EPICARDIAL AND ENDOCARDIAL ST POTENTIAL MAPPING IN ISCHAEMIA

by

Danshi Li

M.B., B.S. MMed (China)

Submitted in fulfilment of the requirements for the degree of Doctor of Philosophy

Division of Clinical Sciences
University of Tasmania

February, 1997

DECLARATION

The investigations described in this thesis constitute my own work. This thesis contains no material which has been accepted for the award of any other higher degree or graduate diploma in any tertiary institution. To the best of my knowledge and belief, this thesis contains no material previously published or written by another person, except where due acknowledgment and reference are made in the text of the thesis.

Signed: Danshi Li

Date: February, 1997

This thesis may be made available for loan and limited copying in accordance with the *Copyright Act 1968*.

Signed: Danshi Li

Date: February, 1997

ABSTRACT

The electrocardiographic change associated with ischaemia is typically ST segment depression which is usually most prominent over the left chest wall. The position of the ST depression does not predict the ischaemic territories in the myocardium or the involved coronary arteries.

To evaluate the source of ST depression, a sheep model of subendocardial ischaemia using partial coronary artery ligation coupled with atrial pacing was developed. Ischaemia was induced initially in either the left anterior descending coronary artery or the left circumflex coronary artery territory and subsequently in the territory of the other vessel. The ischaemic regions were documented by a fluorescent microsphere technique. During ischaemia potentials were mapped simultaneously from the endocardium and the epicardium. The distributions of epicardial potentials from either ischaemic source were very similar (0.77±0.14, P<0.0001), both showing ST depression on the free wall of the left ventricle, and no association between the ST depression and the ischaemic region. At the same time, the endocardial ST elevation was directly associated with the region of reduced blood flow. Insulating the heart from the surrounding tissue with plastic increased the magnitude of epicardial and endocardial ST and QRS potentials and decreased the potentials from limb leads, implying that the ST depression arises from current paths within the myocardium rather than external. Increasing the percent stenosis of a coronary artery increased epicardial ST depression at the lateral boundary and resulted in ST elevation starting from the ischaemic centre as ischaemia became transmural. These results suggest that the major source of ECG changes is the lateral boundary between ischaemic and normal territories. This postulate was supported by the spatial flow distributions which showed a sharp lateral flow change but a gradual transmural flow transition.

In conclusion, ST segment depression can not distinguish an ischaemic region even from the epicardium. The ischaemic source does relate spatially to the endocardial ST change but not to the epicardial ST change. The current paths during subendocardial ischaemia must be in the myocardium and probably originate from the injury current which flows at the lateral boundary. These effects are not explained by conventional ECG theory but they do explain why body surface ST depression does not localise cardiac ischaemia in humans.

The electric and pathophysiologic basis of remote ST depression occurring with ST elevation during acute myocardial infarction remains controversial. To explore the possible mechanism of such ST depression, different sizes of myocardial infarction were produced. The epicardial and endocardial ST potentials were measured and correlated with regional myocardial blood flow measured by fluorescent microspheres. Epicardial ST distributions showed that occluding a small vessel produced the expected ST elevation over the infarcting region with little ST depression over the noninfarcting region, whereas either the occlusion of the left anterior descending coronary artery or the left circumflex coronary artery resulted in a powerful electrical dipole with ST elevation over the infarcted region and ST depression over the noninfarcted region. Examination of fluorescent microsphere delivery into the tissues showed that with smaller infarcts the flow remained unchanged in the noninfarcted region (1.09 ± 0.19 to 1.12 ± 0.15, $P > 0.05$). With large infarcts there was approximately a 30% flow reduction in the noninfarcted region which directly correlated to the perfusion pressure drop ($r = 0.82$, $P < 0.001$). These findings suggest that ST depression reflects extensive infarction and is associated with reduced perfusion of the noninfarcted myocardium. The reduced perfusion may have a significant reversible role in the poor prognosis of these patients.

ACKNOWLEDGMENTS

I wish to sincerely thank my supervisor, **Professor David Kilpatrick**, for his constant guidance, invaluable advice and encouragement throughout the whole project and in the preparation of this thesis.

I am grateful to **Dr. Ah Chot Yong** for his continuous help in the laboratory and in checking and proof-reading the manuscripts; for his encouragement and understanding. Grateful thanks are also extended to:

Ms. Chuanyong Li, Dr. Wojciech Pluta, Dr. Timothy John Gale, and **Mr. David Appleton** for their technical assistance.

Mr. Kevin Pullen, Mr. Malcolm Johnson, Mrs Sue Johnson, and **Miss. Jan Walsh** for their language aid and proof-reading. **Dr. Yiyi Huang** for her discussion and help. **Mr. David Lee** for his assistance in artwork.

Chemistry Department in the University of Tasmania and **Biochemistry Department** in the Royal Hobart Hospital for the use of their spectrofluorimeter. **Catheterisation Laboratory** in the Royal Hobart Hospital for their support of catheters.

Professor G. W. Boyd and **Dr. Janet Vial** for providing the opportunity to undertake this work in the Department of Medicine, and also to my colleagues and staff in this Department and Clinical School who provided a congenial and friendly atmosphere in which to work.

Kunming Medical College and the **Ministry of Education** in China for providing the opportunity to study in Australia. Many thanks to **Professor Guojun Ren** and **Professor Liquan Liang** in China for their moral support and encouragement.

I acknowledge the financial support received from the **Australian Agency for International Development (AusAID)** started from January 1993 to January 1997. I appreciate the help from **Mrs Robin Bowden**, who is the social worker of **AusAID**.

Special thanks to my husband **Xiaoyan Huang**, my father **Lang Li** and my other family members for their support and understanding, without which this task would have been more difficult.

PUBLICATIONS

FULL PAPER

1. Danshi Li, Ah Chot and David Kilpatrick. "Validation of a subendocardial ischaemia sheep model by intracoronary fluorescent microspheres". Clinical and Experimental Pharmacology and Physiology 23: 111-118, 1996.

SHORT PAPERS/ABSTRACTS

1. Danshi Li, Ah Chot and David Kilpatrick. "Validation of a subendocardial ischaemia sheep model by intracoronary fluorescent microspheres". Proceedings of Australian Clinical Physiological and Pharmacological Society 26 (2): 143p, 1995.

2. Danshi Li, Ah Chot and David Kilpatrick. "Effect of subendocardial ischaemia at various myocardial locations on epicardial potential fields". Proceedings of Australian Clinical Physiological and Pharmacological Society 26 (2): 147p, 1995.

3. Danshi Li, Ah Chot and David Kilpatrick. "Origin of epicardial depression in the ischaemic sheep model". Medical & Biological Engineering & Computing. 34(Suppl):101-102, 1996.

4. Danshi Li, Ah Chot and David Kilpatrick. "Epicardial and endocardial potential mapping of ST elevation in experimental myocardial infarction" . Medical & Biological Engineering & Computing. 34(Suppl):111-112, 1996.

5. Danshi Li, Ah Chot and David Kilpatrick. "ST depression is a marker of ischaemia of the noninfarcting myocardium in acute infarction". Scientific Programme of the 44th Annual Meeting of the Cardiac Society of Australia and New Zealand. P203, 1996.

6. Danshi Li, Ah Chot and David Kilpatrick. "The origin of ST depression with partial myocardial wall ischaemia". Scientific Programme of the 44th Annual Meeting of the Cardiac Society of Australia and New Zealand. P233, 1996.

TABLE OF CONTENTS

ABBREVIATIONS IN THE THESIS

bl-grn	blue-green
bpm	beats/min
ECG	electrocardiogram
endo	endocardium or endocardial
endo/epi	endocardial/epicardial
epi	epicardium or epicardial
LA	left atrial or left atrium
LAD	left anterior descending coronary artery
LAP	left atrial pressure
LCX	left circumflex coronary artery
LV	left ventricle
LVEDP	left ventricular end diastolic pressure
LVP	left ventricular pressure
LVSP	left ventricular systolic pressure
OM	obtuse marginal branch of the circumflex coronary artery
PDA	posterior descending coronary artery
RMBF	regional myocardial blood flow
RV	right ventricle
yl-grn	yellow-green

Chapter 1

INTRODUCTION

1.1 BACKGROUND

Myocardial ischaemia remains the major cause of morbidity and mortality in the economically developed countries. Measurements of the electrical activity in the heart have proven to be an extremely valuable tool in detecting and diagnosing ischaemic heart disease. In particular, the electrocardiogram (ECG) has been universally applied as an inexpensive, simple, and noninvasive procedure for diagnosing symptomatic patients as well as for screening healthy subjects.

The ECG is a graphic recording of the electrical potential changes produced by the electrical activation and the electrical recovery of the heart. These electrical events originate from cellular membrane ion fluxes. The ion fluxes generate intracellular and extracellular currents which in turn generate extracellular fields within and on the surface of the body. Myocardial ischaemia and infarction are frequently identified by means of changes in various components of the ECG. For more than 50 years, the most reliable and widely used ECG markers of myocardial ischaemia have been ST segment changes. Typically, ST elevation is thought to represent transmural ischaemia usually leading to infarction, while ST depression is thought to reflect subendocardial ischaemia. Despite the overall acceptance of these criteria, our understanding of the genesis of the ST segment shifts, especially the genesis of ST segment depression, is still very limited. In particular the inability of ST depression to localise ischaemia and the significance of ST depression when it accompanies ST elevation in acute myocardial infarction are not fully explained.

Electrocardiographic ST elevation originates from the injury current flowing from the boundary between normal muscle and its adjacent abnormal area, where resting and/or action potentials are different. The region of ST elevation is closely related to the region of ischaemia (Kleber 1978). At a cellular level, three major mechanisms are considered to underlie ST segment displacement: a localised shortening of action potential duration; a diminishing of the amplitude of the action potential; and a localised decrease in resting membrane potential. The difference in membrane action potentials generates current which produces an ST segment shift. The difference in resting membrane potential generates current which produces a TQ segment shift, opposite to the ST segment shift on the DC-coupled ECG. Conventional electrocardiography with AC coupled amplifiers reflects this as ST elevation.

The origin of ST depression is less well defined. Its mechanism has eluded those workers who have tried to perform animal studies (Holland & Brooks 1975; Vincent et al. 1977). In particular the position of ST depression has no direct relationship to the position of the coronary artery disease (Mark et al. 1987). Classic and modern ECG theories have explained that ST depression is secondary to an injury current in the underlying subendocardium (Wilson et al. 1933; Wolferth et al. 1945; Holland & Brooks 1975). In conventional stress testing, as myocardial demand exceeds the ability of the narrowed coronary arterial bed to increase blood flow in the face of an increased external workload, the ischaemic threshold is exceeded, producing reversible ST segment depression. However, the location of exercise ST depression does not enable the localisation of an ischaemic region. The difficulty in localising myocardial ischaemia from ST depression can not be explained by the classic theories, which all suggest that ST depression should be able to localise ischaemia (Wilson et al. 1933; Holland & Brooks 1975). Progress in this area has been hampered by the lack of models of subendocardial ischaemia. This investigation was proposed to map directly the electrical changes in a model of subendocardial ischaemia to fully define the source of ST depression.

Secondly, the mechanisms responsible for ST depression in ECG leads other than infarct-related ones during acute myocardial infarction have not been completely clarified. Sudden, complete occlusion of a coronary artery is most commonly associated with ST elevation in those ECG leads representing the region of damaged myocardium. "Reciprocal" ST depression may appear in ECG leads remote from the area of infarction. The underlying pathophysiological basis of such ST depression remains controversial. Opinions vary as to whether it is a clinically benign "reciprocal" image of ST elevation in the infarcted zone, or whether it is an independent finding, associated with larger infarction, more extensive coronary artery disease, or a higher risk of poor clinical outcomes. These opinions have been based on the evaluation of ECG in patients with infarction (Wong et al. 1993; Wong & Freedman 1994; Edmunds et al. 1994; Lew et al. 1985 & 1987; Fletcher et al. 1993; Stevenson et al. 1993 & 1994; Birnbaum et al. 1994; Shah et al. 1994; Quyyumi et al. 1986). Although many experimental studies have focused on acute myocardial infarction, few of them have explored the mechanism of ST depression occurring in the remote area other than the primarily damaged myocardium. Remote ST depression was seldom documented in previous studies due to less developed mapping techniques (Rakita et al. 1954; Ekmekci et al. 1961) and limited sizes of myocardial infarction (Holland & Brooks 1975; Smith et al. 1979). The ischaemic models were produced by ligating small branches of a coronary artery to ensure stability of the animal; the electrophysiological changes were only measured at a given site; the transition in electrophysiological measurements with respect to the distance from an ischaemic or infarcted border were not examined and therefore the spatial features of the electrophysiological changes in the infarcted and noninfarcted areas were not estimated (Rakita et al. 1954; Ekmekci et al. 1961; Kleber et al. 1978; Smith et al. 1979). The present study was purposed to map the spatial electrical consequences of different regions and extents of transmural ischaemia to enhance the understanding of mechanisms responsible for ST depression.

1.2 AIMS

This thesis aims to explore the origin of ST segment depression in subendocardial ischaemia, and to investigate the mechanisms of ST depression in acute myocardial infarction.

The design of this study was based on the hypothesis postulated by Kilpatrick et al. (1990). From their clinical studies in patients with inferior infarction and patients having ST depression only, Kilpatrick and his coworkers proposed that ST depression on the ECG originates from current flow from a region of endocardial ischaemia back on to the outside of the heart through the great vessels and atria. This study aimed to test this hypothesis, and to evaluate the source of ST depression in the sheep heart with subendocardial ischaemia.

To carry out this study, the regional myocardial blood flow (RMBF) was used to measure the region, the extent and the degree of ischaemia. A technique for the measurement of RMBF by using fluorescent microspheres was developed. Sheep models with subendocardial and transmural ischaemia in different territories were produced. A forty-pole electrode "basket" apparatus was constructed to map the endocardial ST potentials. Systematic mapping of epicardial and endocardial potentials was performed in the animal models of subendocardial and transmural ischaemia. The electrical consequences were related to the simultaneous measurements of RMBF.

1.3 ORGANISATION OF THE THESIS

The thesis is divided into 8 chapters. Chapter 2 provides background information on basic ECG principles, pathophysiology of myocardial ischaemia and infarction, and reviews the origins of ST segment shifts. Chapter 3 outlines the general methods of the investigation. Special methods for different studies are separated and retained for each chapter. Chapter 4 describes the technique of fluorescent microspheres for the measurement of RMBF. Chapter 5 presents a sheep model of subendocardial ischaemia. Chapter 6 examines the origin of ST depression in subendocardial ischaemia. Chapter 7 studies the possible mechanisms of ST depression occurring with ST elevation in transmural ischaemia. Chapter 8 concludes this study and postulates future directions for research.

Chapter 2

LITERATURE REVIEW

This chapter provides background information on basic electrocardiographic (ECG) principles and the pathophysiology of myocardial ischaemia and infarction and then reviews the origins of ST segment shifts. It includes the cellular membrane potentials, the local current paths, and biological, haemodynamic and electrical effects of myocardial ischaemia and infarction. The classic and the modern ECG models of ischaemia are reviewed. The clinical and experimental aspects of ST elevation and ST depression are also covered. A glossary of terms associated with ECG and ischaemia are also described in this chapter.

2.1 BASIC ECG PRINCIPLES

2.1.1 The Genesis of the Electrocardiogram

The electrical excitation and recovery of the heart generates an electrical field in the body, creating differences of electrical potential between points on the body surface. These potential differences can be measured continuously with a galvanometer producing the electrocardiogram (ECG). The waves in the ECG reflect the sequence of excitation and recovery as it moves through the atria and ventricles.

Four electrophysiological events are involved in the genesis of the ECG (Fozzard & Friedlander 1989): (1) impulse formation in the primary pacemaker of the heart (usually the SA node); (2) conduction of the impulse through specialised conduction fibres; (3) activation (depolarisation) of the myocardium; and (4) recovery (repolarisation) of the myocardium. These events are conducted by five functionally and anatomically separated types of specialised myocardial cells: sinoatrial (SA) node, atrioventricular (AV) node, His-Purkinje system, atrial muscle and ventricular muscle. The first three have the function of impulse formation (pacemaker cells); the second and the third have the primary function of conduction; and the last two have the primary function of mechanical contraction. Each cell type has a characteristic action potential, and the recorded ECG is a summation of these individual action potentials as modified by the electrical field of the thorax and the instrumentation used for their amplification and recording. Thus, the ECG has its origin in cellular electrical events.

2.1.1.1 Membrane potentials and currents

The electrical properties of cardiac cells (myocytes) result from a tightly controlled flow of ions through specialised channels in the cellular membrane; the gap junctions which connect and allow electrical communication between cells; and the extracellular space. The cellular membrane of the cardiac cells is a high-resistance plasma membrane surrounding each of the cardiac cells. The components of the membrane are the molecular bilayer of phospholipids with inserted globular integral proteins functioning as ion channels. This structure acts as a selective barrier to the free flow of ions and other low-molecular-weight substances. The opening and closing of these channels depends on voltage, time or the binding of molecules to receptors. Sodium, potassium, calcium and chloride ion flows are regulated by these protein channels.

Resting membrane potential

The resting myocardial cell is in a state of electrical equilibrium with positive charges on the outer surface of its membrane and negative charges on the inner surface. In this resting state the cell is said to be polarised. No current is recorded if both the exploring electrode and the indifferent electrode are placed on the surface of the cell membrane. However, if the exploring electrode penetrates the cell membrane, a negative potential of -60 mV to -90 mV (i.e. 60-90 mV lower than the extracellular potential) will be recorded. This potential difference between the interior and the exterior of a myocyte at resting state is termed the resting membrane potential. In atrial and ventricular cells this resting membrane potential is stable until external excitation is applied, but in SA nodal cells and other conduction fibres it is unstable, drifting towards zero with time. This process is characterised by a regular, self-induced, progressive depolarisation in the interval between action potentials to a point producing the activation of the action potential and is known as pacemaker behaviour. Because of this electrical property, SA nodal cells and other conduction fibres do not normally have a "resting" potential.

The resting potential is due primarily to two factors: the high concentration of potassium ions in the intracellular fluid and the high permeability of the cell membrane to potassium ions compared with other ions. The latter property is due to the fact that, at resting membrane potential, many K^+ channels are open, whereas Na^+ and Ca^{++} channels are mostly closed. The intracellular K^+ concentration is about 30 times higher than the extracellular K^+ concentration (intracellular 150 meq/L, extracellular 5 meq/L; an opposite gradient exists for Na^+ ions), so there is a continuous tendency for K^+ to diffuse out of the cell down its concentration gradient, via opening K^+ channels. However, the negative intracellular ions, mainly organic phosphates and charged proteins, can not accompany the K^+ ions because the cell membrane is impermeable to them. If the negative intracellular potential was big enough, the electrical attraction of the cell interior for the K^+ could fully offset the outward diffusion tendency of the ions, creating a dynamic equilibrium in which there would be no further net movement of K^+ out of the cell. The electrical potential at which this would happen is called the *potassium equilibrium potential.* This electrical potential is, by definition, equal in magnitude to the outward-driving effect of the chemical concentration gradient. The exact relation between the potassium equilibrium potential and the potassium concentration ratio is given by the Nernst equation:

$$E_{k^+} = (RT/F) \ln([K]_{out}/[K]_{in})$$

where R is the Universal gas constant, T is the absolute temperature and F is the Faraday's constant. Experimentally, it is found that the myocytes' resting potential is indeed close to the potassium equilibrium potential (Page 1962; Levick 1995). It is also found that when the extracellular potassium concentration is increased, as in ischaemia, the myocyte resting potential declines (grows less negative) in proportion to the concentration, as predicted by the Nernst equation (Page 1962; Levick 1995). The K^+ concentration gradient at rest is maintained by an active ion transport mechanism, the Na^+-K^+ exchange pump.

Action membrane potential

The action potential is generated by a sequence of changes in membrane permeability to ions. It commences with an abrupt reversal of the membrane potential to a positive value (depolarisation) (Figure 2.1). The initial depolarisation can be triggered by voltages or currents applied externally or internally to a resting cell. The introduction of a constant current into a cell changes the transmembrane potential to a more positive value by increasing the membrane permeability for positive ions. When more current is passed into the cell, a threshold value between -70 mV and -60 mV is reached, and the cell very rapidly shifts to an inside positive value of +20 mV to +30 mV (depolarisation). In atrial and ventricular cells and in the His-Purkinje system, this response arises from a sudden transient increase in the membrane's permeability for Na^+ ions. At the threshold potential, voltage-sensitive sodium channels (fast channels) open very quickly and increase the Na^+

conductance of the membrane about 100 times. This allows a rapid flux of sodium ions into the myocyte (inward sodium current) and results in a reversal of the intracellular potential. This phase of depolarisation is termed phase 0. Following cellular depolarisation, there is a gradual return of potential to the resting potential. This repolarisation process is divided into 3 phases: Phase 1: an initial rapid return of intracellular potential to 0 mV, the result of inactivation of Na^+ channels and activation of the transient outward K^+ current. Phase 2: a plateau resulting from a small but sustained inward current of Ca^{++} ions flowing into the cell down their electrochemical gradient. A brief change in chloride conductance early in phase 2 may be involved in the transition from peak to plateau; the inward Na^+ current and the outward K^+ current also make a small contribution to the plateau. A balance is achieved between the residual Na^+ current and the developing Ca^{++} current favouring depolarisation and a developing K^+ current favouring repolarisation, which stabilises the potential at 0 mV to -20 mV for a period of 200 ms. The long plateau is important because the cell is electrically inexcitable (refractory) during this long period, and the influx of Ca^{++} triggers mechanical contraction. Phase 3: return of the intracellular potential to resting potential, resulting from the fall in the membrane permeability to inward Ca^{++} and rise in the membrane permeability to outward K^+. With the outward K^+ current virtually unopposed, a rapid repolarisation develops, returning the membrane to its previous polarised state and ending the action potential. The cells then awaits the next signal from its neighbour to repeat the entire process. The total duration of action potentials is about 100 msec in canine ventricular muscle at normal heart rates, and at least twice that long in the human ventricle.

At the end of phase 3, the negative resting potential is reestablished; however, the cell is left with an excess of Na^+ and a deficit of K^+. The Na^+-K^+ exchange pump, an adenosine triphosphate (ATP) dependent transport mechanism in the cell membrane, which transports Na^+ ions out of the cell and K^+ into the cell, becomes effective and restores the change in intracellular ion concentration resulting from the action potential. The pumping is an active process and consumes metabolic energy in the form of ATP. The inhibition of the Na^+-K^+ pump in the early ischaemia can cause an increase in extracellular potassium (Kleber 1983; Wilde & Kleber 1986).

Action Potential

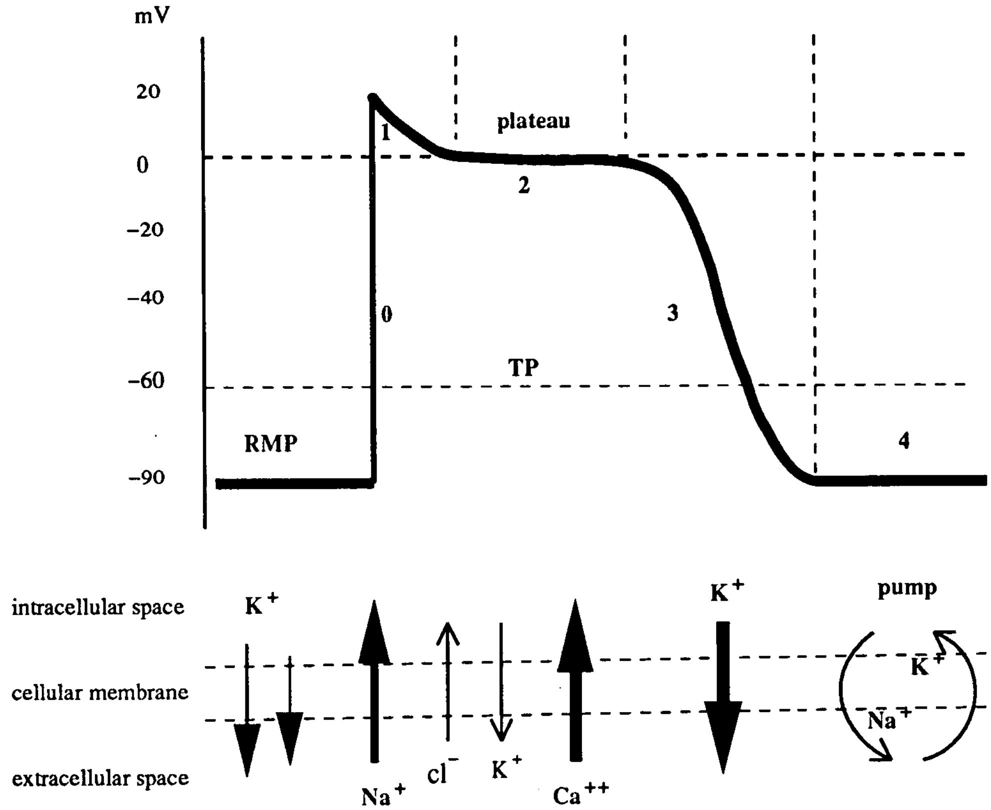

Extracellular Electrogram

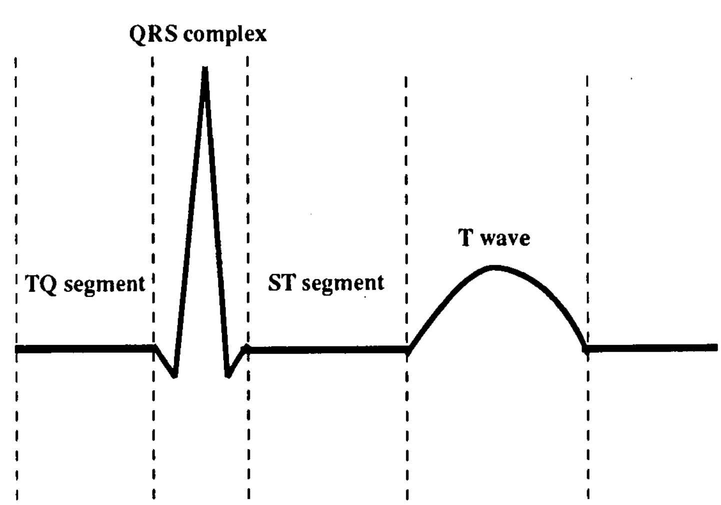

Figure 2.1 Diagrams of the action potential of a ventricular muscle cell (top) and the corresponding extracellular electrogram (bottom). The rapid inward sodium current initiates the rapid depolarization, which, in turn quickly inacitvates the sodium current. A second depolarization current, calcium current, now ensues and generates the plateau of the action potential. During the plateau, the outward patassium current is generated and drives the membrane potential back toward resting potential. RMP=resting membrane potential; 0=depolarization; 1,2,3=repolarization; 4=diastolic phase; TP=threshold potential.

Local circuit currents

The movement of ionic currents through the membrane, within the cells, and back through the extracellular space completes a circuit. As the Na^+ channels open and Na^+ rushes into the cells, these positive charges displace the negative charges stored on the inside of the membrane and result in depolarisation. The intracellular potential in that localised region is now more positive than in neighbouring parts of the cell, so a driving force for the longitudinal current in the myoplasm is established. K^+ is the major carrier of this current (Horan & Flowers 1980). The longitudinal current displaces negative charges off the interior of the membrane, depolarises the adjacent element to the threshold, thereby initialises an action potential of the cell. If the depolarising current reaches the end of a cell and is conducted through a gap junction into an adjacent cell, propagation of the action potential results. However, the conduction of the excitation through the heart is extremely complex and is beyond the scope of this thesis. Readers who wish to explore the full mechanisms of conduction should consult the reviews of Spach (Spach 1995) and Fozzard et al. (Fozzard & Arnsdorf 1992; Fozzard & Friedlander 1989).

2.1.1.2 Relation of cellular events to the electrocardiogram

The cardiac electrical field

Transmembrane potentials are differences in voltage between the inside and outside of a cell; but the ECG records differences of potential in an electrical field at a distance from the heart. At every instant, from the beginning of an action potential in the first excited myocardial cell until the complete repolarisation of the last one, it is possible to identify a boundary between the activated cells and the resting cells. This advancing wave front is usually modelled as the source of the electrical field, because the surface of the depolarised cells is electrically negative with respect to the exterior of those not yet activated. If this wavefront can be replaced by a single moving dipole, then the magnitude and direction of the dipole can be analysed from the body surface. The prototype model of the ECG, the equivalent dipole model, put forward by Einthoven (Einthoven et al. 1913) and developed by Wilson (Wilson et al. 1933b), although oversimplified, has proved to be extremely useful and still dominates traditional electrocardiography. According to this model, at any instant during depolarisation and repolarisation, the heart can be viewed as a dipole consisting of a positive charge (resting cells) and a negative charge (active cells) separated by a small distance, while the body is a homogeneous volume-conductor which acts like a tank full of electrolyte solution and carries electrical current easily in all directions. Since the dipole generates a force that has magnitude and direction, it can be expressed as a vector. As illustrated by Figure 2.2, assuming that the left side is the endocardium and the right side is the epicardium, and the exploring electrodes are placed on the chest wall (B) and the intracavity (A); the indifferent electrode is attached to the leg far away from the heart (considered as being zero potential). At resting state, there is a uniform positive charge outside the heart, no potential difference and no external current field exists, thus the electrodes register an isoelectric line. When the depolarisation begins from the endocardium, the chest electrode facing the positive side of the dipole (also termed the "source") records an upright deflection; the cavity electrode facing the negative side of the dipole (also termed the "sink") records a downward deflection. This occurs as a result of the orientation in the conducting medium of an electrical field created by the advancing dipole. As the dipole is moving away from the endocardium towards the epicardium, the chest electrode records a less positive potential because it faces the less positive electric field; the cavity electrode records a less negative potential. At the end of depolarisation, a uniform negative field occurs and the trace returns to the baseline. When repolarisation starts from the epicardium, a positive field appears in this side and the electrode facing the positive side of the dipole registers an upward deflection.

The general relationship between the dipole source and the cellular activity has been confirmed in tissue-bath experiments by Spach and coworkers (Spach et al. 1972 & 1979). However, the electrical field of the heart is far more complex than a simple dipole generator, because the excitation wave front is equivalent to a great number of dipoles which vary in their orientation. Moreover, the human body is not a homogeneous conductor, and the recording electrodes are not at equidistance as assumed by the equivalent dipole model. Therefore, there are approximations in using this model to interpret the ECG. In recent years, more and more complex mathematical models (Barber & Fischmann 1961; Holt et al. 1969; Miller & Geselowitz 1978a; Holland & Arnsdorf 1977; Colli-Franzone et al. 1982) have been put forward to interpret the ECG. Nevertheless, the general principles that apply in the ECG interpreting are the same as those govern the potentials generated by a single dipole.

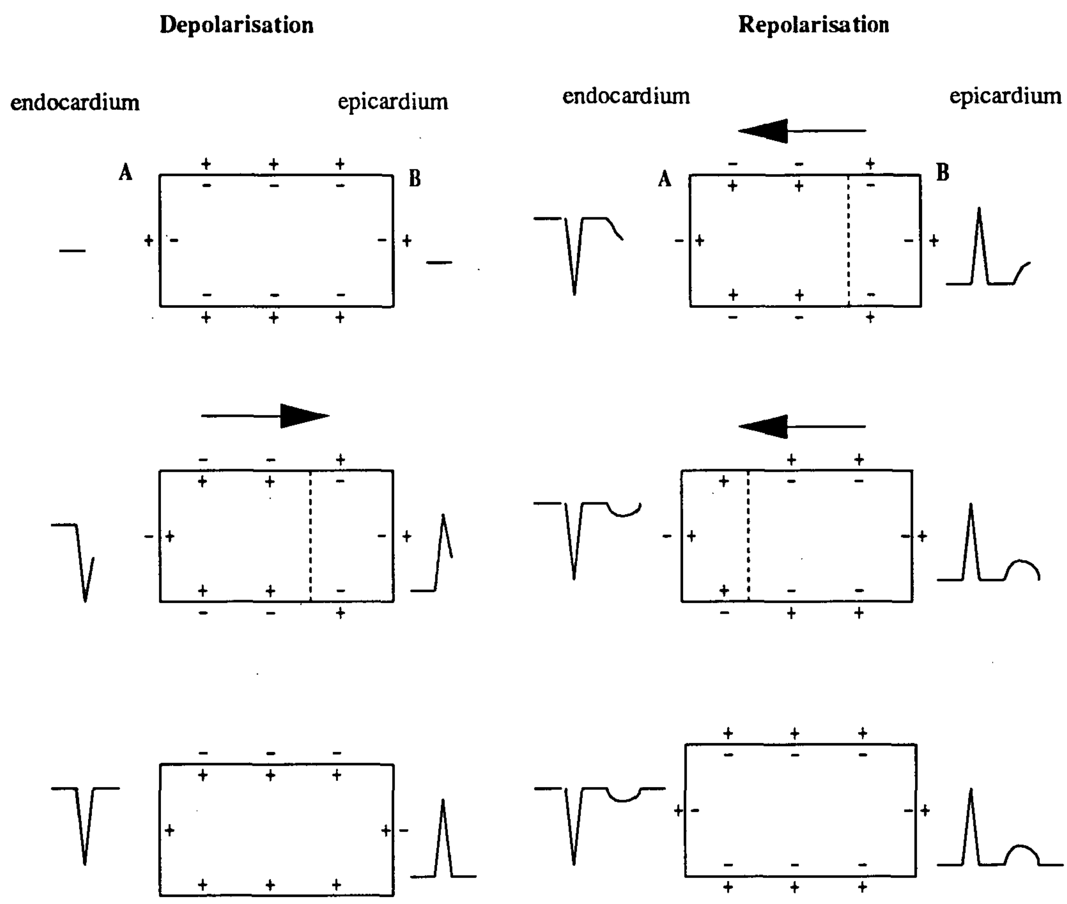

Figure 2.2 Potential generated during depolarization and repolarization recorded with an exploring electrode located at endocardium (A) and precordium (B). The directions of depolarization and repolarization are indicated by arrows. (Modified from Fisch C. Electrocardiography and vectocardiography. In Heart Disease, Braunwald E, ed. W.B. Saunders Company, 1992).

Impulse generation and conduction

The initiating action potential in the normal heart arises in the SA node which is a collection of specialised muscle fibres localised in the high right atrium. The depolarisation impulse leaves the SA node, activates the right atrium first, followed by the activation of the left atrium, producing the outline on an ECG called the P wave. The impulse then reaches the AV node which lies at the top of the interventricular septum bridging the atria and the ventricles. The conduction is delayed due to the slow conduction velocity of the AV node, which allows a full atrial activation before ventricular excitation occurs. The AV node extends the slowed impulse to a bundle of conducting fibres known as the bundle of His. Once passed the His bundle, the impulse proceeds down the rapid conducting Purkinje system which supplies the terminal conduction fibres to the ventricular walls. Then the impulse spreads from the inner surface of the ventricles (endocardium) to the outer surface of the ventricles (epicardium). Conduction through the AV node, the bundle of His, and the Purkinje fibres does not show on ECG because the external recording can discern only the *boundary* between large masses of resting and activated muscle within atrial and ventricular walls, thus only the baseline is drawn on ECG paper during their depolarisation. This isoelectric interval preceding the ventricular depolarisation is called the PR interval. The depolarisation of both ventricles produces a complex in the ECG known as the QRS complex. Ventricular repolarisation produces the T wave corresponding to phase 3 of the action potential. The isoelectric ST segment seen between depolarisation and repolarisation of the heart implies that during this period no great regional differences in potential occur in the ventricle. The transmembrane action potential demonstrates a long plateau phase (phase 2), corresponding to the isoelectric phase, the ST segment in ECG. Factors that shorten or lengthen the plateau phase of repolarisation in individual cells would affect the ST segment. During the resting state, no current is recorded because all the ventricular cells are polarised and no potential difference exists between these cells. This resting period between repolarisation and the next depolarisation is seen in ECG as an isoelectric line between T wave and QRS complex, and is termed the TQ segment.

These ECG features are compared with the underlying cardiac action potential in Figure 2.1. The final surface ECG is primarily a ventricular ECG, and the sequence of activation of the interventricular septum, the right ventricle and the left ventricle plays an important role in the appearance of the ECG. The following approximate correlation exists between the cellular transmembrane potential and the ECG:

The summation of phase 0 potentials of ventricular myocardial cells produces the QRS complex.

Phase 1 corresponds to the J point, the junction of the QRS complex with ST segment.

Phase 2 corresponds to the ST segment.

Phase 3 corresponds to the T wave.

Resting potential corresponds to the TQ segment (the isoelectric baseline between T wave and QRS complex).

2.1.2 Electrocardiographic ST Changes in Myocardial Ischaemia and Infarction

The ST segment is a short section of baseline that begins at the end of the S wave and ends at the beginning of the T wave. Under normal circumstances, the ST segment is isoelectric. However, it may vary from -0.55 to +2.0 mm below or above the baseline. When describing the ST segment as elevation or depression, a comparison is made with that portion of the ECG tracing that lies between the termination of the T wave and the beginning of the following P wave (TP segment) or the preceding PR segment. If part of the myocardium is damaged by ischaemia (a poor blood supply due usually to coronary artery disease), ST segment shifts will occur, as discussed in the following sections.

2.1.2.1 Electrocardiographic ST shifts in myocardial ischaemia

Myocardial ischaemia occurs when the coronary artery blood flow is insufficient to meet myocardial metabolic requirements. It is a transient and reversible phenomenon. The electrocardiographic findings are usually limited to ST segment and T wave abnormalities, although transient changes to the QRS sometimes occur if the ischaemia is of sufficient severity. Since the underlying process is transient, so are the electrocardiographic features.

ST segment depression

ST segment depression is considered to reflect nontransmural myocardial ischaemia. It often involves the subendocardial areas of the heart, which are the most vulnerable to ischaemic injury due to the combination of their limited reserve for vasodilatation, extrinsic compression from the high wall stress and the resultant high metabolic demands in these regions. The typical ECG pattern is ST segment depression with T wave inversion in left precordial leads, and this is usually seen in the clinical setting of exercise induced ischaemia or ischaemia at rest associated with angiographic evidence of fixed or reversible severe coronary stenosis, but not occlusion of a coronary artery. Patients with extensive, angiographically visible collaterals may also have only ST segment depression during total coronary occlusion.

ST segment elevation

ST segment elevation reflects transmural myocardial ischaemia and therefore indicates a more severe degree of ischaemia than that responsible for the pattern of ST segment depression. New ST segment elevation during ischaemic chest pain is usually accompanied by acute total coronary occlusion and occurs in patients with the clinical syndromes of variant angina pectoris or evolving acute myocardial infarction.

2.1.2.2 Electrocardiographic ST shifts in myocardial infarction

Myocardial infarction occurs when insufficient coronary artery blood flow over a critical length of time causes death of myocardial cells. Myocardial cells die from an inadequate blood supply. This usually occurs after 20 minutes of cessation of flow and continues for some hours (vide infra). Occlusion may result from atherosclerotic obstruction in the coronary arteries, thrombotic or embolic occlusion of a coronary artery, or spasm in an artery. The typical ECG manifestations in acute myocardial infarction are those of ischaemia, injury and cellular death and are, within limits, reflected by T wave changes, ST segment shifts and the appearance of abnormal Q waves, respectively.

If the ECG is inscribed at the onset of myocardial infarction, the characteristic early change recorded is often an abnormal T wave. The T wave may be prolonged, increased in magnitude, and either upright or inverted. This is followed by ST elevation in leads facing the area of injury. The upright T wave may exhibit terminal inversion at a time when the ST is still elevated. A Q wave may be present in the first ECG or may not appear for hours or sometimes days. The amplitude of the QRS complex may diminish and may be replaced by a QS pattern. ST elevation begins to diminish soon after the onset of the infarction (several minutes to hours), a change which occurs simultaneously with the deepening of the T wave inversion of ischaemia (McLachlan 1981). As the ST segment returns to the baseline, symmetrically inverted T waves evolve. The time of appearance and the magnitude of the change may vary among patients. Studies in patients have shown that ST elevation is usually maximal during the first hour after onset of chest pain (Selwyn et al. 1977). After this it declines. ST elevation persisting beyond two weeks does not usually resolve within six months, and is a specific but relatively insensitive sign of advanced left ventricular asynergy of a ventricular aneurysm (Mills et al. 1975).

The classic evolution of acute myocardial infarction is documented in approximately one-half to two-thirds of the patients, while in those remaining the infarct is manifested by ST shifts, T wave changes and non-Q QRS changes (Fisch 1992). Evolution of the characteristic ST and T wave changes coupled with appearance of Q waves is highly specific for acute myocardial infarction. In the first ECG, the specificity of the ST change alone is high (Fisch 1992).

ST segment elevation

Frequently the first ECG finding after myocardial infarction is ST segment elevation in leads overlying the area of infarction. Because completely dead muscle is electrically silent, the occurrence of ST segment changes early in the course of infarction indicates the presence of some viable muscle in the epicardial region. Leads opposite to the area of infarction may show reciprocal ST segment depression.

ST segment depression

ST segment depression in acute myocardial infarction may reflect subendocardial ischaemia, infarction or reciprocal changes secondary to infarction at a remote site. The mechanisms and clinical significance of such ST depression will be discussed in the next section.

By observing the ST segment elevation and the developed Q wave in specific ECG leads, the anatomic site of infarction can often be localised. The following types of myocardial infarction are often seen in clinical practice.

Anterior wall infarction. Anterior wall is the left ventricular free wall between the interventricular groove and the lateral margin of the anterior papillary muscle. Anterior wall myocardial infarction is best reflected in the precordial leads (V_{1-6}) that show the infarction pattern depending upon the extent of infarction. Inferior leads (leads II, III and aVF) may show ST depression.

Inferior wall infarction. Inferior wall is the region between the lateral border of the posterior papillary muscle and the posterior septum. Inferior wall myocardial infarction is reflected in leads II, III and aVF. Not infrequently, reciprocal ST segment depression is recorded in precordial leads V_{1-3}.

Posterior wall infarction. Posterior wall is the basal third of the posteroinferior wall. Posterior wall myocardial infarction is unusual. It is characterised by a tall R wave in precordial leads V1-2 because of the loss of the forces normally generated by the posterior portion of the ventricle. ST segment depression in V_{1-2} (and/or V_3) can be seen in this infarction.

2.2 PATHOPHYSIOLOGY OF MYOCARDIAL ISCHAEMIA AND INFARCTION

Myocardial ischaemia has been defined as an imbalance between the supply of oxygenated blood and the oxygen requirements of the myocardium. Ischaemia resulting from increased myocardial oxygen demand in the presence of critical narrowing of a coronary artery is termed *demand ischaemia*; ischaemia caused by the reduction of coronary flow is termed *supply ischaemia* (Ganz & Braunwald 1997). Demand ischaemia is responsible for most of the episodes of stable angina; supply ischaemia is responsible for myocardial infarction and most episodes of unstable angina. In many circumstances, ischaemia results from both an increase in oxygen demand and a reduction in supply. According to the location, ischaemia has been classified as *transmural ischaemia* and *nontransmural* or *subendocardial ischaemia.* Ischaemia is transmural if injury affects the full thickness of the ventricular wall; nontransmural or subendocardial if injury ranges from the inner one-quarter to the inner three-quarters of the ventricular wall (Freifeld et al. 1983). In experimental studies, the degree of ischaemia is defined as *severe* when flow is reduced to 10 to 15% or less of nonischaemic flow; *moderate* when flow is reduced to 15 to 30%; *mild* when flow is reduced to 30 to 50% (Jennings 1975). It is accepted that the severity of ischaemia influences the duration of cell survival and that the time frame of cellular injury may be slower if ischaemia is mild or moderate and faster if ischaemia is severe. Despite the recognition that the time course of injury varies, it is often assumed that the cellular consequences of moderate versus severe ischaemia are qualitatively similar (Reimer & Jennings 1992).

2.2.1 Location and Time Course of Ischaemic Cell Death

2.2.1.1 Transmural progress of ischaemic cell death

After coronary artery occlusion, ischaemic myocytes do not die instantaneously. Necrosis occurs first in the subendocardial myocardium. With longer occlusions, a wavefront of cell death moves from the subendocardial zone across the wall to involve progressively more of the transmural thickness of the ischaemic zone (Warltier et al. 1982; Reimer et al. 1977; Connelly et al. 1982). Mildly ischaemic myocytes may survive indefinitely, even the most severely ischaemic myocytes remain viable for at least 15 minutes in anaesthetised dogs (Jennings et al. 1985).

Beyond 15 minutes of coronary occlusion, increasing numbers of ischaemic myocytes become irreversibly injured, as defined by the fact that reperfusion does not prevent subsequent infarction. By 40 minutes, much of the subendocardial zone has been irreversibly injured (Reimer & Jennings 1979). With increasing duration of coronary occlusion, a transmural wave front of cell death progresses from the subendocardium to the subepicardium. If ischaemia is uninterrupted, infarcts eventually involve an average of 80% of the ischaemic region. By 6 hours, infarcts have reached their full size, and infarct size is not influenced by reperfusion at this time (Reimer & Jennings 1979). The time course of the spatial evolution of infarction varies among species, but in all such experimental models of abrupt coronary occlusion, infarction is complete in 6 hours or less.

2.2.1.2 Lateral boundaries of ischaemia

For many years it was assumed that intramural anastomoses, an element of interdigitation between adjacent coronary beds, gave rise to a quantitatively significant border zone of intermediate perfusion at the interface between an area of ischaemia and adjoining normally perfused tissue; in the acute phase of regional myocardial ischaemia, the central ischaemic area is surrounded by a shell of tissue in which the ischaemic injury is less severe than in the centre because of the intramural lateral circulation (Becker et al. 1973; Jugdutt et al. 1979a & b; Vokonas et al. 1978). This assumed mass of tissue is known as the border zone. It is now well established that there is no quantitatively significant lateral border zone of intermediate ischaemia separating the core of severe ischaemia from the surrounding normal tissue. Instead, the lateral interface is characterised by a sharp transition between ischaemic and normal cells (Factor et al. 1981; Reimer & Jennings 1979; Harken et al. 1981; Janse et al. 1979; Murdock et al. 1983). This interface between normal and ischaemic tissue is characterised by a sharp but irregular profile from the endocardium to the epicardium with severely ischaemic tissue lying adjacent to normal, well perfused tissue. This sharp transition can be explained on the basis that the important collateral anastomoses between major coronary arteries are on the epicardial surface of the heart (Schaper 1971). The myocardium is perfused through smaller penetrating branches of these larger surface arteries. The penetrating intramural arteries are essentially end arteries, with few or no interconnections between adjacent capillary beds (Factor et al. 1981). The existence of any lateral progression of infarction in the subendocardial zone is thus denied based on the vascular anatomical considerations.

2.2.1.3 Determinants of infarct size and transmural extent of injury

The severity of ischaemia varies among individual animals and from area to area within the ischaemic region of a given animal. Collateral blood flow is the major determinant of the extent and transmural progression of infarction (Reimer & Jennings 1992). In dogs even permanent ligation of a major coronary artery often does not result in complete infarction of the occluded vascular region. After the left circumflex coronary artery (LCX) occlusion, there is persistent viable myocardium in the subepicardial zone, averaging about 20% of the ischaemic vascular bed (Reimer & Jennings 1979). In dogs, with permanent occlusion, both the size of the ischaemic vascular bed and the amount of subepicardial collateral blood flow are major determinants of infarct size (Jugdutt et al. 1979a; Reimer & Jennings 1979). In contrast to dogs, baboons (Lavalee & Vatner 1984; Crozatier et al. 1978), pigs (Fedor et al. 1978; Warltier et al. 1982) and sheep (Markovitz et al. 1989; Euler et al. 1983) have few native coronary collateral anastomoses; following a coronary ligation, the subepicardial zone is as severely ischaemic as the subendocardial region; and permanent coronary occlusion is followed by severe transmural ischaemia and by solid transmural infarcts. Thus, in these species, infarct size is determined primarily by the size of the occluded vascular bed. However, ultrastructural and metabolic features of cell injury have occurred more quickly in the subendocardial region than in the subepicardial region, despite the absence of collateral flow (Lowe et al. 1983), suggesting that transmural differences in myocardial work load or basal metabolic needs may contribute to the transmural progression of injury in these species.

2.2.2 Biological, Haemodynamic and Electrical Effects of Myocardial Ischaemia and Infarction

2.2.2.1 Metabolic changes

A series of metabolic, ultrastructural and functional changes of the myocardial cells occur during acute coronary occlusion. There are two essential components behind these events (Gettes & Cascio 1992): (1) absence of arterial inflow, which leads to the deprivation of oxygen (hypoxia) and metabolic substrates, and (2) absence of venous outflow, which leads to accumulation of the end products of anaerobic metabolism in the extracellular space. The abrupt interruption of coronary flow rapidly lowers the pO_2 in the involved tissue, coinciding with the loss of contractility in the ischaemic region (Sayen et al. 1961). Anaerobic glycolysis occurs but is unable to maintain the supply of high-energy phosphates. Within the first 5 minutes of coronary occlusion, 80% of creatinine phosphates are lost (Braash et al. 1968);

within 15 minutes, the ATP level has decreased by 80% (Jennings et al. 1981; Reimer et al. 1981). Intracellular acidosis occurs primarily as a result of ATP hydrolysis and is estimated to exceed one pH unit within 30 minutes (Gevers 1979). The level of pCO_2 rises in the extracellular space (Case et al. 1979), extracellular pH falls, and lactate, phosphate, potassium, free fatty acids, and adenosine accumulate in the extracellular space (Corr et al. 1984; Reimer et al. 1981).

2.2.2.2 Histological and ultrastructural changes

In experimental infarction, the earliest ultrastructural changes in cardiac muscle following the ligation of a coronary artery, noted within 20 minutes, consists of reduction in the size and number of glycogen granules, intracellular edema and swelling and distortion of the mitochondria (Kloner et al. 1980). These early changes are reversible. Changes after 60 minutes of coronary occlusion include myocardial swelling and internal disruption, and development of amorphous flocculent aggregation and margination of nuclear chromatin, and relaxation of myofibrils. After 20 minutes to 2 hours of ischaemia, changes in some cells become irreversible, and there is progression of these alterations. These early ischaemic changes can only be detected by electron microscope. After 8 hours, edema of the interstitium becomes evident, as do increased fatty deposits in the muscle fibres along with infiltration of neutrophilic polymorphonuclear leukocytes and red blood cells. Muscle cell nuclei become pyknotic and then undergo karyolysis, and small blood vessels undergo necrosis (Schlesinger & Reiner 1955). These changes are easily detectable by light microscope.

2.2.2.3 Haemodynamic consequences of ischaemia

The initial consequences of myocardial ischaemia include inhibition of oxidative metabolism and reduced contractile function. Since the heart has virtually no store of oxygen, its high rate of energy expenditure results in a sudden, striking decline of myocardial oxygen tension within seconds of coronary occlusion and loss of contractility. The nonischaemic myocardium exhibits a compensatory increase in its force of contraction (Sayen et al. 1961). Experimental studies show that myocardial function decreases in a graded manner in response to deceases in myocardial blood flow (Vatner 1980; Wyatt et al. 1975; Tomoike et al. 1978). Acute reduction in myocardial flow of 10-20% is consistently associated with mildly deceased mechanical performance (Vatner 1980). Derangement of function of the ischaemic segment increases progressively as myocardial blood flow is reduced below two-thirds to one half of normal levels (Wyatt et al. 1975). With blood flow reduced to 75% of normal, the ischaemic segment function becomes hypokinetic and then diskinetic as heart rate is progressively increased by pacing (Tomoike et al. 1978). Function does not cease entirely until flow falls about 80% from baseline (Vatner 1980). If sufficiently widespread, regional impairment of myocardial contractile activity depresses global left ventricular function, causing reductions of stroke volume, cardiac output, and ejection fraction while elevating ventricular end-diastolic volume and pressure. Heart failure occurs when regional asynergy is severe and extensive enough that the uninvolved myocardium can not sustain the normal haemodynamic burden. Left ventricular failure usually develops when contraction ceases in 20-25% of the left ventricle (Ganz & Braunwald 1997). With loss of 40% or more of the left ventricular myocardium, severe pump failure ensues, and, if this loss is acute, cardiogenic shock develops (Ganz & Braunwald 1997). Myocardial ischaemia also alters the diastolic properties of the heart. Ischaemia increases the end diastolic pressure and thus increase the resistance to ventricular filling (Jennings & Reimer 1983). Therefore ischaemia causes both systolic and diastolic impairment, which eventually leads to heart failure.

2.2.2.4 Changes in regional myocardial blood flow

Following a coronary artery occlusion, the myocardial flow in the ischaemic area decreases immediately, a change occurring prior to the ECG and the metabolic alterations (Theroux et al. 1976). In experimental dogs with total LCX occlusion, the reduction of blood flow in the ischaemic region varies from 0.02±0.01 to 0.56±0.12 mL/g/min (Rivas et al. 1976), an average of 0.25±0.03 and 0.39±0.05 mL/g/min at 45 seconds and 2 hours of total LCX ligation, respectively. In the dog, the reduction in flow to the endocardium is greater than to the epicardium (Rivas et al. 1976; Becker et al. 1973), whereas in the baboon flow reduction to the epi-, mid-, and endocardial zones is equally severe (Lubbe et al. 1974). Studies in the canine model have demonstrated that the regional myocardial blood flow (RMBF) measured from 45 seconds to 2 hours after a coronary occlusion correlated to the subsequent extent and size of histological myocardial infarction after 4-6 days (r=-0.83~0.89) (Reimer & Jennings 1979; Rivas et al. 1976; Irvin & Cobb 1977), suggesting RMBF is a major determinant of the ultimate injury of myocardial tissue. Techniques of RMBF measurement, therefore, have been used to define a region at risk of infarct (Rivas et al. 1976; Irvin & Cobb 1977)).

2.2.2.5 Electrophysiologic alterations

The early electrophysiologic hallmarks of ischaemia include a marked diminution in the resting membrane potential, the action potential amplitude, the rate of upstroke of phase 0, and the action potential duration (Samson & Scher 1960; Kleber et al.

1978). Within 10 minutes of ischaemia, action potential alterations in amplitude and duration become prominent, with subsequent diminution of excitability and conduction block. The early electrophysiological alterations are unstable, rapidly changing, and seem to play a key role in the genesis of ventricular fibrillation resulting from ischaemia. Later on, when the changes stabilise, or even begin to revert toward normal, ventricular fibrillation occurs less often. The effects of ischaemia on the electrophysiologic properties of cardiac cells are also responsible for ST segment shifts. These electrophysiological mechanisms are discussed in the following sections.

The changes in cellular metabolism, tissue ultrastructure, electrical activity and contractile function caused by ischaemia and infarction can be detected clinically and experimentally and have been used to indicate the occurrence of ischaemia and infarction.

2.2.3 Indicators of Myocardial Ischaemia and Infarction in Experimental Studies

2.2.3.1 Histologic evaluation

Microscopic criteria of myocardial necrosis is the absolute criteria for the diagnosis of myocardial infarction. The evaluation of these histopathological features is well described in classic (Mallory et al. 1939) and modern studies (Reimer & Jennings 1992). However, it has certain disadvantages. For example, animals generally must survive more than 20 minutes for necrotic and viable myocardium to be readily distinguishable, because the earliest histological evidence of myocardial injury does not occur until 20 minutes after a coronary ligation (Reimer et al. 1977; Reimer & Jennings 1979). Ischaemia without necrosis generally causes no acute changes that are visible by light microscopy.

2.2.3.2 Measurement of regional myocardial blood flow

The reduction of RMBF is an early, important marker of myocardial ischaemia. The techniques and principles for the measurements of RMBF are presented in chapter 4.

2.2.3.3 Biochemical parameters

A variety of metabolic and physiological parameters have been measured to indicate the occurrence of ischaemia. These parameters include tissue lactate, creatine phosphate and ATP (Dunn & Griggs 1975; Janse et al. 1979; Morena et al. 1980), intramyocardial oxygen and carbon dioxide tension (Khuri et al. 1975). These myocardial metabolites concentrations have been used to measure the extent of myocardial injury and compared with ST segment measurements (Dunn & Griggs 1975; Janse et al. 1979; Khuri et al. 1975; Morena et al. 1980). Since definite studies relating these early parameters of tissue injury to histological indices of necrosis are not available, the quantitative relationship to injured myocardium is uncertain.

2.2.3.4 Measurement of enzyme release

As myocytes become necrotic, the integrity of the sarcolemmal membrane is compromised and intracellular enzymes begin to diffuse into the cardiac interstitium and ultimately into the microvasculature and lymphatics in the region of the infarction (Adams et al. 1993; Ellis 1991). This enzyme leakage can be measured by blood samples from the coronary sinus, from the systemic circulation or from the reduction of tissue content. The time of peak enzyme release may differ between different enzymes when samples are taken from peripheral blood in whole animals. Although enzyme changes are sensitive detectors of myocardial infarction, most enzymes do not rise until 2 hours after myocardial ischaemia; and the results can be false-positive if measured by blood samples (Adams et al. 1993).

2.2.3.5 Electrocardiographic ST segment

ECG ST segment shifts are a convenient indicator of myocardial ischaemia. The distribution of epicardial ST elevation provides an approximation of the extent of myocardial ischaemia in acute infarction (Janse et al. 1979). Although it was found that the epicardial ST elevation shortly after coronary artery occlusion correlated with subsequent depletion of myocardial creatine phosphokinase (CK) activity and with histological evidence of necrosis in the subjacent myocardium (Maroko 1971), no close relation was found between ST elevation and RMBF reduction (vide infra). It must be appreciated that ST segment shifts can be affected by other nonischaemic factors such as temperature changes, drugs or epicardial injury due to pericarditis.

2.2.3.6 Measurement of regional ventricular wall function

Left ventricular wall motion abnormalities are a sensitive marker of early ischaemia. It can be detected by echocardiography; or length changes in the ischaemic segment can be approximated by measurement of the distance between pairs of ultrasonic crystals attached to the myocardium. Abnormalities of the ischaemic segment are detectable by this technique within 10 seconds of coronary ligation and are fully developed within 3 minutes (Theroux et al. 1974).

2.3 THE ORIGIN OF ST SEGMENT SHIFTS

2.3.1 The Origin of ST Segment Elevation

2.3.1.1 Electrophysiological mechanism

The use of ST segment elevation to indicate the appearance of reversible acute myocardial ischaemic injury is based on the classic recognition of the association between ST segment elevation and myocardial injury. In 1918, Smith showed that ST segment elevation occurred during experimental ischaemic injury produced by coronary artery ligation in dogs, establishing the correlation between myocardial injury and ST segment elevation (Smith 1918). In 1920, Pardee first related ST segment elevation of the standard leads of the electrocardiogram to acute myocardial infarction in a patient with an acute inferior wall myocardial infarction (Pardee 1920). Pardee's work directed attention to the ST segment of ECG and many studies have been carried out since then. In spite of the long term clinical and experimental recognition of ST elevation as an ECG sign of ischaemia and infarction, the underlying electrophysiological mechanisms of ST elevation in ischaemic injury were not established until intracellular potentials could be recorded from the intact heart.

Classic electrocardiographic theory explains ST elevation on the basis of a decreased ability of the myocardial cell membrane to depolarise and repolarise. By the application of basic principles of the field theory, Wilson et al. (1933b) and Bayley (1942) proposed that ST elevation is an manifestation of injury currents. Injury currents are classified into two types: injury current at rest or diastolic injury current, and injury current of activation or systolic injury current (Wilson et al. 1933a). These postulates were later confirmed and elaborated by Samson and Scher (1960), Prinzmetal and co-workers (1968), and further explored by Kleber and co-workers (1978).

Using direct-coupled (DC) amplifiers, Samson and Scher (1960) measured electrocardiograms combined with simultaneous intracellular recordings in a model of acute infarction in dogs. The DC recording allowed the differentiation of ST segment shifts from the TQ segment shifts. They found that the first occurrence, some 40 sec after the coronary occlusion, was a primary ST elevation on the ECG which coincided with a shortening of the membrane action potential. This change was followed some 80 sec later by a TQ segment depression (secondary ST elevation) which corresponded to a decrease in the resting membrane potential (less negative). Similar results were subsequently obtained by others (Prinzmetal et al. 1968; Kleber et al. 1978; Janse et al. 1980). The interpretation of these changes was, for the primary ST elevation, an injury current flowing extracellularly from the infarcted area to the normal myocardium due to the alteration in the action potential with earlier repolarisation; for the TQ segment depression, an injury current flowing in the opposite direction due to the loss of resting potential in ischaemic cells (Samson & Scher 1960).

Samson's postulations were later supported by Kleber who measured intracellular potential from subepicardial ventricular cells and local extracellular DC electrograms in isolated pig hearts before and during the LAD occlusion (Kleber et al. 1978; Janse et al. 1980). Kleber and his co-workers observed that the first change was a shift of the resting potential to a more positive value and a concomitant depression of the TQ segment of the extracellular potential, which occurred during the first minute of ischaemia. After 3 minutes, the resting potential decreased further and the upstroke velocity, the amplitude, and the duration of the action potential diminished. The alterations in action potential resulted in ST elevation. Finally, the cells in the ischaemic centre became totally unresponsive at a resting potential of about -65mV. This rendered the extracellular complex monophasic (Figure 2.3). With the use of the Laplacian maps constructed on the basis of the extracellular potential distribution, Kleber also found that during electrical diastole (TQ interval), the injury current flowed from the intracellular compartment of the ischaemic myocardium toward that of the adjacent normal tissue. The diastolic injury current emerged as a current source in the extracellular space at the normal side of the border and flows back into the ischaemic tissue, where it entered, as a current sink, the intracellular space. The distribution of current sources and sinks was localised to the border zone with the extracellular current flowing from the normal zone to the ischaemic zone during the TQ interval, and the current flowing in the opposite direction during the ST interval. The maximal current density during late systole was 1 $\mu A/mm^2$, flowing in the border zone towards normal myocardium; and during diastole a maximal current of 0.3 $\mu A/mm^2$ flowing in the opposite direction (Figure 2.4). The injury current in these studies originated from the ischaemic boundary.

A comparison between precordial ECG leads recorded during the first minutes of acute myocardial infarction in humans, and transmembrane potentials and local DC-extracellular electrogram recorded during the first minutes following coronary artery occlusion in isolated pig hearts was made by Cinca et al. in 1980. They found that in the precordial leads in the patient, the configuration of the complexes and the time course of the changes were very similar to the configuration of the extracellular signals in the pig, suggesting that cellular changes in humans are similar to those in the pig.

There has been little work with direct current coupled amplifiers in humans. However measurements of the magnetic field of patients (Savard et al. 1983; Cohen et al. 1983) have shown that there was an injury current during exercise induced ST depression which was comparable to that recorded in animals. Because the magnetocardiogram is currently an impractical device for systematic evaluation of such patients, the results in animals form the large part of data on the origin of ST potentials.

The ST segment elevation associated with acute ischaemia in the ECG is thus caused by the loss of resting membrane potential (diastolic depolarisation) and the alteration of the transmembrane action potential (early repolarisation or incomplete depolarisation). Both the systolic injury current and the diastolic injury current produce ST segment elevation; ST elevation as seen in the routine ECG is really a combination of true ST segment elevation and TQ segment depression. This electrical mechanism is depicted in Figure 2.4.

The fact that the TQ shift can not be measured on the ECG is explained in the following way (Taccardi 1967). The direct current potentials generated by the heart would be greatly overshadowed by direct current potentials generated by the skin-electrode interface. For this reason, direct current is deliberately filtered out of the clinical ECG by using capacitive coupled amplifiers. Therefore, in the standard ECG with a low cut off frequency of 0.1 Hz for the band-pass filter, both the TQ segment and the true ST segment displacement appear as "ST segment displacement".

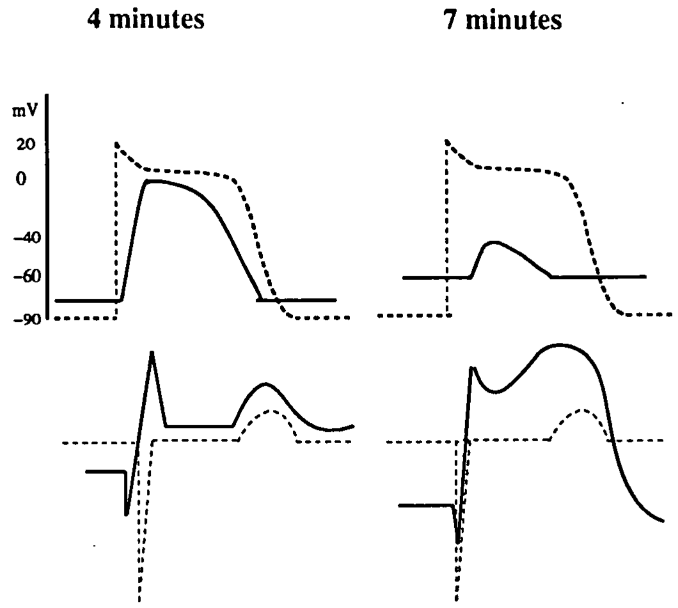

Figure 2.3 Transmembrane potentials (top) and local DC extracellular electrograms (bottom) recorded from a single subepicardial cell in the intact heart during control (dotted line) and ischaemia (solid line). In each panel, the control signals are superimposed over the signals recorded at the same site during ischaemia. See text for explaination (From Kleber 1978 with modifications).

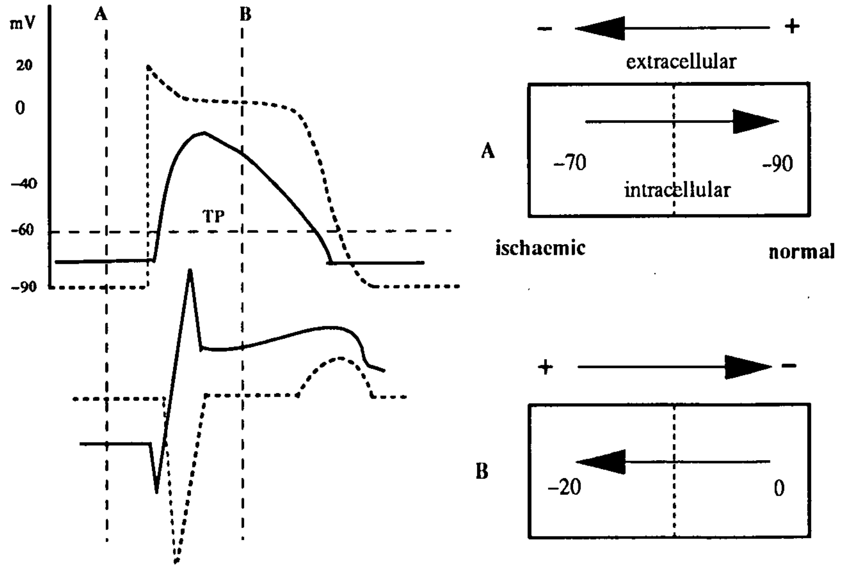

Figure 2.4 Mechanism of ischaemic ST elevation. Action potentials of a normal (dotted) and ischaemic (solid) cell are shown at the top left, with the ECG complex recorded over the ischaemic area before and during ischaemia. Directions of extracellular current flow during electrical diastole (A) and during electrical systole (B) are shown at the right. During diastole, the ischaemic region is negative with respect to the normal myocardium, so current flows from the normal region to the ischaemic region, and produces TQ depression in ECG. During systole, current flows from the ischaemic myocardium to the normal myocardium, and produces ST elevation in ECG.

2.3.1.2 Metabolic changes behind the electrical changes

As discussed in section 2.2, acute ischaemia increases anaerobic metabolism and leads to accumulation of the end products of anaerobic metabolism in the extracellular space. The accumulation of extracellular potassium parallels with the electrical changes (Harris et al. 1954; Morena et al. 1980; Kleber 1983; Wilde & Kleber 1986; Coronel et al. 1988) and thus merits special mention.

A characteristic biphasic time course of extracellular potassium accumulation has been described during myocardial ischaemia (Kleber 1984; Hill & Gettes 1980): an initial fast rise is followed by a plateau, during which a transient decrease in extracellular potassium may occur, until a second phase of increase in extracellular potassium heralds the onset of irreversible injury. The increase in extracellular potassium causes a decrease in resting membrane potential; the decrease in resting membrane potential further reduces the maximum rate of rise of the action potential upstroke, and thus lowers the action potential amplitude. The shortening of action potential duration is due primarily to the effects of hypoxia, via activation of the ATP-dependent potassium channel, which is opened by the fall in intracellular ATP level and the rise in intracellular H^+ level (Nakayama et al. 1990; Kubota et al. 1993).

2.3.2 The Origin Of ST Segment Depression

Unlike ST elevation, the origin of ST depression is not clear. Much of the current opinion regarding the genesis of ST depression is derived from interpretations based on certain theoretical considerations and indirect evidence from animal studies. Results of early experimental studies by Wolferth et al. (1945) and Pruitt (Pruitt and Valencia 1948) documented the occurrence of ST depression after chemical or physical damage to the endocardium and the epicardium in animal hearts. By bathing the entire ventricular epicardium of in-situ canine heart in 0.2 molar potassium chloride solution, Wolferth et al recorded ST depression from needle electrodes inserted into the cavity of left and right ventricles; when only the left ventricular epicardium was treated, ST depression was only recorded over the surface of the right ventricle (Wolferth et al. 1945). A similar result was obtained by Pruitt and Valencia (1948) in the isolated turtle heart. Epicardial ST depression was generated by burning the subendocardium, and endocardial ST depression was generated by burning the epicardium. The ST shifts were thus divided into the primary and the secondary types, defined as follows: the primary type resulted from injury directly beneath the exploring electrode; the secondary type is recorded over the surface of uninvolved muscle as a result of the potential changes generated in injured muscle elsewhere in the heart (Wolferth et al. 1945). ST elevation is considered as the primary, and ST depression is considered as the secondary or reciprocal. These studies together with dipole theory form the basis of the modern theory of ST depression.

2.3.2.1 Dipole theory

Einthoven and co-workers (Einthoven et al. 1913) first idealised the cardiac source as an electrical dipole which was fixed in location at the centre of an equilateral triangle. The dipole theory was developed by Wilson and co-workers by relating the dipole sources to cellular activity in 1930s (Wilson et al. 1933c; Pruitt and Valencia 1948; Bayley et al. 1942). As discussed in section 2.1, the dipole model considered the active myocardial event as a single dipole source which contained both the maximum and the minimum potentials; the distance from the recording electrode to the heart is large in comparison with the electrically active boundaries of the heart; and that the heart and surrounding thoracic structure together comprise a uniform, homogeneous volume conductor. Accordingly, an injured region of the myocardium acts in systole as the positive pole of a layer of dipoles situated on its boundary with normal myocardium whereas the latter acts as the negative pole. In the event of subendocardial ischaemia, the ventricular surface and the precordium over the ischaemic region face the negative pole of the dipole while the cavity faces the positive pole. Thus, the electrodes on the epicardium or precordium should record depressed ST while the cavity should yield elevated ST (Bayley 1946; Cook et al. 1958; Yu & Stewart 1950).

Work in isolated animal hearts with physical injury in the endocardium suggested that the ST segment response to myocardial injury is elevation; ST segment depression recorded at the epicardium is the reciprocity of ST elevation in the underlying subendocardium (Wolferth et al. 1945; Bayley 1946; Pruitt & Valencia 1948). It was also documented that the injury currents in transmural ischaemia could be represented by a single moving dipole model of the heart's electrical activity (Mirvis et al. 1978). These studies amplified the dipole theory. However, this theory does not explain the clinical difficulty in localising ischaemia by ST depression, and there are certain limitations in the practical application of this model. Firstly, instead of being a single, relatively small layer as required by the single dipole model, the ischaemic lesions are complex geometries with irregular boundaries, suggesting nondipolarity. Secondly, the heart, filled with highly conductive blood, is surrounded by lung, bone, muscle, fat and skin tissues in irregular shape which all have different resistivity, suggesting a nonuniform, inhomogeneous conductor. Finally, most endocardial, epicardial and precordial electrodes are too close to the source in relation to the size of the boundary to meet the requirements of the single dipole model (Taccardi 1958). The limitations of the single dipole model, have been demonstrated (Schmitt et al. 1953; Okada et al. 1959; Scher et al. 1960) and discussed (Holland & Arnsdorf 1977; Horan & Flowers 1972; Plonsey 1966) extensively. Because of the limitations of dipole theory, the following models have been developed to explain the genesis of ST shifts.

2.3.2.2 Solid angle theory

The solid angle theory, a concept developed from a mathematical formula and applied to interpret ECGs by Wilson et al. in 1933, was expanded to ECG theory by Holland and Brooks (1975). The solid angle model considers each boundary present in the heart to be composed of an infinite number of dipoles, each representing an infinitesimally small region of the boundary. This model more accurately represents the electrical activity of the heart because more dipoles are considered, each dipole is permitted to move in the direction of its segment of the boundary, and each dipole has exactly the same strength or magnitude which equals the transmembrane potential difference across the boundary (Holland & Arnsdorf 1977). Since this boundary separates two cell populations that differ in transmembrane potential, it has been represented as a distributed dipole layer.

According to Holland and Brooks' solid angle model (Holland & Brooks 1977a), ST segment elevation is a boundary phenomenon, because it depends on diastolic and systolic injury currents flowing at the boundary between ischaemic cells and normal myocardium. The magnitude and polarity of the TQ-ST segment deflection recorded at an electrode site can be calculated by solid angle formulation: $\mathbf{E_{TQ\text{-}ST} = \Omega/4\pi \cdot (Vm_N - Vm_I) \cdot K}$. As depicted in Figure 2.5, ($\mathbf{E_{TQ\text{-}ST}}$) is the potential recorded at point P. Ω is the solid angle subtended by the ischaemic boundary at the electrode site P. The magnitude of this solid angle varies directly with size of ischaemic area and inversely with the distance between the boundary and the recording electrode. The polarity of Ω is positive or negative depending on whether an observer at point P views first the positive or negative side of the surface enclosed by the boundary. $\mathbf{Vm_N}$ and $\mathbf{Vm_I}$ denote the transmembrane potentials of the normal and ischaemic regions; and $\mathbf{K}$ is a term correcting for differences in intracellular and extracellular conductivity and the occupancy of much of the heart muscle by interstitial tissue and space. The electrocardiographically recorded potential is thus directly proportional to both solid angle and the difference in transmembrane potentials between two regions. Consideration of ST elevation in this way shows that it has spatial and non-spatial determinants (Holland & Brooks 1975 & 1977b). Since the solid angle depends only on the position of the recording electrode and the geometry of the boundary (ischaemic size and shape, and ventricular wall thickness), it reflects spatial influences on the magnitude of TQ-ST segment deflection. The difference in transmembrane potential between the two regions does not, however, depend on geometry and thus reflects nonspatial influences on the magnitude of TQ-ST segment deflection.

In a combined theoretical and experimental analysis, Holland and Brooks (1975 & 1977b) verified the dependence of the TQ-ST deflection on the spatial factor Ω. Assuming a transmural ischaemia in a spherical heart model with outer and inner wall radii of 3 and 2 cm, respectively, they calculated the solid angles subtended by transmural ischaemic boundary at centrally overlying precordial and epicardial electrodes. For the precordial site, these solid angles increased with the size of the ischaemic area. On the other hand, at the epicardial site the solid angle decreased with an increase in the ischaemic area because the ischaemic boundary moves further away from the electrode following an increase in ischaemic area. Also, the thicker the ventricular wall at the ischaemic boundary, the larger the solid angle, and hence the TQ-ST deflections, at both sides. The preceding theoretical contentions were verified experimentally by Holland and Brooks (1975 & 1977b) in the porcine heart. In their experiment, sequential coronary ligations were performed in pigs by ligating different segments of the LAD to produce different sizes of ischaemia. They showed that, when the size of the ischaemic area was increased by ligating the LAD more proximally, the magnitude of precordial TQ-ST deflections was increased while the magnitude of epicardial TQ-ST deflections was reduced.

Another theoretical prediction was that differences in ischaemic position would change the polarity of the ischaemic TQ-ST deflections. Subepicardial and transmural ischaemia would yield positive ST deflection at either precordial or epicardial location, because the polarity of the solid angle is positive at electrodes sites overlying epicardial and transmural ischaemic regions. In contrast, subendocardial ischaemia would yield negative ST deflection in overlying leads, because the direction of ionic current flow during systole is away from the recording electrodes, and the solid angle and the ST deflection is negative in all overlying leads, and that this ST depression should be able to localise ischaemia (Figure 2.6). They did prove some of these assertions experimentally in their porcine models when epicardial and transmural ischaemia were produced by ligating different coronary arteries (Holland & Brooks 1975 & 1977b). However, they failed to produce subendocardial ischaemia in their porcine model (Holland & Brooks 1975), and were unable to confirm their theoretical prediction of subendocardial ischaemia.

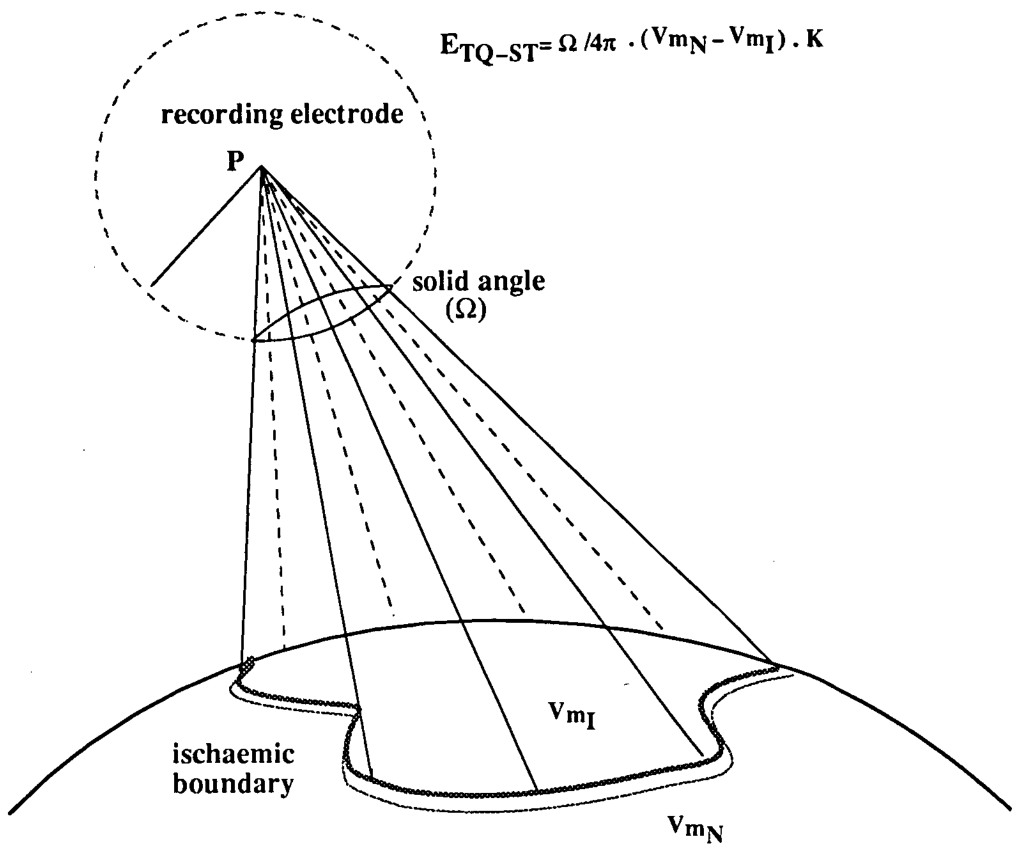

Figure 2.5 Mathematical and pictorial characterisation of the solid angle theory. The TQ–ST segment potential recorded at the electrode (P) is given by the equation. The ischaemic boundary is a source of current flow established by differences in the transmembrane potentials of normal and ischaemic cells during diastole and systole. See text for explaination (From Holland RP, Arnsdorf MF. Prog Cardiovasc Dis. 1977; 19:431–457).

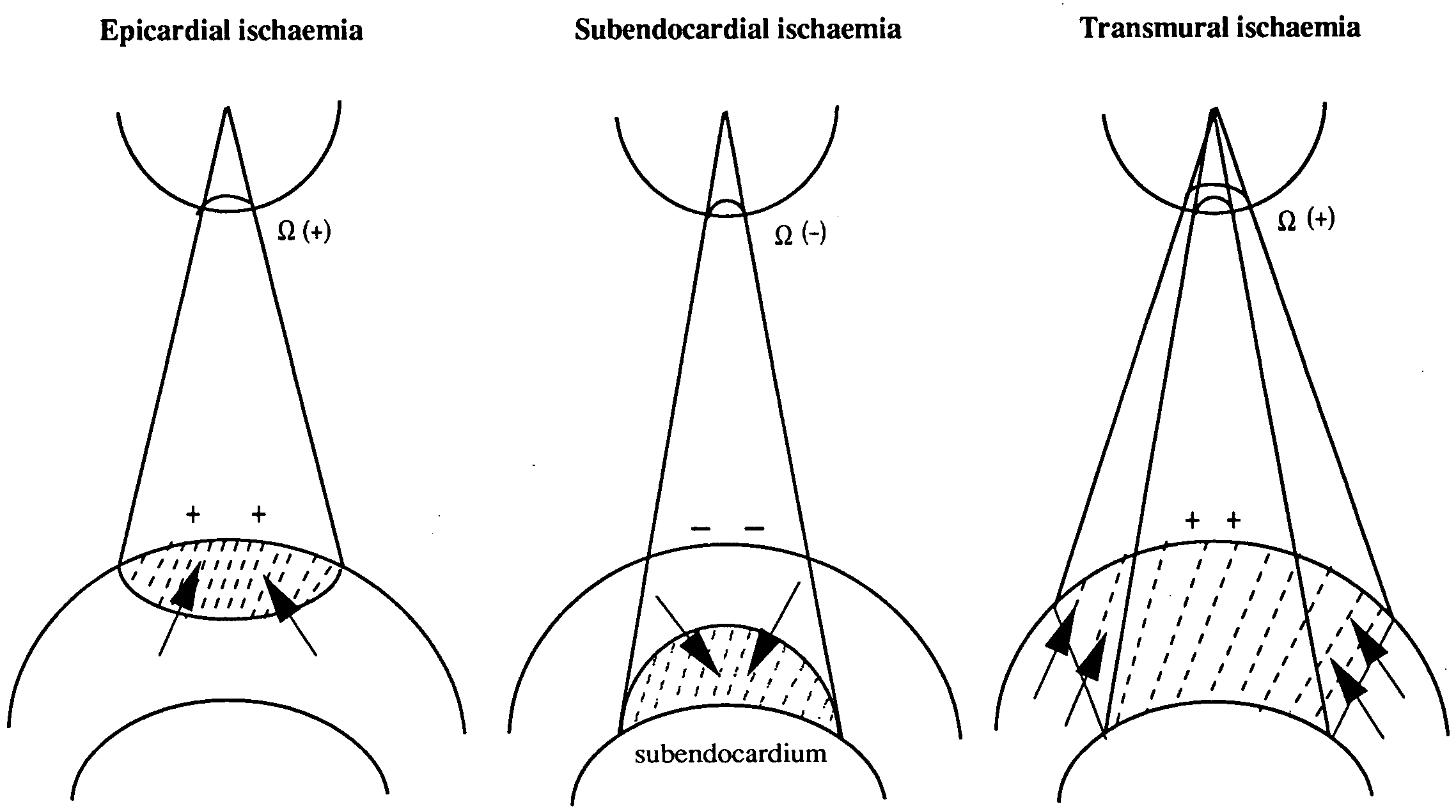

Figure 2.6 The production of ST shifts by epicardial, subendocardial and transmural ischaemia is explained in terms of the solid angle theory. The direction of current flow during systole at the ischaemic boundary is indicated by arrows. During subendocardial ischaemia, the current flow is away from the electrode and ST depression is observed from overlying electrodes;during epicardial and transmural ischaemia the current flow is towards the electrode and ST elevation is observed.

With regard to nonspatial influences on the TQ-ST deflection, Holland and Brooks (1977b) identified four agents that are capable of significantly influencing the action potential waveform, namely: hypoxia, lack of glucose, low pH, and extracellular K^+ accumulation. They focused on extracellular K^+ accumulation in their experiment and demonstrated that increasing in the plasma K^+ level resulted in a decrease in the magnitude of the TQ-ST deflections during ischaemia (Holland & Brooks 1977b), a result which is opposite to those of others (Harris et al. 1954; Morena et al. 1980; Kleber 1083; Wilde & Kleber 1986).

The solid angle theory has provided a geometric ischaemic heart model that quantitatively links changes in ST elevation to the distribution of transmembrane potential changes in the ischaemic region. In spite of the innovative work, the solid angle analysis is limited (Holland & Arnsdorf 1977), as is the classical dipole theory, by the fact that the thorax is neither a homogeneous nor an infinite volume conductor. The major limitations in the solid angle model to the analysis of the TQ-ST deflections have been summarised in a paper by Smith et al. (1983).

2.3.2.3 Miller-Geselowitz model

The Miller-Geselowitz model (Miller & Geselowitz 1978a & b), a bidomain model developed by Miller and Geselowitz in the late 70's, has provided a good simulation of the body surface ECG for the normal heart and infarction by relating cellular electrical activity to myocardial sources. In this digital computer model, 1426 plane triangular elements were used to represent a realistically shaped torso surface, and a three-dimensional array of approximately 4000 points were used to simulate the ventricles of a human heart (Miller & Geselowitz 1978a). The model generates time-varying dipole sources at each one of the 4000 points. The heart was divided into 23 regions and a resultant dipole was assigned to each region by summing vectorially the appropriate subset of the 4000 dipoles. To model ischaemia and infarction, the region of injury is identified in the heart cross sections and the appropriate abnormal action potentials are assigned to the cells in this region (Miller & Geselowitz 1978b). A simulation in which altered action potentials with decreased resting potentials were assigned to an anterior subendocardial region has resulted in body surface ST depression in leads V_2-V_5 and leads I, aVL (Miller & Geselowitz 1978b). Unfortunately, ST depression was not fully evaluated in this model because neither the endocardial nor the epicardial potential was simulated (Miller & Geselowitz 1978b). In addition, anisotropy and inhomogeneity of the body as a volume conductor were ignored in this model (Miller & Geselowitz 1978a & b).

A new model, the oblique dipole layer model has more recently been developed (Colli-Franzone et al. 1982). This model, by taking into account the influence of cardiac fibre orientation on extracellular potentials, generalised the classical uniform dipole layer model, upon which the solid angle theory was based, by adding to it an axial component. In this model, the cardiac sources may depend on fibre orientation both in strength and in direction. Unfortunately, no one has yet applied it to interpret ST changes (Watabe et al. 1990).

2.3.2.4 Other theories

Electrocardiographic ST depression, according to Prinzmetal and co-workers (Ekmekci et al. 1961; Toyoshima et al. 1964), is a primary effect of abnormal membrane polarisation rather than a reciprocal effect of ST elevation. Prinzmetal and his associates carried out multiple studies of the mechanism of ST depression during the 1950s and 1960s. From clinical observations, they found that (Prinzmetal et al. 1959b): (1) In some instances of myocardial infarction, ST depression rather than elevation occurs. They noted, subendocardial infarction without some extension either anatomically or chemically to the outer layers was quite rare; (2) In conditions classified as "idiopathic hypertrophy of the heart", ST depression was often found. The endocardium and subendocardium of these hearts, they commented, were not diseased disproportionately to the remainder of the heart. They then postulated that ST depression was a primary change rather than a reciprocal change of subendocardial ischaemia. In a series of experiments carried out in dogs, Prinzmetal and his co-workers investigated the chemical origin (Prinzmetal et al. 1959a) and the cellular electrophysiology (Prinzmetal et al. 1961; Ekmekci et al. 1961; Toyoshima et al. 1964) of ST depression. They recorded relative ST depression (true TQ segment elevation) from the epicardium of "mild" ischaemic areas produced by severe haemorrhagic hypotension in in-situ canine hearts (Prinzmetal et al. 1961; Ekmekci et al. 1961; Toyoshima et al. 1964). The TQ segment elevation coincided with the increase in membrane resting potential. Injection of high concentration of sodium or low concentration of potassium solutions produced the same results. They then alternatively suggested that mild subepicardial ischaemia may generate ST depression independent of subendocardial damage. In conditions of mild ischaemia, they explained, glucose and potassium uptake of the cell was increased. The transmembrane ionic gradients for potassium and probably sodium were increased. These caused increased negativity of the membrane resting potential or hyperpolarization. The result was TQ elevation and relative ST depression. In the absence of ischaemia, low potassium ion concentration or high sodium ion concentration in the extracellular fluid would also increase the transmembrane ionic gradient and the same electrocardiographic changes might result as in mild ischaemia. In spite of their detailed studies, these postulates have never been pursued to further clarification and have lost ground over the years. Both precordial ST segment depression and simultaneous TQ segment elevation have been recorded in a patient with typical coronary artery disease during exercise by using a direct-current magnetocardiograph (Cohen et al. 1983), suggesting that subendocardial ischaemia, not epicardial ischaemia, produces ST depression. There are two major concerns in Prinzmetal's experiments: firstly, the model they used was not a real ischaemic model produced by vessel stenosis, and regional myocardial flow was not measured in those experiments, thus the "mild epicardial ischaemia" could not been validated; secondly, the reference electrode used for intracellular potential recording was placed in a small pool of Ringer's solution in the region of the exposed femoral vein (Prinzmetal et al. 1962; Toyoshima et al. 1964) instead of on the epicardial surface of the recording cell. The intracellular electrogram could be affected by extrinsic cardiac potentials using this long distance reference electrode (Woodbury & Brady 1956).

Based on his studies using body surface mapping and an inverse transformation (Kilpatrick et al. 1990; Walker & Kilpatrick 1987; Kilpatrick & Walker 1987) in 219 patients with acute inferior infarction and 93 patients with ST depression and no infarction, Kilpatrick postulated that ST depression on ECG originates from current flowing from an endocardial ischaemic region to the outside of the heart through the great vessels and atria (Kilpatrick et al. 1990). Kilpatrick and his co-workers found that the epicardial ST potential maps of the inferior infarction showed a positive region over the superior aspect of the heart in addition to the expected inferior ST elevation in 96% of the patients. They then postulated that the current flow out of the heart during the ST segment comes from two regions, ie, the infarction region and the region over the great vessels. Later, they examined 93 patients with ST depression on the 12-lead ECG, not associated with ST elevation (Kilpatrick et al. 1990), and they found 94% of the patients had a region of ST elevation superiorly. Thus, epicardial potentials are elevated over the superior aspect of the heart in both inferior infarction with inferior ST elevation and in patients with ST depression only. Hence, they deduced that a selective current path from the infarcting endocardium travelled out of the heart through the great vessels. Accordingly, the surface of heart as a sink will show general ST depression. Although the hypothesis explains the difficulty in localising ischaemia from body surface ST depression, it needs further verification.

The electrophysiological mechanism of ST depression remains unclear and further exploration is necessary to fully define the origin of ST depression.

2.4 ST SEGMENT SHIFTS IN EXPERIMENTAL STUDIES AND CLINICAL PRACTICE

2.4.1 ST Segment Elevation in Experimental Studies

Previous investigators have reported a wide range of ST changes after acute coronary occlusion in experimental animals, depending on the experimental model and technique used. These variabilities fall into three categories. The first category has a pattern of ST elevation over the ischaemic region, and ST depression at surroundings, with (Prinzmetal et al. 1962; Ekmekci et al. 1961) or without (Bruyneel 1975) reciprocal ST depression at the opposite region, depending on the distribution of recording electrodes and the size of ischaemia. In this category, the highest ST elevation occurred near the centre of the ischaemic region, with a progressive decrease in amplitude approaching the ischaemic boundary (Prinzmetal et al. 1962; Ekmekci et al. 1961). The typical representation of this pattern was shown by Prinzmetal and his associates in their canine model (Rakita et al. 1954; Ekmekci et al. 1961). Following experimental ligation of the left anterior descending coronary artery in dogs, unipolar epicardial electrogram leads taken in the centre of the cyanotic area showed elevation of the ST segments within 30-60 seconds, which occurred somewhat later than the regional loss of contraction and tended to reach a maximum in 5 to 7 minutes (Rakita et al. 1954; Ekmekci et al. 1961). Exploration of the epicardial surface in adjacent areas showed somewhat more gradual development of ST-segment elevation in the peripheral regions, and a gradation of less severe ST-segment elevations occurred from central to peripheral cyanotic areas (Rakita et al. 1954; Ekmekci et al. 1961). Reciprocal ST depressions were noted in leads taken from the posterior wall of the heart (Rakita et al. 1954). However, ST depression was noted just outside the cyanotic area when only a branch of LAD was ligated (Ekmekci et al. 1961). It was further observed that if a small coronary artery supplying such a region of ST depression was ligated, ST elevation promptly replaced the depression (Ekmekci et al. 1961). When small plunge electrodes were used to record intramural leads across the left ventricular wall, simultaneous ST elevation also was observed, but it was less marked than ST elevations in epicardial leads (Rakita et al. 1954). Intracavity leads immediately beneath the subendocardium also showed ST elevation of a slight degree (Rakita et al. 1954). In addition, ST elevations could be recorded with subendocardial and intramural electrodes after coronary occlusion when ST segments in epicardial leads overlying a site on the periphery of the cyanotic region remained normal (Rakita et al. 1954). In regions where ST depression developed later after coronary occlusion, as described above, ST elevation was not recorded from subendocardial leads at the same location, which suggested that the depression could not be explained on the basis of a local reciprocal effect of subendocardial injury (Ekmekci et al. 1961). Such ST depression was also observed from the posterior wall of the left ventricle after LAD ligation in an isolated, perfused rabbit heart (Brody et al. 1973) and in an in-situ baboon model (Crawford et al. 1984).

The second category of ST segment changes in transmural ischaemia had a pattern of uniform ST elevation over the infarcted region and no ST depression over the remaining regions. The typical representation of this pattern was the potential recording by Kleber and his co-workers (1978). Kleber et al. showed uniform ST elevation over the infarcted region and little change over the border region after LAD ligation in an isolated pig heart, which led to a dipole moment density just at the border between normal and ischaemic tissues, and this agrees with the solid angle model of Holland and Brooks (1977 & 1975).

The third category generalised the previous two and was represented by Smith's experiment and his "polarised surface models" (Smith et al. 1979 & 1983). In experiments involving baboons and pigs, Smith and his co-workers noted a spatially uniform degree of epicardial ST elevation overlaying the ischaemic area for approximately the first 20 mins of ischaemia. This changed to exhibit increasing ST elevations from the periphery to the centre of the ischaemic area after 20 minutes. Since the solid angle theory predicts maximal ST elevation at the periphery of the ischaemic region with a relatively slight decrease at the centre (Holland and Brooks 1977), Smith et al. suggest that Holland and Brooks' hypothesis is applicable for early ischaemia. On the other hand, to explain the larger ST elevations at the centre of the ischaemic zone after 20 mins of ischaemia, Smith et al. assumed that the entire ischaemic region may be characterised by a uniform dipole moment per unit volume instead of one distributed solely around the border between healthy and ischaemic tissues. Computation shows that this does lead to a bell-shaped spatial distribution for epicardial ST elevation with a maximum in the centre of the ischaemic region, together with an increase in epicardial ST elevations everywhere when the ischaemic region is increased. Thus, according to Smith et al. (1979) the amplitude and the distribution of epicardial ST segment elevation was related to the duration of ischaemia, and the results during early ischaemia may be represented by Holland's model in which injury current arises only at the ischaemic boundary. The results during later ischaemia may be represented by other models (Rakita et al. 1954; Ekmekci et al. 1961) in which ST elevation is considered dependent on injury currents generated throughout the ischaemic region. ST depression was not observed in Smith's model.

The limitations of the above experiments are in the number and the distribution of the electrodes. The epicardial recordings were only obtained from the ischaemic and the border regions by a limited number of epicardial electrodes; the endocardial recordings were either not applied at all or only one or two applied to the ischaemic regions. Therefore, detailed evaluation of the ST source during transmural ischaemia is not fully evaluated by these studies. Furthermore, ischaemic size in these studies was relatively small to ensure stability of the animal, either only a branch of the LAD or the distal end of the LAD was ligated (Holland & Brooks 1975; Smith et al. 1975; Prinzmetal et al. 1961).

2.4.2 ST Segment Depression in Animal Experiments

Although many of the reported studies have focused on subendocardial ischaemia, relatively few of them have documented the presence of subendocardial ischaemia, and the recording of ST segment depression has been disappointing because of the difficulty in producing subendocardial ischaemia. Studies by Guyton et al. (1977) in dogs showed epicardial ST depression when the LCX was partially ligated and the heart was paced at the rate of 150-200 bpm. The epicardial ST depression was associated with normal flow to the epicardium and decreased blood flow to the deeper myocardial layers. They also found that as the degree of arterial obstruction increased and the perfusion pressure decreased, endocardial ST elevation developed progressively as did epicardial ST depression. Only when the perfusion pressure fell to less than 50 mmHg did the primary epicardial ST elevation develop. Intracavitary ECG during the development of ischaemia in dogs showed ST elevation before it could be seen in the epicardial ECG. Unfortunately, the origin of ST depression was not evaluated and only a limited number of epicardial electrodes were applied to the ischaemic region.

Studies by Vincent et al. (1977) in the same species failed to show epicardial ST depression when partial occlusion of a coronary artery and tachycardia were applied, although T-Q depression and ST elevation were found in the subendocardial leads. They accounted for their results by the small magnitude of the subendocardial injury currents which they obtained in their study.

Holland and Brooks (1975) have also failed to produce epicardial ECG changes from attempts to produce subendocardial ischaemia in a pig model although they predicted from solid angle theory that subendocardial ischaemia would cause relative depression of the ST segment.

Mirvis and Gordey (1983) developed an excellent model of chronic subendocardial ischaemia in dogs by gradual but complete vascular obstruction using an ameroid occluder. Collateral development during the period of gradual constriction maintained regional flow at rest. However, abnormal regional blood flow could be provoked in this model by rapid pacing (about 185 bpm), which increased oxygen demand beyond the ability of the expanded collateral system to supply oxygen. Subendocardial underperfusion resulted with a fall in the endocardial/epicardial (endo/epi) flow ratio. The onset of body surface ST depression corresponded to an endo/epi flow ratio of 0.74 for the anterior descending bed and 0.65 for the left circumflex bed. Unfortunately, the spatial origin of ST depression was not investigated.

2.4.3 Relations of ST Segment Changes to Regional Myocardial Blood Flow

In 1949, Wegria first reported the correlation between ST segment changes in the ECG and coronary blood flow in experimental animals (Wegria et al. 1949). Reduction in flow by two-thirds or more always produced marked ST segment changes, while minor changes occurred when coronary blood flow was reduced by between one-third or two-thirds of control; no changes were noted with reductions in coronary flow by less than one-third. More detailed studies have been performed since using microspheres for the measurement of regional myocardial blood flow (RMBF). Most of these studies have showed that no simple, quantitative relation exists between ST elevation and the acute reduction in total or subepicardial myocardial blood flow early after coronary occlusion. Becker et al. (1973) measured RMBF and correlated it with epicardial electrograms recorded at 10 to 15 sites, 30 to 60 minutes after coronary occlusions in dogs. Of 22 sites overlying low-flow zones, ST segment was substantially elevated in most, but one-quarter showed no significant change. Smith et al. (1975) studied dogs at intervals from 15 minutes to 2 hours after LAD occlusion, and they found that there was a general correlation between ST elevation and blood flow reduction. However, at individual sites in central areas of markedly reduced blood flow, one-third of the areas did not show significant ST elevations at 15 minutes. Studies in awake dogs (Irvin & Cobb 1977) have also demonstrated that the epicardial ST elevation was poorly correlated to the simultaneous transmural and epicardial RMBF reduction measured by radioactive microspheres at 15 minutes and 2 hours of LAD ligation ($r=0.59$). Similar results were reported by Heng et al. (1976), who found a weak although significant inverse correlation ($r=-0.41$) between the ST voltage and transmural RMBF 15 minutes after LAD occlusion in a canine model. In contrast, Kjekshus et al. (1972) reported a linear relationship between the degree of ST elevation and reduction of subepicardial RMBF 15 minutes after coronary occlusion in anaesthetised dogs. The different result from the later study might be due to a less detailed sampling method. Indeed, it would be surprising if there were an excellent correlation between ST elevation and coronary blood flow under a wide variety of circumstances since the severity and extent of ischaemic injury are dependent not only on myocardial perfusion, but also on myocardial oxygen needs, ie, on the balance between supply and demand (Stephan et al. 1975). At a given level of blood flow reduction, various degrees of ischaemia can be present, depending on the instantaneous metabolic requirements. In addition, the magnitude of ST changes is also influenced by electrophysiological events remote from the ischaemic myocardium.

2.4.4 ST Segment Depression in the Exercise Test

The electrocardiographic exercise stress test is a standard method for detecting clinically significant coronary artery disease. The test is based on the premise that exercise increases the demands on the coronary blood supply, which may be adequate at rest but inadequate during exercise. The exercise thus results in a relative ischaemia and an inability of the coronary circulation to maintain the metabolic needs of the heart muscle. The most important ischaemic ECG manifestation is ST depression. And this exercise-induced ST depression in patients with effort angina pectoris is generally believed to be a reflection of subendocardial ischaemia. In order to understand the significance of the exercise test, it is important to review the relevant pathophysiology.

2.4.4.1 Pathophysiology of the exercise test

Myocardial ischaemia in exercise testing results from increased myocardial oxygen demand in the presence of critical narrowing of a coronary artery (Ganz & Braunwald 1997). The oxygen requirements of the myocardium include requirements for basal metabolism, for electrical activation and for the performance of internal and external mechanical works (Reimer & Jennings 1992). Basal oxygen requirements, eg, the requirements of an electrically arrested, normothermic heart on cardiopulmonary by-pass, have been estimated to be about 0.7-2.0 mL O_2/min/100g (McKeever et al. 1958), or 20% of total myocardial oxygen consumption (MVO_2) in a beating heart (8-15ml/min/100g). The energy requirement of electrical activation is about 0.5 mL/min/100g, about 5% of total oxygen requirements (Klocke et al. 1966). Contractile work thus accounts for the majority of myocardial oxygen consumption. The MVO_2 per contraction is determined mainly by the tension developed by the myofibrils and by the inotropic (contractile) state. The latter is reflected in the rapidity with which tension is generated and shortening occurs. MVO_2 per minute is the product of MVO_2 per beat and heart rate. Therefore, the three major determinants of myocardial oxygen demand are myocardial wall tension, the intrinsic contractile state of the myocardium, and the heart rate (Reimer & Jennings 1992). All of the three determinants of MVO_2 are increased by exercise (Sheffield 1988; Hoffman 1987), resulting in an increase in MVO_2 per minute. Under normal circumstances, oxygen extraction of myocardium is fairly constant and high, averaging about 75% (the highest in the body) (Reimer & Jennings 1992). The additional oxygen needed at increased workload is met, not primarily by increased oxygen extraction, but by corresponding change in the local rate of blood flow, ie, coronary blood flow is tightly matched to myocardial oxygen needs (Reimer & Jennings 1979; Rivas et al. 1976). This metabolic regulation of coronary blood flow is achieved through control of the vascular resistance of precapillary arterioles (Hoffman 1987). At rest, the coronary vascular system behaves as a low-flow, high-resistance system in which flow is determined by the peripheral resistance (Ross et al. 1990). During maximal exercise or during pharmacological vasodilation, peripheral resistances in normal individuals decrease by a factor of four to five. Studies have shown that, in the absence of coronary stenosis, coronary blood flow increases proportionally as diastolic perfusion time decreases during stress tests (Holmberg & Varnauskas 1971; Holmberg et al. 1971; Nabel et al. 1990; Momomura et al. 1991) due primarily to a decrease in coronary vascular resistance (Holmberg & Varnauskas 1971; Holmberg et al. 1971; Momomura et al. 1991), which maintains uniform net transmural perfusion even if a marked reduction in diastolic perfusion time or higher heart rates are achieved (Flynn et al. 1992; Bache & Cobb 1977). In the case of epicardial narrowing, flow is determined by resistances in series: the resistance of coronary stenosis and the resistance of the coronary vascular bed. At rest, the proximal stenosis has to be severe before its resistance exceeds that of the resting coronary vascular bed. Resting blood flow will not be hampered by the narrowing until the lesion reaches approximately 80% diameter stenosis (Gould et al. 1974; Uren et al. 1994). In contrast, during maximal vasodilation, the peripheral resistances are minimal and hyperaemic flow is determined mainly by the severity of the narrowing. Therefore, it is likely that during stress tests, when the compensating mechanism caused by coronary vasodilation is exhausted (Nabel et al. 1990), myocardial ischaemia becomes dependent primarily on the interaction between the reduction of diastolic perfusion time and the degree of coronary stenosis (Ferro et al. 1995). Accordingly, if there is an obstructive disease of a major coronary artery, the degree of coronary flow increase may not take place, and regions of the heart that are adequately perfused at rest may therefore become ischaemic during exercise. The exercise test, therefore, is an ECG test for the adequacy of the coronary blood supply when the demand for the latter is increased by exercise. If the supply is inadequate, subendocardial ischaemia would occur (Ross 1989), and the subendocardial ischaemia is shown in ECG as ST segment depression (Brazier et al. 1974).

Why does exercise testing often provoke subendocardial ischaemia but not transmural ischaemia? The explanation is that the subendocardium is vulnerable to flow reduction, and the vulnerability of the subendocardium to ischaemia is related to mechanical and haemodynamic factors that limit systolic flow to the inner layers of the myocardium (Hoffman 1987). Extravascular compressive forces during systole are greater in subendocardial zones of the heart compared with subepicardial ones (Sabbah & Stein 1982). Therefore, systolic flow is greatly reduced in this region. The deeper muscle will thus be perfused mainly in diastole (Bache & Cobb 1977), and any substantial decrease of diastolic perfusion time or pressure (as occurs with coronary obstruction, elevation of ventricular diastolic pressure, and tachycardia) will lower the ratio of subendocardial to subepicardial flow and may cause the subendocardium to become ischaemic. Subepicardium, being perfused in systole and diastole, will be at lower risk of ischaemia. Nevertheless, under physiological conditions, the mean blood flow to the subendocardium is slightly higher than to the subepicardial, yielding an endo/epi flow ratio of above 1 (Ross et al. 1990; Hoffman 1987). In the conscious dog (Bache & Cobb 1977; Bache et al. 1981), sheep and lamb (Archie et al. 1974; Fisher et al. 1980; Fisher 1984), flow per gram in the subendocardium is usually 20% to 40% higher than that in the subepicardium, with flow in the midwall usually being between the two. Total flow is greater in the subendocardium because the calculated wall stress and the oxygen consumption are greater in this region than in the subepicardium. The combination of a greater wall stress, and hence greater resistance to flow, and higher metabolic demands results in lower coronary vascular tone in the subendocardium than in the subepicardium. As a consequence, the reserve for vasodilatation is also less in the subendocardium than in the subepicardium Bache et al. 1977), and as perfusion is reduced, the deeper layers of myocardium become ischaemic before the more superficial ones.

Another important factor that determines the forms of ischaemia is collateral circulation. It has been consistently observed in experimental models of coronary occlusion that if there is collateral blood flow available, it is distributed disproportionately to the subepicardial zone of the ischaemic region (Reimer & Jennings 1979; Becker et al. 1971; Rivas et al. 1976). In dogs even permanent ligation of a major coronary artery often does not result in complete infarction of the occluded vascular region because of their rich collateral circulation. Observations in humans also found that collateral function is an important determinant of the direction of ST response to ischaemia during acute total coronary occlusion (Macdonald et al. 1986). Patients with extensive, angiographically visible collaterals may have only ST segment depression during total coronary occlusion (Yasue et al. 1981; Tada et al. 1983; Yamagishi et al. 1985).

Factors such as systemic arterial pressure and ventricular diastolic pressure could play a role in the mechanism underlying stress-induced myocardial ischaemia (Ross et al. 1990; Hoffman 1987). An elevated left ventricular end diastolic pressure, by causing either a diastolic tissue pressure gradient or an increased myocardial wall stress, may contribute to subendocardial ischaemia (Dunn & Griggs 1983; Kjekshus 1973). A perfusion pressure lower than 60 mmHg may cause subendocardial ischaemia, although the coronary blood flow is relatively independent of coronary perfusion pressure when the pressure changes between 60 to 150 mmHg(Ross et al. 1990).

Exercise is currently the most convenient means of stimulating the myocardium to demand maximal blood flow and is the only way of stimulating such a rigorous demand for oxygen delivery that even moderate impairment of coronary blood flow capacity becomes detectable. In experimental studies, pacing instead of exercising is applied to increase the myocardial oxygen demand because of the inconvenience in exercising the animals (Guyton et al. 1977; Vincent et al. 1977; Mirvis & Ramanathan 1987; Mirvis & Gordey 1983). The premise is that tachycardia increases oxygen demand, and it is unaffected by the mode of tachycardia induction such as exercise or pacing (Mirvis & Gordey 1983; Heller et al. 1984).

2.4.4.2 ST Depression and the Location of Coronary Artery Disease

During the exercise test, ST segment depression is most frequently seen in the left anterior chest leads, regardless of which coronary artery is diseased. The classic study of Blackburn and Katigbak (Blackburn & Katigbak 1963) concluded that the most sensitive lead of the standard 12-ECG for detecting exercise-induced ST depression was V_5. Many workers have recently shown that, although body surface ST elevation was highly related to the region of ischaemia, body surface ST depression was poorly related if at all (Kubota et al. 1985; Dunn et al. 1981; Fuchs et al. 1982; Abouantoun et al. 1984; Mark et al. 1987). With the use of 12-lead exercise ECGs, Dunnet et al. (1981) and Fuchset et al. (1982) reported no differences in the distribution of exercise-induced ST segment depression in patients with isolated LAD lesions nor in those with single LCX or right coronary artery (RCA) lesions. For example, ST depression in both inferior and anterior leads occurred in 43% of patients with LAD disease and in 29% of subjects with right or LCX disease. Furthermore in a study undertaken by Abouantoun et al. (1984), the sites of exercise-induced thallium-201 scintigraphic defects could not be specifically identified by exercise-induced ST vector shifts in 54 patients with coronary artery disease. These findings showed no relation between the spatial orientation of the ST segment vector during exercise and the location of myocardial ischaemia as detected from thallium scintigraphy. Studies using body-surface mapping also indicate that ST depression is most prominent in the precordium. The actual position where the largest ST depression occurs varies widely, from the level of the third intercostal space to the tenth intercostal space. However, even analysis of precordial surface maps does not permit an accurate prediction of the location of coronary artery disease (Kubota et al. 1985 & 1989; Macfarlane et al. 1984), although this has been claimed by some authors (Fox et al. 1979). From a study using 16-lead precordial mapping during exercise in 19 patients with single vessel disease and 61 with multivessel disease, Fox et al. (1979) postulated that isolated disease of the LAD, the LCX or the right coronary artery was confined to the anterior leads (V_1 to V_5), inferior leads (II, III, aVF) and lateral leads (I, aVL, V_6), respectively. They also found that all patients with ST depression in all three regions had triple vessel disease. Conflicting results were obtained by others using more detailed body surface mapping system. Kubota et al. (1985) performed 87-lead ECG mapping in 61 patients with effort angina pectoris without myocardial infarction before and 1.5 and 5 minutes after treadmill exercise. They found that there was considerable overlap in the sites of ST segment depression among patients with LAD disease, those with LCX disease, and those with RCA disease although patients with RCA disease tended to have ST segment depression in more lower leads than those with LAD disease. These findings were further supported by the latest studies from the same workers (Kubota et al. 1989) and others (Mark et al. 1987) in patients with single-vessel disease. Reports (Kubota et al. 1989) from the same workers demonstrated that ST-segment maps immediately recorded after exercise showed the minimal potential in the left anterior chest region for all patients, irrespective of the diseased coronary arteries. Another study (Mark et al. 1987), which was carefully performed in 452 patients by Mark et al, demonstrated that ST depression provides no information about the location of the responsible coronary lesion, whereas exercise ST elevation, although uncommon, is a reliable guide to the underlying coronary anatomy. Therefore, body surface ST depression detected by either body surface mapping or 12-lead ECG provides no information on the site of coronary stenosis even in patients with one-vessel disease. An index, the ST segment/heart rate slope, has been recently introduced to analyse ST depression in exercise testing. However, this index does not improve the poor prediction of stenotic arteries by ST depression (Okin & Kligfield 1994a & b). This clinical problem can not be explained by the classic (Wilson et al. 1933a) and modern ECG theories (Tung 1978; Holland & Brooks 1977), which all suggest that ST depression should be able to localise.ischaemic region. The bidomain model worked in one situation but did not evaluate the clinical anomaly (Miller & Geselowitz 1978 a & b; Tung 1978).

2.4.5 ST Segment Depression in Acute Myocardial Infarction

Patients suffering an acute myocardial infarction may develop ST segment depression in the ECG leads remote from the primary site of myocardial damage. In clinical studies, two findings are generally discussed, ie, the anterior ST depression associated with inferior myocardial infarction, and inferior ST depression associated with anterior myocardial infarction. Approximately 65% to 72% of patients with inferior myocardial infarction have anterior ST segment depression (aVL, V_1 to V_4), and 37% to 62% of patients with anterior myocardial infarction have inferior ST depression (II, III, and aVF) (Mirvis 1988; Katz et al. 1986). The underlying pathophysiologic mechanism of such ST depression is not clear. Two hypotheses have been advanced to explain these ECG findings (Wong et al. 1993b; Haraphongse et al. 1984; Lew et al. 1987; Fletcher et al. 1993; Mirvis 1988; Schuster & Bulkley 1980; Quyyumi et al. 1986; Billadello et al. 1983): (1) ST depression dependent on ST elevation and (2) ST depression independent of ST elevation. These two subtypes conceivably have two different pathogenesis (Shah et al. 1994). The first type probably occurs as a reciprocal image of ST elevation in the infarcted region. In the latter pattern, however, ST depression probably occurs due to ischaemia outside the infarcted zone (ischaemia at a distance). Thus these two proposals with very different pathophysiologic bases may produce the same ECG result.

2.4.5.1 Reciprocal ST depression

Mirvis (1988) explained, based on dipole theory, that ST depression in myocardial infarction is a biophysical phenomenon, which should always be expected with primary ST elevation, and such ST depression is termed "reciprocal" ST change. A reciprocal ECG pattern is produced by viewing the myocardial event or lesion from the opposite perspective. Thus myocardial injury on the posterior wall would produce ST elevation in leads over the posterior wall and body surfaces while producing reciprocal ST depression on the anterior cardiac and torso surfaces. The ST elevation may be termed primary or intrinsic, reflecting damage to the myocardium "directly" under the exploring electrodes; the ST depression may be termed reciprocal, secondary, or extrinsic, reflecting events in cardiac regions remote from those electrodes (Mirvis 1988). Accordingly, such ST depression should always change reciprocally with fluctuations of ST elevation. This reciprocal change has been described in the setting of coronary angioplasty. In the presence of single vessel coronary artery disease, intermittent occlusion of the diseased coronary artery can cause concomitant ST segment depression in leads other than those showing ST segment elevation (Brymer et al. 1985). Others observed that ST depression during percutaneous transluminal coronary angioplasty (PTCA) occurs with coronary occlusion and resolves with reperfusion in a remarkable mirror-image manner of ST elevation resolution (Shah et al. 1994; Shenasa et al. 1993). Furthermore, reciprocal ECG patterns have also been documented in experimental models, although RMBF was not measured in these studies. ST depression was recorded from the histologically normal posterior wall of the left ventricle 15 minutes after LAD ligation in an isolated, perfused rabbit heart (Brody et al 1973). A similar finding was observed after the distal one-third of the LAD was ligated in an in-situ baboon model (Crawford et al. 1984). Some other clinical studies have also reported a clinically benign "reciprocal" ST depression remote from the region of myocardial infarction (Putini et al. 1993; Fletcher et al. 1993; Stevenson et al. 1993 & 1994; Birnbaum et al. 1994).

2.4.5.2 Ischaemia at a distance

The concept of "ischaemia at a distance" in the setting of myocardial infarction, as originally proposed by Schuster and Bulkley, concerned the mechanism of angina pectoris in the immediate postinfarction period (Schuster & Bulkley 1980). Among 20 patients with postinfarction angina who underwent necropsy, all 8 of the patients with ECG ST segment depression in areas remote from the infarction occurring during angina had significant narrowings of other coronary arteries with collateral connections from the occluded artery supplying the infarcted area. Also, they noted that ST-segment depression at rest in leads remote from the infarcted area was predictive of the eventual occurrence of angina with further ST-segment depression in these leads and predicted death or other severe complications in these same patients (Schuster & Bulkley 1981). Thus, they suggested that some patients with ST-segment depression in leads remote from the infarction may already have ischaemia of these adjacent areas due to the lack of collateral blood flow from the occluded blood vessel. While these findings are supported by both experimental (Naccarella et al. 1984; Gascho & Beller 1987) and clinical (Salcedo et al. 1981; Jennings et al. 1983; Billadello et al. 1983) studies, it is possible that multiple mechanisms interact to produce such remote ischaemia (Naccarella et al. 1984; Gascho et al. 1987; Mirvis 1988; Edmunds et al. 1994; Schuster & Bulkley 1980 & 1981). Firstly, the increased oxygen demand after arterial ligation, resulting from factors including increased heart rate and increased chamber size, may provoke new ischaemia in the noninfarcted region. Secondly, increased back pressure on the distal coronary bed produced by increased left ventricular end-diastolic pressure may reduce the transcoronary pressure gradient to reduce flow. Thirdly, acute occlusion may reduce collateral flow to the adjacent bed, this mechanism would be more effective under conditions of chronic ischaemia producing augmented collaterization. Finally, the stress to sustain cardiac output by overcompensation by the noninfarcted myocardium may result in a "relative" ischaemia in the noninfarcted region (Scott & Kerber 1992; Trevi GP & Sheiban 1991).

Regardless of the operative mechanism, myocardial infarctions accompanied by ST depression in remote myocardial zones are associated with greater infarcts with more extensive left ventricular dysfunction (Wong et al. 1993; Wong & Freedman 1994; Edmunds et al. 1994; Berland et al. 1986; Gibson et al. 1982; Lew et al. 1985), a higher incidence of multivessel disease (Haraphongse et al. 1984; Salcedo et al. 1981; Jennings et al. 1983; Krone et al. 1993), worse haemodynamics, more clinical complications and a higher risk of poor clinical outcomes (Bates et al. 1990; Kilpatrick et al. 1989; Krone et al. 1993; Gheorghiade et al. 1993). It was evident that the amount of ischaemia and infarction was greater in the patients with ST segment depression in both inferior myocardial infarction and anterior myocardial infarction (Wong & Freedman 1994; Edmunds et al. 1994; Willems et al. 1990; Berland et al. 1986; Gibson et al. 1982; Lew et al. 1985); arterial size and distribution are smaller in patients without ST depression (Bates 1988; Sato et al. 1989; Brymer et al. 1985). Patients with ST depression also had worse ventricular function than those without (Bates et al. 1990; Billadello et al. 1983; Mukharji et al. 1984; Shah et al. 1980; Haraphongse et al. 1984). Furthermore, in a study of patients with acute inferior infarction and using inverse transformation of the body surface electrocardiogram to derive epicardial maps, Kilpatrick and his coworkers (1989) observed localised ST elevation corresponding to good prognosis; whereas an epicardial dipole consisting of ST elevation over the infarcted region and adjacent ST depression over the normal region corresponded to a bad prognosis. The analysis shows clearly that the dipoles were present in patients with single vessel disease as well as in those with triple vessel disease and the dipole predicted the death of those with single vessel disease (Kilpatrick et al. 1989).

While the debate on the physiological mechanism and clinical significance of remote ST depression in acute myocardial infarction continues, patients with ST depression do, as a group, have more severe functional abnormalities and postinfarction complications. The discrepancy between published studies concerning the clinical significance of remote ST depression may come from differences in diagnostic tools utilised, different time frames, and inhomogeneousity between patient groups (Mirvis 1988; DeWood et al. 1982; Bates et al. 1990; Becker & Alpert 1988; Kornreich et al. 1993).

2.5 GLOSSARY

Cardiac source. The cardiac source is the electromotive forces which give rise to currents. It results from the excitation and recovery of cardiac cells.

Dipole. A dipole is a description of potential distributions. It consists of positive charges and negative charges separated by a certain distance. The positive side of the dipole is termed *source*, and the negative side *sink*.

Electrical diastole and systole. The interval between the repolarisation and the next depolarisation is called diastole (interval between action potentials), implying a correlation with the mechanical diastolic period of the cardiac cycle; the action potential period is called systole, implying a correlation with the mechanical systolic period of the cardiac cycle. Electrical diastole and electrical systole correspond respectively to TQ segment and ST segment in ECG.

Injury current. The currents flow between ischaemic and normal regions created by the potential differences between these two areas during ischaemia. They appear in the periods of electrical diastole (TQ segment) and electrical systole (ST segment). The injury current during ST segment is termed *systolic current of injury*, and the current during TQ segment is termed *diastolic current of injury*.

Subendocardium. The inner one quarter or one third of the ventricular myocardium.

Subepicardium. The outer one quarter or one third of the ventricular myocardium.

Chapter 3

MATERIALS AND METHODS

3.1 EXPERIMENTAL ANIMALS

A total of 73 sheep bred on the University of Tasmania's animal farm with the following general characteristics were used:

Species:	Polworth (ram) / Comeback (ewe) cross
Sex:	both male and female
Weight:	25-41 Kg
Age:	6-9 months

Table 3.1 shows the animal numbers used in different experiments.

Table 3 Animal Numbers in Different Experiments

Experiments	Animal Numbers	Study Protocols
1	10	Methodology of regional myocardial blood flow measurement using fluorescent microspheres
2	18	Production and validation of subendocardial ischaemia in sheep
3	30	Epicardial and endocardial ST potential distributions in subendocardial ischaemia - in relation to regional myocardial blood flow
4	33	Epicardial and endocardial ST potential distribution in transmural ischaemia - in relation to regional myocardial blood flow

3.2 DRUGS AND CHEMICALS

Table 3.2 shows the drugs and chemicals used in this investigation.

Table 3.2 Drugs and Chemicals Used For This Investigation

Name	Supplier	Usage
Pentobarbitone sodium	Boehringer Ingelheim	Induction and continuous anaesthesia
Physiological Saline	Royal Hobart Hospital (R.H.H.) Pharmacy	1) Slow drip into jugular vein to compensate for the loss of body fluid during the experiments 2) Flushing all the lines to prevent the coagulation of blood in the catheters 3) Making up drug or chemical solutions 4) Soak flowmeter probes for calibration
Heparin	R.H.H. Pharmacy	Systematically for sheep to avoid blood coagulation
Dobutamine Hydrochloride	R.H.H. Pharmacy	Slow drip into jugular vein to maintain blood pressure when necessary
Fluorescent Microspheres	Molecular Probes, Inc.	Measurement of regional myocardial blood flow
Ethyl Acetate	Sigma	Extraction of fluorescent dye
KOH	Sigma	Digestion of myocardial tissue
Methylene Blue	Sigma	Delineation of ischaemic regions
Tween 80	Sigma	Dispersion of microspheres

3.3 ANIMAL PREPARATION AND EXPERIMENTAL SETUP

Studies were performed in an acute, open-chest sheep preparation. Anaesthesia was induced intravenously with Pentobarbitone sodium (30 mg/kg) and then maintained with continuous infusion (3-8 mg/kg/hour) through a jugular vein catheter. The animals were artificially ventilated (3.5-3.0 L/min) by a positive pressure respirator via a cuffed tracheal tube with room air. Tidal volume and respiratory rate were constant during each experiment. A left thoracotomy was performed in the fourth intercostal space, and the heart was suspended in a pericardial cradle. The left circumflex coronary artery (LCX) and the left anterior descending coronary artery (LAD) were each isolated proximally for the electromagnetic flow transducer (NARCO, Carolina Medical Inc, P.O. Box 307, 157 Industrial Drive, King, NC 27021, USA) for blood flow measurement, and 10-20 mm more distally for the hydraulic occluder (IN VIVO METRIC, Healdsburg, CA) for inducing arterial stenosis. In the study of transmural ischaemia, the obtuse marginal branch of the circumflex coronary artery (OM) was also isolated near its origin for arterial stenosis. Another cannula (PE 90) was inserted into the left atrial appendage for microsphere injection and pressure measurement. Two epicardial wires were sutured to the left atrial appendage for left atrial pacing.

Statham P23ID transducers were used for the pressure measurements. The arterial pressure was measured via a 7F catheter in the left carotid artery. The left ventricular pressure was measured via a 7F catheter in the left ventricular cavity introduced through the left carotid artery. The left atrial pressure was measured via a PE 90 cannula implanted in the left atrium. Both the LCX and the LAD flow were measured with the electromagnetic flow transducer. Epicardial and endocardial electrograms were recorded with an epicardial sock and an endocardial basket respectively as described in the next section.

Sheep were instrumented as shown in Table 3.3.

Table 3.3 Experimental Instruments and Their Purposes

Instruments	Locations	Usage
F7 fluid filled catheter	Carotid artery and left ventricle	Pressures
PE 90 cannula	Left atrium	Pressure, microsphere injection
2.5-3.0 mm NARCO RT 500 magnetic flow probe	LAD and LCX	Coronary flow measurement
Hydraulic occluder	OM, LAD/LCX	Coronary artery stenosis
Two pacing wires	Left atrial appendage	Pacing
Epicardial sock electrodes	Surface of left and right ventricles	Epicardial potential recording
Endocardial basket electrodes Quadripolar electrode catheter	Left ventricular cavity	Endocardial potential recording

3.4 REGIONAL MYOCARDIAL BLOOD FLOW MEASUREMENT

Regional myocardial blood flow was measured by using fluorescent microspheres. The full techniques and procedures are described in chapter 4.

3.5 EPICARDIAL AND ENDOCARDIAL ST POTENTIAL MAPPING

3.5.1 Potential Recording

3.5.1.1 Epicardial sock

The epicardial potentials were recorded using an epicardial sock containing 64 electrodes (Cardiovascular Research and Training Institute, the University of Utah, USA) which was placed around the heart. The arrangement of the 64 electrodes provided extensive coverage of the epicardial surfaces of the left and the right ventricles (Figure 3.1).

3.5.1.2 Endocardial basket

The endocardial potentials were recorded using a home-made 40-electrode basket mapping apparatus (Figure 3.2). The apparatus was oval-shaped and constructed with spring steel wire (0.25 mm in diameter) as the skeleton, and polyethylene tube (1.27 mm in outer diameter) as the outer covering, on which 40 silver electrodes were mounted. The steel skeleton consisted of 8 arms. Each arm was insulated with a polyethylene tube and mounted with 5 unipolar silver electrodes (0.15 x 4 mm). To avoid injury current, the electrodes were mounted in such a manner that they were not in direct contact with the endocardium. The 8 arms were at equal distance and were connected to each other at both ends so that when the apparatus was expanded, a uniform distribution of electrodes resulted. Two arms were marked with different colours for orientation. The apparatus was 50 mm long and 32 mm across when fully opened. Placement of the apparatus was accomplished by using a thin wall tubing (inserter) with an outer diameter of 8 mm via the apex. The closed apparatus was placed inside the inserter; a left apical ventriculotomy of approximately 10 mm, simulating the clinical approach, was performed. The inserter was introduced into the apex, and the apparatus placed into the left ventricle while withdrawing the inserter. The apparatus was secured by a purse string suture around the point of insertion. The time for positioning the apparatus was a matter of seconds. Once inside the left ventricle, the apparatus deploys, placing the eight arms into position, with each maintaining constant contact with the endocardium. The electrodes were not in direct contact with the endocardium, but they detected the potential changes from the nearest endocardium. From the postmortem examination, the distance between the electrodes and the endocardium ranged from 1.3 to 3.0 mm. The apparatus enabled the author to record the signal from a working heart, and to map the whole endocardial surface at one time, although at a moderate spatial resolution.

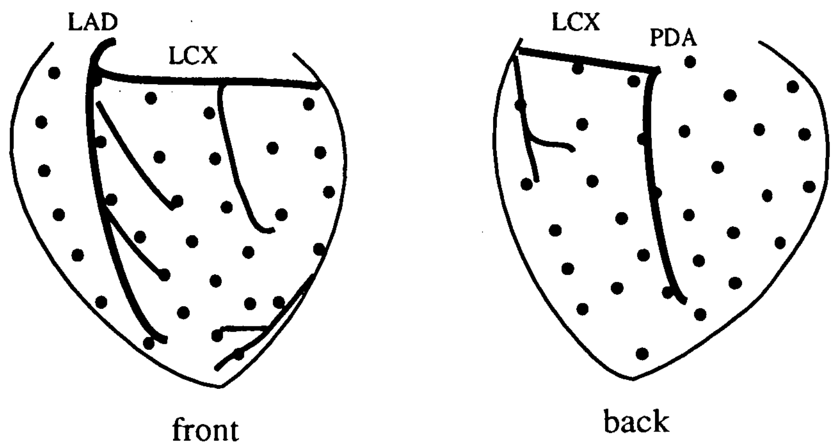

Figure 3.1 Epicardial electrode matrix. Schematic drawings represent the electrode matrix on the front and the back surfaces of the heart. Distances between electrodes were approximately 10 mm.

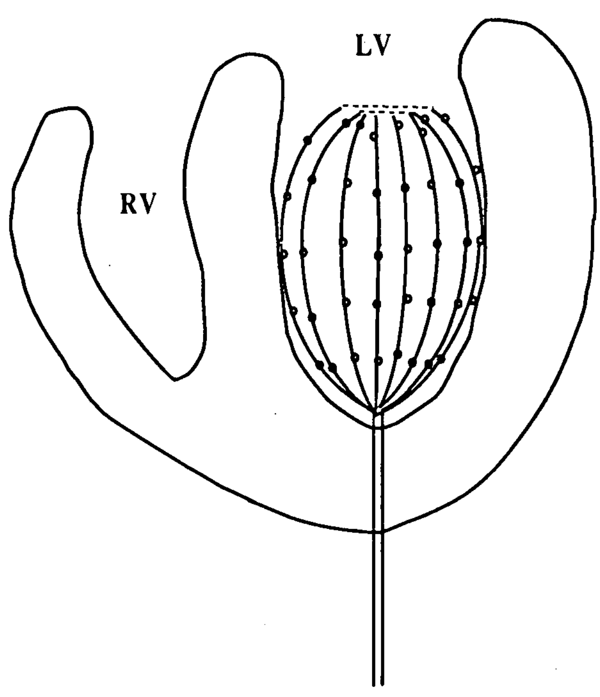

Figure 3.2 Schematic drawing illustrating the 40–electrode basket apparatus fully opened in the left ventricle. It was 50 mm long and 32 mm across. The 40 silver electrodes were regularly distributed along 8 arms with 5 electrodes in each, at a distance of 5–8 mm between electrodes.The size of each electrode is about 0.15 x 4.0 mm. The arms were attached to each other at both ends. Each arm maintained constant contact with the endocardium, without the electrodes touching the endocardium. The distance between the electrodes and the endocardium ranged from 1.3 to 3.0 mm. Each electrode detected the potential changes from the nearest endocardium.

Simple haemodynamic measurements during experiments suggested that the insertion of the apparatus into the left ventricle did not cause significant haemodynamic deterioration. The apparatus did not provoke arrhythmias or injury currents. All the electrodes remained in their positions throughout the experiments. The quality of all unipolar electrical signals remained satisfactory (Figure 3.3).

In some experiments, the endocardial electrograms were recorded by using a quadripolar electrode catheter implanted in the left ventricular cavity (see chapters 5 and 6).

3.5.1.3 Recording system

The epicardial and the endocardial electrodes were connected to a 120 channel data acquisition system (Walker et al. 1983 & 1987a). The signal from each electrode was passed through a differential amplifier with a gain of 1000. The amplifier outputs were connected through an 8x16-1 channel multiplexer to a high speed 12 bit analog to digital converter (Burr Brown ADC803). A sample and hold on the output of each amplifier allows the signal at all electrodes to be sampled simultaneously. Potentials were sampled at 1000 samples/sec per channel by the data acquisition system directly on to computer memory (DMA) through an S11W (Engineering Design Team, Inc., 1100 NW Compton, Suite 306, Beaverton, Oregon USA 97006) interface to an SBus on a portable computer (BriteLite RDI Computer Corp., 2300 Faraday Avenue, Carlsbad, CA 92008). An immediate display of the sampled electrocardiographic signals enabled a check on the quality of the data. All the potentials were recorded in reference to the left leg. During data acquisition, the pericardial cradle was released, the opening in the chest wall was covered by moisturised warm saline pads without touching the myocardium, so that the anterior wall of the left ventricle was not directly exposed to the air. Both the atria, right ventricle and the posterior and lateral walls of the left ventricle were in contact with the lung, the great vessels and the back of the thoracic cavity. To avoid the interference of injury currents, recordings were obtained at least 20 minutes after setting up, when the ST-T shifts had disappeared almost completely.

Figure 3.3 illustrates the epicardial and the endocardial electrograms recorded by the epicardial sock and the endocardial basket electrodes via the 120-channel recording system.

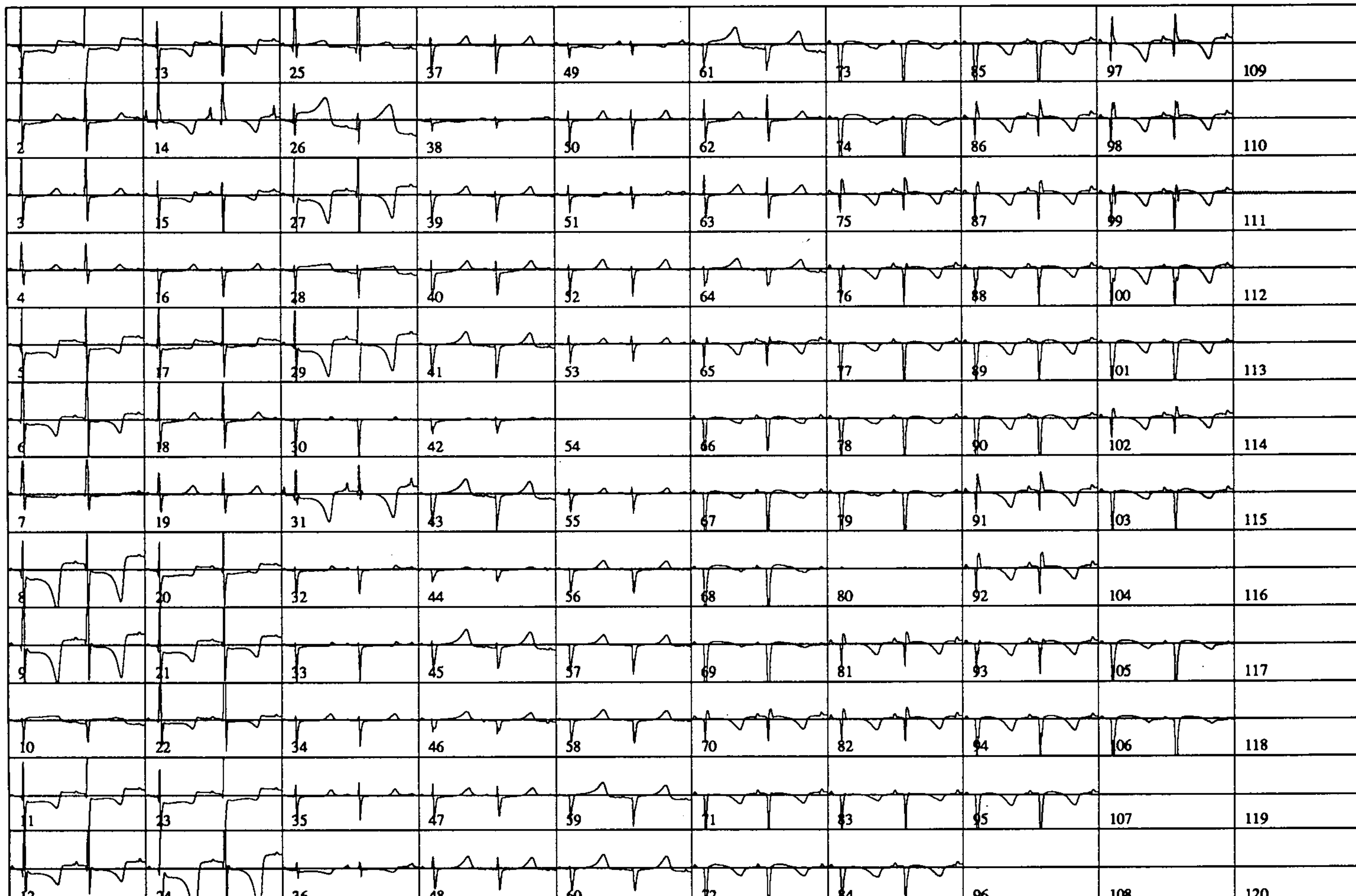

File : exper.830 Range Min: -5418 (uV) Range Max: 5418 (uV) 0 ms to 1024 ms

Figure 3.3 Epicardial electrograms (1-64) and endocardial electrograms (65-106) recorded by the 64-electrode sock and the 40-electrode basket via a 120-channel recording system.

3.5.2 Construction of Isopotential Maps and Map Display

3.5.2.1 Confirmation of the electrode position and reconstruction of the heart outline

At the termination of each experiment, the sheep was sacrificed and the heart carefully removed from the chest cavity. After marking the epicardial electrode position with mapping pins, the heart was opened and the endocardial electrode positions verified and marked. The electrode positions corresponded to the tissue samples subsequently taken for measurement of the regional myocardial blood flow, so that the ST segment changes after the coronary artery occlusion could be correlated with the blood flow of each sample. By making an incision from the posterior edge to the apex, the ventricles could be opened flat (for endocardial mapping, the incision was made from the middle of the septum). The electrode positions, the epicardial vascular patterns and the outlines of the ventricles were traced on transparent plastic and transferred to paper, where the coordinates of the whole picture were measured and reconstructed using our own mapping program and the S-Plus statistical package. The picture was then combined with the ST potential contour map to give either an epicardial or an endocardial potential map as illustrated in Figure 3.4.

3.5.2.2 Computer analysis

Data from the recording system were transferred to a SUN workstation (SUN Microsystems, Inc., 2550 Garcia Avenue, Mountain View, CA 94043, USA), and then analysed using the mapping program in this laboratory (Walker et al. 1983 & 1987a) and S-Plus statistical package, which are both run under UNIX system. The electrograms were plotted, and their qualities evaluated. Missing or poor electrograms were discarded. Bad leads were picked out and replaced by interpolation from the surrounding leads. The onset of the QRS complex was chosen manually from the plots, and the potentials during a 10 msec portion of the PR segment were averaged for use as a zero-potential reference level. The ST segment maps were each constructed from data averaged over a 20 msec interval centred on a point 80 msec after the QRS onset (the QRS interval of the sheep is shorter than that in the humans, about 40 msec). The epicardial potential maps were constructed from the epicardial ST potentials of the left and the right ventricles. The endocardial potential maps were constructed from the endocardial ST potentials of the left ventricle. In some studies, the epicardial and the endocardial potential maps were further combined with the flow maps constructed from the simultaneously measured regional myocardial blood flow (see chapter 6). The ST segment potential distributions were displayed as isopotential contour maps in the format shown in Figure 3.4. Isopotential contours were drawn at 1, 2 or 4 mV intervals using linear interpolation. Maps were also displayed and analysed in the patterns as described below.

Isopotential maps. Individual maps were constructed as contour lines, connecting the points of equal voltage at the selected time instants, representative of the ST segment. In the sheep these varied from animal to animal and were recorded as an integral of 20 msec after the J point.

Isopotential difference maps. Difference maps were computed by subtracting the control voltage from each ischaemic voltage at each electrode site during the ST segment. The resultant pattern depicted the electrical field generated by the intervention, ie, reduced blood supply and increased heart rate, while controlling for biological variability in the baseline potential distributions.

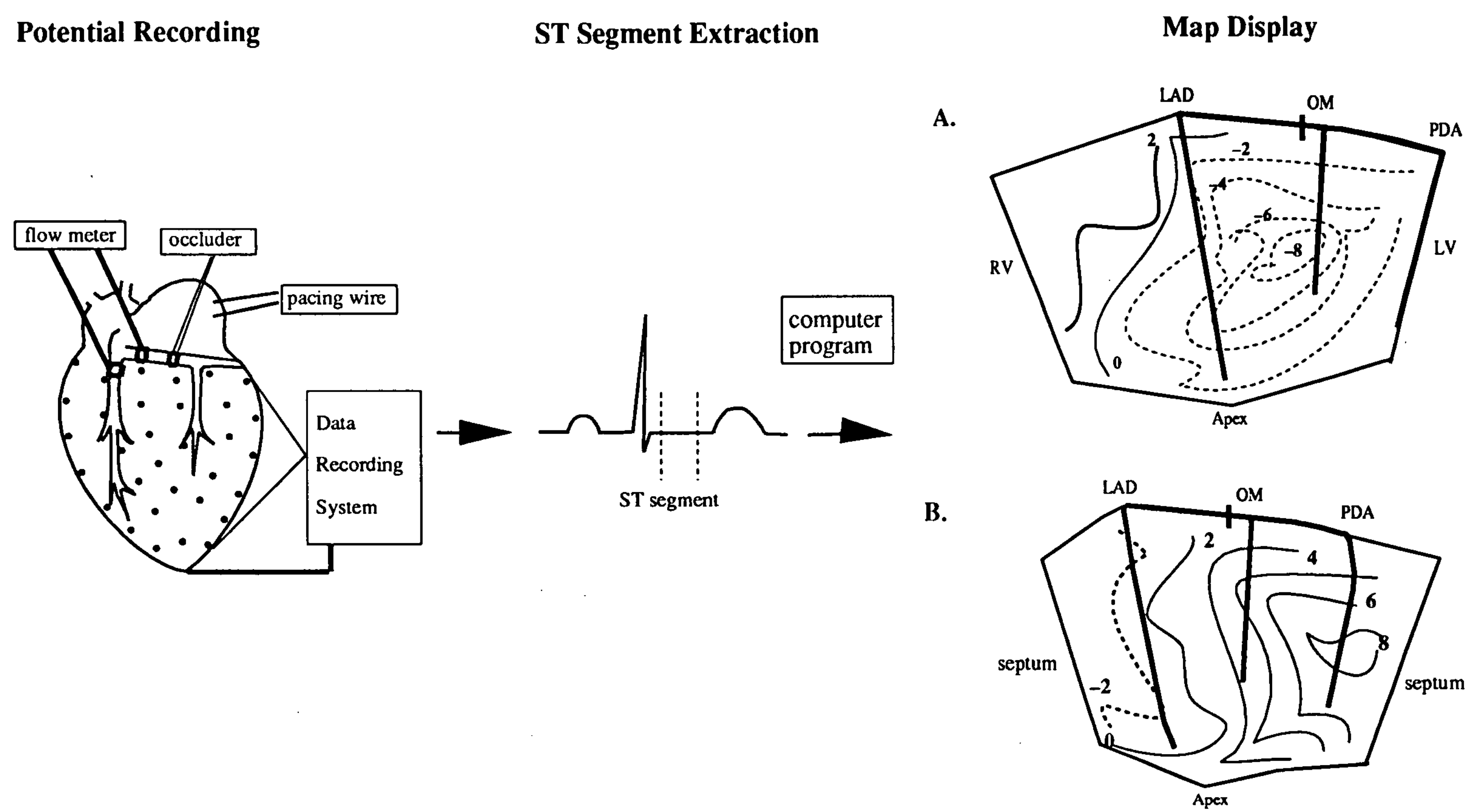

Figure 3.4 Schematic drawings illustrating the potential recording, the map construction and the map display. The left diagram represents the heart preparation. The right diagrams depict epicardial (A) and endocardial (B) contour maps constructed from ST potentials. Schematic drawing of the frames represent the unwrapped epicardial surface of the left and the right ventricles (A), and the unwrapped endocardial surface of the left ventricle (B). The thick solid lines reflect coronary arteries. The thin solid and dotted lines indicate ST elevation and ST depression respectively. Numbers inside maps indicate values of voltages in millivolts. Ligated arteries are indicated by bars. All the contour maps in this thesis are in this format.

3.5.2.3 Computer programs

Computer programs written on the UNIX system to process data and to display results are as follows:

premap	Extracts ST potential data from the electrogram data collected by the recording program.
get_con	Combines ST potential of each channel with its corresponding electrode position, and picks out bad or missing signals.
mycontour	Displays the ST potentials or blood flow values in the format of contour map or image map together with the picture of the heart.
sub	Subtracts the control ST potential from each ischaemic ST potential at each electrode site.
flow.spatial	Displays the spatial distribution of regional myocardial blood flow.

3.6 HAEMODYNAMIC MEASUREMENTS

3.6.1 Blood Pressures

Statham P23ID pressure transducers (Statham Laboratory Inc.) were used for blood pressure measurements with size 7 catheters. Each sheep was anticoagulated with heparin sodium (initial dose 5000 IU, followed by 5000 IU every 1-2 hours) throughout the whole experiment to ensure there was no clotting during each experiment.

3.6.2 Coronary Blood Flow

Electromagnetic flow transducers (2.5-3.0 mm, NARCO) were used for the LAD and the LCX blood flow measurements. Each transducer was calibrated by measuring its reading against the actual flow rate at the specified calibration factor of the transducer. At the flow rate range of 20-100 mL/min, the flowmeter reading correlated exceptionally well with the actual flow ($r \geq 0.98$) (Appendix B). At the start of each experiment, the flow transducer was cleaned thoroughly and soaked in saline for at least 30 minutes, and then calibrated according to the manufacturer's instructions. The calibration was again carefully performed at the end of the experiment.

3.6.3 Data Recording and Analysis

The left ventricular pressure, the carotid artery pressure, the left atrial pressure and the coronary flows were recorded on a multichannel recorder (Grass Instrument Co., Quincy, Mass., 02169, USA); they were also recorded by a Macintosh II computer via an analogue-to-digital converter (NB-DMA-8, NI-488 for Mac-SN 3643 and LabView software: National Instruments Corporation, 12109 Technology Boulevard, Austin, TX 78727-6204, USA). The data recorded by Macintosh II computer were transferred to a SUN workstation (SUN Microsystems, Inc., 2550 Garcia Avenue, Mountain View, CA 94043, USA), where they were decoded and processed using the computer programs in this laboratory. All data points were averaged over at least 40 cardiac cycles.

3.7 STATISTICAL ANALYSIS

Results were expressed as the mean ± SD. Paired data were analysed by two-tailed Student's paired t-test with the 0.05 level of probability considered as being significant. Simple linear regression and correlation were used to analyse the relationship between two sets of data.

The following statistical packages were used to analyse data.

Excel	was used to calculate regional myocardial blood flow (see Chapter 4), the mean, the standard deviation (SD), and the P value for student t-test.
Cricket Graph	was used to graph data and to compare two groups of data by linear regression and correlation.
S-Plus	was used to compare two groups of data by linear correlation, and to do t-test of correlation coefficient.
Sigma plot	was used to graph data.

Chapter 4

MEASUREMENT OF REGIONAL MYOCARDIAL BLOOD FLOW BY FLUORESCENT MICROSPHERES

4.1 INTRODUCTION

The measurement of regional myocardial blood flow (RMBF) is essential in experimental cardiology, it allows more detailed observation of blood flow change in the target region of the heart. The traditional method for the measurement of the RMBF is the radioactive microsphere technique. This method has become the standard technique since its first introduction by Rudolph and Heymann in 1967 (Rudolph and Heymann 1967). However, radioactive microspheres have their disadvantages, such as radioactivity which requires special disposal and limited shelf-life which makes them expensive. Recently, several nonradioactive microspheres (Hale et al. 1988; Kowallik et al. 1991; Abel et al. 1993; Glenny et al. 1993) have been developed. One of these products is the fluorescent-labelled microspheres. Their use for measuring RMBF on dogs and pigs is reported by Abel et al. (1993) and Glenny et al. (1993) and the method has proven to be equivalent to the radioactive microsphere method (Abel et al. 1993; Glenny et al. 1993). Nevertheless, there are some concerns on the techniques applied in these studies. Firstly, the tissue filtering not only makes this technique tedious, but also causes error due to the loss of microspheres (Glenny et al. 1993). Secondly, the traditional left atrial injection wastes approximately 95% of the microspheres if only the RMBF is measured, because only about 5% of the cardiac output supplies the heart.

The primary objective of this study was to investigate the use of a fluorescent technique without filtering the myocardial tissues and to validate this modified fluorescent technique in sheep with heart in-situ. The secondary objective was to evaluate the measurement of the RMBF by direct coronary artery injection of fluorescent-labelled microspheres. The results were compared with those measured by the conventional left atrial injection method.

4.2 METHOD

4.2.1 Animal Preparation and Instrumentation

Ten sheep (25-41 kg) of both sexes were used. Animal preparation and instrumentation were as described in chapter 3, except that a fine cannula (PE 50) was implanted into the left circumflex coronary artery (LCX) for intracoronary injection of microspheres. The cannula was placed distally to the flow transducer with the tip of the cannula pointing against the blood flow direction (Figure 4.1).

4.2.2 Fluorescent Microspheres and Their Preparation

The fluorescent-labelled microspheres were bought as a kit containing seven vials of different fluorescent dyes from Molecular Probes, Inc., USA. Table 4.1 lists the seven colours with their excitation and emission wavelengths in Cellosolve® acetate (Glenny et al. 1993) and in ethyl acetate (author's measurement).

Table 4.1 Excitation and Emission Wavelengths of Fluorescent Microspheres in Cellosolve® Acetate and Ethyl Acetate

	Excitation Wavelength (nm)		Emission Wavelength (nm)	
colour	Cellosolve® Acetate	Ethyl Acetate	Cellosolve® Acetate	Ethyl Acetate
blue	360	360	420	430
blue-green	430	420	457	470
green	450	450	488	495
yellow-green	490	490	520	505
orange	530	530	552	550
red	565	565	598	590
crimson	600	600	635	630

The microspheres were 10.3±0.27 micrometers in diameter suspended in 10 ml of distilled water with 0.01% Tween-20. Each vial contained 3.33×10^7 microspheres. The microspheres were diluted by normal saline to provide a dose of $0.08\text{-}0.33 \times 10^6$ in a volume of 1-2 ml for the intracoronary injection, and $3.33\text{-}6.67 \times 10^6$ in a volume of 10 ml for the left atrial injection. Tween-80 was added to the suspensions (0.02% by volume) to avoid aggregation. Each microsphere preparation was ultrasonically agitated for 5 minutes, followed by a vigorous vortex for 10 minutes prior to injection.

In order to avoid errors caused by spillover (overlapping) of fluorescence into adjacent colours, non-adjacent colours were chosen for each experiment. The fluorescent dyes were also randomised between injection methods for different sheep. As specified by the spectrofluorimeter, the following colours of microspheres and optimum excitation/emission wavelengths were used: blue-green (420, 470 nm), green (450,495 nm), yellow-green (490, 505 nm), orange (530, 550 nm), red (565, 590 nm) and crimson (600, 630 nm). The excitation/emission slit widths were set at 5/5 nm.

Due to the weak red signal in the spectrofluorimeter used in this study, 2-4 times more orange and crimson microspheres were used in the preparation. On average, approximately 2,600 microspheres for blue-green, green and yellow-green, and 5,000-6,000 microspheres for orange, red and crimson dyes per myocardium sample were used.

4.2.3 Administration of Microspheres

Both LCX and left atrial injections were applied in eight sheep for comparison. The RMBFs were calculated using the coronary inflow as the reference flow. In five sheep, the reference flow was also collected from the femoral artery during left atrial injection and the calculated RMBFs using classic technique were compared with those determined by using the coronary inflow as the reference flow.

4.2.3.1 LCX injection

Microsphere suspensions were mixed with 2 ml of warm blood and the whole mixture injected against the direction of flow over 90 seconds via the implanted LCX cannula. The cannula was flushed with 3 ml of saline. Administration of both the microspheres and the flushing were carried out at a slow speed to avoid changes in the coronary artery flow.

4.2.3.2 Left atrial injection

Ten minutes after the LCX injection, another set of microsphere suspensions were mixed with 10 ml of warm blood and the mixture administered over ten seconds via the implanted left atrium cannula. The cannula was flushed with 10 ml of saline. As for the LCX injection, the reference flow was established using an in-line electromagnetic flow transducer. In five sheep, an arterial reference sample, initiated at the time of microsphere injection and continued for 100 sec after completion of the injection, was also withdrawn at a speed of 6 mL/minute from a catheter implanted in the femoral artery via a calibrated pump (MasterFlex®, Cole-Parmer Instrument Co., Chicago, ILL, USA).

4.2.3.3 Distribution between different fluorescent dyes

Two sheep were used to study the distribution of different fluorescent dyes in the myocardium by receiving a LCX injection of blue-green and crimson mixture, followed by a left atrial injection of yellow-green and orange mixture.

During each injection, the coronary blood flow, the arterial pressure and the ECG were monitored.

4.2.4 Tissue Samples

After completion of the experiment, 10 mL of 0.1% methylene blue dye (Sigma) were injected into the LAD, and 10 mL of normal saline were simultaneously injected into the LCX to delineate the nonischaemic and the ischaemic areas respectively. Each sheep was killed by sodium pentobarbital overdose. The heart was excised, and rinsed with normal saline to remove superficial blood. The left ventricle was isolated, and the gross epicardial fat and blood vessels trimmed off. Then the heart was stored in a refrigerator at -10°C for 10 hours to facilitate sectioning. The left ventricle was divided into 3-5 circumferential rings from the base to the apex (Figure 4.1). The circumferential rings were then cut into sections of epicardial arc length 12 mm per piece. Sections of the myocardium were divided into the endocardial, the middle and the epicardial thirds. The anatomic location of each myocardial piece was recorded. The dimension of each piece was approximately 12x10x3 mm. Each sample was individually weighed, placed into a screw-cap polystyrene tube to which 2 ml of 4M KOH was added, and the tube containing the mixture placed in a 37°C water bath for 12 hours. After the tissue had been digested, 3 ml of ethyl acetate was added, the tube vortexed for 1 minute, and then centrifuged for 2 minutes at 2,500 rpm. The upper layer of solvent was transferred to a quartz cuvette where fluorescent intensity was read, at the appropriate excitation/emission wavelengths, with a Perkin-Elmer 650-10S fluorescence spectrophotometer. All the samples from the same experiment were measured on the same day.

Xylene was initially used as a solvent in two sheep. However, great difficulty was experienced in separating the aqueous and the organic layers. Unfortunately, the addition of a large quantity of sodium sulphate resulted in small particles suspended in the aqueous layer, distorting the fluorescence reading. The results were discarded, and the xylene method was abandoned.

The blood reference samples were processed in the same manner as the tissue samples.

The solvents, the blood and the myocardial tissues were measured for their intrinsic fluorescence.

The process of tissue sampling and digesting, fluorescence extraction and measurement are illustrated in Figure 4.1.

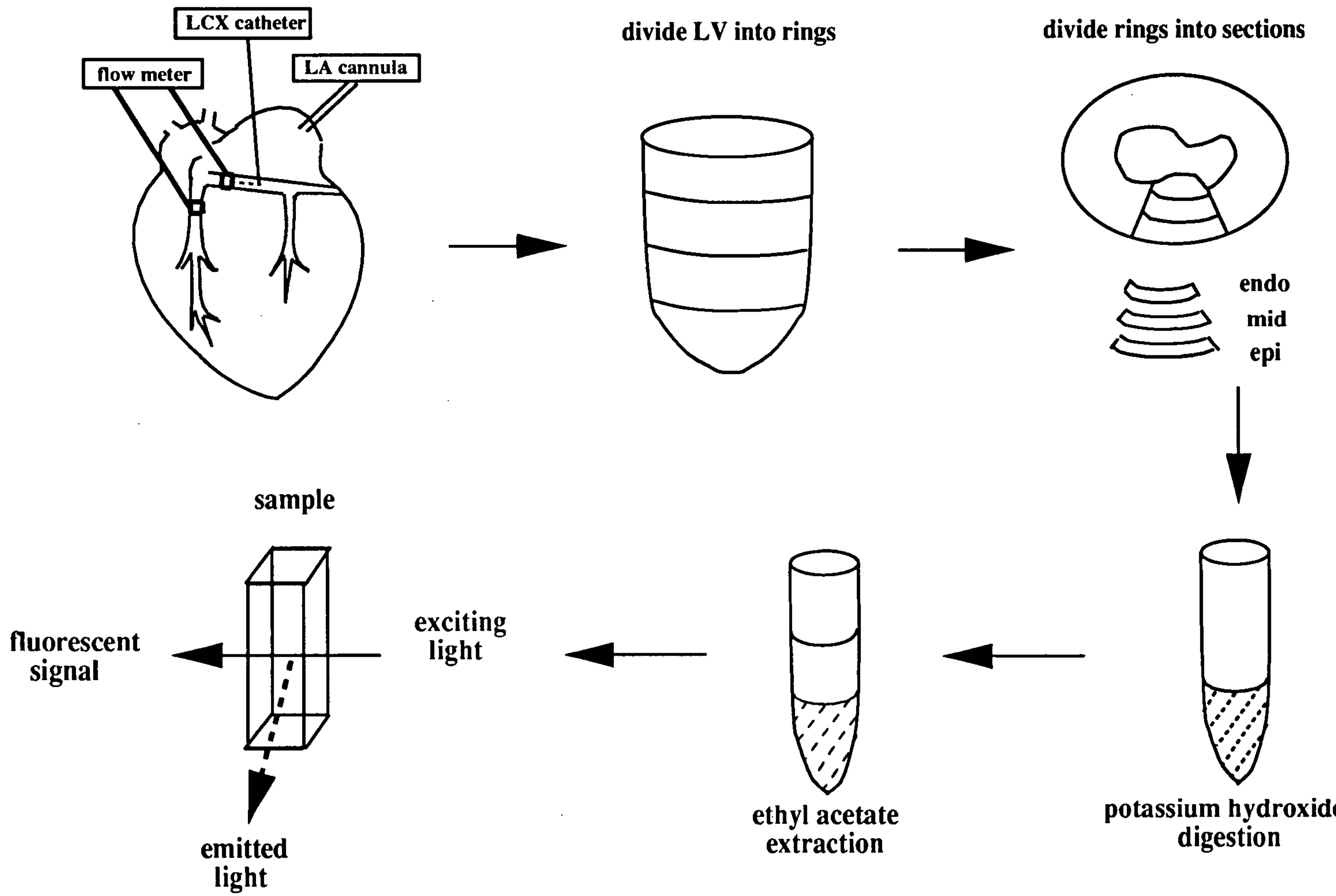

Figure 4.1 Schematic drawings illustrate microsphere injection, tissue sampling and digesting, fluoresence extraction and measurement. The emitted light is read at right angles to the exciting light (see discussion). LA: left atrium, LV: left ventricle.

4.2.5 Evaluation of the Linearity of the Fluorescent signal

The linearity of the fluorescent signals with respect to the dye concentration was evaluated in the following manner.

With the exception of the blue dye, one mL of each fluorescent dye was obtained from the stock solution and the six 1-mL solutions were pooled, yielding a new 6-mL solution which contained 6 different fluorescent dyes. Nine serial dilutions with different fluorescent dye concentrations were made from this new solution. Each dilution was then divided into two equal half and one gram of myocardial tissue was added to one of them. Two nine-serial dilutions were thus produced, with one containing pure fluorescent dyes, the other a mixture of fluorescent dyes and myocardial tissue. The linearity of the fluorescent signals of the pure samples and the microsphere-myocardium mixed samples was evaluated by reading fluorescent intensity of each sample from the serial dilutions.

4.2.6 RMBF Calculation and Statistics

4.2.6.1 RMBF calculation using coronary inflow as reference

The RMBFs for both the LCX and the left atrial injections were calculated using the formula

$$Fs = Is * Ft / It$$

where

Fs = flow rate per gram tissue sample (mL/min/g)
Is = intensity of fluorescence per gram tissue sample (units/g)
Ft = total flow rate to the LCX area (mL/min)
It = total intensity of fluorescence of the LCX area

The blood flow of the LCX area (**Ft**) was used as a flow reference and measured with the electromagnetic flow transducer.

4.2.6.2 RMBF calculation using femoral artery blood as reference

The RMBF for the left atrial injection (n=5) was also calculated using the formula below for comparison.

$$Fi = Is * R / Iref$$

where

Fi = flow rate per gram tissue sample (mL/min/g)
Is = intensity of fluorescence per gram tissue sample (units/g)

R = reference withdrawal rate (mL/min)
Iref = fluorescence in the reference blood sample

4.2.6.3 Relative flow calculation

Relative flow was determined by:

$$\frac{\text{fluorescent intensity of each individual sample (units/g)}}{\text{mean fluorescent intensity from all samples (units/g)}}$$

4.2.6.4 Statistics

Linear regression was used to evaluate the linearity of fluorescent signals by correlating the fluorescent intensity to the number of microspheres (Glenny et al 1993). Linear correlation was used to estimate the similarity between two microsphere injection methods and the similarity between two fluorescent dye distributions. The similarity between two measurements were further assessed by the method of Bland and Altman (Lancet 1986) using the percent difference between two measurements.

4.3 RESULTS

4.3.1 Fluorescent Intensity of Pure Microsphere Samples Versus Fluorescent Intensity of Myocardium-containing Samples

Figure 4.2a and Figure 4.2b are the calibration curves showing the fluorescent intensity as a function of microsphere number for six different colours. Curves from the pure fluorescence samples (Figure 4.2a) are similar to the curves from the fluorescence plus the myocardial tissue samples (Figure 4.2b). Their combined emission spectrum is presented in Figure 4.3a and Figure 4.3b.

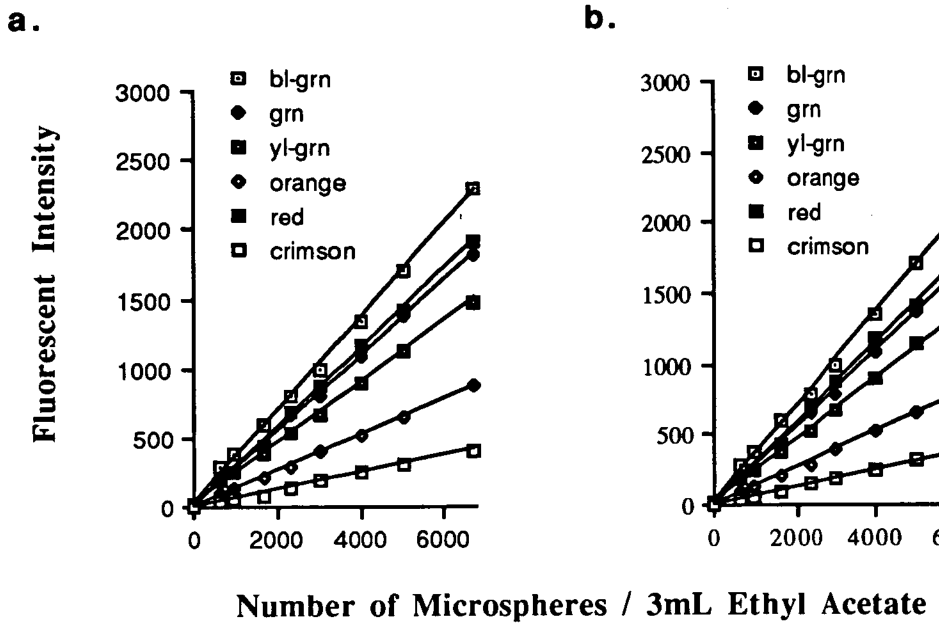

Figure 4.2 Calibration curves from six mixed dyes. a. Samples were made by mixing six dyes; b. Samples were made by mixing six dyes and one gram of myocardial tissue. Sensitivity: blue-green, green, yellow-green and orange=0.1, red and crimson=1. r>0.97.

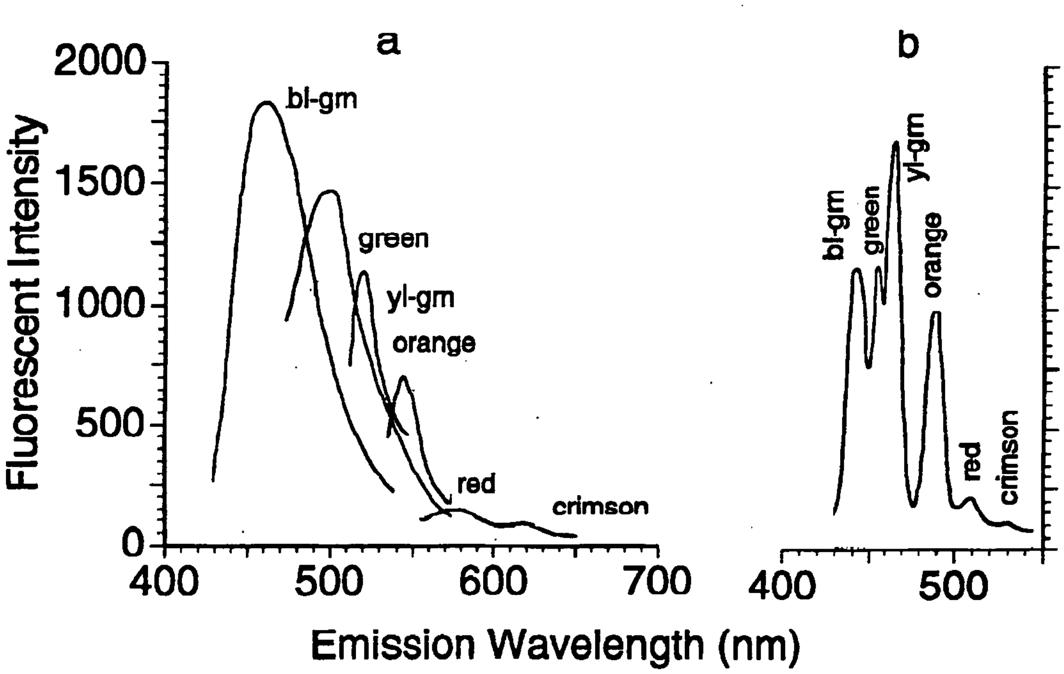

Figure 4.3 a. Combined emission spectrum of 6-colour mixture at their optimal excitations; b. Synchronous scan of 6-colour mixture using a 15 nm wavelength interval. Scan at a speed of 30 nm/minute, 5/5 slit widths.

4.3.2 Intrinsic Fluorescence in the Myocardium, the Blood and the Solvents

The results were similar to Abel's (Abel et al. 1993). At the blue excitation wavelengths (360 nm), an emission peak of 1571 fluorescent units/g of the myocardial tissue occurred at 430 nm. This corresponded to 7,500 blue microspheres. An excitation peak of 100 fluorescent units/ml of the blood was also recorded at the same excitation/emission wavelengths. Neither KOH nor ethyl acetate alone showed any significant fluorescent peaks. To avoid the natural excitation of the myocardium and the blood in the blue region, the blue microspheres were omitted from this study.

4.3.3 Myocardial Blood Flow Determination

The LCX supplied area was cut into 30 pieces on average; and an average of 17 pieces were obtained from the LAD supplied areas. The average weight of each piece was 1.1 g (0.5-1.5g). With four different dyes in each piece of the myocardial tissue per sheep for a total of two sheep, and two in another eight sheep, a total of 1128 readings were made. Injections had no discernible effect on the coronary or the systemic haemodynamics.

4.3.3.1 Comparison of the two injection methods and the distribution of different fluorescent dyes in the myocardium

Figure 4.4a. shows the RMBF from the two injection methods. Transmurally, the average flow in both injections is identical: 0.97±0.17 mL/min/g. Although slight differences are seen in the RMBF between the endocardial, the middle and the epicardial layers for the two injection methods, the differences are not significant. The correlation of the RMBF between these two methods is excellent ($r=0.92$, $n=107$, Figure 4.4b), and there is a good agreement between these two methods (Figure 4.4c). Both methods resulted in a similar distribution of the different coloured microspheres in the myocardium (Figure 4.5 and Figure 4.6).

a.

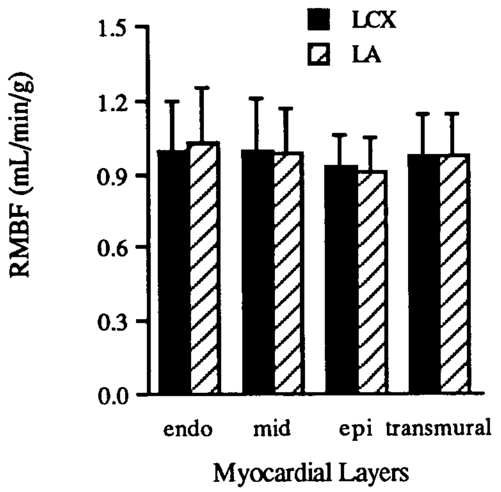

Figure 4.4a Comparsion of RMBF determined by the LCX and the left atrial (LA) injection methods (n=8, all non-significant).

b.

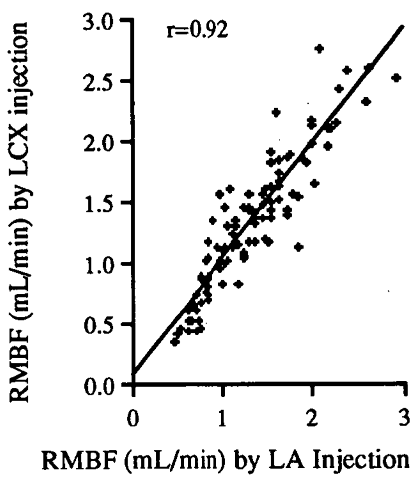

Figure 4.4b Flow correlation between the LCX and the left atrial injection methods (107 myocardial pieces of four sheep).

c.

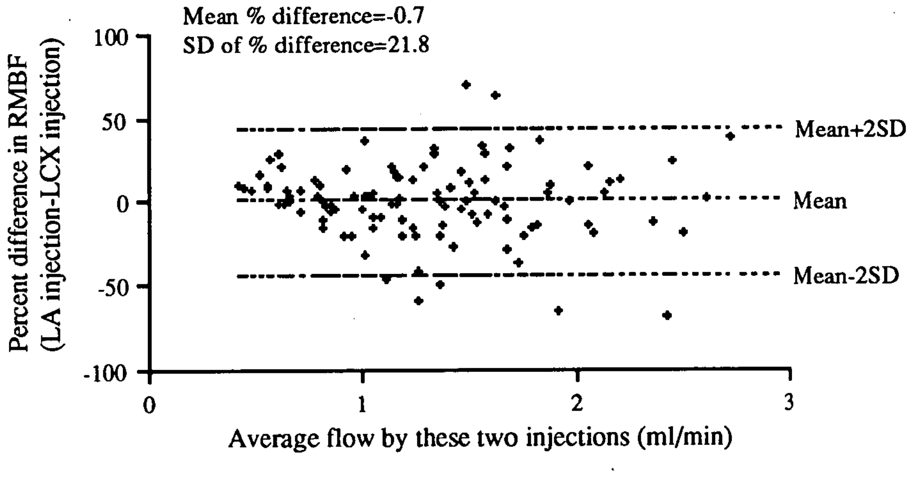

Figure 4.4c Percent difference between regional flow determined by the left atrial (LA) and the LCX injections as a function of average flow by the two injection methods.

a.

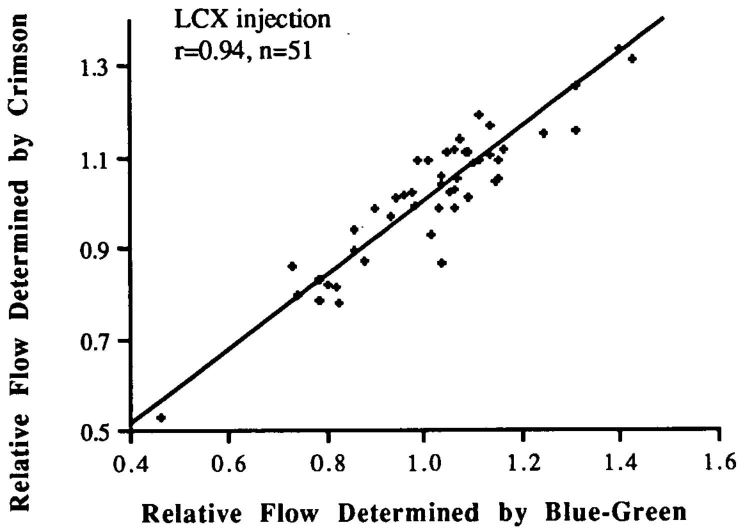

Figure 4.5a Comparison of crimson vs blue-green microsphere distributions to all layers of the myocardial wall.

b.

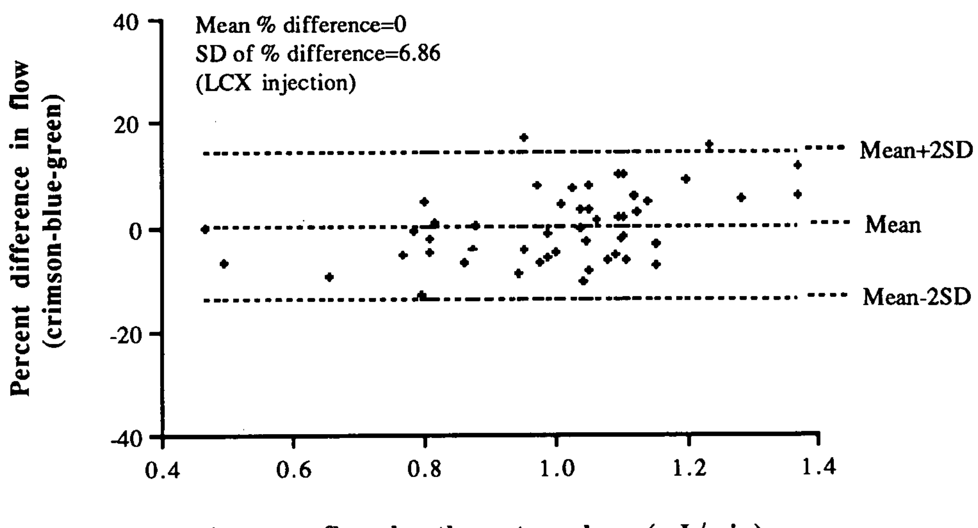

Figure 4.5b Percent difference between regional flow determined by crimson and blue-green as a function of average flow by these two dyes.

a.

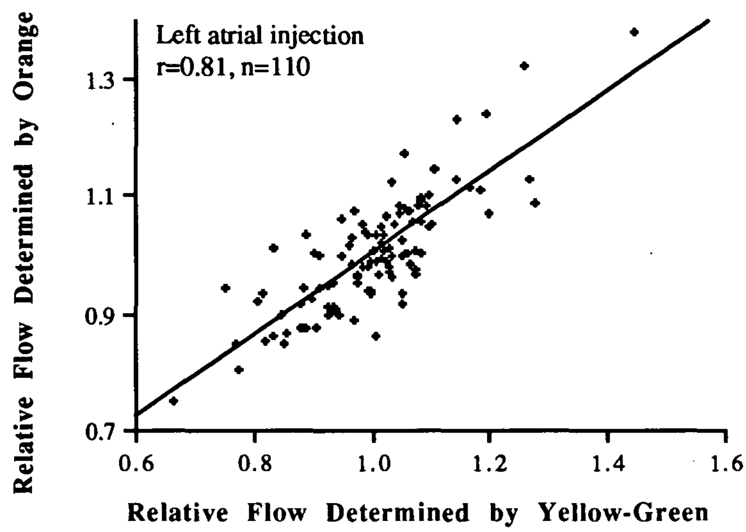

Figure 4.6a Comparison of orange vs yellow-green microsphere distributions to all layers of the myocardial wall.

b.

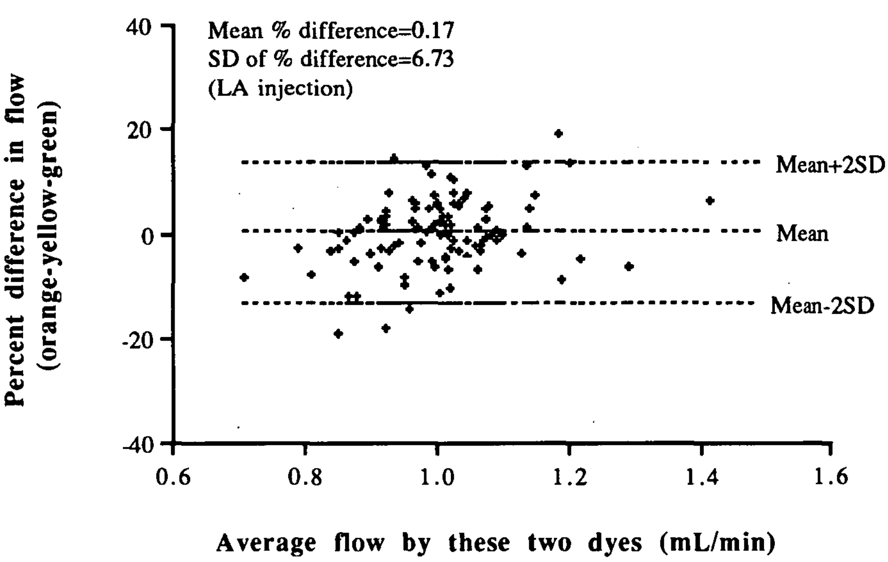

Figure 4.6b Percent difference between regional flow determined by orange and yellow-green as a function of average flow by these two dyes.

4.3.3.2 Comparison of two calculation methods

The traditional arterial reference method and the electromagnetic flowmeter measurements were compared and great discrepancies were found in the results between these two methods (Table 4.2). Possible reasons are amplified in the discussion.

Table 4.2 Myocardial Blood Flow Measured By Electromagnetic Flow Transducer And Fluorescent Microspheres

Sheep No.	Body Wt (kg)	Heart Wt of LCX region (g)	LCX flow F_1 (mL/min)	F_2 (mL/min/g)	RMBF (mL/min/g) Fc	Fl	Fi
1	25.00	24.57	23.20	0.94	0.90	0.89	7.09
2	30.00	33.94	27.50	0.81	0.79	0.83	4.23
3	35.00	32.86	28.71	0.87	0.88	0.89	6.43
4	35.00	40.75	33.30	0.82	0.83	0.83	4.82
5	41.00	51.02	40.04	0.78	0.92	0.89	3.62
mean	33.20	36.63	30.55	0.85	0.86	0.87	5.24
SD	6.02	9.89	6.41	0.06	0.05	0.03	1.47
P					NS	NS	0.002

F_1: Flow to the left circumflex coronary artery measured by electromagnetic flow probe

F_2: F_1/g of myocardium weight

Fc: RMBF determined by the LCX injection

Fl: RMBF determined by the left atrial injection

Fi: RMBF calculated by using the femoral arterial blood as reference

P value: Fc, Fl and Fi VS F_2 respectively

4.4 DISCUSSION

4.4.1 Principle Involved in the Use of Fluorescent Microspheres

The measurement of blood flow to small myocardial regions can not be made with flowmeters or the direct Fick technique, since the vascular inflow to and outflow from these regions can not be isolated. It is therefore necessary to use techniques involving an indicator which is distributed to various myocardial regions in proportion to the regional blood flows. The indicator should be trapped in the myocardium. By determining the amounts of indicator remaining in the regions, the regional flow can be calculated by comparing to a reference blood flow. Fluorescent dye is one of the latest indicators.

Fluorescent microspheres are polystyrene latex beads in which different fluorescent dyes are encapsulated. By using different colours the flow can be measured several times in one experiment. The principle of the method is to inject the well mixed microspheres into the blood upstream from the target organ. After the experiment, the organ is sectioned into the desired number of pieces, each tissue sample is digested to liberate the microspheres, and the fluorescence in the tissue hydrolysate is extracted with an appropriate solvent that dissolves the microspheres and the fluorescent dyes. In another variation, the microspheres are collected by filtration through a polyester filter, which removes the soluble fluorescent substances originating from the tissue hydrolysate which may cause interference with subsequent measurement of the microsphere fluorescence. The filtered microspheres are dissolved, and the fluorescence of the dye-containing solvent is then quantitated with a fluorometer.

Several important factors have to be considered in order to accurately measure the flow distributions within an organ (Heymann et al. 1977). These factors are discussed below.

4.4.1.1 Dispersed state of microspheres

Aggregation of the microspheres should be minimised by all means to ensure an even distribution of the microspheres in the bloodstream. Since the microspheres are polystyrene-based, they always retain some hydrophobic characteristics which make them tend to aggregate. According to others' reports (Heymann et al. 1977) and the author's experience, the following techniques can minimise the aggregation: a. keep the microsphere suspensions dilute and pure; b. add an appropriate amount of Tween 80; c. mechanically and ultrasonically agitate the microsphere suspension before injection; d. mix the suspension with warm blood immediately before injection. In this study, microsphere suspensions were checked under the microscope before each injection to ensure that there was no aggregation.

4.4.1.2 Number of microspheres injected

More than 200 microspheres per tissue sample should be injected to ensure an adequate fluorescent signal (Glenny et al. 1993), and more than 400 microspheres per tissue sample should be injected to minimise statistical errors (Buckberg et al. 1971; Dole et al. 1982). In the author's own measurement, it was ensured that there were at least 1000 microspheres per tissue sample.

4.4.1.3 Complete entrapment of the microspheres in the vascular beds of the organ

The microspheres should trap in the vascular beds of the target organ during the first circulation, and must remain entrapped until the termination of the experiment. This requires the proper size of microspheres. According to Utley et al. (1974), microspheres which approximate red cell diameter (9-10μ) are the best for measuring regional myocardial blood flow. Experiments in ovine and canine hearts showed that 99% of the microspheres with a diameter of 8-10μ were trapped in the coronary circulation after being injected into the left ventricle or the left atrium (Buckberg et al. 1971; Utley et al. 1974).

4.4.1.4 Lodging of the microspheres in the capillary must have no effect on local perfusion

The microspheres lodge in only a few capillaries, but the number of microspheres trapped per unit of myocardial tissue is directly proportional to the myocardial blood flow to that region. Hales and Cliff (1977) observed directly, in a rabbit ear chamber preparation, that 15μm spheres lodged in precapillary sphincter regions and capillaries and did not stop the flow of erythrocytes (Hales and Cliff 1977).

4.4.2 Evaluation of Fluorescent Technology

The linear correlation coefficient between the fluorescent intensity and the number of microspheres was > 0.97 for all colours. This linear relationship held over the range of 600 to 7,000 microspheres per 3 ml of solvent, indicating that both low and high flows were accurately measured. The similarity between the curves from the pure fluorescence samples (Figure 4.2a) and the curves from the fluorescence plus the myocardial tissue samples (Figure 4.2b.) suggests that extraction of the six fluorescent dyes (blue-green, yellow-green, green, orange, red and crimson) directly from the aqueous solution using ethyl acetate is extremely efficient and effective. This method not only reduces the sample processing time but also the container transfer, thus lessening the chances of error due to the loss of microspheres. According to Glenny et al. (1993) microsphere loss is the most important source of error in fluorescent technology, and therefore this method is superior to the filtering method used in other studies (Glenny et al. 1993).

However limitations do exist. The blue colour was avoided because of the intrinsic blue fluorescence of the myocardium and the blood. If the blue colour is to be used, then the intrinsic blue fluorescence of these media has to be corrected from the flow calculation. Xylene was also avoided because of the difficulty in separating the aqueous from the organic layers. Finally, if the flow reference is obtained by collecting an arterial reference sample, the filtering method should be used. This is because extraction of fluorescence directly from the blood was always incomplete, resulting in an overestimation of the regional blood flow (Table 4.2). The myocardial samples were not filtered, and in order to keep the method uniform, the arterial reference samples were therefore not filtered.

4.4.3 Evaluation of Direct Coronary Artery Injection

As shown in Figure 4.4c, most of the flow differences between the direct coronary injection and the traditional left atrial method lie between the mean±2SD, suggesting a good agreement between these two methods (Bland & Altmna 1986). Traditionally, the use of the left atrial injection is to ensure adequate microsphere mixing in blood (Heymann et al. 1977). Comparing to the LCX injection, this technique requires at least 20 times the number of microspheres since the heart receives about 5% of the cardiac output, which makes this technique much more expensive. The use of the intracoronary injection described earlier (Kowallik et al. 1991; Schulz et al. 1989) differed from the direct coronary injection in this study. In the former method, the coronary inflow was controlled by a pump in an extracorporeal circuit. It was unsuitable for the intention of producing subendocardial ischaemia in situ in later studies. In this study, to ensure even distribution of microspheres in the bloodstream, the microspheres were first mixed with heparinised warm blood, and then slowly injected in a direction opposing the blood flow. The results (Figure 4.4) showed that RMBF measurement could be achieved by this method without affecting the coronary circulation. This technique of direct coronary injection uses only 1/20th of the number of microspheres required by the traditional left atrial injection method, which greatly reduces the cost, making the microsphere technique more feasible and far more economical.

4.4.4 Distribution of Different Fluorescent Dyes in the Myocardium

Different fluorescent dyes were also injected simultaneously in the same animals by both coronary artery injection and left atrial injection. Figures 4.5 and 4.6 demonstrate that the fluorescent dyes, per se, had no significant effect on microsphere distribution.

4.4.5 Evaluation of Calculation Methods

All the results were calculated using the coronary inflow as the reference flow. Traditionally, the reference flow was measured at the time of microsphere injection by collecting an arterial reference sample (Makowski et al. 1968). In five experiments, the arterial reference flow samples were also collected from the femoral artery. As summarised in Table 4.2, the flow was approximately six times that measured by electromagnetic flow transducer (5.24±1.47 mL/min/g vs. 0.85±0.06 mL/min/g, n=5, $P<0.001$), which was obviously unrealistically high. Nonetheless the RMBF calculated using the coronary inflow as reference was 0.86±0.05 mL/min/g by the LCX injection, and 0.87±0.03 mL/min/g by the left atrial injection, which was identical to the flow (0.85±0.06 mL/min/g) measured by the electromagnetic flow transducer. These values were also similar to those measured by other workers using radio-labelled microspheres in the same species (0.88±0.28 mL/min/g, n=11, anaesthetised sheep, Bassingthwaighte et al. 1990; 1.19±0.5mL/min/g, n=6, awake sheep, Archie et al. 1974; 1.33±0.14 mL/min/g, n=12, awake sheep, Nesarajah et al. 1983).

The most plausible explanation for the overestimation of RMBF is the disproportionately low fluorescence in the arterial reference sample (Domenech et al. 1969). A comparison with pure fluorescent samples demonstrated that less than 30% of the fluorescence was extracted from the arterial reference samples due to the immediate clotting of the blood on addition of KOH. As a result, the fluorescence was underrepresented in the arterial reference samples due to the incomplete extraction. Another possible explanation is the anatomical configuration of the aortic arch in sheep (Heymann et al. 1977; Buckberg et al. 1971), because their brachiocephalic trunk arises just above the aortic valve and incomplete mixing or streaming occurs in this region (Heymann et al. 1977; Buckberg et al. 1971). Ideally, the reference samples should be obtained from both the upper and the lower arteries

(Heymann et al. 1977). In this study, the reference samples were only obtained from the femoral artery, which might increase the reference error.

In order for the reference sample technique to be accurate, several factors should be considered. Firstly, the number of microspheres present needs to be more than 400 (Buckberg et al. 1971). Secondly, the concentration of microspheres in the reference sample has to be representative of that target organ (Heymann et al. 1977). For any given injection dose, changes in blood withdrawal period and speed can cause a change in microsphere number in the reference sample (Domenech et al. 1969; Dole et al. 1982). Furthermore, the anatomical configuration of the animal, as discussed above, also influences the regional microsphere distribution. Compared to the arterial reference technique in this experiment, the use of the coronary inflow as the reference flow is simpler and has less chance of reference error (Dole et al. 1982; Austin et al. 1989).

4.4.6 Advantages of Fluorescent Microspheres

There are three different types of microspheres currently available, ie, radioactive microspheres, coloured microspheres and fluorescent microspheres. Radioactive microspheres have become the gold standard for measuring regional organ perfusion since their first introduction by Rudolf and Heyman in 1967. Unfortunately, because of the radioactivity, these microspheres pose health risks, require special precautions for use and disposal, have limited shelf-lives, and consequently are relatively expensive.

Coloured microspheres are nonradioactive. The different coloured spheres can be easily distinguished under the microscope and counted. They are cheap to buy, and the equipment needed is simple, but preparing the samples is time consuming and labour intensive, and the samples must be small. There is also some question about the ability of these spheres to measure high flows as compared with radioactive microspheres (Hale et al. 1988).

Fluorescent microspheres are new products which have a longer shelf life (at least one year) and are cheaper in price. In addition, fluorescent methods have other three significant advantages over radioactive technology (Glenny et al. 1993). First, fluorescent colours are easily separable because each colour has a unique and narrow excitation spectra. This selectivity can be further enhanced by narrowing the slit width of the emission monochrometer so that only emitted light within a narrow spectral range is measured. Measurement of multiple fluorescent colours within a sample can be accomplished by reading the sample multiple times with specific matched excitation and emission wavelength filters for each colour. The second advantage is that since the emitted light can be read at right angles to the exciting light, there is no background signal from which the fluorescent signal must be measured. The third advantage is that fluorescent methods have a greater range of linearity. Both the radioactive microsphere and the colour microsphere methods require corrections for signal spillover into adjacent spectral windows, which make these techniques more complicated (Kowallik et al. 1991; Schosser et al. 1979). The ability to resolve the separate fluorescent signals without having to correct for spillover also removes one more potential source of error in data collection (Zwissler et al. 1991).

4.5 SUMMARY

1. The use of a fluorescent technique without filtering the myocardial tissue was investigated. The calibration curves from the fluorescence plus myocardial tissue samples were similar to those of the pure fluorescence samples, and both showed a linear relationship between fluorescent intensity and the number of microspheres ($r>0.97$). These results indicated that the extraction of six fluorescent dyes (blue-green, yellow-green, green, orange, red and crimson) directly from the aqueous solution using ethyl acetate is effective.

2. Injection of fluorescent-labelled microspheres directly into the coronary artery was compared with the left atrial injection. There was a good correlation in the measurement of RMBF between these two injection methods ($r=0.92$, $n=107$ data points). Injection into the coronary requires less fluorescent-labelled microspheres (1/20th of that required by the atrial injection) and is more economical.

3. RMBF calculation using the coronary inflow as the reference flow was also compared with that using the traditional method. In this study, in which nonfiltering technique was applied, using the coronary inflow as the reference flow was superior to the conventional distal sampling method.

Chapter 5

THE SUBENDOCARDIAL ISCHAEMIC MODEL AND ITS VALIDATION

To explore the origin of ischaemic ST depression, it is essential to have a reliable subendocardial ischaemic model. This study was designed to develop a subendocardial ischaemic model in sheep and to validate this model.

5.1 METHOD

5.1.1 Animal Groups

Eighteen sheep of both sexes were used in this study. They were randomised into three groups as described below and in Table 5.1.

Group 1 Pacing alone (n=5): The left atrium was paced with an initial rate of 120 beats/min (bpm), and increased gradually by 10 bpm every 2 minutes to 180 bpm. The regional myocardial blood flow (RMBF) was measured before and at 20 minutes of pacing by the left atrial microsphere injection method.

Group 2 Subendocardial ischaemia in the left circumflex coronary artery (LCX) territory: Five animals from the study mentioned in chapter 4 were used. Posterior subendocardial ischaemia was produced by a combination of the LCX partial ligation and pacing. The occurrence of ischaemia was validated by measuring the RMBF before and during the LCX stenosis. For comparison, both the left atrial and the LCX microsphere injection methods were applied.

Group 3 Subendocardial ischaemia in alternate LCX or left anterior descending coronary artery (LAD) territory (n=8): Posterior and anterior subendocardial ischaemia were produced in the same animal by alternate LCX or LAD partial ligation coupled with pacing. Each partial ligation lasted for 20 minutes, followed by 30 minutes rest before the next partial ligation. The RMBF was measured before and 20 minutes after each artery ligation by the left atrial injection method.

Table 5.1 Animal groups and treatment

group	n	treatment	RMBF measurement
1	5	pacing, 180bpm	left atrial injection
2	5	LCX partial occlusion with pacing	left atrial and LCX injections
3	8	alternate LAD/LCX occlusion with pacing	left atrial injection

5.1.2 Subendocardial Ischaemia

In groups 2 and 3, coronary artery stenosis was achieved by inflating the hydraulic occluder causing a flow reduction to about 50% of the control level, then the left atrium was paced by a stimulator (SRI, England). The pacing started with a rate of 120 beats/min (bpm), and increased gradually by 10 bpm every 2 minutes until it reached 180 bpm. Subendocardial ischaemia was considered to occur when the intracavity leads showed ST segment elevation and the epicardial leads showed ST depression (Guyton et al. 1977).

5.1.3 Perfusion Beds and Regional Myocardial Blood Flow Measurement

After completion of the experiment, 10 mL of 0.1% methylene blue dye (Sigma) were injected into the LAD, and 10 mL of normal saline were simultaneously injected into the LCX to delineate the nonischaemic and the ischaemic areas respectively. The ischaemic boundary was expected to be well defined due to fewer functionally significant collateral blood vessels (Markovitz et al. 1989). The LCX and the LAD supplied areas were cut into 30 pieces on average. The average weight of each piece was 1.1 g (0.5-1.5g). The fluorescent microsphere technique for the RMBF measurement was as described in chapter 4.

5.1.4 Epicardial and Endocardial Electrogram Recording

The epicardial electrograms were recorded by the sock electrodes as described in chapter 3. For group 2, the endocardial electrograms were recorded by a 4-pole electrode catheter. For group 3, the endocardial electrograms were recorded by the basket apparatus as described in chapter 3.

The haemodynamic measurements, the animal preparation and instrumentation were as described in chapter 3.

5.2 RESULTS

5.2.1 Tachycardia Without Stenosis

The haemodynamic and the flow responses to pacing are shown in Tables 5.2 and 5.3, and Figure 5.1. Pacing alone to the rate of 180 bpm increased the left ventricular pressure and the left atrial pressure slightly, but the increase was not significant (Table 5.2). There was a similar increase in the anterograde coronary flow (measured by an electromagnetic flow meter) and RMBF (measured by microspheres) to each third of the myocardium (Tables 5.2 and 5.3, Figure 5.1). Although the RMBF to the epicardial third increased slightly more than that to the endocardial third, the endo/epi flow ratio reduction was not significant (P>0.05, Table 5.3).

Table 5.2 Haemodynamic changes before and during pacing

sheep	LCX flow (mL/min)		LVEDP (mmHg)		LVSP (mmHg)		LAP (mmHg)	
	control	pace	control	pace	control	pace	control	pace
1	40	47	2	2	80	87	1	0
2	26	34	3	3	81	88	2	7
3	39	50	2	2	92	90	2	7
4	32	35	1	2	97	101	-3	-3
5	30	40	3	5	77	80	2	5
mean	34	41	2	3	85	89	1	3
SD	6	7	1	1	9	8	2	5
P		0.01		0.15		0.09		0.10

LCX flow: flow to the left circumflex coronary artery territory measured by flow probe

LVEDP: left ventricular end-diastolic pressure.

LVSP: left ventricular systolic pressure.

LAP: mean left atrial pressure.

Table 5.3 Regional myocardial blood flow (mL/min/g) before and during pacing

sheep	endo		mid		epi		transmural		endo/epi ratio	
	control	pacing	control	pacing	control	pacing	control	pacing	control	pacing
1	1.35	1.50	1.51	1.79	1.05	1.48	1.30	1.59	1.29	1.01
2	0.94	1.22	0.96	1.18	0.86	1.06	0.92	1.15	1.09	1.15
3	1.32	1.37	1.12	1.24	0.94	1.19	1.13	1.27	1.40	1.15
4	0.89	1.05	0.82	0.97	0.79	0.95	0.83	0.99	1.13	1.11
5	1.21	1.43	1.20	1.47	1.08	1.42	1.12	1.39	1.12	1.01
mean	1.14	1.31	1.12	1.33	0.94	1.22	1.06	1.28	1.21	1.09
SD	0.21	0.18	0.26	0.31	0.12	0.23	0.19	0.23	0.13	0.07
P		0.01		0.00		0.01		0.00		0.13

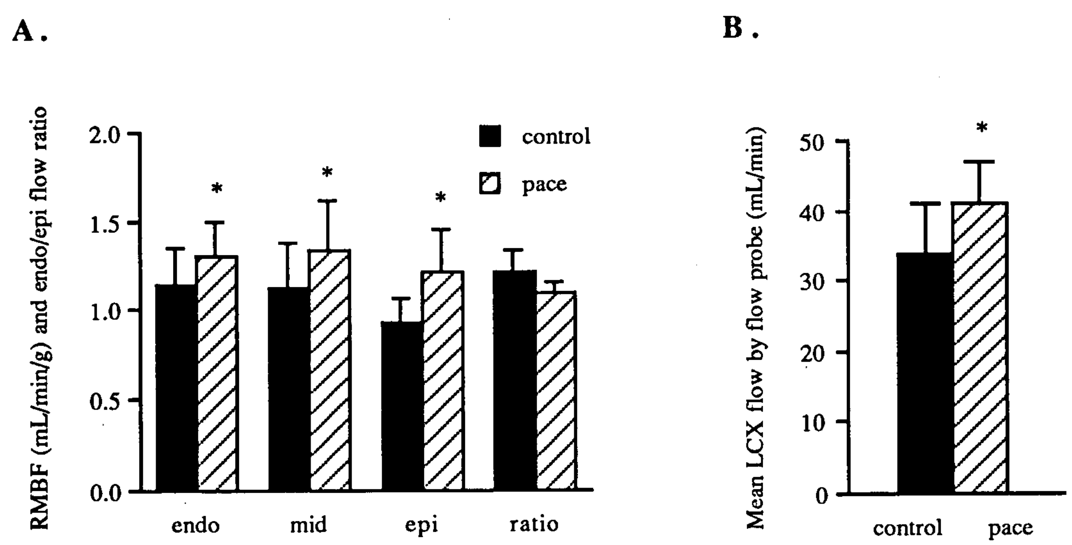

Figure 5.1 (A) Mean RMBF and endo/epi flow ratio measured by microspheres at control and pacing at a rate of 180 bpm. (B) Simultaneous measurement of mean coronary blood flow by magnetic flow probe (n=5, *P<0.05 VS control).

5.2.2 LCX Stenosis With Tachycardia

The flow and the haemodynamic responses to partial LCX ligation with pacing are presented in Table 5.4 and Figure 5.2. Partial stenosis with tachycardia caused a marked decrease in flow to the endocardial third of the ischaemic area, from 0.90±0.09 to 0.34±0.12 mL/min/g (66% decrease, $p<0.05$) in the LCX injection method; from 0.93±0.08 to 0.31±0.07 mL/min/g (67% decrease, $P<0.05$) in the left atrial injection method. However, flow to the epicardial third was unchanged with the LCX injection, from 0.88±0.03 to 0.75±0.22 mL/min/g (NS), but decreased slightly with the left atrial injection, from 0.87±0.07 mL/min/g to 0.61±0.09 mL/min/g (29% decrease, $P<0.05$). There were no significant differences between the LCX injection and the left atrial injection methods for either the control flow or the ischaemic flow (all $P>0.05$, Table 5.4). The endo/epi flow ratios (Figure 5.2C) in the ischaemic region (LCX territory) reduced from 1.04±0.12 to 0.47±0.17 in the LCX injection (55% decrease, $P<0.05$) and from 1.08±0.12 to 0.51±0.05 in the left atrial injection (53% decrease, $P<0.05$) during ischaemia. The ratio in the nonischaemic region (the LAD territory) was unchanged (1.12 ± 0.26 to 1.01±0.22, NS, left atrial injection) (Figure 5.2C). The LCX flow reduced by 50% (from 31 mL/min to 16 mL/min, Table 5.4) during ischaemia. The decrease in the carotid artery pressure was not significant ($P>0.05$, Table 5.4).

Table 5.4 Myocardial blood flow and haemodynamics before and during ischaemia

Sheep	AP (mmHg)		LCX flow (mL/min)		RMBF (mL/min/g)											
					left atrial injection						LCX injection					
					endo		mid		epi		endo		mid		epi	
	contr	isch	contr	isch	contr	isch	contr	isch	contr	isch	contr	isch	contr	isch	contr	isch
1	75	73	23	13	1.01	0.35	0.86	0.56	0.90	0.65	0.95	0.23	0.95	0.53	0.88	0.80
2	80	68	28	10	0.98	0.30	0.91	0.42	0.79	0.58	0.92	0.33	0.92	0.45	0.83	0.50
3	78	75	33	14	0.86	0.21	1.02	0.34	0.80	0.50	0.89	0.33	0.95	0.37	0.87	0.55
4	84	75	29	19	0.98	0.41	0.82	0.60	0.90	0.73	0.98	0.27	0.79	0.56	0.91	0.86
5	83	75	40	25	0.84	0.30	0.89	0.38	0.94	0.60	0.76	0.53	0.96	0.67	0.91	1.04
mean	80	73	31	16	0.93	0.31	0.90	0.46	0.87	0.61	0.90	0.34	0.91	0.52	0.88	0.75
SD	4	3	6	6	0.08	0.07	0.08	0.11	0.07	0.09	0.09	0.12	0.07	0.11	0.03	0.22
P1		0.07		0.01		0.00		0.03		0.00		0.00		0.01		0.08
P2											0.18	0.73	0.37	0.35	0.49	0.22

AP: carotid artery pressure.

contr: control

isch: ischaemia

LCX flow: flow to the left circumflex coronary artery territory measured by electromagnetic flow probe.

P1: P value of ischaemia versus control.

P2: P value of left atrial injection versus LCX injection.

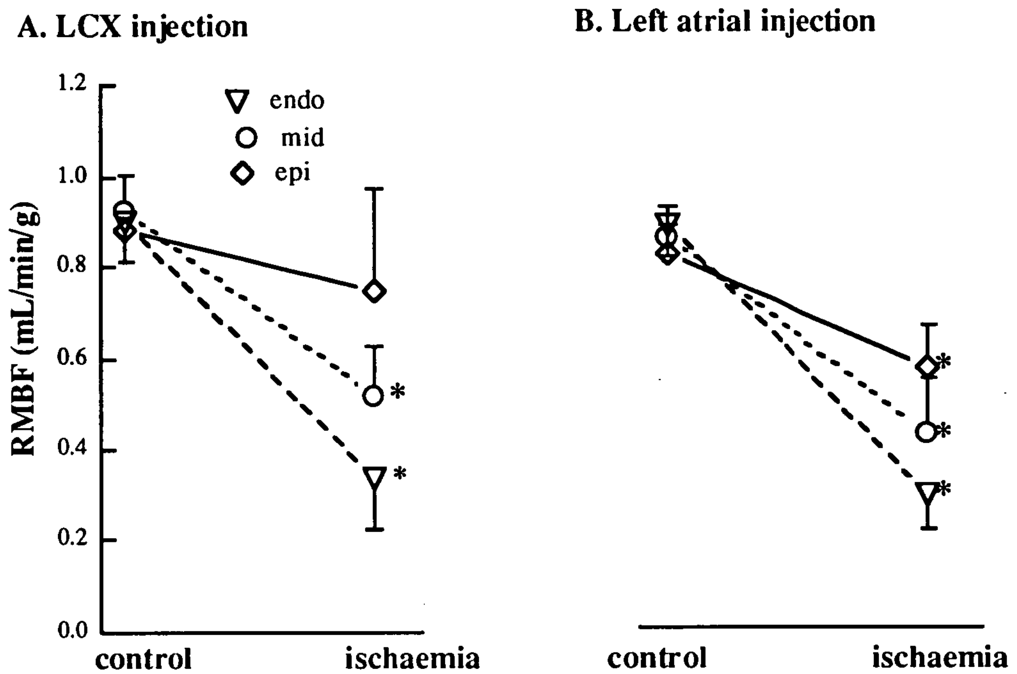

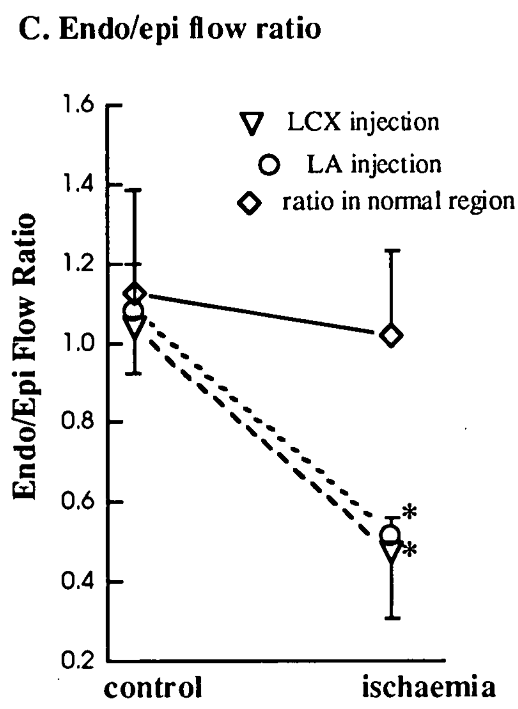

Figure 5.2 RMBF determined by LCX injection (A) and left atrial injection (B) before and during ischaemia.

C. Endo/Epi flow ratio before and during ischaemia, n=5. (*P<0.05, student's paired t test).

5.2.3 Alternate LCX or LAD Stenosis With Tachycardia

In 5 of the 8 animals, regional ischaemia was induced in different territories by alternate LAD/LCX ligation coupled with pacing. In 3 animals, both the anterior and posterior ischaemia developed during the second ligation, and the data were excluded.

Changes in haemodynamics and myocardial blood flow by ischaemia are tabulated in Table 5.5. In the LAD ligation, the ischaemia was accompanied by a slight increase in the left ventricular end-diastolic pressure and a decrease in the left ventricular systolic pressure ($P<0.05$, Table 5.5). However, pressure changes were not significant in the LCX ligation. The LAD bed weighed 54±3%, and the LCX bed 46±3% of the left ventricle respectively. Either the LAD or the LCX ligation caused a similar 41% flow reduction to the corresponding territory (from 39±5 mL/min to 23±5 mL/min, and from 34±8 mL/min to 20±6 mL/min, respectively).

Table 5.5 Haemodynamic changes before and during ischaemia

LAD ligation	% Wt of LV	CBF (mL/min)		LVSP (mmHg)		LVEDP (mmHg)		LAP (mmHg)	
		contr	isch	contr	isch	contr	isch	contr	isch
1	58	39	20	87	84	1	4	4	4
2	51	41	30	78	72	-3	1	0	0
3	55	37	21	102	86	2	6	1	11
4	55	46	25	71	43	3	13	0	14
5	52	31	19	105	78	4	6	-1	1
mean	54	39	23	89	73	1	6	1	6
SD	3	5	5	15	17	3	4	2	7
P			0.00		0.04		0.03		0.16
LCX ligation									
1	42	34	22	103	91	0	0	6	4
2	49	38	21	64	69	3	3	0	5
3	45	35	21	85	57	-1	9	0	10
4	45	40	25	85	63	1	12	-1	12
5	48	21	10	96	100	8	8	1	1
mean	46	34	20	87	76	2	6	1	6
SD	3	8	6	15	19	4	5	3	4
P			0.00		0.18		0.19		0.13

For LAD ligation, % Wt of LV = weight of LAD territory/weight of left ventricle x 100%;

CBF = LAD flow measured by magnetic flow probe.

For LCX ligation, % Wt of LV = weight of LCX territory/weight of left ventricle x 100%;

CBF = LCX flow measured by magnetic flow probe.

contr: control; isch: ischaemia.

LVSP: left ventricular systolic pressure

LVEDP: left ventricular end-diastolic pressure

LAP: mean left atrial pressure.

The transmural flow distributions at 20 minutes of ischaemia in the ischaemic and the nonischaemic regions are displayed in Tables 5.6 and 5.7 respectively. In the ischaemic regions (Table 5.6), stenosis with tachycardia caused a marked decrease in flow to the endocardial third, from 1.04±0.10 to 0.55±0.11 mL/min/g with the LAD ligation (47% decrease, $p<0.01$), from 1.13±0.13 to 0.58±0.06 mL/min/g with the LCX ligation (48% decrease, $p<0.01$). Flow to the epicardial third had a less significant change, from 0.83±0.06 to 0.74±0.06 mL/min/g in the LAD ligation (11% decrease, $P>0.05$), from 0.94±0.18 to 0.74±0.06 mL/min/g in the LCX ligation (19% decrease, $p<0.05$). The endo/epi flow ratios (Table 5.6, Figure 5.3) decreased from 1.25±0.08 to 0.74±0.10 mL/min/g (41% decrease, $P<0.01$) with the LAD ligation, and decreased from 1.23±0.26 to 0.78±0.11 mL/min/g (36% decrease, $P<0.05$) with the LCX ligation. In the nonischaemic regions, flow to the inner third also decreased slightly (20% reduction with the LAD ligation, $P=0.05$; 13% reduction with the LCX ligation, $P>0.05$, Table 5.7), but endo/epi flow ratio had no significant change with the LAD ligation (from 1.26±0.17 to 1.09±0.32, $P>0.05$), and only marginally decreased with the LCX ligation (from 1.22±0.22 to 1.05±0.22, $P=0.04$). Comparisons of the haemodynamic and the flow variables between the LAD and the LCX ligations showed that there were no differences in these variables (Table 5.8). The weight of the LAD territory was slightly greater than the LCX territory (54±3 VS 46±3 % of left ventricle, $P<0.05$, Table 5.8).

Table 5.6 RMBF(mL/min/g) in ischaemic areas before and during ischaemia

LAD ligation	control mL/min/g			ischaemia mL/min/g			ischaemia % of control			endo/epi flow ratio: ratio		endo/epi flow ratio: % of control
	endo	mid	epi	endo	mid	epi	endo	mid	epi	contr	isch	
1	1.02	1.03	0.84	0.65	0.74	0.75	64	72	89	1.22	0.87	71
2	0.99	0.86	0.75	0.56	0.63	0.80	57	73	107	1.32	0.70	53
3	1.19	1.06	0.90	0.65	0.77	0.79	55	73	88	1.32	0.82	62
4	1.07	0.97	0.87	0.43	0.55	0.65	40	57	75	1.23	0.66	54
5	0.92	1.01	0.81	0.44	0.60	0.70	48	59	86	1.14	0.63	55
mean	1.04	0.99	0.83	0.55	0.66	0.74	53	67	89	1.25	0.74	59
SD	0.10	0.08	0.06	0.11	0.09	0.06	9	8	11	0.08	0.10	8
P				0.000	0.001	0.090					0.000	
LCX ligation												
1	1.03	0.94	0.83	0.59	0.69	0.75	57	74	91	1.24	0.78	63
2	0.99	0.90	0.95	0.54	0.63	0.68	55	70	71	1.04	0.80	77
3	1.17	1.24	1.09	0.63	0.77	0.81	54	62	75	1.07	0.77	72
4	1.30	1.21	1.15	0.49	0.69	0.79	38	57	69	1.13	0.62	55
5	1.18	1.01	0.70	0.65	0.67	0.69	55	66	99	1.69	0.94	56
mean	1.13	1.06	0.94	0.58	0.69	0.74	52	66	81	1.23	0.78	64
SD	0.13	0.16	0.18	0.06	0.05	0.06	8	7	13	0.26	0.11	10
P				0.001	0.002	0.040					0.007	

Table 5.7 RMBF(mL/min/g) in nonischaemic areas before and during ischaemia

LAD ligation	control			ischaemia						endo/epi flow ratio		
	mL/min/g			mL/min/g			% of control			ratio		% of
	endo	mid	epi	endo	mid	epi	endo	mid	epi	contr	isch	control
1	1.15	1.02	0.78	1.07	0.96	0.80	93	94	102	1.47	1.34	91
2	1.39	1.29	1.25	1.27	1.08	1.03	91	84	82	1.11	1.23	111
3	1.27	1.17	1.06	0.74	0.79	0.75	58	68	71	1.19	0.99	83
4	1.10	0.91	0.78	0.87	0.78	0.67	79	86	86	1.41	1.30	92
5	0.79	0.86	0.72	0.63	0.88	1.09	80	102	151	1.10	0.58	53
mean	1.14	1.05	0.92	0.92	0.90	0.87	80	87	98	1.26	1.09	86
SD	0.23	0.18	0.23	0.26	0.13	0.18	14	13	32	0.17	0.32	21
P				0.05	0.09	0.69					0.17	
LCX ligation												
1	0.98	0.95	0.76	0.93	0.86	0.72	95	90	95	1.29	1.29	100
2	0.98	0.95	0.89	0.70	0.69	0.69	72	73	78	1.09	1.01	92
3	1.11	0.73	0.74	0.84	0.78	0.72	76	107	98	1.50	1.17	78
4	1.08	1.02	0.85	1.10	0.99	1.01	101	97	119	1.28	1.09	85
5	0.81	1.00	0.88	0.75	1.01	1.06	93	101	120	0.92	0.71	77
mean	0.99	0.93	0.82	0.86	0.87	0.84	87	94	102	1.22	1.05	86
SD	0.12	0.12	0.07	0.16	0.14	0.18	13	13	18	0.22	0.22	10
P				0.10	0.29	0.81					0.04	

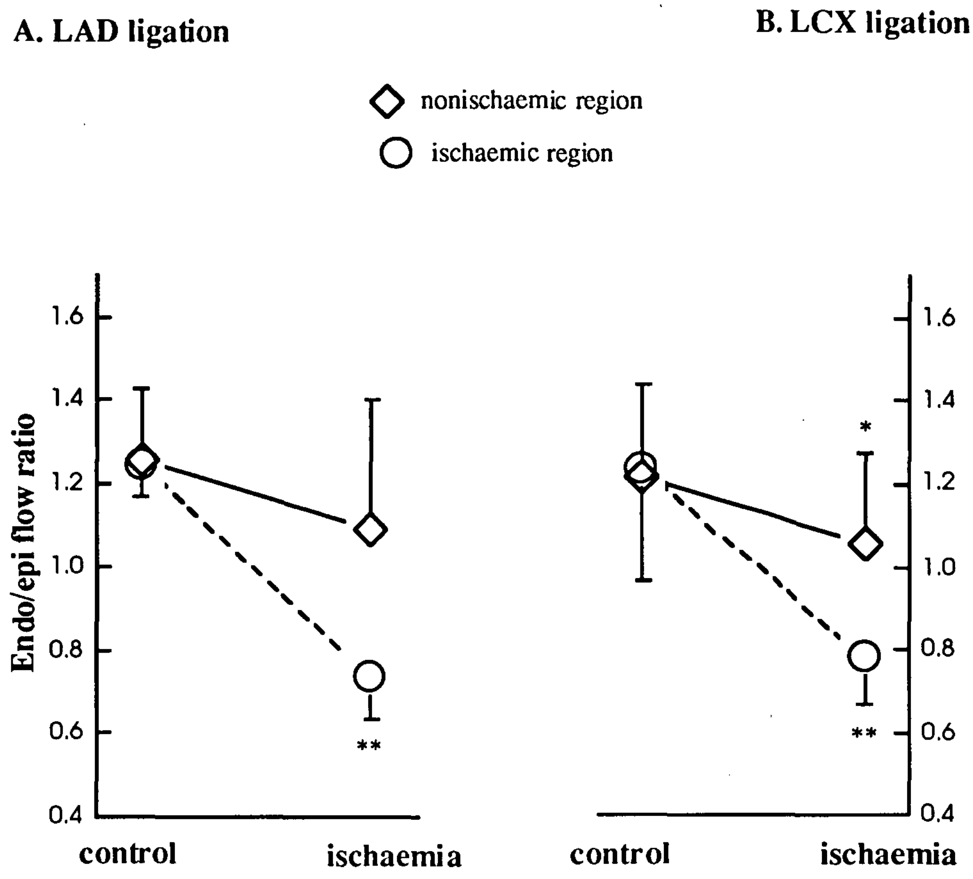

Figure 5.3 Endo/epi flow ratio with LAD (A) and LCX (B) ligations at control and 20 minutes of ischaemia. (n=5, *P<0.05, **P<0.01 VS control).

Table 5.8 Comparisons of haemodynamic and flow changes by LAD and LCX ligations

		LAD ligation	LCX ligation	P
Haemodynamics				
	% Wt of LV	54±3	46±3	<0.05
	LVSP	83±15	88±17	>0.05
	LVEDP	5±3	4±6	>0.05
	LAP	5±7	5±6	>0.05
	CBF	62±9	58±7	>0.05
RMBF				
ischaemic areas				
	endo	53±9	52±8	>0.05
	mid	67±8	66±7	>0.05
	epi	89±11	81±13	>0.05
	flow ratio	59±8	64±10	>0.05
normal areas				
	endo	80±14	87±13	>0.05
	mid	87±13	94±13	>0.05
	epi	99±32	102±18	>0.05
	flow ratio	87±21	86±10	>0.05

Values are mean±SD.

LVSP, CBF and RMBF are percent of the control value.

LVEDP and LAP are the differences between the control and the ischaemic values.

CBF: coronary blood flow measured by magnetic flow probe.

LAP: left atrial pressure.

LVSP: left ventricular systolic pressure.

LVEDP: left ventricular end-diastolic pressure.

% Wt of LV: the percent weight of the left ventricle for the LAD and the LCX territories.

5.2.4 Comparison of Flow Distributions Between Pacing Alone and Pacing With Stenosis

Figure 5.4 was plotted with the data from group 1 and group 3. As illustrated in this figure, at resting state, flow to the inner third of the myocardium is higher than to the outer third, which produced an endo/epi flow ratio > 1. Pacing alone increased myocardial blood flow, but did not alter transmural flow distribution because of the uniform flow increase across the ventricular wall. However, when one of the coronary arteries was partially constricted, pacing caused a marked fall in the blood flow to the subendocardial region supplied by that vessel. Although the flow to the epicardium also decreased, the change was not significant (P>0.05, data were the average of the LAD and the LCX ligations).

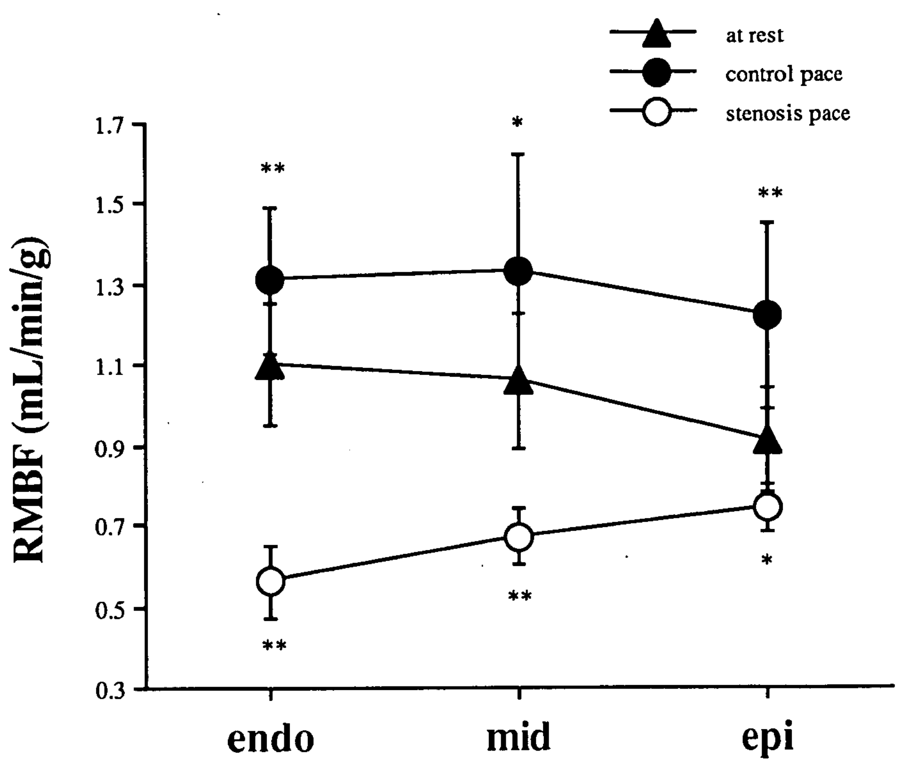

Figure 5.4 RMBF distributions across the left ventricular wall at rest (n=15), control pace (n=5) and stenosis pace (n=10). (*P<0.05, **P<0.01 VS the rest flow).

5.2.5 Spatial Myocardial Blood Flow Distributions

Figure 5.5 was plotted with the data of one experiment from group 3. It displays the spatial flow distributions across the left ventricular wall before and during alternate LCX and LAD ligations. Before ischaemia (control), there were marked variations of RMBF from piece to piece within a layer and from layer to layer across the ventricular wall. Generally speaking, flow to the inner layer was higher than to the outer layer. During ischaemia, flow to the ischaemic regions decreased, with the maximum reduction in the inner layer and the minimum reduction in the outer layer. This disproportionate flow reduction produced a gradual flow transition from endocardium to epicardium. Figure 5.6 was plotted with the data of two experiments from group 3. It displays the endocardial flow distributions before and during LCX and LAD ligations. During ischaemia, flow to the ischaemic regions decreased remarkably, with a comparatively uniform change from the ischaemic centre to the boundary, and thus produced a sharp lateral interface between ischaemic and normal regions.

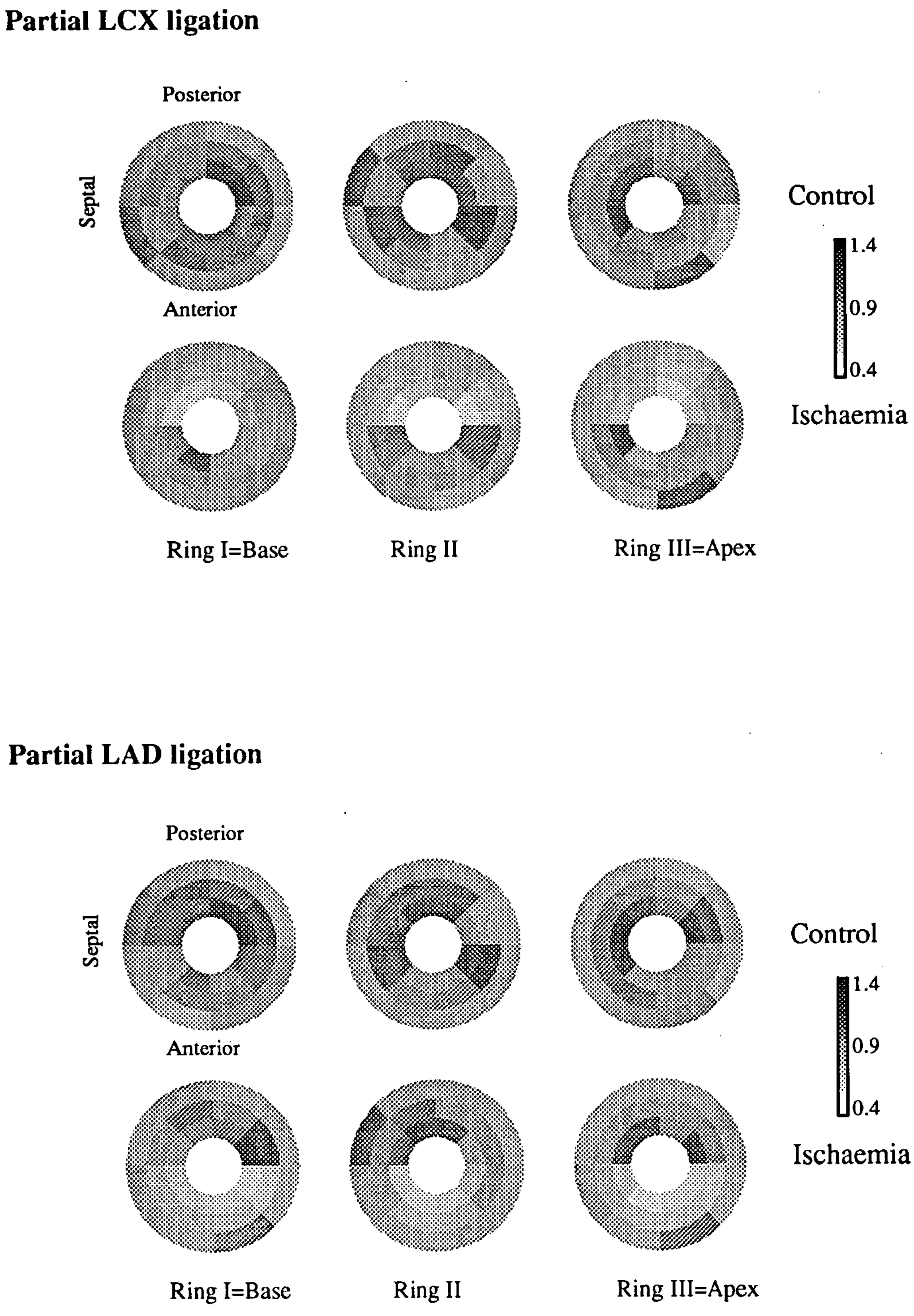

Figure 5.5 Spatial flow distributions in the left ventricular myocardium of a sheep before and during alternate LCX and LAD ligations. Intensities represent the quantity of RMBFs (mL/g/min). Each circle represents about 1-cm thick left ventricle rings. In each 45° arc there are three slices from endocardium to epicardium. The four arcs above represent the myocardium of the LCX bed; the four arcs below represent the myocardium of the LAD bed. For each ring, septum is left, free wall is right, posterior wall is above, and anterior wall is below.

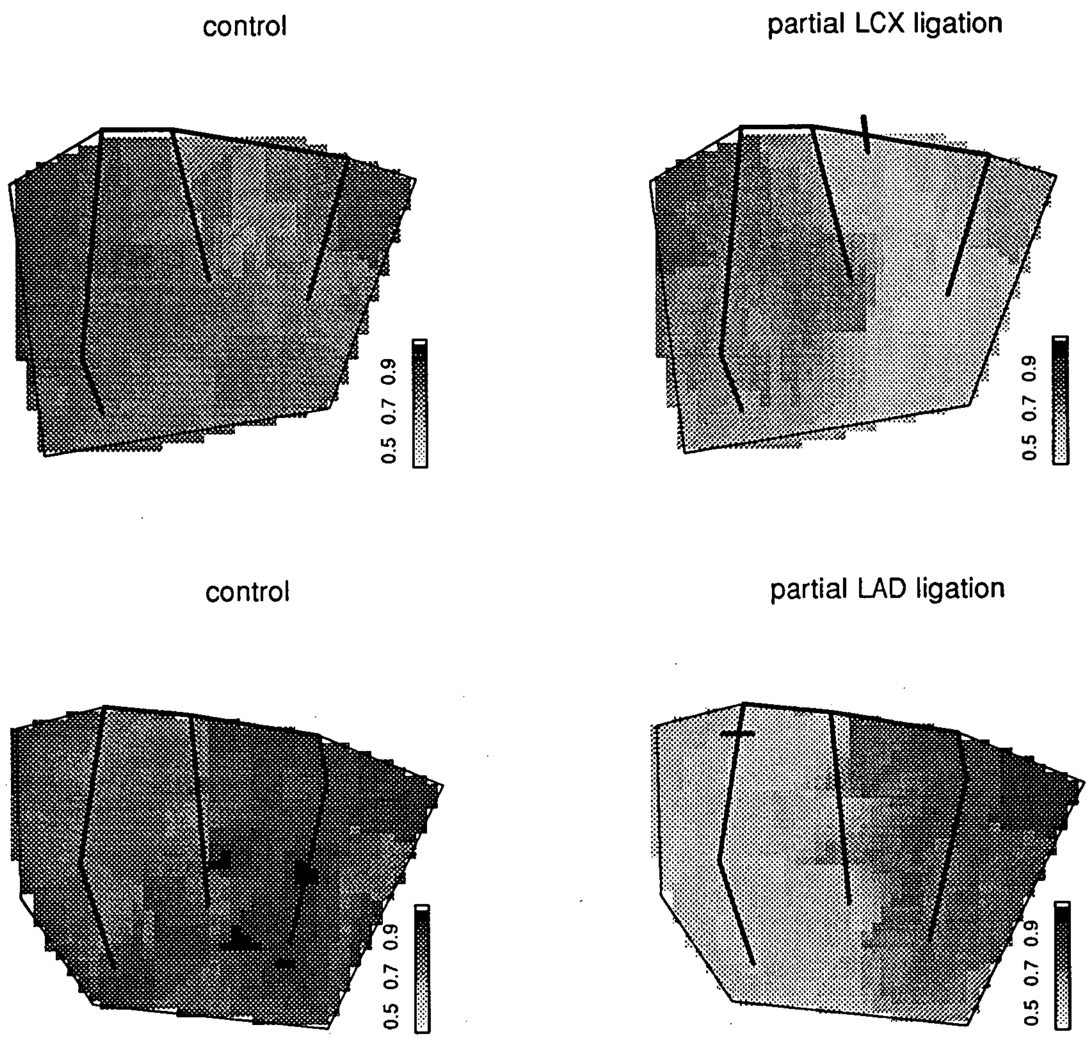

Figure 5.6 Myocardial blood flow distributions in the inner third of the left ventricles of two animals before and during LCX and LAD ligations. Intensities represent the quantity of RMBFs (mL/g/min). Schematic drawing of the frames represents the unwrapped endocardial surface of the left ventricles with the septum on the left and right sides, and the free walls in the middle. The thick solid lines represent coronary arteries. Ligated arteries are indicated by bars.

5.3 DISCUSSION

5.3.1 Validation of Subendocardial Ischaemia

The design of this model was based on the principle of the exercise stress test for detecting coronary artery disease, ie, the transient subendocardial ischaemia was produced by an insufficient coronary blood supply in the face of an increased myocardial oxygen demand. Pacing rather than exercise was used to augment oxygen demand because of the inconvenience in exercising animals. The premise is that tachycardia increases oxygen demand, and it is unaffected by the mode of tachycardia induction such as exercise or pacing (Mirvis & Gordey 1983; Heller et al. 1984). As demonstrated in both clinical and animal studies (Guyton et al. 1977; Mirvis & Gordey 1983; Cohen et al. 1983), the increased demand produces alterations in RMBF and electrocardiographic patterns. These changes can be detected by the RMBF and electrocardiographic techniques. The fluorescent microsphere technique provides the most sensitive way of measuring blood flow to small myocardial regions (Glenny et al. 1993; Li et al. 1996).

In order to assess subendocardial flow, the ratio of subendocardial to subepicardial flow is used in experimental studies (Mirvis et al. 1986). This ratio is termed the endo/epi flow ratio. The rationale for its use is that subepicardial flow is seldom inadequate so that it usually reflects the myocardial demand for blood flow. Thus as long as the endo/epi flow ratio remains constant, it is reasonable to infer that all layers are receiving an adequate blood flow. When the ratio falls it is likely that subendocardial flow is decreasing below a required level. Under physiological conditions, the mean blood flow to the subendocardium is slightly higher than to the subepicardial, yielding an endo/epi flow ratio of above 1 (Ross et al. 1990; Hoffman 1987). In the conscious dog (Bache & Cobb 1977; Bache et al. 1981), sheep and lamb (Archie et al. 1974; Fisher 1984), the flow per gram in the subendocardium is usually 20% to 40% higher than that in the subepicardium, with flow in the midwall usually being between the two. Even in anaesthetised animals the endo/epi flow ratio is usually above 1.0 (Rouleau et al. 1979; Boatwright et al. 1980). We also obtained an endo/epi flow ratio above 1.0 from the animals at both resting and pacing state (Table 5.3, Figure 5.1). Total flow is greater in the subendocardium because the calculated wall stress and oxygen consumption are greater in this region than in the subepicardium (Ross et al. 1990). However, at low perfusing pressures the endo/epi flow ratio is usually under 1.0, and the lower the pressure the lower the flow ratio (Rouleau et al. 1979; Bache & Schwartz 1982). Therefore, the presence of subendocardial ischaemia was evidenced by the reduction in the endo/epi flow ratio in the ischaemic area (Guyton et al. 1977; Mirvis et al. 1986), which was caused by a marked decrease in subendocardial flow with a less significant change in subepicardial perfusion (Figures 5.2 and 5.3).

In the absence of a stenosis, the myocardial blood flow increased with a pacing rate of 180 bpm (Table 5.3, Figures 5.1 and 5.4). This is due primarily to a decrease in the coronary vascular resistance (Holmberg & Varnauskas 1971; Holmberg et al. 1971; Momomura et al. 1991), which maintains uniform net transmural perfusion even if a marked reduction in diastolic perfusion time or higher heart rates are achieved (Flynn et al. 1992; Bache & Cobb 1977). In the presence of a coronary artery obstruction, pacing to a rate of 180 bpm caused a decrease in the subendocardial flow with a less significant change in the subepicardial perfusion; thus a reduction in the endo/epi flow ratio in the ischaemic area (Figures 5.2 and 5.3) (Guyton et al. 1977; Mirvis et al. 1986; Li et al. 1996). The subendocardium's susceptibility to ischaemia is due to its limited reserve for vasodilation, the extrinsic compression from the higher wall stress to which it is subjected, and the resultant high metabolic demands in this region (Ross et al. 1990). Atrial pacing was associated with a decrease in diastolic perfusion time, an increase in oxygen demand (Hoffman 1987), and an increase in stenosis resistance (Schwartz et al. 1981). Therefore, partial coronary occlusion plus the added atrial pacing would produce a degree of subendocardial ischaemia similar to that reported during the exercise, as indicated by the elevation of the ST segment in the endocardial recording and depression of the ST segment in the epicardial recording.

As shown in Table 5.7, the endo/epi flow ratio also decreased slightly (a 14% reduction for both the LAD and LCX ligations) in the nonischaemic region, although not significantly. This reduction is probably caused by the elevated left ventricular end-diastolic pressure (Dunn & Griggs 1983; Kjekshus 1973) and the decreased systolic pressure (Ross et al. 1990) (Table 5.5), which may be attributed to the stress produced by pacing and ischaemia in the nonischaemic region. The shared border region by the LAD and the LCX might also be responsible for the nonischaemic region's flow reduction. Since the RMBF was the average of the whole nonischaemic region, it was possible that reduced RMBF measurement from the ischaemic border region was included. However, this 14% endo/epi flow ratio reduction was not enough to produce ischaemic ECG changes. In a chronic canine model, the ST depression corresponded to an endo/epi flow ratio of 0.74 and 0.65 for the anterior descending bed and the left circumflex bed respectively (a 30-35% of ratio reduction, Mirvis & Ramanathan 1987). From this study, it was not possible to judge the endo/epi flow ratio threshold for the exact onset of ischaemic ST changes, however, it was observed that the appearance of ischaemic ST changes did not occur until the endo/epi flow ratio reduced by about 23% (Table 5.6).

5.3.2 Ovine Model Versus Canine Model

Studies in both acute (Guyton et al. 1977) and chronic (Mirvis et al. 1986) canine models demonstrated that coronary stenosis with pacing reduced flow to the subendocardium while flow to the epicardium was unchanged or slightly increased. In this sheep model, flow to the epicardium was either unchanged or slightly decreased. The alterations may be attributed to the differences in the coronary circulations between these two species. Dogs have rich collateral circulations which distribute disproportionately to the subepicardial zone of the ischaemic region (Reimer & Jennings 1979; Becker et al. 1971; Rivas et al. 1976). After permanent LCX occlusion, there is persistent viable myocardium in the subepicardial zone, averaging about 20% of the ischaemic vascular bed (Reimer & Jennings 1979). In a canine model, both the size of the ischaemic vascular bed and the amount of subepicardial collateral blood flow are major determinants of ischaemic size. In contrast to dogs, the ovine heart is devoid of an intrinsic coronary collateral circulation and is similar to humans (Markovitz et al. 1989; Euler et al. 1983). Even in the presence of gradual coronary stenosis, there is no demonstrable growth of coronary collateral vessels (Euler et al. 1983). This explains the mild flow reduction to the epicardium which occurred in some sheep during subendocardial ischaemia. The ischaemic size of the ovine heart is thus determined primarily by the size of the occluded vascular bed because of the lack of collateral connections (Euler et al. 1983). Another anatomic distinction of the ovine heart is its remarkably consistent and left side dominant coronary arterial circulation (Markovitz et al. 1989; Euler et al. 1983). The arterial circulation of the ovine left ventricle is exclusively supplied by the left main coronary artery and its branches. The LAD supplies the anterior wall and the apex, and the anterior two thirds of the septum. The LCX supplies the remainder of the left ventricle and extends around to the posterior wall to give off two to three marginal branches and a short posterior descending vessel with septal branches in the posterior interventricular sulcus. The posterior descending artery never originates from the right coronary artery. Postmortems of the ovine heart during this study validated these coronary anatomic features. Data from this study also showed that the LAD supplies 54±3%, and the LCX 46±3% of the left ventricle (Table 5.8). These coronary anatomic features in sheep permit predictable and reproducible myocardial ischaemia with small standard deviations.

5.3.3 LCX Ischaemia Versus LAD Ischaemia

Studies in canine models suggested that the LAD bed is more susceptible to ischaemia than the LCX bed because of differences in collateral blood flow patterns (Becker 1983; Mirvis & Ramanathan 1987). The endocardial flows and the endo/epi flow ratio fell to lower levels in the ischaemic LAD bed than in the LCX perfusion zone (Mirvis & Ramanathan 1987). Occlusion of the LAD resulted in more necrosis than did similar obstruction of the LCX, and this finding was related to more reduced collateral flow to the anterior bed (Becker et al. 1983). In this study, no significant differences were found in the haemodynamic and flow variables between the LAD and the LCX ligations (Table 5.8), although there were more changes in the left ventricular pressures and in the endo/epi flow ratio in the anterior ischaemia than in the posterior ischaemia. The different results from this study may be attributed to the different anatomy of the coronary arterial circulation in the ovine heart in which native coronary collateral anastomoses are absent (Markovitz et al. 1989).

5.3.4 Flow Distribution Across the Ventricular Wall Versus Flow Distribution at the Lateral Boundary

As shown in Figures 5.5 and 5.6, during subendocardial ischaemia, flow reduction across the ventricular wall was quite different from the flow change at the lateral boundary. Transmurally, flow changed gradually from the endocardium to the epicardium; Laterally, flow shifted sharply from the ischaemic region to the normal region, producing a sharp lateral interface between ischaemic and normal regions. No studies on the flow mapping of subendocardial ischaemia have been previously performed. However, electrophysiological, metabolic, and histological studies on transmural ischaemia have demonstrated that the lateral interface between normal and ischaemic tissue is characterised by a sharp but irregular profile from the endocardium to the epicardium with severely ischaemic tissue lying adjacent to normal, well perfused tissue (Factor et al. 1981; Reimer & Jennings 1979; Harken et al. 1981; Janse et al. 1979; Murdock et al. 1983). Results of the present study are consistent with these reports.

5.3.5 LCX Microsphere Injection Versus Left Atrial Microsphere Injection

There was no significant difference in the RMBF measured by the left atrial and the LCX injection methods. However, the flow reduction in the epicardial layer measured by the LCX injection was not significant during ischaemia, but the flow reduction in the same myocardium measured by the left atrial injection was significant. The reasons for this variation were not clear. It was possible that the LCX injection might increase the LCX perfusion pressure and thus increase the epicardial perfusion, although no significant changes in the LCX flow was observed during the injection. A minor increase in the perfusion pressure might produce a significant change during the stenosis because of the great reduction in the perfusion pressure distal to the stenotic LCX. In order to avoid this possibility, left atrial injection rather than LCX injection was used in the subsequent studies.

Chapter 6

EPICARDIAL AND ENDOCARDIAL ST POTENTIAL MAPPING OF THE SUBENDOCARDIAL ISCHAEMIA -In Relation to Regional Myocardial Blood Flow

6.1 INTRODUCTION

Electrocardiographic ST segment depression has long been recognised as a sign of ischaemia (Wolferth et al. 1945; Bayley 1946), but the responsible mechanisms have been controversial (Prinzmetal et al. 1959 & 1961; Ekmekci et al. 1961; Holland & Brooks 1975). Much of the current opinion regarding the genesis of ST segment depression is derived from interpretations based on certain theoretical considerations (Holland & Brooks 1975 & 1977a) and indirect evidence from animal experiments (Wolferth et al. 1945; Bayley 1946). Ischaemic muscle generates intracellular currents which effectively cause TQ depression and ST elevation over the ischaemic area (Samson & Scher 1960; Kleber et al. 1978). Conventional electrocardiography with AC coupled amplifiers reflects this as ST elevation. ST segment depression recorded at the epicardium was considered to be secondary to an injury current in the underlying subendocardium (Otto 1929; Odle et al. 1950; Sodi-Pallares & Calder 1956).

In conventional stress testing, as myocardial demand exceeds the ability of the narrowed coronary arterial bed to increase blood flow, the ischaemic threshold is exceeded and reversible ST segment depression is produced. However, the location of this ST depression does not enable the localisation of an ischaemic region (Kubota et al. 1985; Dunn et al. 1981; Fuchs et al. 1982; Abouantoun et al. 1984; Mark et al. 1987). The difficulty in localising myocardial ischaemia from ST depression can not be explained by the classic theories (Wilson et al. 1933; Holland & Brooks 1975), which all suggest that ST depression should be able to localise ischaemia.

Recent work (Kilpatrick et al. 1990) comparing epicardial maps of patients with inferior infarction to maps of patients with pure ST depression showed superior ST elevation in both. The author hypothesised that ST depression on the ECG was secondary to current flow from a region of endocardial ischaemia through the great vessels and atria and back on to the outside of the heart. This study aimed to test this hypothesis, and to evaluate the source of ST depression by measuring epicardial and endocardial potential distributions in the sheep heart with subendocardial ischaemia, and relating these to the regions of ischaemia confirmed by fluorescent microspheres.

6.2 EXPERIMENTAL PROCEDURES

6.2.1 Animal Groups

A total of 30 sheep (30-40 kg) of both sexes were used in this study. They were randomly divided into 4 groups.

Group 1 (pacing without stenosis): Five animals from the study of chapter 5 (group 1) were used in this study. The epicardial ST potential fields were recorded before and during pacing at the rate of 120, 140, 160, 180, 200, 220 and 240 beats per minute (bpm).

Group 2 (Subendocardial ischaemia in either the LCX or the LAD territory in different animals with intervention): In this group, either posterior subendocardial ischaemia or anterior subendocardial ischaemia was produced in different animals (LAD ligation, n=4, LCX ligation, n=7). The epicardial ST potential distributions were recorded prior to and after 2, 5, 10, 15, and 20 minutes of ischaemia. The endocardial electrograms were simultaneously recorded by a quadripolar electrode catheter. The following tests were performed to investigate the nature of the ischaemic source after the production of subendocardial ischaemia:

(1) Insulating the heart from surrounding tissues (n=8):
A thin plastic bag was placed onto the heart, covering the right and left ventricles and portions of both atria, to insulate the heart from the surrounding tissues during ischaemia, the epicardial ST potential changes were recorded; the insulator was quickly removed, the potentials were again recorded and compared with those during insulation. The time difference between the two recordings was about 10 seconds.

(2) Intracavity injection of low conductivity fluid (n=7):
High concentration glucose (50%) of 25-50 mL was injected into the left ventricular cavity to change the conductivity of the blood. The epicardial ST potentials were measured before and during the injection and the induced changes were compared. 20 mL of blood was withdrawn from the left ventricle via an implanted catheter before and during the glucose injection to measure the resistance by using a device

manufactured by the author and illustrated in Figure 6.1. The resistance of the pure glucose measured at 1 kHz at room temperature by this device was 690 kΩ, the pure blood was 4.75 kΩ, and the mixture of these two (10ml+10ml) in vitro was 11.9 kΩ.

(3) Transforming subendocardial ischaemia to full-thickness ischaemia (n=5):
The percent stenosis of a coronary artery was increased by fully inflating the hydraulic occluder at 10-15 minutes of partial coronary ligation, to transform the subendocardial ischaemia to full-thickness ischaemia. In 2 animals, the potential changes were recorded before and 2, 30, 60, 90 and 120 seconds after the transition. In another 3 animals, the potential changes during the transition were recorded continuously for a period of 30 seconds (n=2) and 50 seconds (n=1).

Group 3 (Alternate LAD and LCX partial ligation in the same animal): In this group, alternate posterior and anterior subendocardial ischaemia was produced in the same animal by alternate partial constriction of the LAD and the LCX coupled with pacing (see chapter 5, Section 5.1). The epicardial potential maps were constructed and the epicardial potential distributions between these two ischaemic regions were compared.

Group 4 (Epicardial and endocardial potential mapping in relation to RMBF): Eight animals from the study mentioned in chapter 5 (group 3) were used. The subendocardial ischaemia production is similar to that in group 3, ie., alternate LAD and LCX ligation in the same animal. Both the epicardial and the endocardial ST potentials were then recorded and compared. The RMBF was measured prior to and during ischaemia and the flow maps constructed. The flow changes were then correlated to both the epicardial and the endocardial ST potential changes.

The animal groups and their treatments are summarised in Table 6.1.

Table 6.1 Animal Groups and Treatments

Group	N	Treatments
1	5	pacing without vessel ligation, epicardial mapping
2	11	pacing and partial ligation of either LAD or LCX in different animals epicardial mapping, epicardial insulation endocardial electrograms by quadripolar electrode catheter intracavity injection of 50% glucose transition of subendocardial to transmural ischaemia
3	6	pacing and alternate partial ligation of LAD and LCX in the same animal epicardial mapping comparing the similarity between two epicardial maps
4	8	pacing and alternate partial ligation of LAD and LCX in the same animal epicardial and endocardial mapping, RMBF correlation between ST potentials and RMBF

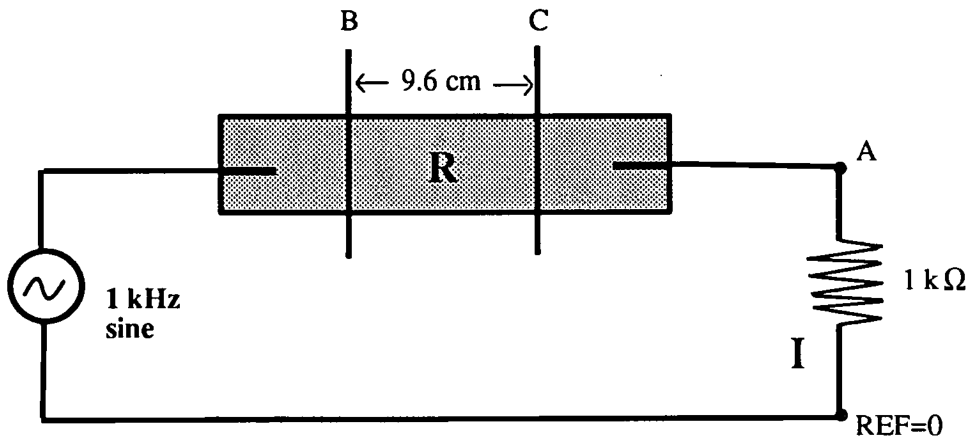

$$I = (V_A - V_{REF}) / 1k\Omega$$

$$R = (V_B - V_C) / I$$

Figure 6.1 Circuit for the measurement and calculation of the blood resistance. The blood container is 20 mL in volume, and 20 cm in length. The length of B–C segment is 9.6 cm. The resistance was estimated at 1 kHz at room temperature.

6.2.2 Subendocardial Ischaemia

Subendocardial ischaemia was produced as described in Chapter 5, Section 5.1.2.

6.2.3 Perfusion Beds and Regional Myocardial Blood Flow Measurement

The LAD and the LCX perfusion beds were delineated by methylene blue dye as described in Chapter 5, Section 5.1.3. The RMBF was measured prior to and at 20 minutes of ischaemia as described in Chapter 4.

During the sectioning of the myocardium, the anatomic location of each myocardial piece was recorded onto the tracing of the left ventricular wall and related to the positions of the electrodes, so that the simultaneous measurements of the potentials and the RMBF could be compared and mapped together.

The RMBF in each sample was expressed both in absolute terms, as mL/min/g of myocardium and in relative terms as a percentage of the control flow obtained before ischaemia. After the flow for each sample was calculated, maps of the left ventricular blood flow were constructed from both the absolute flow and the relative flow. The flow maps were combined with the epicardial and the endocardial contour potential maps .

6.2.4 Potential Recording, Map Construction and Map Display

See Chapter 3, Section 3.5.

6.2.5 Data Analysis and Statistics

The correlation coefficient was used to measure the similarity between two epicardial potential maps. The correlation coefficient r was calculated by considering two maps as vector A and B, r was given by

$$r = A \bullet B / |A|\,|B|$$

where

$$A \bullet B = \sum_{i=0}^{n} a_i b_i, \quad |A| = \sqrt{\sum_{i=0}^{n} a_i a_i}, \quad |B| = \sqrt{\sum_{i=0}^{n} b_i b_i}$$

and n is the total number of components in the vector, a_i and b_i are the ith components of A and B.

The resulting correlation coefficient is between -1 and 1. Two maps with a similar pattern have a correlation coefficient approaching 1 and dissimilar maps have a correlation coefficient approaching zero. Maps with the same pattern but with the positive and negative areas exchanged have a correlation coefficient approaching -1. This technique has been used to analyse body surface ECG maps in clinical studies (Walker et al. 1987a; Bell et al. 1993) and to assess the similarity between modelled and measured body surface potential maps in theoretical studies (Stanley et al. 1986).

The correlation coefficient was also used to analyse the association between the RMBF and the epicardial and the endocardial potentials. The correlation coefficient is also between -1 and 1; a correlation coefficient approaching 1 if the data sets are identically shaped; a zero correlation coefficient if there is no association between the two data sets.

6.3 RESULTS

6.3.1 Epicardial Potential Distributions in Pacing Alone

Table 6.2 presents epicardial ST potential changes at different pacing rates. At baseline, the epicardial ST potentials showed a slight variation in magnitude. Over all the epicardial sites, the ST magnitude ranged from +2 mV to -3 mV. In all the 5 animals, pacing to the rate of 180 bpm without coronary ligation had no significant effect on the magnitude of ST potentials. ST potential changes appeared at the pacing rate of 200 bpm or more in 3 of the 5 animals. In 2 animals, ST potential was not altered even when the pacing rate reached 240 bpm. Representative maps of epicardial ST potential distributions from one typical experiment are displayed in Figure 6.2. Pacing up to the rate of 180 bpm without coronary ligation had no significant effect on the ST potential distributions and their spatial features.

Table 6.2 Epicardial potential variables (mV) before and during pacing

No.	control (mean±SD)	pacing (mean±SD) 120bpm	140bpm	160bpm	180bpm	200bpm	220bpm	240bpm
1	-0.49±1.36	-0.57±1.09	-0.35±1.38	-0.55±1.12	-0.53±0.94	-0.72±1.01*	-0.82±1.06*	-0.53±1.57*
2	-0.19±0.53	-0.29±0.58	-0.30±0.79	-0.36±0.85	-0.33±0.52	-0.31±0.50	-0.34±0.83	-1.07±1.49
3	-0.39±0.58	-0.46±0.72	-0.40±0.79	-0.41±0.76	-0.47±0.89	-0.27±0.95	-0.50±0.96	-0.11±0.57*
4	-0.34±0.73	-0.20±0.61	-0.52±0.96	-0.59±0.90	-0.09±0.75	-0.63±0.67	-0.74±0.76*	-0.38±0.65*
5	-0.76±1.94	-0.55±1.43	0.03±1.65	-0.55±1.67	0.13±1.38	-0.55±2.5	-0.29±2.31	0.09±3.15

For each animal, the mean±SD was calculated from ST potentials of 64 epicardial recording sites.

*P < 0.05 versus control.

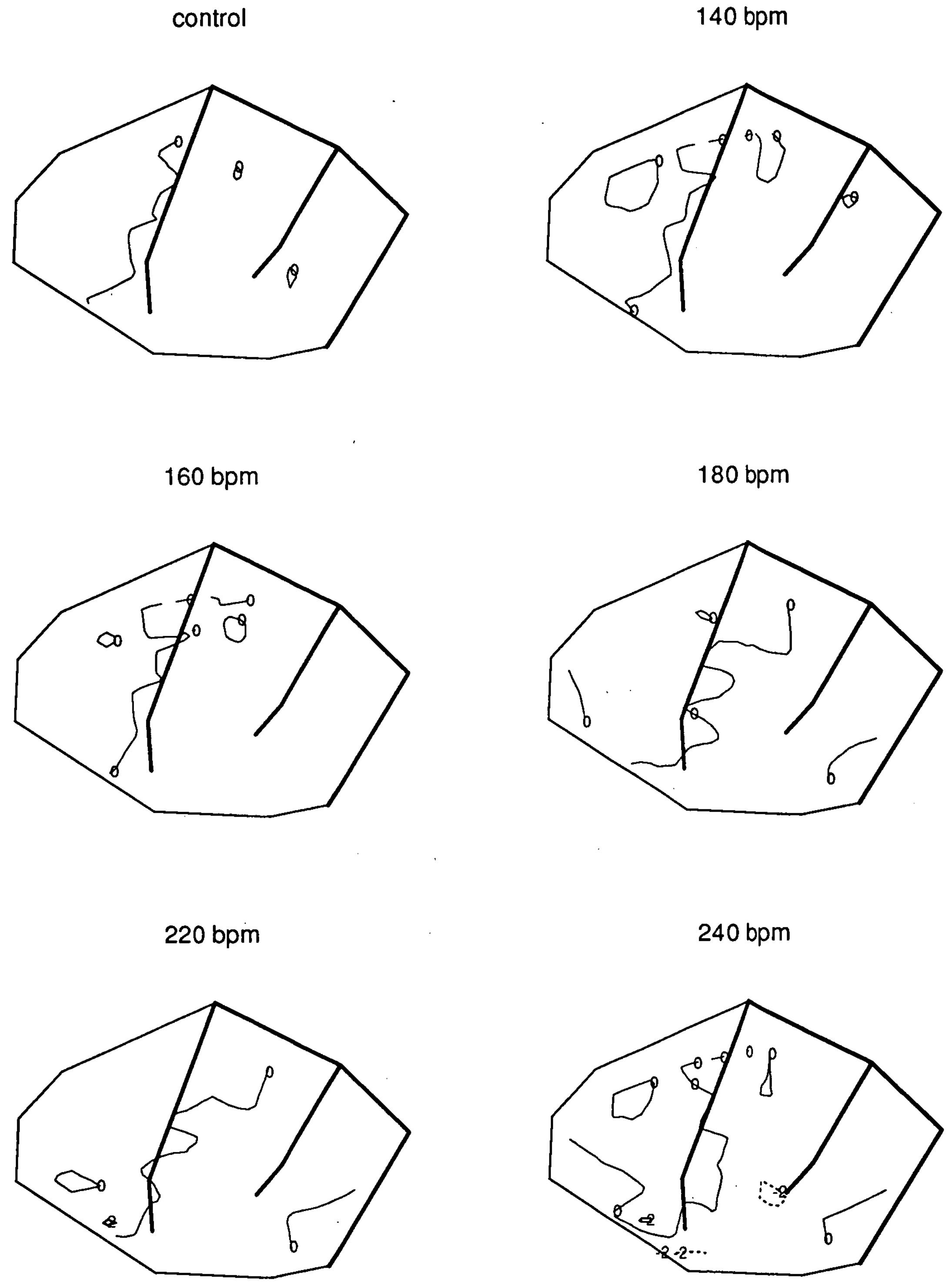

Figure 6.2 Epicardial ST potential distributions at different pacing rate. Schematic drawing of the frames represents the unwrapped epicardial surface of the left and right ventricles. The thick solid lines represent coronary arteries. The thin solid and dotted lines indicate ST potentials. Numbers are in mV.

6.3.2 Epicardial Potential Distributions in Posterior and Anterior Ischaemia - *in different animals*

Representative maps of epicardial ST potential distributions from six typical experiments are displayed in Figures 6.3 and 6.4. Before coronary ligation and pacing (control), the epicardial ST potentials showed a slight variation in magnitude. Over all the epicardial sites, the ST magnitude ranged from +2 mV to -4 mV. The distribution patterns of ST depression during ischaemia showed ST depression occurred over the whole surface of the left ventricle, with a maximum change at the anterolateral wall in both the LCX and the LAD ligations, and the patterns of potential distributions were similar in these two ligations.

Figures 6.5 and 6.6 demonstrate the potential distributions at different times of ischaemia in the LCX and the LAD ligations. ST depression started from the lateral wall of the left ventricle; as ischaemia progressed, ST depression spread to the whole surface of the left ventricle, with the position of maximum change of potential being variable although on the lateral wall. Minor ST elevation occurred in the apex region at 20 minutes after the ligation of either the LCX or the LAD. ST elevation also appeared in a small area of the anterior wall of the right ventricle in the LAD ligation (Figure 6.6).

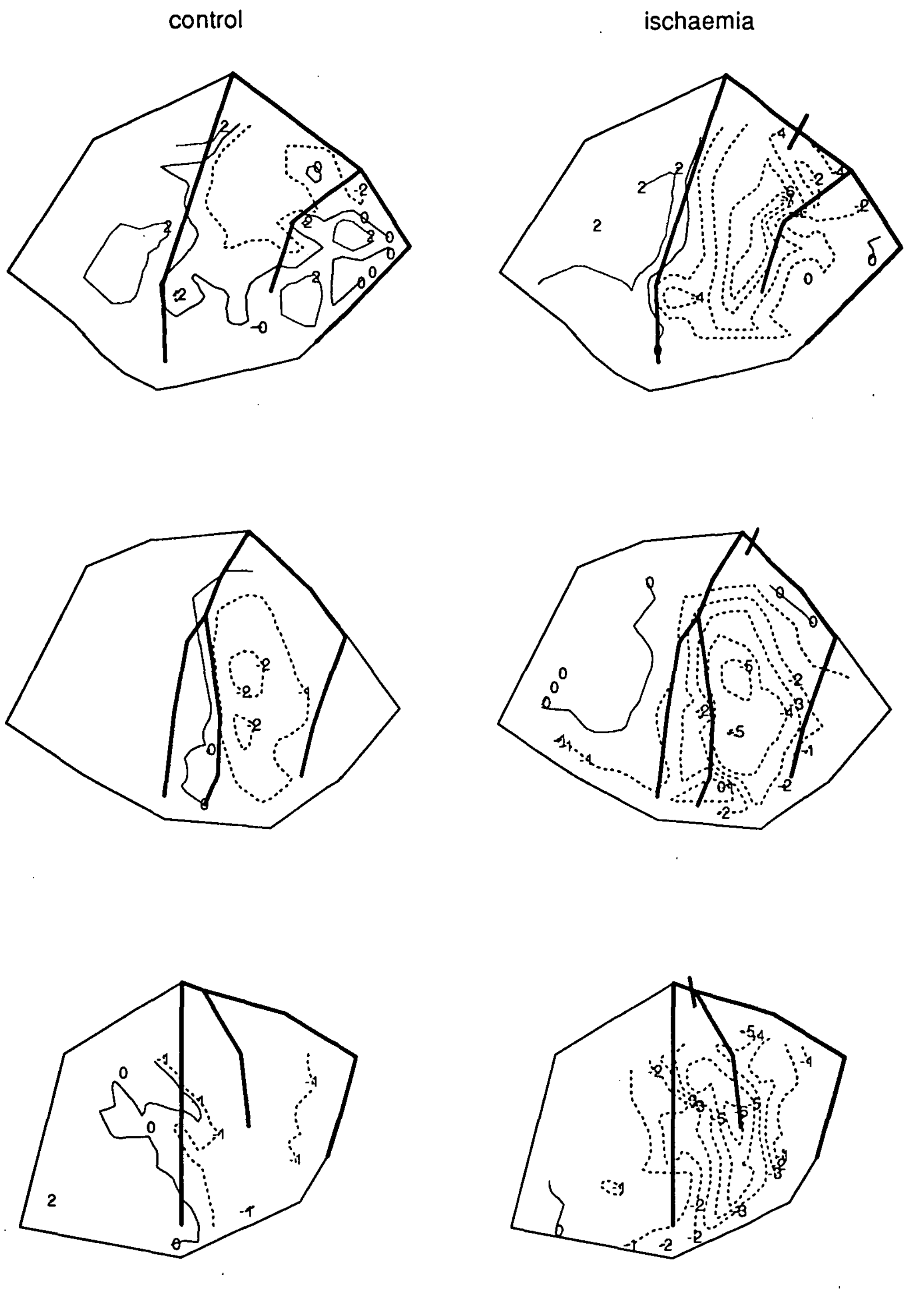

Figure 6.3 Epicardial potential distributions at control and 10 minutes of LCX ligation. The thin solid lines represent zero potential and ST elevation and dotted lines ST depression. Numbers are in mV. Ligated arteries are indicated by bars. Maps are plotted with the data of 3 animals from group 2 (every two parallel maps are from one animal).

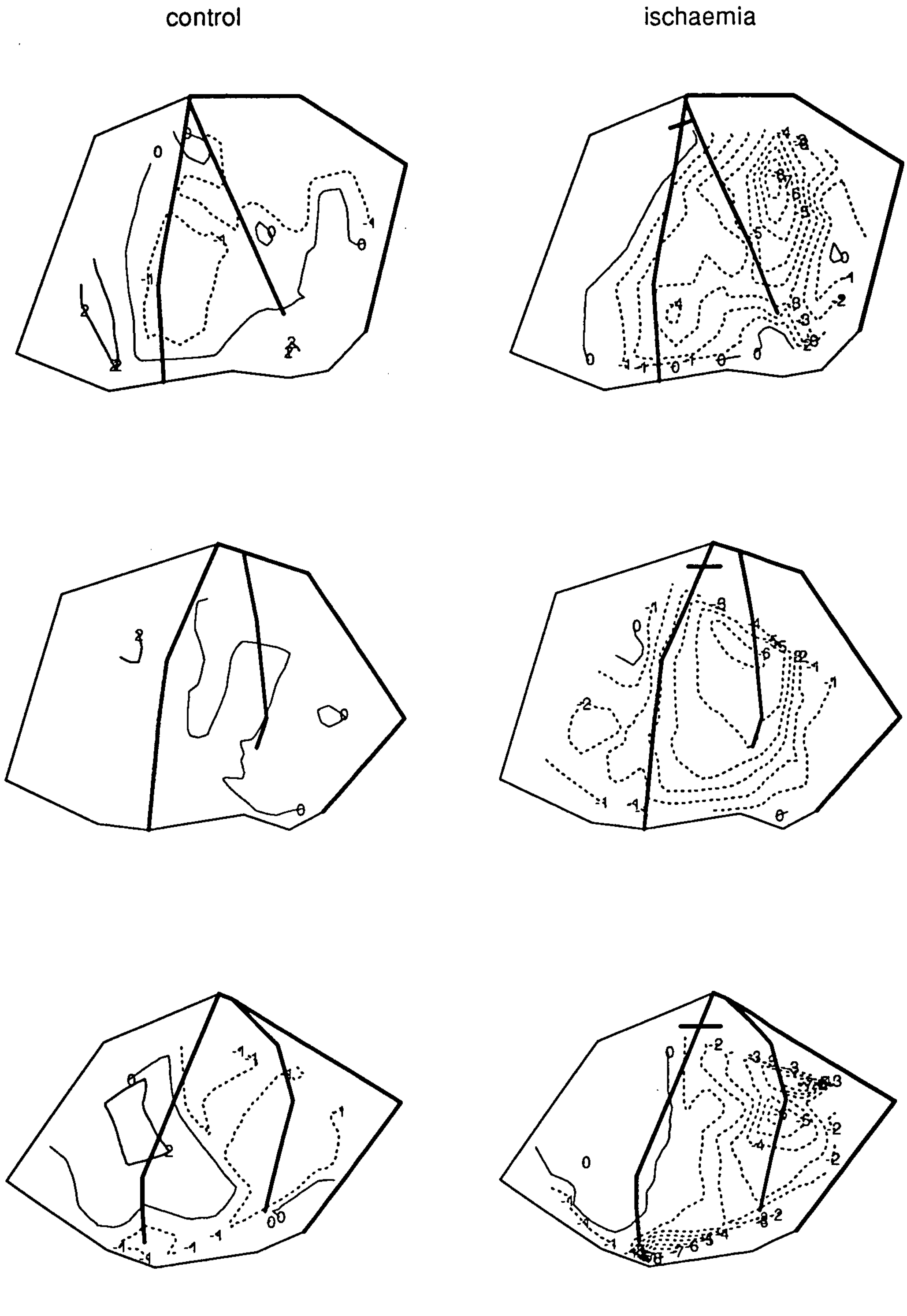

Figure 6.4 Epicardial potential distributions at control and 10 minutes of LAD ligation. The thin solid lines represent zero potential and ST elevation and dotted lines ST depression. Numbers are in mV. Ligated arteries are indicated by bars. Maps are plotted with the data of 3 animals from group 2 (every two parallel maps are from one animal).

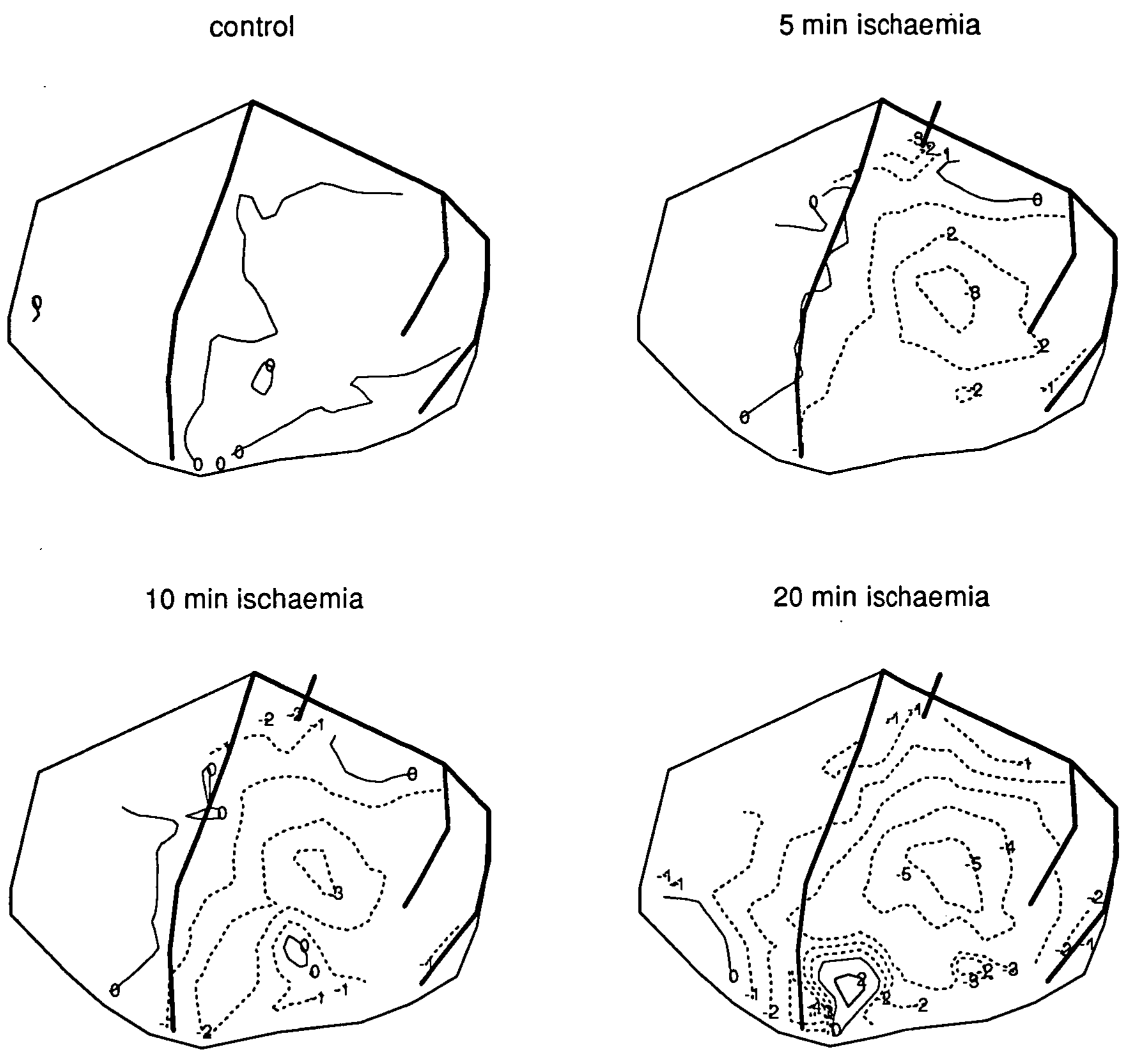

Figure 6.5 Epicardial potential distributions at control and during various time intervals of LCX ligation. Maps are plotted with the data of one animal from group 2. The thin solid lines represent zero potential and ST elevation and dotted lines ST depression. Numbers are in mV. Ligated arteries are indicated by bars.

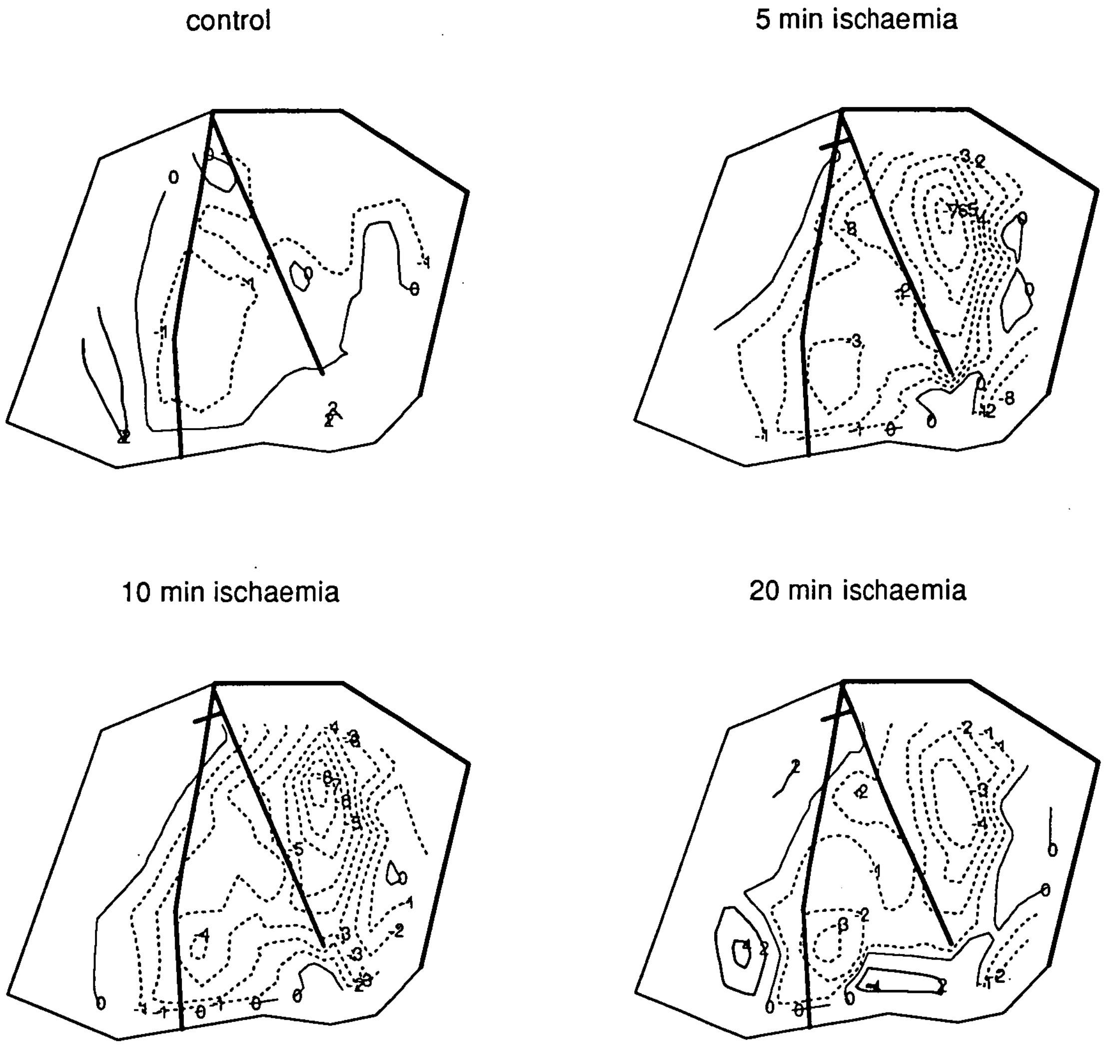

Figure 6.6. Epicardial potential distributions at control and during various time intervals of LAD ligation. Maps are plotted with the data of one animal from group 2. The thin solid lines represent zero potential and ST elevation and dotted lines ST depression. Numbers are in mV. Ligated arteries are indicated by bars.

6.3.3 Epicardial Potential Distributions in Posterior and Anterior Ischaemia - *in the same animal*

When alternate LAD and LCX partial ligation was tested in the same animal (group3), even more similar ST potential distribution patterns were obtained. Representative maps of epicardial ST potential distributions from three typical experiments are displayed in Figure 6.7. The potential distributions were characterised by general epicardial ST depression with a minimum potential in the anterolateral epicardium. The epicardial ST potential change in each individual electrode position during the LAD ligation was compared to that during the LCX ligation. When such potential changes from the 64 electrode positions in each of 6 sheep of group 3 were tested, a correlation coefficient of 0.77±0.14 (ranged from 0.66 to 0.97, all $P<0.0001$, Table 6.3) was obtained.

Table 6.3 Correlation coefficient of the epicardial ST potential changes between LCX and LAD ligations in the same animal

No.	r
1	0.75
2	0.65
3	0.97
4	0.91
5	0.69
6	0.66
mean	0.77
SD	0.14

partial LAD ligation partial LCX ligation

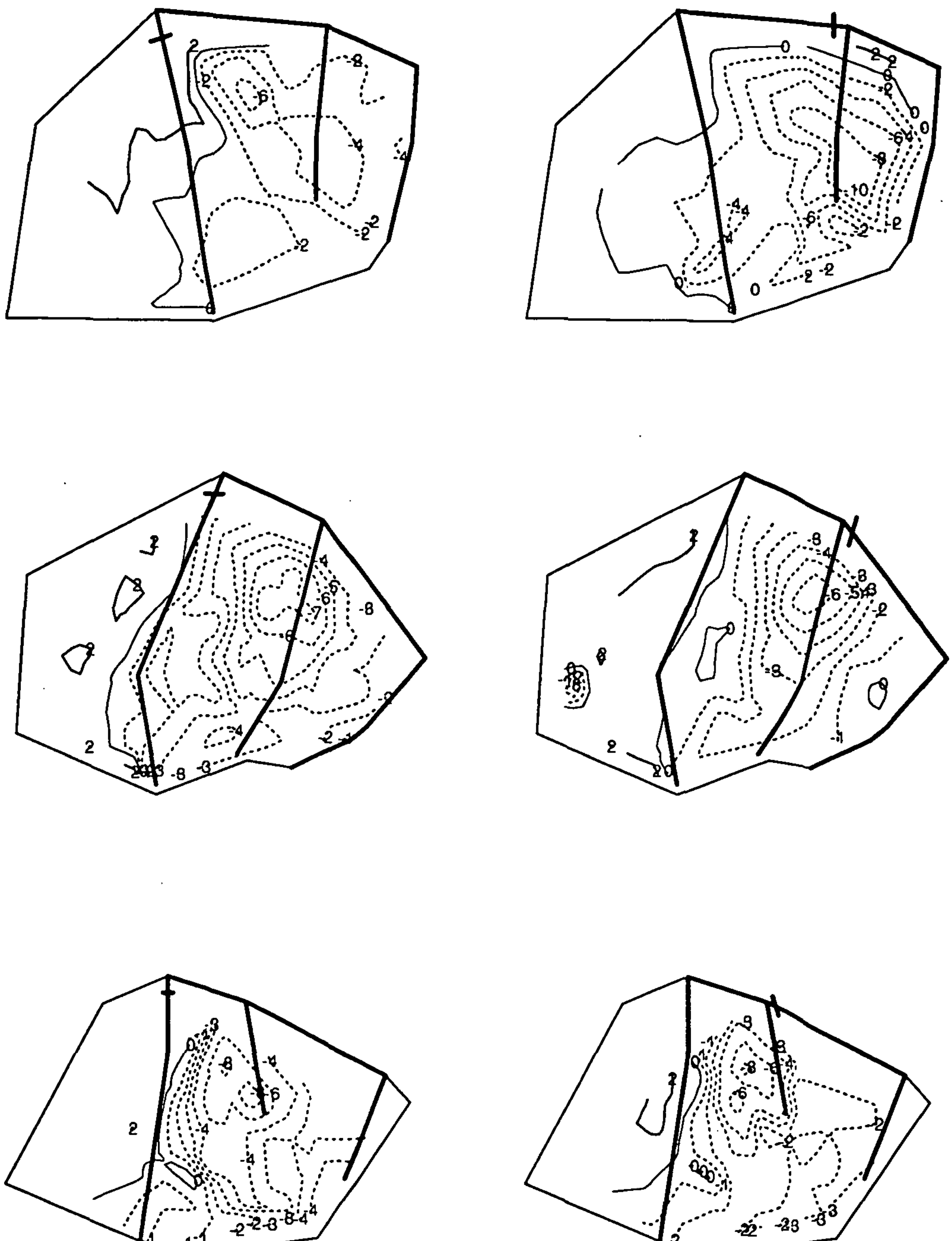

Figure 6.7 The diagrams are isopotential difference maps plotted with the data of 3 animals from group 3 (every two parallel maps are from one animal). They represent epicardial ST potential distributions in alternate partial LAD and LCX ligation in the same sheep. The thin solid lines represent zero potential and ST elevation and dotted lines ST depression. Numbers are in mV. Ligated arteries are indicated by bars.

6.3.4 Epicardial Potential Distributions in Posterior and Anterior Ischaemia

- in relation to the endocardial potential distributions

Regional subendocardial ischaemia was alternatively produced by alternate LAD and LCX ligations in 5 of the 8 animals in group 4. The representative maps from two animals are shown in Figures 6.8 and 6.9. The maps display the simultaneous epicardial and endocardial ST potential changes induced by ischaemia. On the epicardium, ST depression was recorded in most leads. The potential changes were independent of the ligated artery. From the endocardium, localised ST elevation was recorded, with the ST elevation corresponding to the territory of the ligated artery.

In 3 of the 8 animals the second ligation produced ischaemia in both territories. Figures 6.10 and 6.11 demonstrate the simultaneous epicardial and endocardial ST potential changes in one of the three animals. During the initial LCX ligation (Figure 6.10), posterior ischaemia developed. A localised ST elevation occurred in the posterior epicardium at 10 minutes of ischaemia, indicating more severe ischaemia. The ischaemia transformed to a pure subendocardial ischaemia after 10 minutes. During the subsequent LAD ligation (Figure 6.11), endocardial ST elevation occurred in both the anterior and posterior regions, indicating a broader subendocardial ischaemia in these two regions, which was confirmed by the measurements of RMBF (Figure 6.16).

partial LCX ligation | Partial LAD ligation

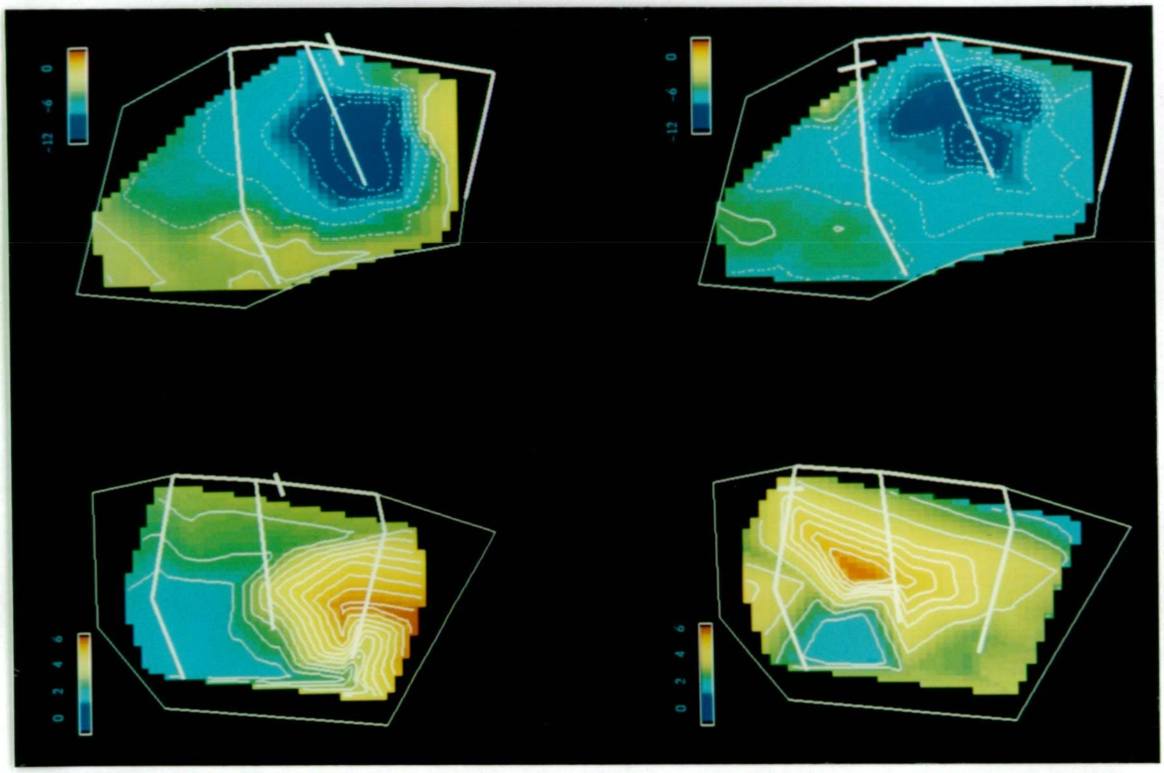

Figure 6.8 Epicardial and endocardial potential distributions during partial coronary artery ligations. The diagrams are isopotential difference maps constructed from the simultaneous epicardial and endocardial recordings of one sheep from group 4. Schematic drawing of the frames represents the unwrapped epicardial surface of the left and right ventricles (top), and the endocardial surface of the left ventricle (bottom). The solid contour lines reflect ST elevation and the dotted lines ST depression. The red colour represents positive potential and the blue colour negative potential. Ligated arteries are indicated by bars.

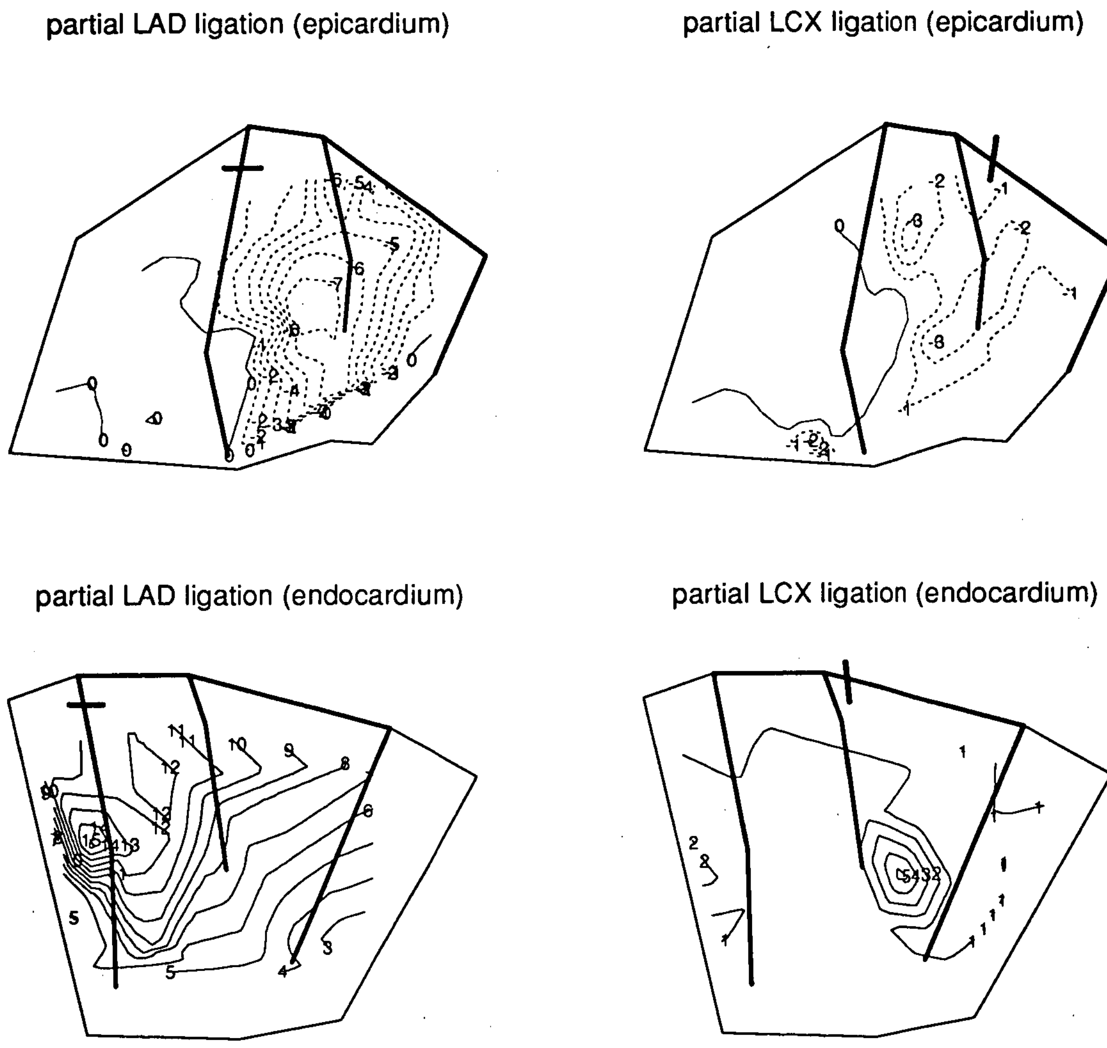

Figure 6.9 Epicardial and endocardial potential distributions during partial coronary artery ligations. The diagrams are isopotential difference maps constructed from the simultaneous epicardial and endocardial recordings of one sheep from group 4. Schematic drawing of the frames represents the unwrapped epicardial surface of the left and right ventricles (top), and the endocardial surface of the left ventricle (bottom). The solid contour lines represent ST elevation and the dotted lines ST depression. Numbers are in mV. Ligated arteries are indicated by bars.

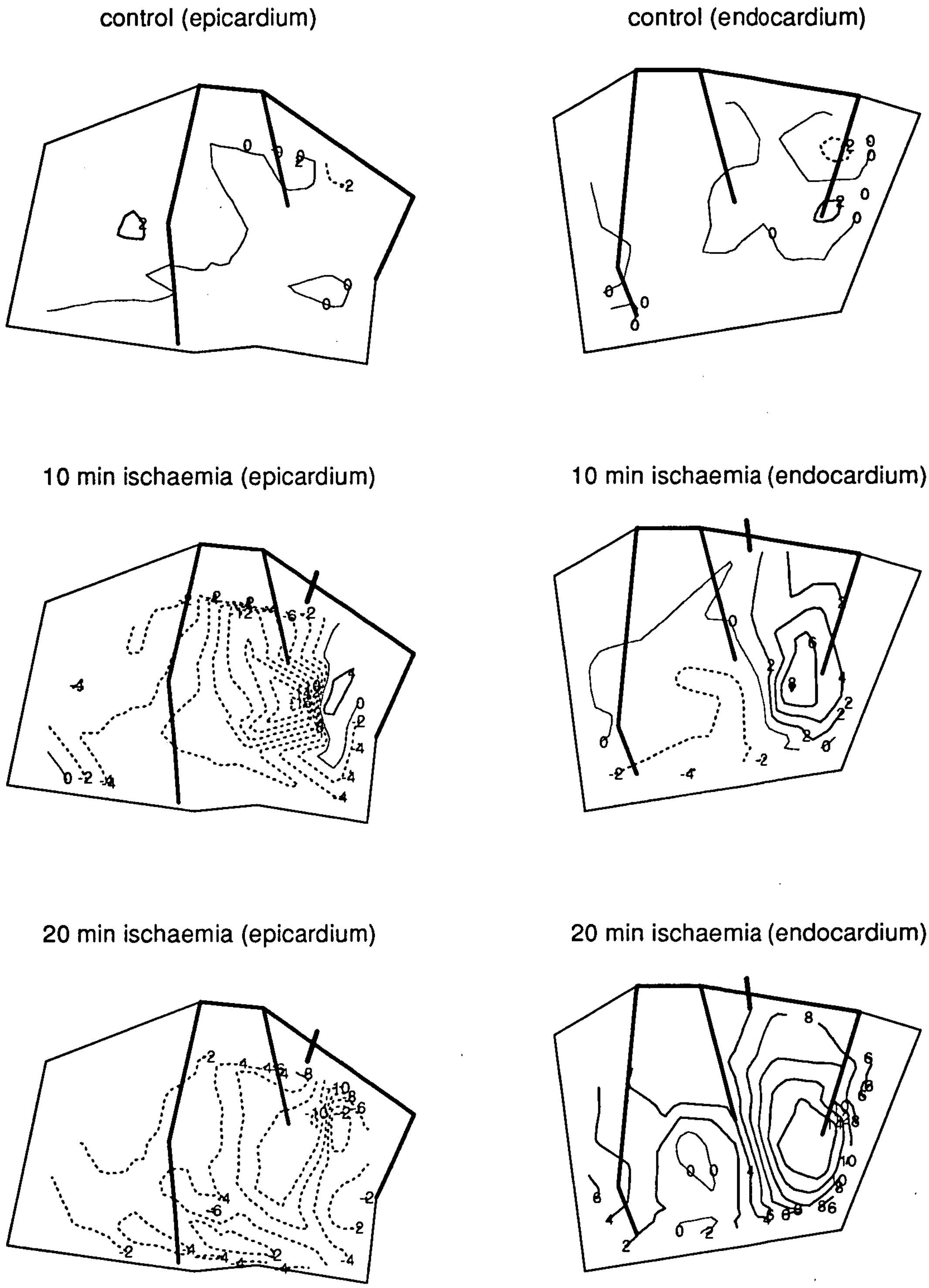

Figure 6.10 Simultaneous epicardial and endocardial potential distributions during LCX ligation. Schematic drawing of the frames represents the unwrapped epicardial surface of the left and right ventricles (left), and the endocardial surface of the left ventricle (right). The solid contour lines represent ST elevation and the dotted lines ST depression. Numbers are in mV. Ligated arteries are indicated by bars.

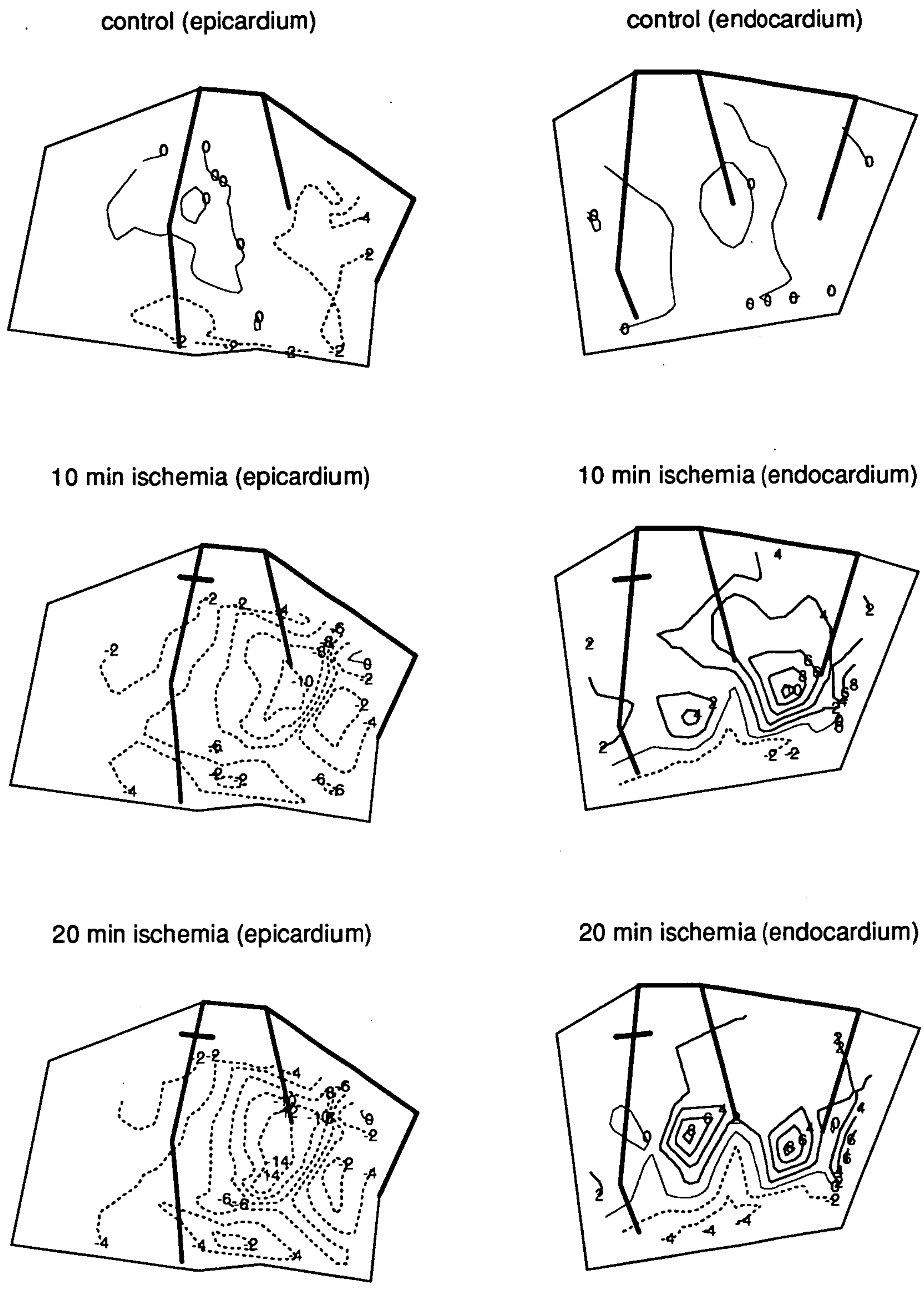

Figure 6.11 Simultaneous epicardial and endocardial potential distributions during LAD ligation. Schematic drawing of the frames represents the unwrapped epicardial surface of the left and right ventricles (left), and the endocardial surface of the left ventricle (right). The solid contour lines represent ST elevation and the dotted lines ST depression. Numbers are in mV. Ligated arteries are indicated by bars. Data are from the same animal as in Figure 6.10.

6.3.5 Epicardial and Endocardial Potential Distributions
- *in relation to the RMBF*

The relationship between the described changes in the ST potentials and the RMBF were examined in two ways. The ST potential changes were computed by subtracting the control voltage from each ischaemic voltage at each electrode site during the ST segment. The flow change was represented either by the endo/epi flow ratio or by the percent decrease in the RMBF during ischaemia.

First, linear correlation was used to determine whether a statistically significant relation existed between the simultaneous measurements of flow change and the epicardial potential changes during ischaemia. As shown in Figure 6.12, the epicardial potential changes at 20 minutes did not correlate with either the endo/epi flow ratio or the percent decrease in the RMBF in the inner third of the myocardium underlying the electrodes (r=0.02, and r=-0.02, respectively). The author further tested whether the peak negative potential difference correlated with the average endo/epi ratio (Figure 6.13), but no significant correlation (r=0.28, P=0.30) was found between these two. Figure 6.15 (top) shows that when the epicardial potential contour maps were combined with the endocardial RMBF image maps, the lowest ST depression did not coincide with the lowest flow area.

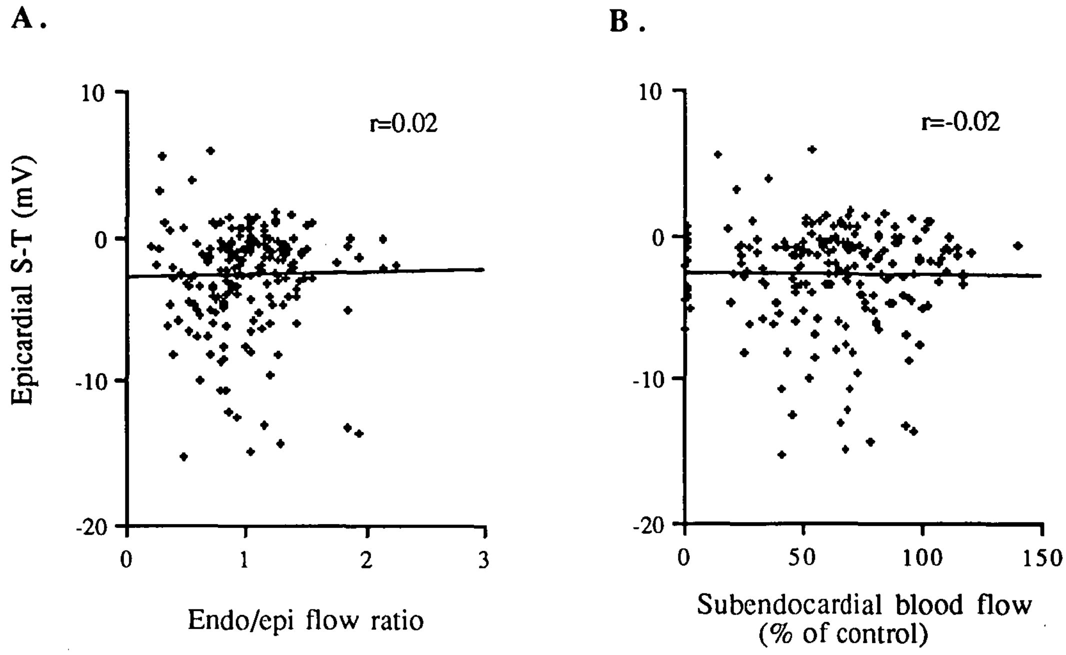

Figure 6.12 Epicardial ST changes from control are plotted as a function of the endo/epi flow ratio (A) and subendocardial blood flow (B) to the region of the electrodes (204 data points from 8 sheep).

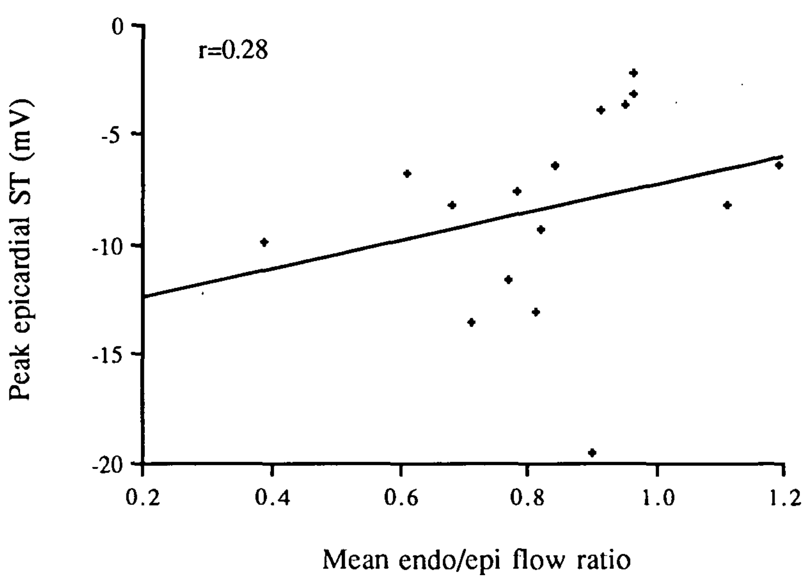

Figure 6.13 Relationship between peak epicardial ST changes from control and mean endo/epi flow ratio in ischaemic region (16 data points from 8 sheep).

A similar analysis was performed with the endocardial potential changes. Figure 6.14 demonstrates the overall relationship between myocardial blood flow and endocardial ST elevation at 20 minutes of ischaemia in 220 myocardial samples from the left ventricle of eight animals. It is evident that, although there was a wide variation in the levels of ST elevation for each range of myocardial blood flow, a weak but highly significant negative correlation (r=-0.25, r=-0.27, respectively, both P<0.001) was found between the endocardial potential changes to individual electrode site, and the endo/epi flow ratio, as well as the percent decrease of control RMBF, in which the endocardial electrodes were located. This correlation implies an inverse association between the endocardial potential increase and the endocardial flow decrease. Figures 6.15 (bottom) and 6.16 demonstrate that when the endocardial potential contour maps were superimposed with the RMBF image maps, a general relationship existed between the positive endocardial ST potentials and the low flow regions.

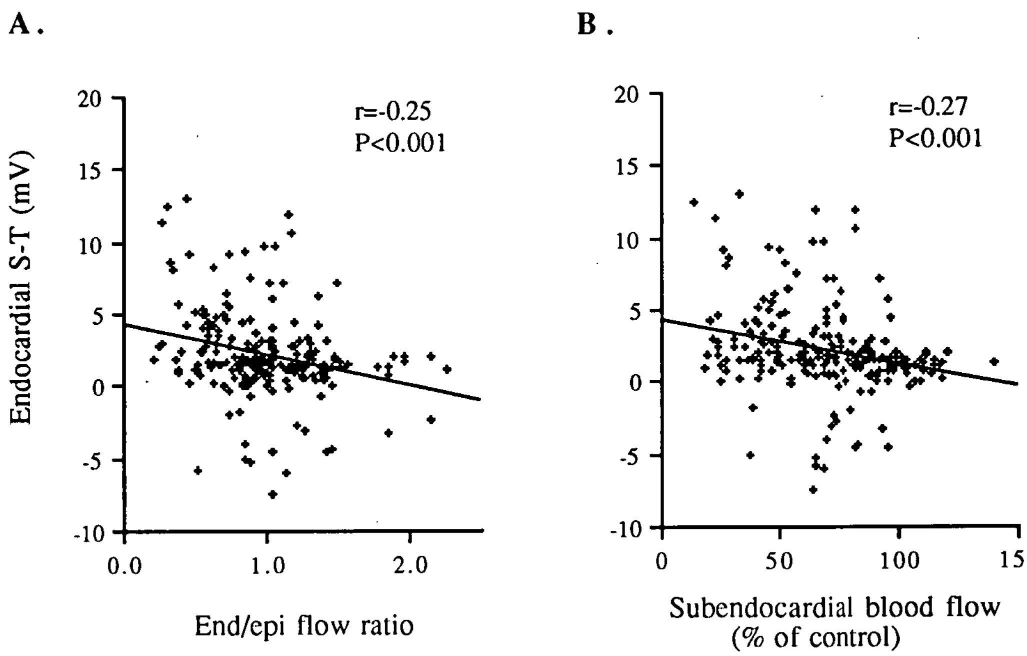

Figure 6.14. Endocardial ST changes from control are plotted as a function of the endo/epi flow ratio (A) and subendocardial blood flow (B) to the positions of the electrodes (220 data points from 8 sheep).

partial LAD ligation　　　　partial LCX ligation

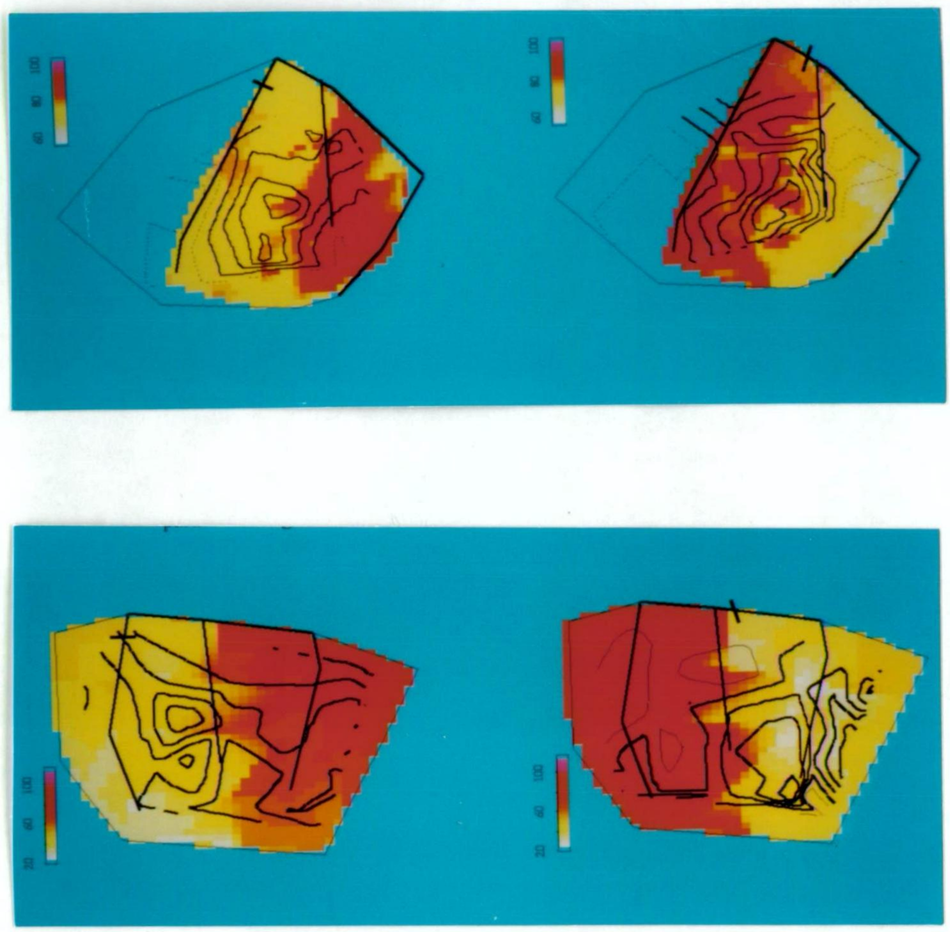

Figure 6.15 The top two maps are epicardial ST potential distributions (contour line) and endocardial flow distributions (colour). The bottom two maps are endocardial ST potential distributions (contour line) and endocardial flow distributions (colour). The flow maps were constructed from the simultaneous measurements of RMBF (as % of control flow). The red colour represents high flow and light colour low flow.

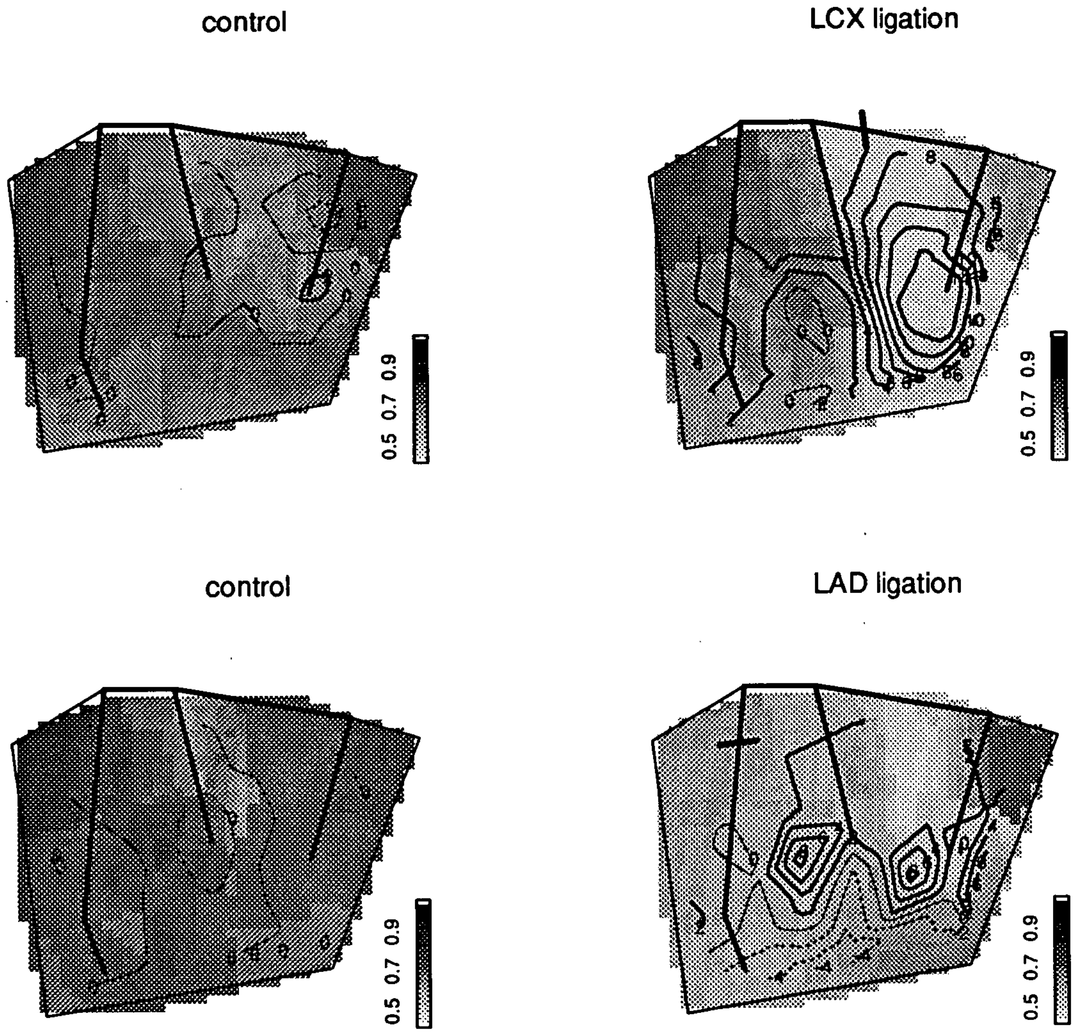

Figure 6.16 Endocardial ST potential distributions (contour line) overlayed by the endocardial flow distributions (shaded area) at control and 20 minutes of ischaemia. The flow maps were constructed from the simultaneous measurements of RMBF (mL/min/g). Intensities of the shade represent the quantity of flow.

6.3.6 Potential Changes by Insulation

The minimum epicardial ST potentials before and during insulation are tabulated in Table 6.4, and the epicardial potential distributions before and during insulation are shown in Figure 6.17. In 6 of the 8 sheep, insulation increased the magnitude of the epicardial ST depression by 2 to 8 mV (Table 6.4, $P<0.05$) without altering the distribution patterns (Figure 6.17). The magnitude of epicardial QRS complex was also significantly increased by insulation (Figure 6.18), while the magnitude of the QRS and ST potentials from the intracavity leads had less significant changes (Figure 6.19). In both the epicardial and endocardial electrograms, the R wave changed more than the S wave. Routine ECG limb leads showed a significant decrease in the magnitude of QRS complex and T wave (Figure 6.20). In 2 sheep, the epicardial potentials remained unchanged (Table 6.4).

Table 6.4 Minimum epicardial ST potentials (mV) with and without insulation

No.	without insulation	with insulation
1	-8	-16
2	-10	-12
3	-3	-3
4	-5	-8
5	-6	-10
6	-8	-10
7	-8	-8
8	-8	-10
mean	-7.00	-9.63
SD	2.20	3.70
P		0.02

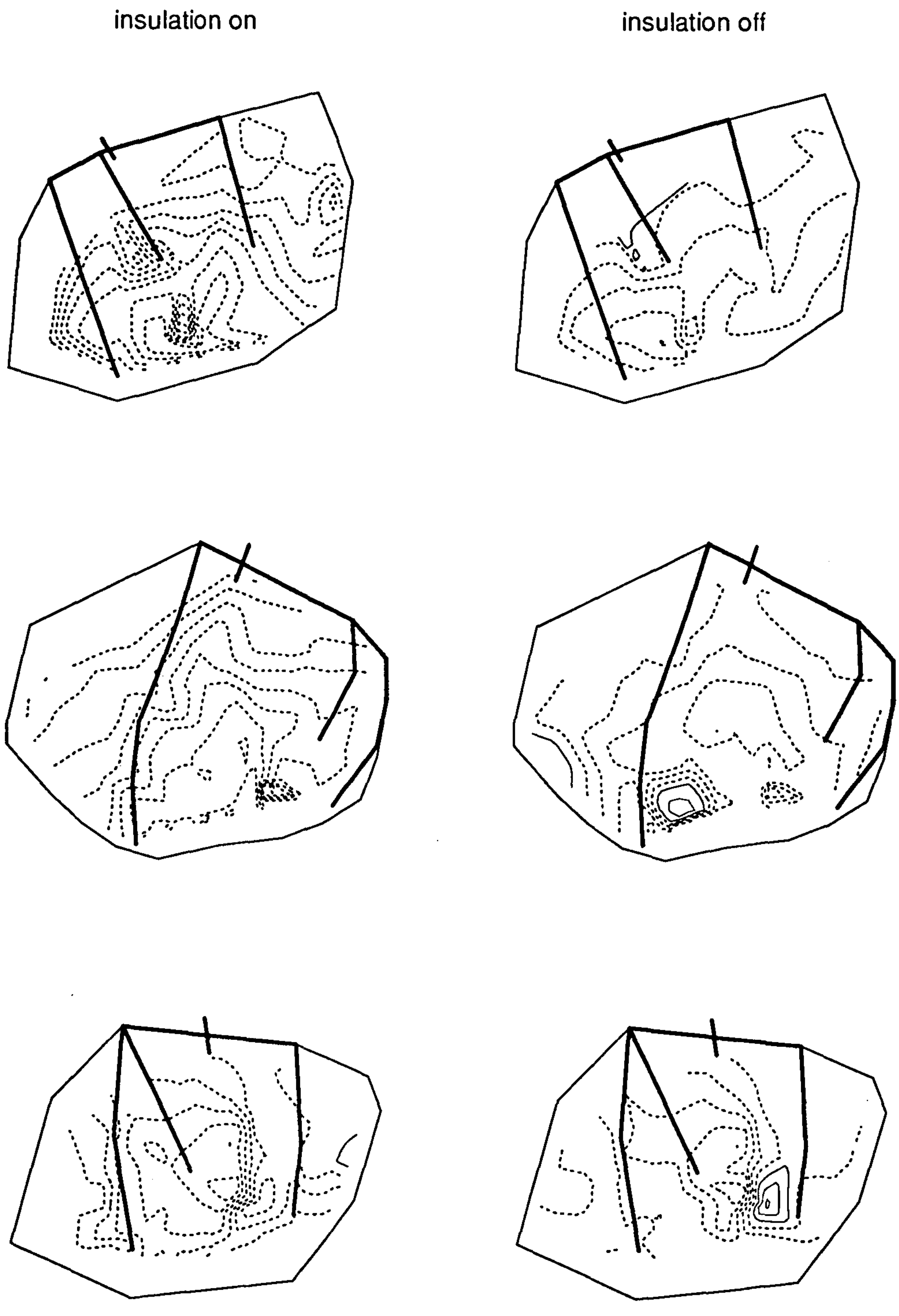

Figure 6.17 The diagrams are isopotential difference maps plotted with the data of 3 animals from group 2 (every two parallel maps are from one animal). They depict epicardial ST potential distributions with and without insulation. The increase in the magnitude of ST depression during insulation of the heart is shown by the increased number of isopotential lines. The potential distribution patterns are similar with and without insulation (contour interval = 2 mV. The solid contour lines represent ST elevation and dotted lines ST depression. Ligated arteries are indicated by bars).

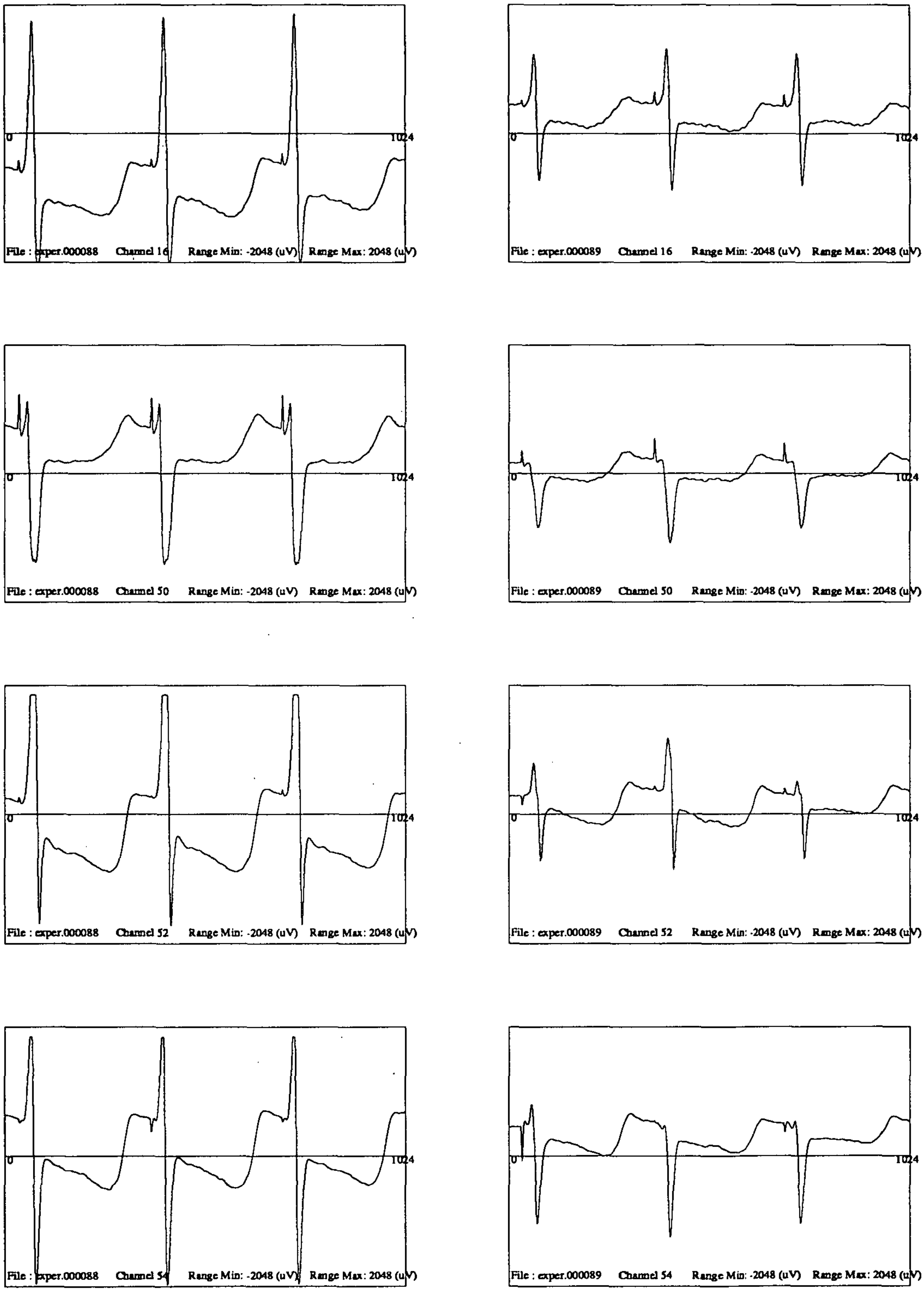

Figure 6.18 Epicardial electrograms with (left) and without (right) insulation during ischaemia. Insulation increased the magnitude of both ST depression and QRS waves significantly. The electrograms are selected from 64 epicardial recordings of one animal. The spikes before QRS complex are pacing signals.

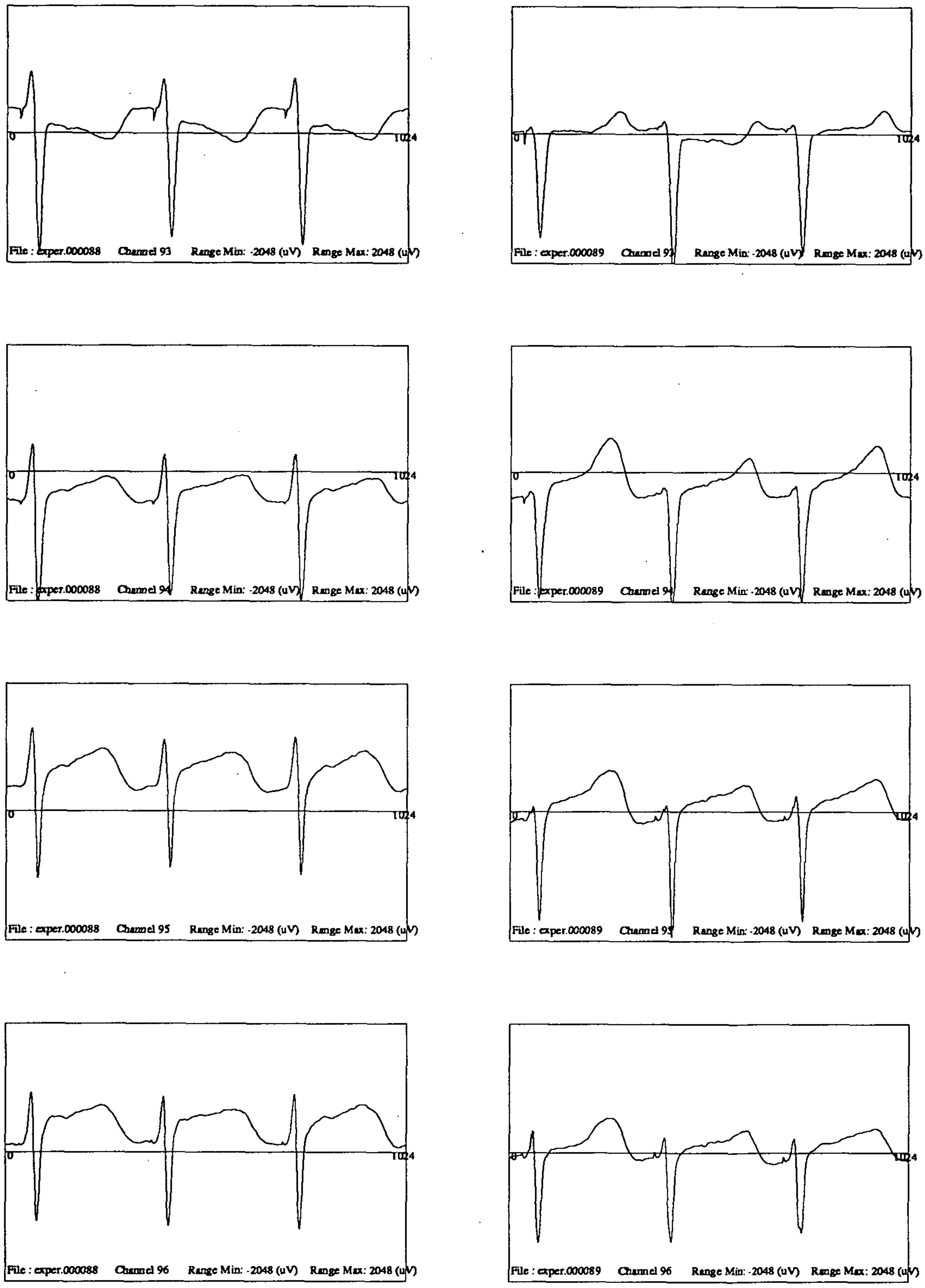

Figure 6.19 Endocardial electrograms with (left) and without (right) insulation during ischaemia. Insulation changed both the magnitude and the morphology of the QRS waves and the ST segment. The electrograms were simultaneously recorded with the epicardial electrograms in Figure 7.18 by a quadripolar electrode catheter. The spikes before QRS complex are pacing signals.

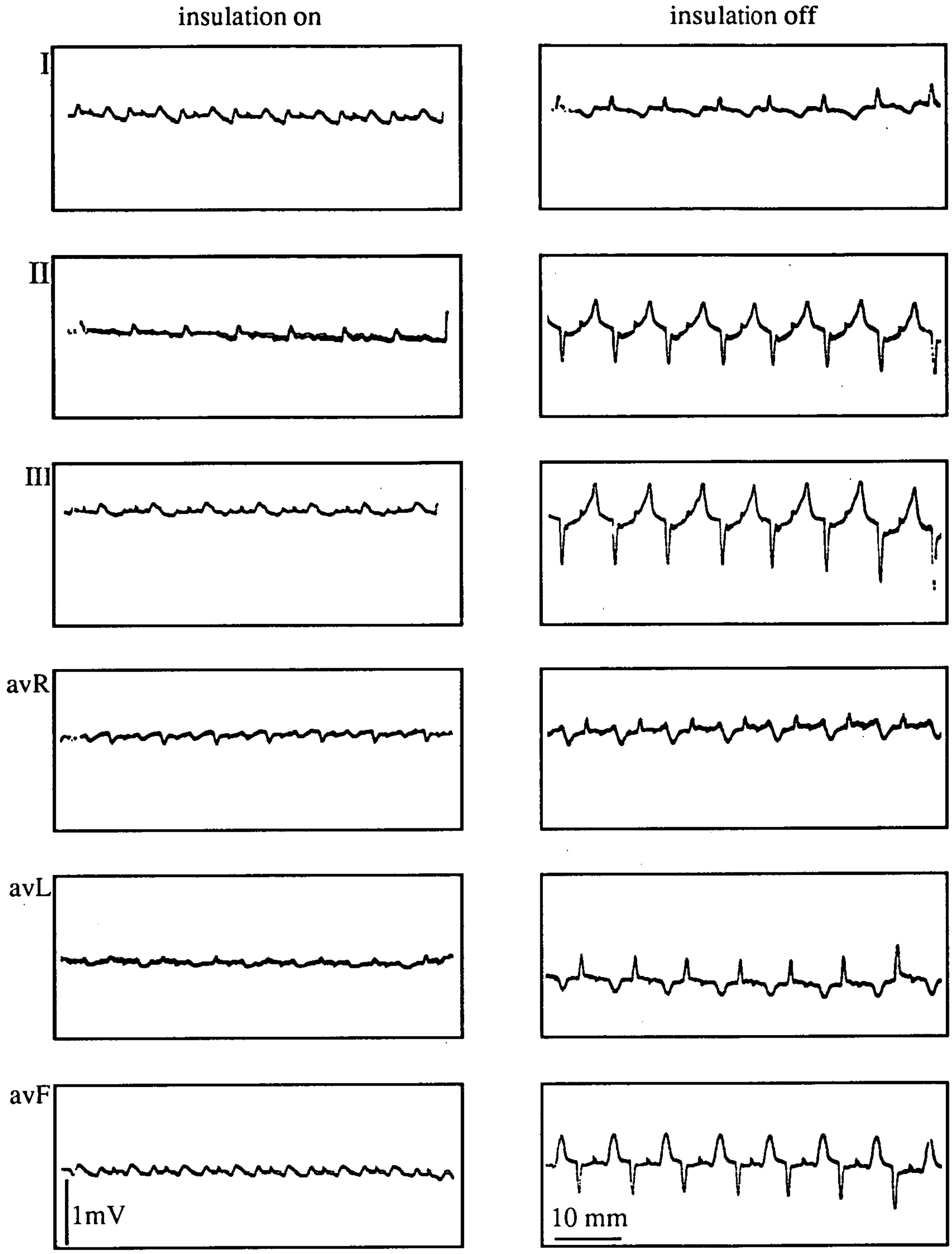

Figure 6.20 Routine ECG recordings with and without insulation. During insulation, the magnitudes of QRS and T waves were significantly reduced. The ECGs were recorded at a speed of 25 mm/sec, a calibration of 10 mm = 1 mV.

6.3.7 Epicardial Potential Changes by Intracavity Glucose Injection

The minimum epicardial ST potentials and the resistance of the blood before and during intracavity glucose injection are tabulated in Table 6.5. The potential distributions before and during glucose injection are shown in Figure 6.21. In 3 of the 7 sheep, glucose injection caused minor changes in the magnitude of epicardial ST depression (either increase or decrease by 1-2 mV, Table 6.5, $P>0.05$). In 4 sheep, the magnitude remained unchanged. The pattern of the potential distributions was not altered by the glucose injection (Figure 6.21). The measurement of the left ventricular blood resistance in three experiments before and during the glucose injection showed a marginal increase (from 4.84±0.15 to 5.40±0.12, $P=0.05$, Table 6.5).

Table 6.5 Minimum epicardial ST potentials and left ventricular blood resistance before and during glucose injection

	minimum ST (mV)		blood resistance (kΩ)	
No.	control	glucose	control	glucose
1	-5	-4	4.75	5.31
2	-4	-5	4.75	5.53
3	-3	-3	5.01	5.36
4	-6	-4		
5	-3	-3		
6	-5	-5		
7	-5	-5		
mean	-4.43	-4.14	4.84	5.40
SD	1.13	0.90	0.15	0.12
P		0.46		0.05

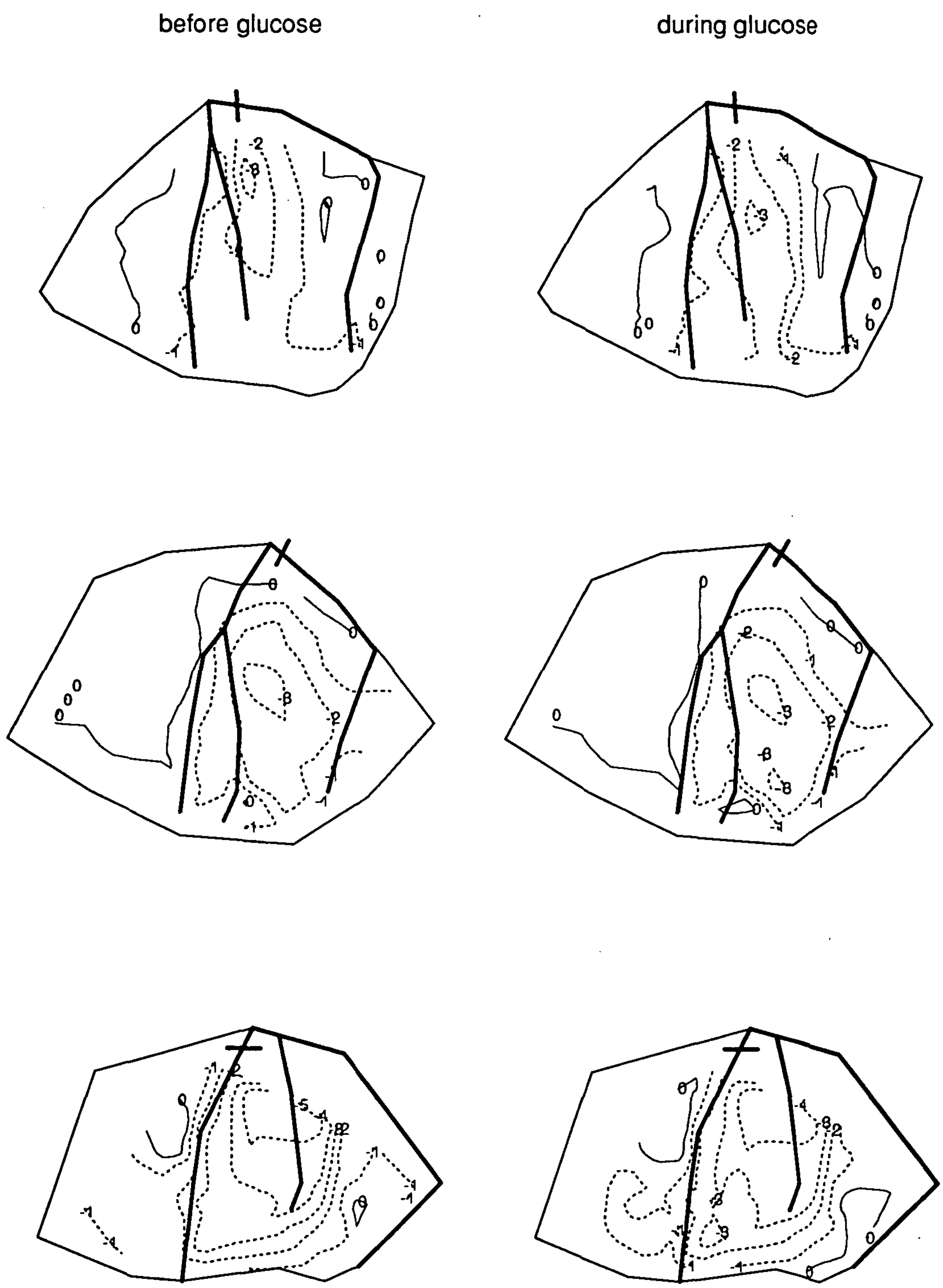

Figure 6.21 The diagrams are isopotential difference maps plotted with the data of 3 animals from group 2 (every two parallel maps are from one animal). They depict the epicardial ST potential distributions before and during glucose injection. The solid contour lines represent zero potential and dotted lines ST depression. Ligated arteries are indicated by bars.

6.3.8 Transition of Subendocardial Ischaemia to Transmural Ischaemia

To transform subendocardial ischaemia into full-thickness ischaemia, the percent stenosis of a coronary artery was increased by fully inflating the hydraulic occluder at 10-15 minutes of subendocardial ischaemia in 5 sheep of group 2, and the instant potential changes were recorded. In the early experiments, the potential changes were recorded intermittently (n=2). Maps of one animal with LCX ligation were displayed in Figure 6.22. Minor ST elevation first occurred in the posterior region 2 seconds after the transition. As ischaemia progressed, ST elevation expanded to the inferior region with a gradual increase in the magnitude. The expanding of the ST elevation shifted the boundary toward the lateral wall. Two minutes after the transition, ST changes reached a maximum of +24 mV, and a minimum of -32mV. In the later experiments, the potential changes during transition were recorded continuously for 30 seconds (n=2) and 50 seconds (n=1). From 50 second recording, it was found that ST depression increased gradually as ischaemia progressed until ST elevation ensued at 30-35 seconds (Figures 6.23 & 6.24). The increase of the ST depression occurred at the lateral boundary in either the LCX or the LAD ligation, whereas the ST elevation started from the posterior wall of the heart in LCX ligation (Figure 6.23) and the anterior wall in LAD ligation (Figure 6.24). The ST changes were not captured in the 30 second recording either because the recording was started too early, too late, or because the recording period was not long enough.

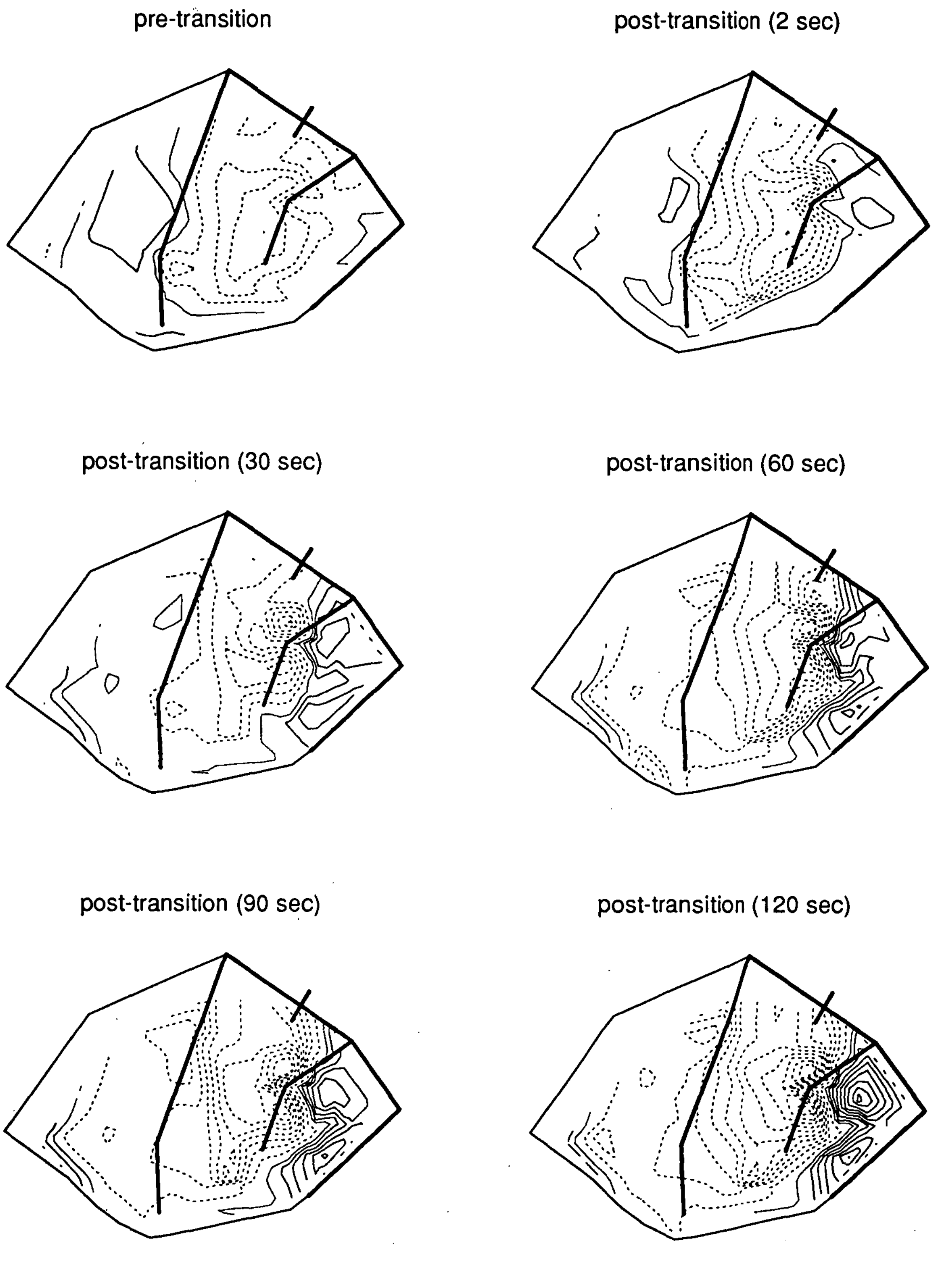

Figure 6.22 Sequential epicardial potential distributions before and after the transition of subendocardial to full-thickness ischaemia in the LCX ligation (intermittent recording). The thin solid and dotted contour lines represent ST elevation and depression respectively. The thinner contour lines indicate zero potential. For the top two maps, the contour interval=2 mV; for the bottom four maps, the contour interval=4 mV.

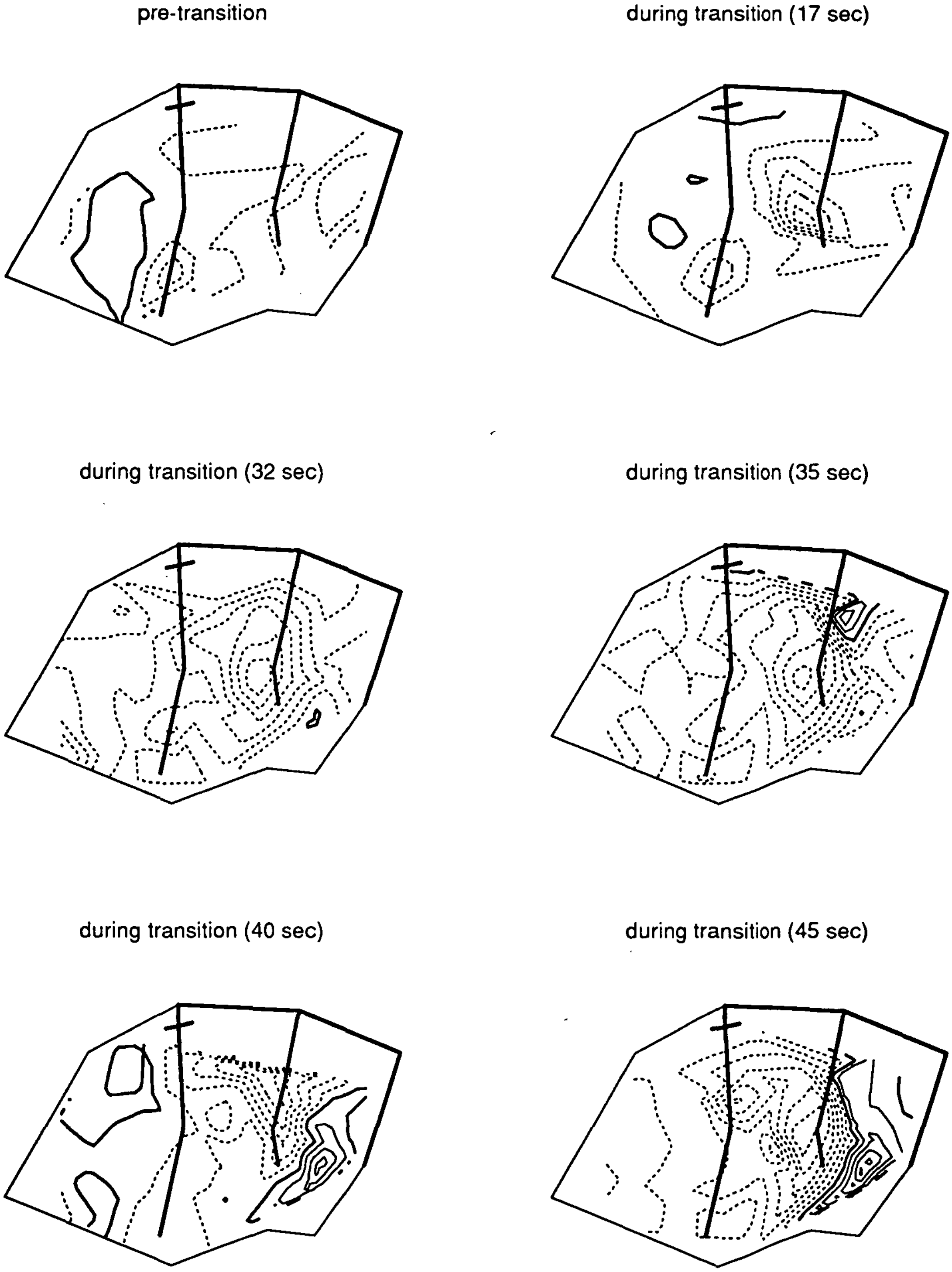

Figure 6.23 Sequential epicardial potential distributions during the transition of subendocardial to full-thickness ischaemia in the LCX ligation (continuous recording). Thin solid and dotted contour lines represent ST elevation and depression respectively. The thick solid contour lines indicate zero potential. For the first map, the contour interval=2 mV; for the other 5 maps, the contour interval=4 mV.

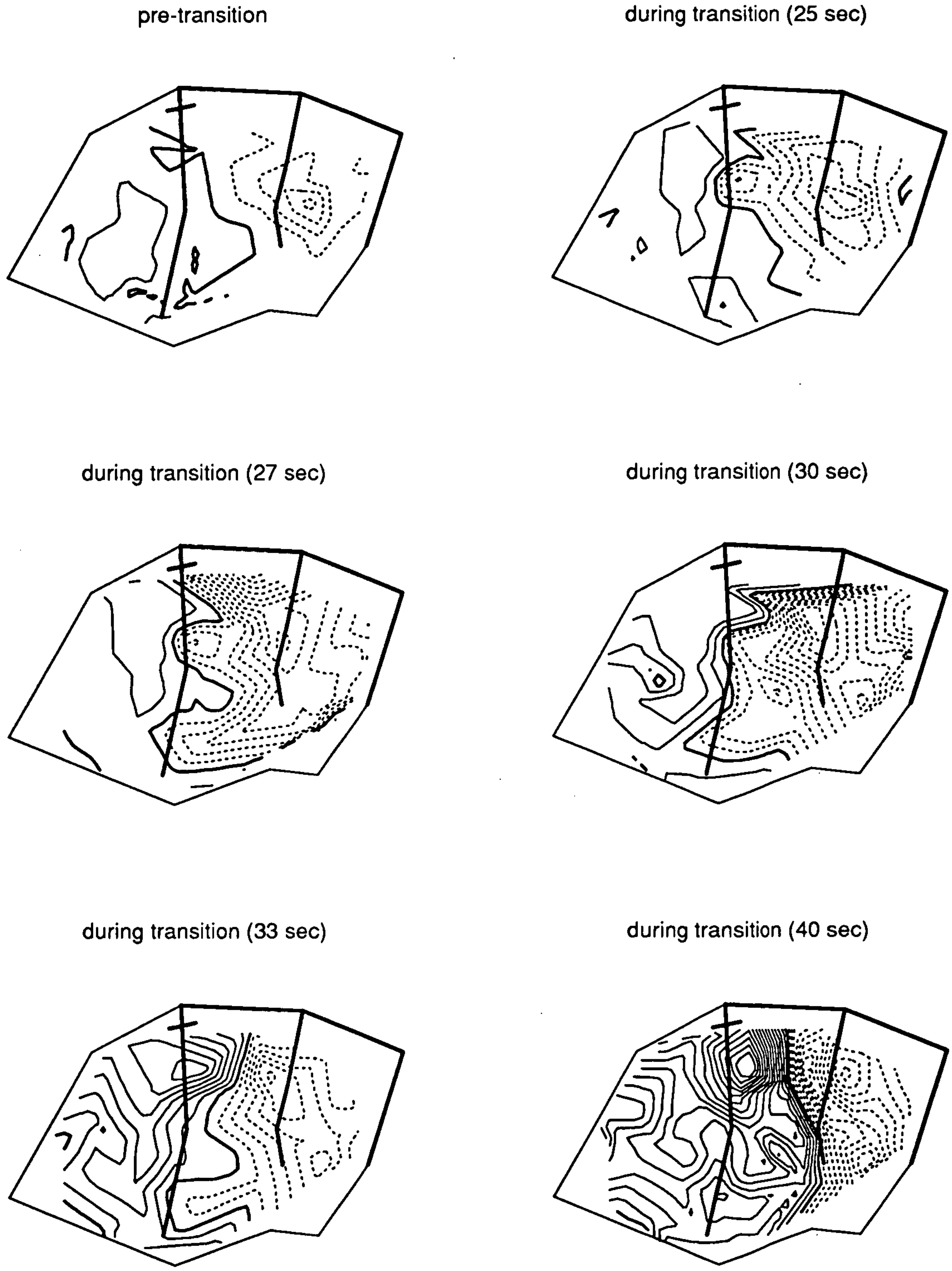

Figure 6.24 Sequential epicardial potential distributions during the transition of subendocardial to full-thickness ischaemia in the LAD ligation (continuous recording). Thin solid and dotted contour lines represent ST elevation and depression respectively. The thick solid contour lines indicate zero potential. For the top 4 maps, the contour interval=1 mV; for the bottom 2 maps, the contour interval=2 mV.

6.4 DISCUSSION

6.4.1 Epicardial ST Depression Does Not Predict Ischaemic Region

A major finding of the present study is that even from the epicardium, ischaemic ST depression can not predict the location of an ischaemic region. As shown in Figures 6.3, 6.4, and 6.7, the distributions of epicardial ST depression are independent of the responsible ischaemic location. Either the LAD or the LCX ischaemia gives a similar epicardial ST distribution pattern although the absolute values of the potentials varied. Pacing alone to the rate of 180 bpm did not change the ST potentials and their spatial features (Table 6.2, Figure 6.2), indicating that rapid atrial pacing was not responsible for the patterns of ST depression. Therefore, although epicardial ST depression reflects subendocardial ischaemia, its position does not locate the responsible myocardium. Unlike body surface recording, epicardial potential recordings are free of the intervening structures such as lungs, bone, and skeletal muscle, and therefore directly relate to the underlying myocardium. If epicardial ST depression can not distinguish an ischaemic region, neither can the body surface ST depression. These results explain the difficulty in localising ischaemia from body surface ST depression (Kubota et al. 1985; Dunn et al. 1981; Fuchs et al. 1982; Abouantoun et al. 1984; Mark et al. 1987). However, they can not be explained by the classic ECG theories (Wilson et al. 1933; Holland & Brooks 1975), which all suggest that ST depression should be able to localise ischaemia.

6.4.2 The Source of Epicardial ST Depression Is Related to the Ischaemia of the Subendocardium

In transmural ischaemia, epicardial ST elevation occurs when injury currents flow between the ischaemic regions and the normal myocardium (Kleber et al. 1978, Samson & Scher 1960). The region of ST elevation is closely related to the region of ischaemia (Kleber et al. 1978). At cellular level, two major mechanisms are considered to underlie ST segment displacement: a localised shortening of action potential duration and diminishing of the amplitude of the action potential, or a localised decrease in resting membrane potential. The former generates current only during the ST segment. The latter generates a steady injury current that is interrupted during the ST segment when all the cells are depolarised. The injury current produces a TQ segment shift that can not be directly detected on the ECG because the amplifiers are AC-coupled, but the interruption of the injury current during the ST segment produces an apparent ST shift, which is opposite to the TQ segment shift on the AC-coupled ECG.

With ST depression, there is no satisfactory explanation of the cardiac electrophysiological changes. Early work (Wolferth et al. 1945; Bayley 1946; Pruitt & Valencia 1948) in isolated hearts suggested that the ST segment response to myocardial injury is elevation; the ST segment depression recorded at the epicardium is the reciprocity of ST elevation in the underlying subendocardium. These works confirmed the dipole theory, which was developed by Wilson and co-workers in 1930s (Wilson et al. 1933b; Bayley 1942). The dipole model considered the active myocardial event as a single dipole source which contained both the maximum and the minimum potentials. Accordingly, an injured region of the myocardium acts in systole as the positive pole of a layer of dipoles situated on its boundary with normal myocardium which acts as the negative pole. In the event of subendocardial ischaemia, the ventricular surface and the precordium over the ischaemic region face the negative pole of the dipole while the cavity faces the positive pole. Thus, the electrodes over the ischaemic region should record depressed ST while the cavity should yield elevated ST (Bayley 1946; Cook 1958; Yu & Stewart 1950). However, this theory does not explain either the clinical difficulty in localising ischaemia by ST depression, or the present findings. The limitations of the single dipole model have been reviewed in Chapter 2 (Section 2.3.2).

Prinzmetal and co-workers (Ekmekci et al. 1961; Toyoshima et al. 1964) proposed that epicardial ST depression was the direct result of mild local ischaemia causing an increased epicardial intracellular negativity, rather than a reciprocal effect of subendocardial ST elevation. But they did not perform local measurements of RMBF. The simultaneous epicardial and endocardial electrogram recordings from our experiments (Figures 6.8 & 6.9) did not support their point of view. Furthermore, the RMBF measurement in this study (Chapter 5) and others' (Guyton et al. 1977; Mirvis & Gordey 1983) revealed that epicardial ST depression occurs when blood flow to the deeper myocardial layers decreases. The ECG reflects the potential difference between two electrodes or points on the body surface; a region of ST depression implies that there is a region of potential that is more negative than the reference electrode. The endocardial recording of the ST elevation in the ischaemic region during subendocardial ischaemia along with Kleber's work (1978) with intracellular recording have suggested that the source of the ischaemic ST depression is related to the ischaemia of the endocardium (Figures 6.8, 6.9 and 6.15).

In this study, the general epicardial ST depression during ischaemia was not correlated with the simultaneously measured flow changes (Figures 6.12 & 6.13); when the epicardial contour maps were combined with the endocardial flow maps, the minimum potential was independent of the lowest flow region (Figure 6.15 top). These results suggest that the changes in epicardial ST potential during subendocardial ischaemia do not directly relate to the concomitant RMBF changes in the ischaemic region. However, a weak but highly significant inverse correlation existed between the endocardial ST elevation and the endocardial flow reduction (Figure 6.14). This correlation implies an inverse association between endocardial potential increase and endocardial flow decrease (Figures 6.15 bottom & 6.16). Nevertheless, the results do not suggest a simple quantitative relationship between these two variables. Since the ischaemic state results from an imbalance between the energy requirements of the myocardium and its metabolic supply, the measurement of the regional blood flow provides only a partial assessment of the magnitude of myocardial ischaemia. This could explain the low correlation coefficient between the endocardial ST elevation and the flow changes, but it does not negate the value of RMBF change as an indicator of myocardial ischaemia. The combined endocardial potential maps and the endocardial flow maps demonstrated that the maximum potential was related to the low flow region (Figures 6.15 bottom & 6.16). These results suggest that the ischaemic source relates to the endocardial ST changes but not the epicardial ST changes. This finding can not be interpreted by the solid angle theory.

The solid angle theory (Holland & Arnsdorf 1977), by taking into account the geometry of the ischaemic boundaries, the degree of transmembrane action potential duration differences, and alterations in intra- and extra- cellular conductivities, has provided a geometrical ischaemic heart model that quantitatively links changes in ST elevation to the distribution of transmembrane potential changes in the ischaemic region. From this model, Holland and Brooks also predicted that endocardial ischaemia would cause relative depression of the ST segment in epicardium and precordium due to the reversed current flow at the boundary of the normal and the ischaemic myocardium (Holland & Arnsdorf 1977; Holland & Brooks 1975 & 1977b) and that this ST depression should be able to localise ischaemia. However, they did not produce subendocardial ischaemia in their porcine model and this proposition remained untested (Holland & Brooks 1975).

Since the endocardial ST elevation predicts the location of subendocardial ischaemia, while the simultaneous epicardial ST depression does not (Figures 6.8 & 6.9), it is possible that the injury current has been altered when it flows from the endocardium to the epicardium by some unknown factors such as the great vessels and other tissues surrounding the heart, and the intracavity blood, which may be important in the origin of ischaemic ST depression (Kilpatrick et al. 1990). These factors and the current path are discussed in the following section.

6.4.3 The Current Path of Subendocardial Ischaemia Is Inside the Heart

The primary source currents generated by the heart itself flow throughout the conductive body and contribute to the ECG. The relative contributions of the primary ischaemic source currents to epicardial ST depression were evaluated experimentally in the present study by insulating the heart in vivo in an effort to eliminate the flow of currents through the body. The results demonstrate that insulation increased the magnitude of epicardial ST depression by 2 to 8 mV (Table 6.4, $P<0.05$) without altering the distribution patterns (Figure 6.17). The magnitude of epicardial QRS complex was also increased by insulation (Figure 6.18), while the magnitude of the QRS and ST potentials from the intracavity leads had less significant change (Figure 6.19). Routine ECG limb leads showed a significant decrease in the magnitude of QRS complex and T wave (Figure 6.20).

A few experiments have been done in which the conductivity of the area external to the heart has been altered. Wilson, Hill, and Johnston (1934) showed that the potentials recorded by the leads on the turtle heart were greatly reduced when the heart was surrounded by saline. Conrad and Cuddy (1960) also observed decreases in potentials when the dog chest cavity was filled with conducting fluid. In these experiments, the loss in potentials was due to the shunting action of the low-resistance fluid. Lindner and Katz (1939) put rubber sheeting between various parts of the heart and the surrounding medium. The electrical current flow through the lungs, anterior chest wall, diaphragm and adjacent organs, and through the tissues behind the heart was assessed individually by measuring the decrease in QRS voltage when insulators were placed in lateral, anterior, inferior and posterior locations, respectively. In order of decreasing importance, they found the relative proportion of the heart's current transferred to the body field to be the posterior, superior, inferior, and anterior surfaces of the heart. A recent study has also demonstrated that the amplitude of the epicardial QRS potentials from both intact and isolated hearts was markedly higher when the heart was surrounded by an insulating medium, but the QRS potential distribution patterns were less affected by the surrounding medium (Green et al. 1991). The introduction of the insulating material has the effect of reducing the net flow of current from the heart into the surrounding medium. Because of this effect, the magnitudes of the epicardial and endocardial QRS potentials increased (Figures 6.18 & 6.19) while the magnitudes of the limb QRS potentials decreased (Figure 6.20). The excitation of the heart can be detected by the ECG primarily because of the existence of the potential difference between the activated cells and the resting cells during the propagation of the action potential in the ventricles. The similar increase in the magnitudes of the epicardial and endocardial ST potentials might represent the same behaviour, suggesting the current path is inside the heart itself, ie, from the endocardium to the epicardium either via the myocardium or via both the intracavity blood and myocardium. This contention was further tested by the transition of subendocardial ischaemia to transmural ischaemia and by changing the conductivity of the intracavity blood.

From the transition of subendocardial ischaemia to full-thickness ischaemia, it was found that epicardial ST depression increased gradually over the boundary region as ischaemia progressed and ST elevation ensued over the ischaemic region as ischaemia became transmural (Figures 6.23 & 6.24, n=1). In the early experiments, intermittent recording (n=2) and 30 seconds recording (n=2) were used due to the computer memory shortage, and the increase in the ST depression before transmural ischaemia was not captured because of the short-time recording. However, the epicardial potential distributions before and after the transition did show a progressive ST elevation which started from the ischaemic region and extended to the lateral boundary (Figure 6.22). The increase of ST depression before the occurrence of ST elevation was also observed in a study with a perfused canine heart (Guyton et al. 1977). The electrical transition from ST depression to ST elevation was consistent with the contention that the current path is in the myocardium.

In the normal ECG, the ST segment remains isoelectric because there are no great potential differences occurring in the myocardium during this period. In transmural ischaemia, epicardial ST elevation occurs when injury currents flow at the *boundary* between the ischaemic region and the normal myocardium because of the potential difference between these two regions (Kleber et al. 1978; Samson & Scher 1960). Since the myocardial cells in subendocardial ischaemia undergo qualitatively similar changes as those in transmural ischaemia (Reimer et al. 1992), it is possible that the injury currents in subendocardial ischaemia also originate from the ischaemic boundary. As the subendocardial ischaemia involves only the inner layer of the ventricular wall, the boundary between the ischaemic region and the normal myocardium should include transmural boundary and lateral boundary. However, the flow distribution during subendocardial ischaemia demonstrated that transmurally, there was a gradual flow transition from the endocardium to the epicardium (Figure 5.5, chapter 5) (Guyton et al. 1977; Mirvis & Gordey 1983) while at the lateral boundary, flow changed sharply from the ischaemic zone to the nonischaemic zone, producing a sharp lateral interface between ischaemic and normal regions (Figure 5.6, chapter 5). Studies on transmural ischaemia also found a sharp lateral interface between ischaemic and normal cells with severely ischaemic tissue lying adjacent to normal, well perfused tissue (Factor et al. 1981; Reimer et al. 1979; Harken et al. 1981). Transmembrane action potential recordings from ischaemic pig heart by using floating microelectrodes also demonstrated a sharp and distinct transition from electrophysiologically abnormal to normal cells (Janse et al. 1979). Therefore, it can be assumed that the greatest potential difference between ischaemic and nonischaemic cells appears at the lateral boundary, which, in turn produces the strongest injury current. Under such circumstances, the greatest epicardial potential change should appear at the lateral boundary regions with less change in the ischaemic centre where the transmural boundary locates and less injury current occurs. Accordingly, in this study, the maximum epicardial potential change should be at the lateral wall and middle septum where the LAD and the LCX share their borders, and this explains the experimental results. To verify this contention, intramural recordings were performed. Four quadripolar needle electrodes with a diameter of 0.9 mm and a length of 17 mm were applied to record intramural potentials from the boundary, the ischaemic and the nonischaemic regions. Unfortunately, the data recorded were not satisfactory due to the strong injury currents produced by the intramural electrodes themselves (Figure 6.25). This problem should be solved by reducing the diameter of the intramural electrodes and improving the skills of electrode implantation in the future studies. Nevertheless, the transition of subendocardial ischaemia to full-thickness ischaemia showed that as ischaemia progressed, ST depression increased gradually until ischaemia became transmural and ST elevation ensued in the ischaemic centre (Figures 6.23 & 6.24). The change of ST depression occurred at the lateral while the change of ST elevation started at the ischaemic centre. ST elevation gradually progressed toward the ischaemic border, shifting the boundary almost to its original position, ie, the lateral wall. These results support the postulate that the major source of subendocardial ischaemia may be the lateral boundary.

In addition, data from this experiment showed that ST depression in nonischaemic region did not disappear when full-thickness ischaemia occurred, instead, the magnitude of ST depression increased as did ST elevation as ischaemia progressed. The reasons for these changes are not clear. It might be a simple electrical reciprocity of ST elevation or it might reflect subendocardial ischaemia (Mirvis 1988) (see Chapter 7 for further discussion). Furthermore, the recordings demonstrated that the epicardial ST distribution during partial coronary stenosis was totally different from that of ST elevation resulting from total coronary stenosis; the former provided no information on the coronary artery involved, while the latter localised in the ischaemic region.

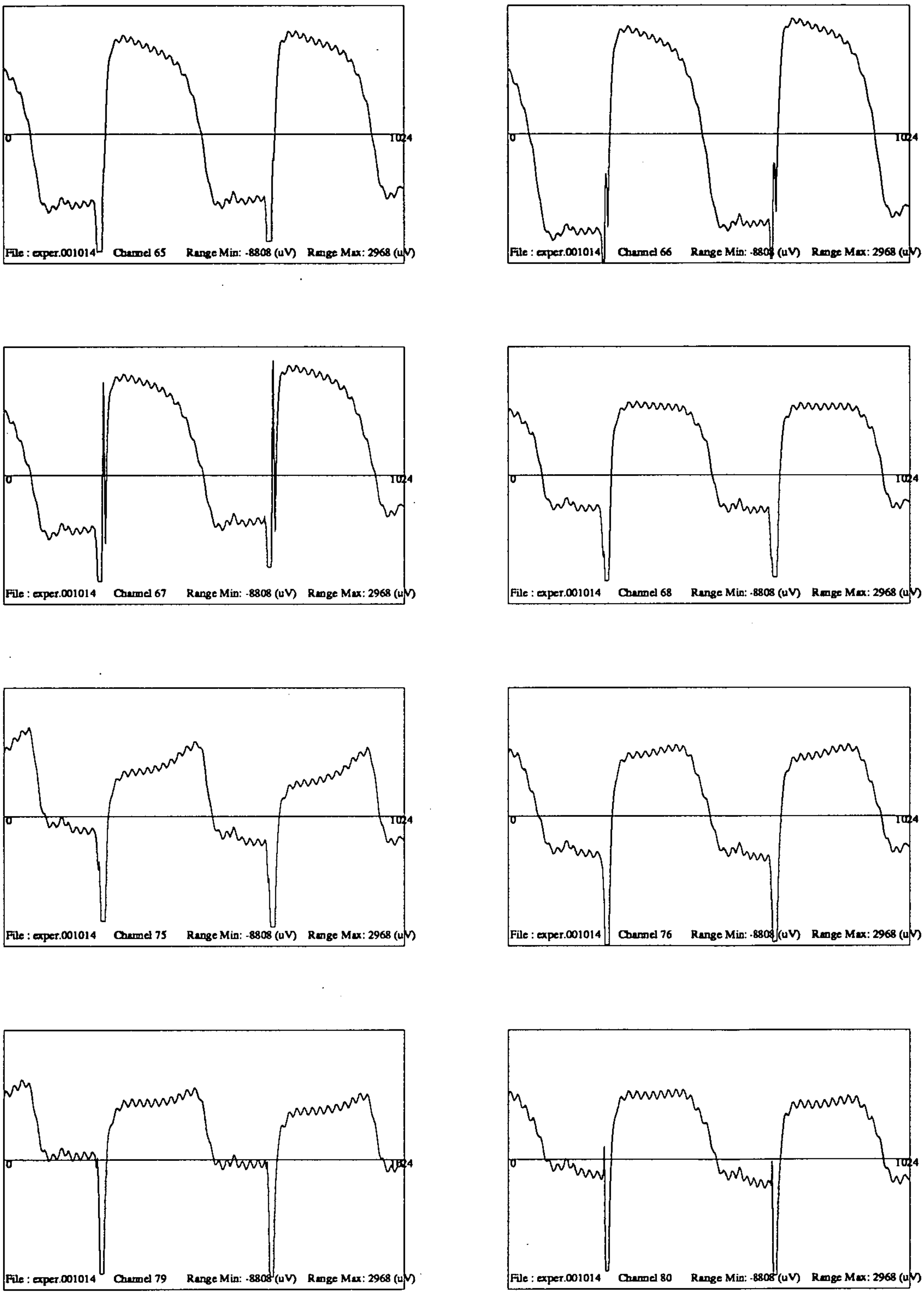

Figure 6.25 Intramural recordings by two quadripolar needle electrodes from one experiment. The electrograms were recorded 3 hours after the implantation of the electrodes. The ST elevation was still obviously high.

Findings from this study are inconsistent with the hypothesis that a low-resistance current path from the ischaemic endocardium travels out of the heart through the intracavity blood and the great vessels and then returns back to the epicardium (Kilpatrick et al. 1990). Insulating the heart from surrounding tissues should have changed or prevented the epicardial ST depression if the hypothesis was correct. Since this study was carried out in an open chest preparation with the anterior wall of the left ventricle not in contact with the thorax, insulating the heart would change the amount of the lateral and posterior wall of the left ventricle and the right ventricle in contact with the surrounding tissues. The ventricles were supposed to be well insulated as they were nearly encircled by the plastic bag. However, there was a small leakage path existing upwards through the atria and the great vessels to conduct currents to the body surface that resulted in potentials at the limb leads, and this explains why the QRS waves did not totally disappear from the limb leads (Figure 7.20).

During insulation, why did the endocardial QRS and ST segment have less change in the magnitude and more change in the QRS morphology than that of the epicardial (Figures 6.18 & 6.19)? One possible explanation is that the high conductivity of the intracavity blood (3 times that of the myocardium (Rush et al. 1963)) might dilute the current intensity by shunting the current, when considering that the current also flows at the boundary between endocardium and intracavity blood.

It has been suggested that the presence of blood within the heart strongly influences the cardiac electrical potentials recorded at the thoracic surface (Brody 1956). This effect may result either from an alteration in intracardiac blood volume or from different blood resistivity as determined by the proportions of red blood cells (high resistivity) and plasma (low resistivity). The presence of relatively low resistivity blood within the heart was postulated by Brody (Brody 1956) to augment the radially oriented cardiac forces associated with endocardial-to-epicardial excitation and to attenuate tangentially oriented forces occurring during apex-to-base directed depolarisation. It is postulated that, if haematocrit (and therefore resistivity) increased, voltages due to radial forces would be diminished and voltages due to tangential ones augmented. Evidence supporting the hypothesis has been found in models (Brody 1956) and in animals (Nelson et al. 1956 & 1972; Hodgkin et al. 1977; Nelson 1980).

In the present study, the contribution of the intracavity blood to the ischaemic ST changes was tested by injection of high resistance glucose into the left ventricle. Since the blood has a lower resistivity than myocardium (Rush et al. 1963), to increase the resistivity of the blood to equal that of the myocardium should produce a homogeneous myocardium-cavity situation, and eliminate the endocardium-blood boundary, and thus alter the electrical field. The results of this attempt were not conclusive. As shown in Table 6.5 and Figure 6.21, the distribution and the magnitude of the epicardial potentials were not altered significantly by this manoeuvre. The failure of the glucose injection to change the epicardial ST depression is probably due to the fact that glucose injection did not produce sufficient change in the resistivity of the intracavity blood. As showed in Table 6.5, glucose injection caused a nonsignificant increase of blood resistance (from 4.84±0.15 kΩ to 5.40±0.12 kΩ, P=0.05). Since the resistance of the pure glucose was 690 kΩ, the pure blood was 4.75 kΩ (from the author's experiment), it is obvious that the 50 mL glucose injection did not produce enough change in the resistance of the intracavity blood. Thus, the contribution of the intracavity blood to the epicardial ST depression can not be excluded. It was decided not to pursue this further in this study as other manoeuvres were likely to yield more definitive results.

From the above discussion, the origin of ST depression remains unclear. The exact current path and the contribution of the intracavity blood to the ischaemic ST depression need further scrutiny. In theory this can be provided by intramyocardial electrical recordings but in practice injury currents make the ST segment very difficult to analyse.

The cardiac ischaemic source-surface potential relationship which is fundamental in electrocardiography is recognised to be complex. Source orientation and strength, volume-conductor characteristics of the body, and source location are all factors in the relationship. This multiplicity of factors makes it difficult to rigidly prove and quantitatively define the roles for each. Despite this, findings in the present study strongly suggest that: epicardial potential patterns are not substantially affected by the cardiac locations of responsible subendocardial ischaemia; ST depression may originate from the injury current which flows at the lateral boundary of the endocardial ischaemia; and the current path for the ischaemic ST source is mainly in the myocardium.

6.4.4 Evaluation of Present Method

The present study was based on the previously validated subendocardial ischaemic sheep model produced by a combination of partial coronary arterial stenosis coupled with left atrium pacing (Li et al. 1996) (Chapter 5). The methods in the present study differed in certain aspects from those used by others. To avoid variables introduced by the isolated heart, the study was carried out with the heart in-situ. The epicardial ST potentials were recorded from 64 electrodes spread over the whole surface of the heart. The endocardial ST was recorded by a 40-pole basket electrode. The precise determination of the electrode position together with the detection of the RMBF in each experiment enabled the author to correlate electrophysiology with anatomy and the regions of ischaemia. Such precise and detailed mapping on the simultaneous epicardial and endocardial potentials in an in-situ heart with subendocardial ischaemia has not been performed previously. Previous studies have been performed in the isolated heart in which the epicardial ST changes after physical or chemical injury were only recorded in the injured region with a limited number of electrodes (Wolferth et al. 1945; Bayley 1946; Pruitt & Valencia 1948). For those studies in the in-situ heart, ST depression was either not produced (Holland & Brooks 1975; Vincent et al. 1977), or the epicardial and the endocardial potential changes during subendocardial ischaemia were not investigated (Mirvis et al. 1986).

6.4.5 Limitation

The intramural recordings were not successful, thus, the actual current flow path was unable to be determined.

6.4.6 Clinical Implication

The findings of the present study have special relevance to the interpretation of ST depression. Many workers have shown that, although body surface ST elevation was highly related to the region of ischaemia, body surface ST depression was poorly related if at all (Kubota et al. 1985; Dunn et al. 1981; Fuchs et al. 1982; Abouantoun et al. 1984; Mark et al. 1987). The results from this study explain this poor localisation of ischaemia by ST depression in humans, but do not yet define the source.

Chapter 7

EPICARDIAL AND ENDOCARDIAL ST POTENTIAL MAPPING OF THE TRANSMURAL ISCHAEMIA -In Relation to Regional Myocardial Blood Flow

7.1 INTRODUCTION

The ST segment elevation typical of acute myocardial infarction is located over the infarcted region and is often associated with ST segment depression in the contralateral leads (Mirvis 1988; Katz et al. 1986). The pathogenesis and clinical significance of such ST depression remains controversial. Most of the clinical studies have showed that the presence of ST depression in the remote myocardial region is associated with larger infarction (Wong et al. 1993a; Wong & Freedman 1994; Edmunds et al. 1994; Lew et al. 1985), more extensive coronary artery disease (Haraphongse et al. 1984; Salcedo et al. 1981; Krone et al. 1993), and a higher risk of poor clinical outcomes (Bates et al. 1990; Lembo et al. 1986; Pichler et al. 1983; Gheorghiade 1993; Krone et al. 1993; Kilpatrick et al. 1989). However, other clinical studies have failed to reach the same conclusion, and the remote ST depression has been attributed to a purely benign electrical phenomenon in these studies (Camara et al. 1983; Putini et al. 1993; Fletcher et al. 1993; Stevenson et al. 1993 & 1994; Birnbaum et al. 1994). Published results of animal models of acute myocardial infarction showed uniform ST elevation over the infarcted region with little change over the remaining epicardium (Holland & Brooks 1975; Smith et al. 1979; Kleber et al. 1978). Typical infarction size was small to ensure stability of the animal (Holland & Brooks 1975; Smith et al. 1979).

This chapter presents different results from 33 sheep when both large and small infarctions were generated. To assess the significance of ST depression in acute myocardial infarction, the epicardial and the endocardial ST potential distributions were mapped in both the infarcted and the noninfarcted regions in an in-situ sheep model, and the potentials were related to the regions of ischaemia confirmed by fluorescent microspheres.

7.2 EXPERIMENTAL PROCEDURES

7.2.1 Animal Groups

A total of 33 sheep (20-37 kg) of both sexes were used in this study. They were randomised into three groups.

Group 1 Ligation of the obtuse marginal branch of the left circumflex coronary artery (OM, n=8). Epicardial potentials were mapped in 8 animals, regional myocardial blood flow (RMBF) was measured before and 20 minutes after the artery was occluded in 6 animals.

Group 2 Ligation of the left circumflex coronary artery (LCX, n=12). Epicardial potentials were measured in all the 12 animals. In 5 of the 12 animals, RMBF was measured before and 20 minutes after the artery was occluded, and the endocardial potential distributions were simultaneously recorded with the epicardial potentials.

Group 3 Ligation of the left anterior descending coronary artery (LAD, n=13). Epicardial potentials were measured in all the 13 animals. In 5 of the 13 animals, RMBF was measured before and 20 minutes after the artery was occluded, and the endocardial potential distributions were simultaneously recorded with the epicardial potentials.

7.2.2 Transmural Ischaemia

Transmural ischaemia was achieved by completely ligating the OM in group 1, the proximal LCX (after the first branch) in group 2, and the proximal LAD (before any branches) in group 3 for a minimum of 20 minutes. Each ligation was conducted by applying an artery clip on the intended artery near its origin. Immediately after the artery ligation, the epicardial ST potential fields were recorded at 1, 2, 5, 10, 15, and 20 minutes for a period of 2 seconds respectively.

The measurement of regional myocardial blood flow and perfusion beds are as described in Chapters 4 and 5; the epicardial and endocardial potential recording, map construction and map display are as described in Chapter 3.

7.2.3 Data Analysis and Statistics

Linear correlation was used to analyse the relationship between the epicardial ST elevation and depression, the RMBF and the epicardial ST potentials, as well as the RMBF and the pressures. Curves for paired data were plotted.

7.3 RESULTS

7.3.1 Regional Myocardial Blood Flow and Haemodynamic Response

Immediately following the OM ligation, the heart rate, the left ventricular systolic pressure and the LAD flow (measured by flow probe) often increased slightly and then gradually returned to the control level after 20 minutes. No ventricular arrhythmias and conduction blocks were observed, and all the 8 animals survived till the end of the experiment in this group.

Immediately following the LCX/LAD ligations, the left ventricular systolic pressure and the coronary flow to the nonischaemic regions (measured by magnetic flow probe) increased slightly, but the left ventricular systolic pressure and the coronary flow to the nonischaemic regions started to drop after 2 minutes in all but 2 animals. The left ventricular end diastolic pressure increased in all but 2 animals within 15 minutes. In 9 of the 25 animals with either the LAD or the LCX ligation, ventricular fibrillation developed within 5 minutes, and the animals died within 15 minutes (no data from these 9 animals were included). Ventricular fibrillation developed within 20 minutes in 7 animals all of which died within 30 minutes. The occurrence of ventricular fibrillation was preceded by a period of sustained (0.5-3 min) ventricular tachycardia. Nine animals survived the 30-60 minute observation period, however, five developed ventricular ectopics and nonsustained ventricular tachycardia, and one developed atrio-ventricular block. The average weight of each coronary artery bed was 20±4% of the left ventricle for the OM territory, 46±6% for the LCX territory, and 52±6% for the LAD territory. The above results are summarised in Table 7.1.

Table 7.1 Animal survivals in OM, LCX and LAD ligations

vessel ligated	OM	LCX	LAD
N	8	12	13
% Wt of LV	20±4	46±6*	52±5*
VF within 5'	0	4(33%)	5(38%)
VF within 20'	0	3(25%)	4(31%)
ventricular ectopics & nonsustained VT	0	3(25%)	2(15%)
AVB	0	0	1(7.6%)
30-60' survivals	8(100%)	5(42%)	4(31%)

Abbreviations:
N: number of animals
% Wt of LV: percent weight of OM, LCX and LAD territory of the left ventricle
VF: ventricular fibrillation   VT: ventricular tachycardia
AVB: atrio-ventricular block   *: $P<0.001$ versus OM ligation

Haemodynamic results and changes in the myocardial blood flow at 20 minutes of different vessel ligations are presented below. The RMBF was averaged for each layer of myocardium in each coronary artery territory (infarcted and noninfarcted regions).

7.3.1.1 OM ligation (Group 1)

Haemodynamics were measured in all the 8 animals tested. RMBF was measured in 6 animals. As shown in Table 7.2, there were no significant changes in the heart rate, the left ventricular end diastolic pressure and the left ventricular systolic pressure at 20 minutes of the OM ligation. In all the six animals, total OM ligation caused a significant reduction in flow to each third of the infarcted areas (from 1.06±0.18 to 0.37±0.12 mL/min/g, from 0.99±0.19 to 0.39±0.16 mL/min/g, from 0.97±0.22 to 0.40±0.16 mL/min/g for the endo-, mid- and epicardial third respectively, all $p<0.01$) (Table 7.3 top, Figure 7.1A), with slightly less decrease to the epicardial layer, and thus a marginal reduction in the endo/epi flow ratio (from 1.13±0.23 to 0.95±0.23, $P=0.01$). The flow to the noninfarcted regions increased nonsignificantly (from 1.09±0.19 to 1.12±0.15 mL/min/g for the transmural flow, $P>0.05$) (Table 7.3 bottom, Figure 7.1B).

Table 7.2 Haemodynamic changes in OM ligation

	HR (bpm)		LVSP (mmHg)		LVEDP (mmHg)		LAP (mmHg)	
NO.	before	after	before	after	before	after	before	after
1	120	120	95	100	5	7	2	3
2	140	160	96	106	7	3	-2	-2
3	130	100	115	114	3	3	-2	-2
4	110	108	101	98	1	3	-3	-3
5	130	140	101	109	1	2	-1	-1
6	115	120	84	84	-3	-3	3	4
7	110	100	91	93	0	0	1	0
8	100	100	93	88	1	1	-1	0
mean	119	119	97	99	2	2	0	0
SD	13	22	9	10	3	3	2	2
P		0.87		0.32		0.83		0.17

Table 7.3 Regional myocardial blood flow (mL/min/g) in OM ligation

infarcted region

	endo		mid		epi		transmural			endo/epi ratio	
No.	before	after	before	after	before	after	before	after	% of before	before	after
1	1.00	0.46	1.07	0.60	1.13	0.62	1.07	0.56	52.71	0.88	0.75
2	1.38	0.30	1.25	0.25	1.19	0.22	1.27	0.26	20.16	1.16	1.36
3	0.88	0.39	0.86	0.40	0.86	0.46	0.87	0.42	48.08	1.02	0.85
4	1.06	0.53	0.89	0.53	0.70	0.51	0.88	0.52	59.25	1.51	1.04
5	0.92	0.18	0.76	0.20	0.75	0.24	0.81	0.21	25.51	1.23	0.75
6	1.10	0.34	1.14	0.34	1.16	0.35	1.13	0.34	30.29	0.95	0.97
mean	1.06	0.37	0.99	0.39	0.97	0.40	1.01	0.38	39.33	1.13	0.95
SD	0.18	0.12	0.19	0.16	0.22	0.16	0.18	0.14	16.08	0.23	0.23
P		0.00		0.00		0.00		0.00			0.01

noninfarcted region

1	1.46	1.35	1.36	1.32	1.29	1.33	1.37	1.33	97.46	1.13	1.02
2	1.30	1.32	1.17	1.28	1.22	1.14	1.23	1.25	101.36	1.07	1.16
3	1.14	1.18	1.09	1.15	1.06	1.15	1.10	1.16	105.78	1.08	1.03
4	1.07	1.15	0.97	0.97	0.78	0.85	0.94	0.99	105.32	1.37	1.35
5	0.93	1.06	0.85	0.92	0.80	0.88	0.86	0.95	110.85	1.16	1.20
6	1.05	1.16	1.04	1.01	0.99	0.95	1.03	1.04	101.30	1.06	1.22
mean	1.16	1.20	1.08	1.11	1.02	1.05	1.09	1.12	103.68	1.14	1.16
SD	0.19	0.11	0.17	0.17	0.21	0.19	0.19	0.15	4.65	0.12	0.13
P		0.24		0.29		0.40		0.13			0.65

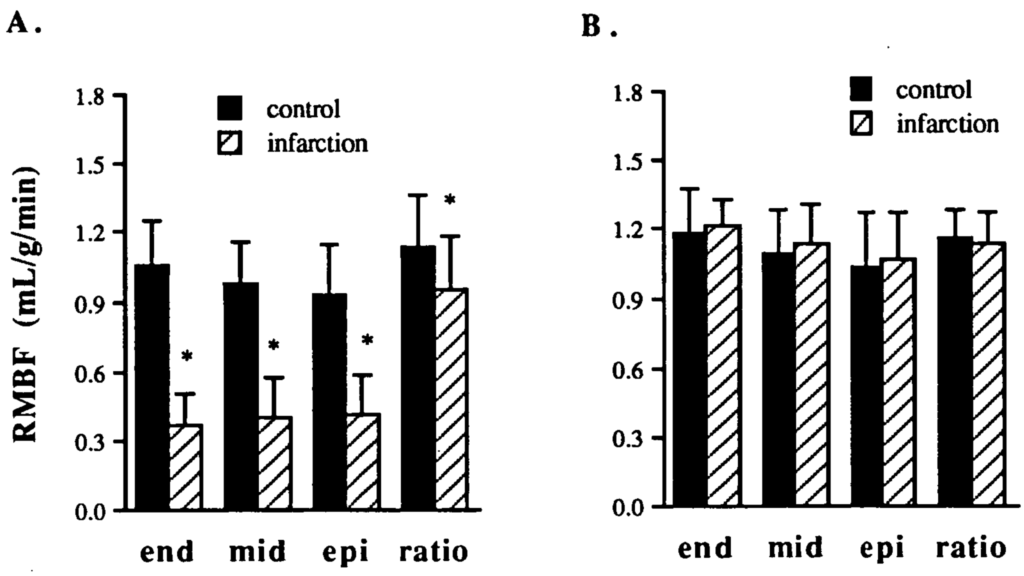

Figure 7.1. RMBF distributions across the left ventricular wall in the infarcted (A) and the noninfarcted (B) regions before and 20 minutes after OM ligation (n=6, *P<0.05 vs control).

7.3.1.2 LCX ligation (Group 2)

Haemodynamic data are from the 8 animals which survived 20 minutes of the LCX ligation (4 animals died in less than 20 minutes). RMBF are from 5 animals. As tabulated in Table 7.4, the LCX ligation caused a marked decrease in the flow to each third of the infarcted areas (from 1.16±0.20 to 0.20±0.08 mL/min/g, from 1.05±0.10 to 0.19±0.06 mL/min/g, from 0.86±0.13 to 0.17±0.07 mL/min/g for the endo-, mid- and epicardial third respectively, all $p<0.01$). In the noninfarcted regions, there was also a considerable decrease in the RMBF (from 1.12±0.10 to 0.75±0.20 mL/min/g, from 1.07±0.14 to 0.76±0.22 mL/min/g, from 0.92±0.19 to 0.70±0.22 mL/min/g for the endo-, mid- and epicardial third respectively, all $p<0.05$). The infarction was accompanied by an increase in the left ventricular end diastolic pressure (from 3±1 to 8±3 mmHg, $P<0.01$) and a decrease in the left ventricular systolic pressure (from 81±12 to 72±20 mmHg, $P=0.05$) (Table 7.5).

Table 7.4 Regional myocardial blood flow (mL/min/g) in LCX ligation

infarcted region

	endo		mid		epi		transmural			endo/epi ratio	
No.	before	after	before	after	before	after	before	after	% of before	before	after
1	0.83	0.28	0.94	0.22	0.96	0.23	0.91	0.24	26.74	0.86	1.22
2	1.28	0.24	1.19	0.25	1.00	0.21	1.16	0.23	20.17	1.28	1.14
3	1.18	0.08	1.01	0.10	0.70	0.11	0.96	0.10	10.03	1.69	0.73
4	1.16	0.22	1.02	0.24	0.74	0.22	0.97	0.22	23.10	1.56	0.99
5	1.34	0.18	1.12	0.15	0.88	0.09	1.11	0.14	12.52	1.53	2.12
mean	1.16	0.20	1.05	0.19	0.86	0.17	1.02	0.19	18.51	1.38	1.24
SD	0.20	0.08	0.10	0.06	0.13	0.07	0.11	0.07	7.06	0.33	0.53
P		0.00		0.00		0.00		0.00			0.64

noninfarcted region

1	1.14	0.69	1.13	0.58	0.95	0.48	1.07	0.58	54.35	1.20	1.44
2	1.21	0.89	1.20	0.87	1.08	0.79	1.16	0.85	73.07	1.12	1.13
3	1.08	0.44	1.02	0.52	0.85	0.61	0.98	0.52	53.22	1.27	0.72
4	0.97	0.80	0.85	0.75	0.63	0.56	0.82	0.70	86.04	1.54	1.43
5	1.21	0.95	1.14	1.07	1.10	1.04	1.15	1.02	89.06	1.10	0.91
mean	1.12	0.75	1.07	0.76	0.92	0.70	1.04	0.74	71.15	1.25	1.13
SD	0.10	0.20	0.14	0.22	0.19	0.22	0.14	0.20	16.96	0.18	0.32
P		0.01		0.04		0.04		0.02			0.40

Table 7.5 Haemodynamic changes in LCX ligation

	HR (bpm)		LVSP (mmHg)		LVEDP (mmHg)		LAP (mmHg)	
NO.	before	after	before	after	before	after	before	after
1	120	170	90	73	5	10	1	3
2	100	110	85	93	5	10	-1	0
3	110	120	65	50	2	10	0	8
4	130	120	65	40	3	10	1	9
5	100	160	80	62	1	4	0	4
6	120	140	89	86	4	2	-1	2
7	130	140	97	95	3	7	0	0
8	100	110	78	75	4	9	2	7
mean	114	134	81	72	3	8	0	4
SD	13	23	12	20	1	3	1	4
P		0.05		0.05		0.00		0.01

The average flow distributions across the left ventricle after 20 minutes of LCX ligation are presented in Figure 7.2. During infarction, there were similar decreases in the RMBF to each third of the myocardium in both of the infarcted and the noninfarcted regions, the endo/epi flow ratio remained unchanged (from 1.38±0.33 to 1.24±0.53 for the infarcted regions; from 1.25±0.18 to 1.13±0.32 for the noninfarcted regions, both $P>0.05$).

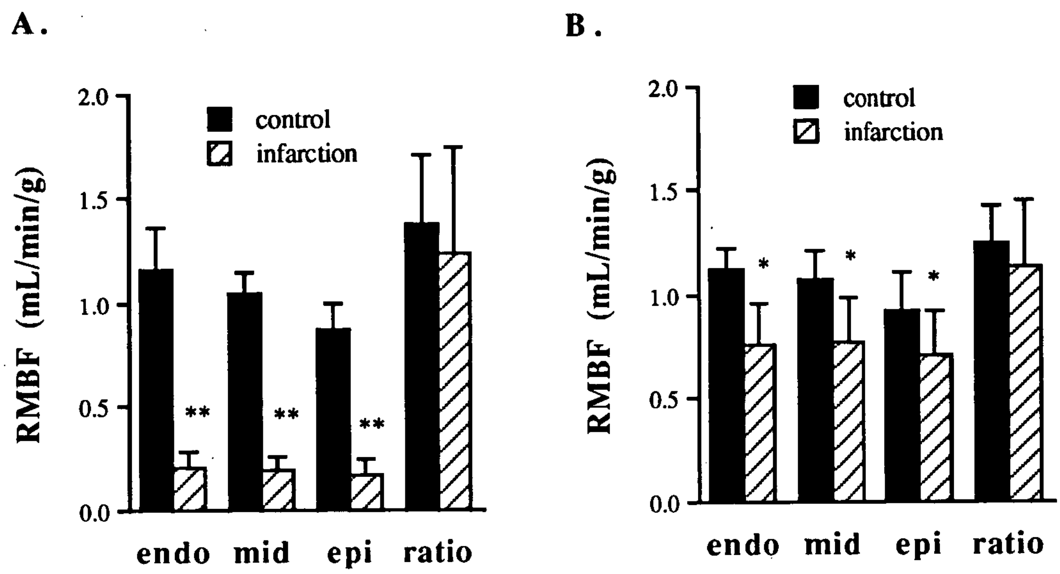

Figure 7.2 RMBF distributions across the left ventricular wall in the infarcted (A) and the noninfarcted (B) regions before and 20 minutes after LCX ligation (n=5, *P<0.05, **P<0.001 vs control).

7.3.1.3 LAD ligation (Group 3)

Haemodynamic data are from the 8 animals who survived 20 minutes of the LAD ligation (5 animals died in less than 20 minutes). RMBF are from 5 animals. As tabulated in Table 7.6, the LAD ligation caused a marked decrease in the flow to each third of the infarcted areas (from 1.08±0.21 to 0.16±0.08 mL/min/g, from 0.98±0.22 to 0.16±0.11 mL/min/g, from 0.90±0.23 to 0.16±0.10 mL/min/g for the endo-, mid- and epicardial third respectively, all $p<0.01$). In the noninfarcted regions, there was also a considerable decrease in the RMBF (from 1.01±0.23 to 0.71±0.24 mL/min/g, from 0.87±0.22 to 0.64±0.21 mL/min/g, from 0.78±0.22 to 0.58±0.21 mL/min/g for the endo-, mid- and epicardial third respectively, all $p<0.05$). The infarction was accompanied by an increase in the left ventricular end diastolic pressure (from 1±4 to 6±7 mmHg, $P<0.05$) and a decrease in the left ventricular systolic pressure (from 92±11 to 69±13 mmHg, $P<0.01$) (Table 7.7).

Table 7.6 Regional myocardial blood flow (mL/min/g) in LAD ligation

infarcted region

	endo		mid		epi		transmural			endo/epi ratio	
No.	before	after	before	after	before	after	before	after	% of before	before	after
1	0.94	0.09	0.96	0.1	0.86	0.1	0.92	0.08	8.33	1.09	1.50
2	1.25	0.26	0.90	0.32	0.75	0.30	0.97	0.29	30.37	1.66	0.86
3	1.31	0.16	1.30	0.13	1.24	0.13	1.29	0.14	10.92	1.06	1.26
4	0.82	0.08	0.71	0.06	0.64	0.11	0.72	0.08	11.28	1.30	0.71
5	1.05	0.19	1.04	0.21	0.99	0.22	1.03	0.21	20.13	1.06	0.86
mean	1.08	0.16	0.98	0.16	0.90	0.16	0.98	0.16	16.21	1.23	1.04
SD	0.21	0.08	0.22	0.11	0.23	0.10	0.20	0.09	9.09	0.26	0.33
P		0.00		0.00		0.00		0.00			0.44

noninfarcted region

1	0.71	0.33	0.57	0.30	0.63	0.27	0.64	0.30	47.12	1.13	1.22
2	1.16	0.97	0.86	0.80	0.72	0.69	0.91	0.82	89.61	1.62	1.41
3	1.18	0.69	0.98	0.60	0.72	0.53	0.96	0.61	63.60	1.63	1.30
4	0.81	0.73	0.77	0.69	0.64	0.58	0.74	0.67	89.99	1.25	1.27
5	1.20	0.81	1.16	0.82	1.17	0.83	1.18	0.82	69.69	1.03	0.98
mean	1.01	0.71	0.87	0.64	0.78	0.58	0.89	0.64	72.00	1.33	1.24
SD	0.23	0.24	0.22	0.21	0.22	0.21	0.21	0.21	18.23	0.28	0.16
P		0.01		0.03		0.04		0.02			0.28

Table 7.7 Haemodynamic changes in LAD ligation

NO.	HR (bpm)		LVSP (mmHg)		LVEDP (mmHg)		LAP (mmHg)	
	before	after	before	after	before	after	before	after
1	150	140	110	70	3	5	0	3
2	90	120	100	80	-5	-5	-1	0
3	110	160	92	60	0	3	0	8
4	120	120	86	71	2	4	0	0
5	170	180	91	78	4	7	0	0
6	140	110	70	40	6	15	-1	8
7	120	120	94	80	4	15	1	9
8	95	106	91	67	-2	3	0	5
mean	124	132	92	69	1	6	0	4
SD	27	26	11	13	4	7	1	4
P		0.41		0.00		0.01		0.02

The average flow distributions across the left ventricle at 20 minutes of LAD ligation are presented in Figure 7.3. During infarction, there were similar decreases in the RMBF to each third of the myocardium in both of the infarcted and the noninfarcted regions, so the endo/epi flow ratio remained unchanged (from 1.23±0.26 to 1.04±0.33 for the infarcted regions; from 1.33±0.28 to 1.24±0.16 for the noninfarcted regions, both $P>0.05$).

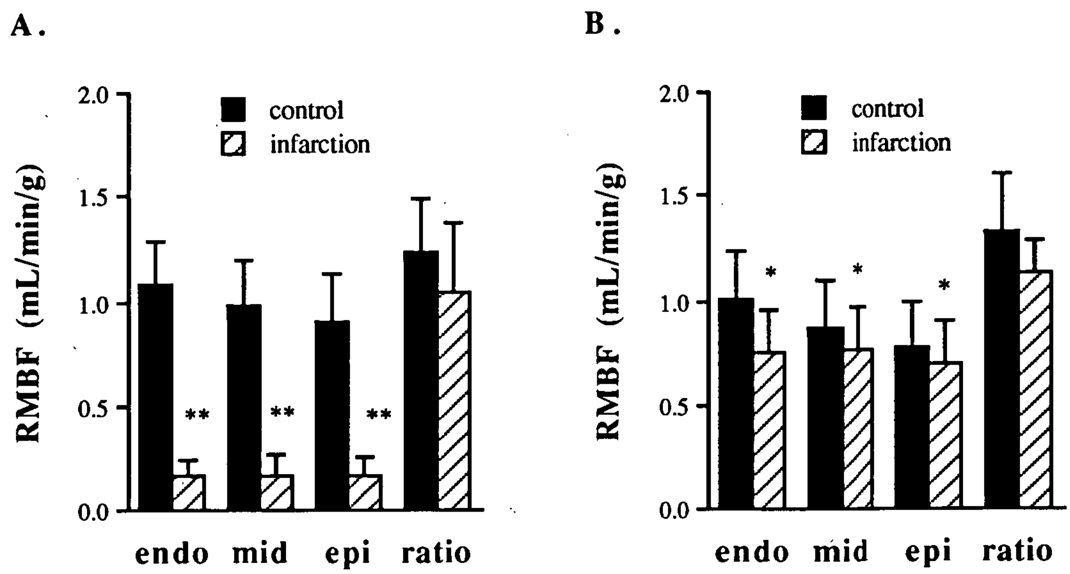

Figure 7.3 RMBF distributions across the left ventricular wall in the infarcted (A) and the noninfarcted (B) regions before and 20 minutes after LAD ligation ($n=5$, $*P<0.05$, $**P<0.001$ vs control).

Changes in the myocardial blood flow and the haemodynamics in different artery occlusions are compared in Table 7.8 and Figures 7.4 and 7.5, which show significantly different flow and haemodynamic changes with varied infarctions. In either the LAD or the LCX ligation, the flow to the noninfarcted regions decreased significantly (Figure 7.4); the flow reduction was accompanied by an increase in the left ventricular end diastolic pressure and a decrease in the left ventricular systolic pressure (Table 7.8). However, in OM ligation, the flow to the noninfarcted regions increased nonsignificantly (Figure 7.4). There were no changes in the left ventricular diastolic pressure and the left ventricular systolic pressure during OM ligation (Table 7.8). Figure 7.5 was plotted with the data of three animals from groups 1, 2 and 3, respectively. It displays the spatial flow distributions of the left ventricles in different artery occlusions. In OM occlusion, the flow reduction occurred only in the infarcted regions (Figure 7.5A). In either the LCX or the LAD occlusion, however, flow to the noninfarcted regions also reduced considerably (Figures 7.5B and C). In all the three occlusions, flow reduction to each third of the ventricular wall was similar.

Table 7.8 Haemodynamic responses to OM, LCX and LAD ligations

	OM ligation		LCX ligation		LAD ligation	
	control	infarction	control	infarction	control	infarction
HR	119±13	119±21	113±13	133±22	124±27	132±26
LVSP	97±9	99±10	81±12	72±20*	92±11	69±13*
LVEDP	2±3	2±3	3±1	8±3*	1±4	6±7*
LAP	0±2	0±2	0±1	4±4*	0±1	4±4*

Mean ± SD, n=8, *P<0.05 versus control.

Abbreviations:

HR: heart rate (beats/min)

LVSP: left ventricular systolic pressure (mmHg)

LVEDP: left ventricular end diastolic pressure (mmHg)

LAP: mean left atrial pressure (mmHg)

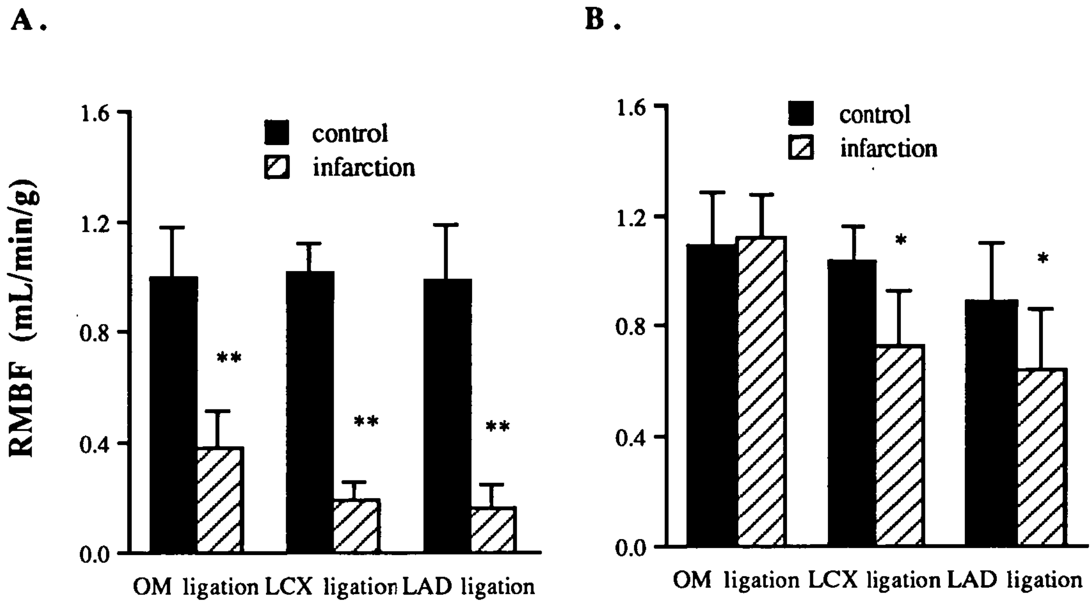

Figure 7.4 RMBF distributions across the left ventricular wall in the infarcted (A) and the noninfarcted (B) regions before and 20 minutes after different coronary artery ligations (OM=6, LCX/LAD=5, *P<0.05, **P<0.001 vs control).

A. OM ligation

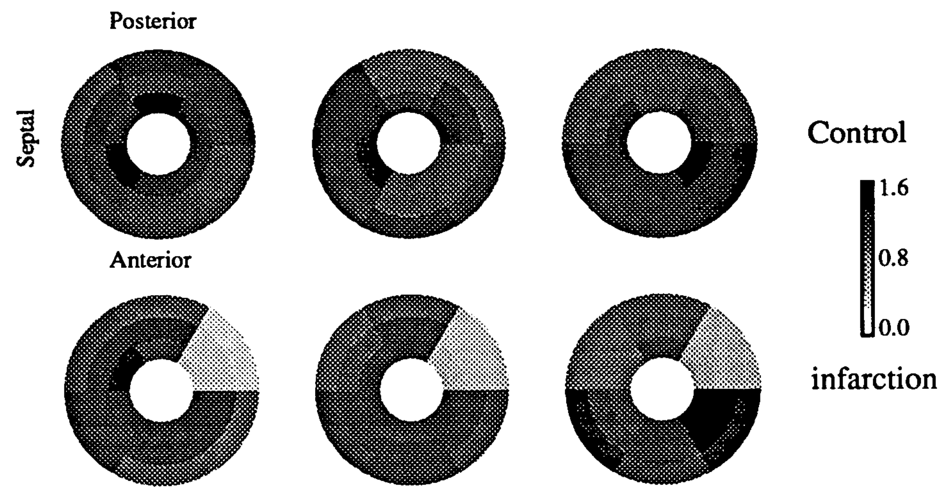

B. LCX ligation

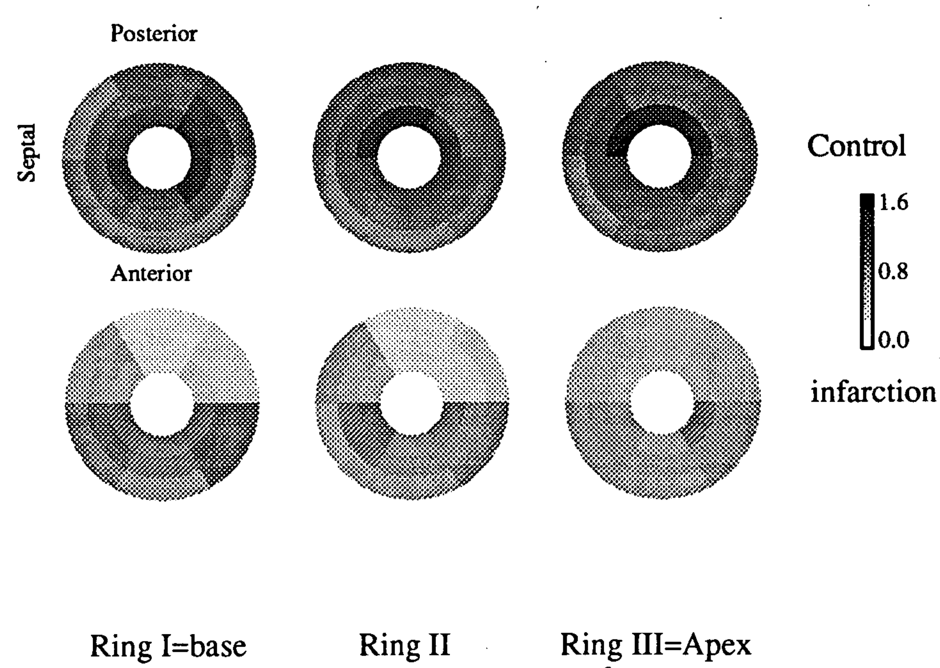

C. LAD ligation

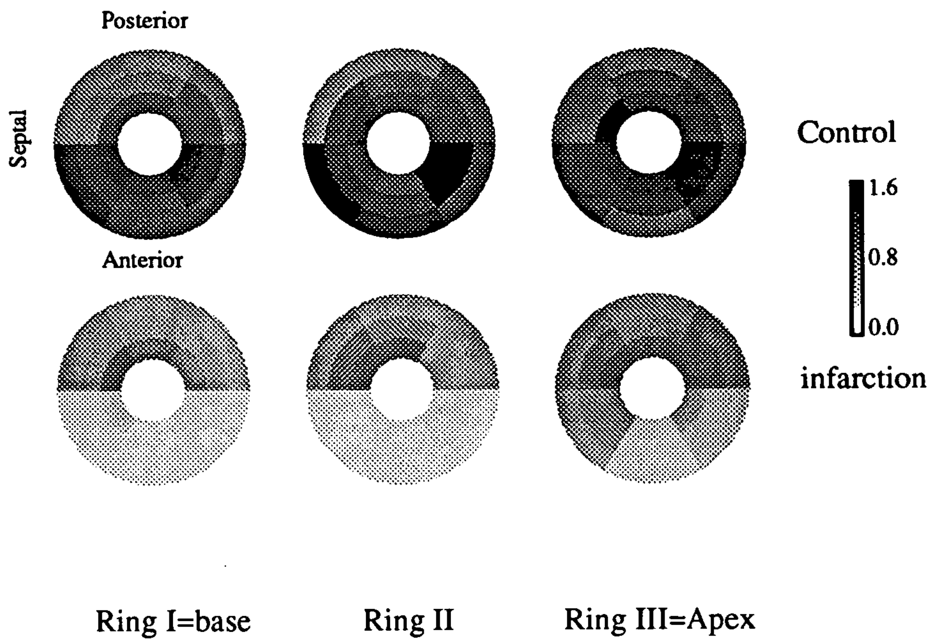

Figure 7.5 Spatial flow distributions in the left ventricular myocardium before and during OM ligation (A), LCX ligation (B) and LAD ligation (C). Intensities represent quantity of RMBFs (mL/min/g). Each circle represents about 1-cm thick left ventricle ring. In each 60° arc there are three slices from endocardium to epicardium. The three arcs above represent the myocardium of the LCX bed; the three arcs below represent the myocardium of the LAD bed. For each ring, septum is left, free wall is right, posterior wall is above, and anterior wall is below. Data are from three animals with each from group 1, group 2 and group 3, respectively.

7.3.2 Relationships Between RMBF and Haemodynamics

Linear correlation was used to determine whether a statistically significant relation existed between the RMBF changes in the noninfarcted regions and the simultaneous measurements of the left ventricular diastolic pressure, the left ventricular systolic pressure, the mean left atrial pressure and the heart rate during ischaemia. As shown in Figure 7.6, the RMBF during ischaemia in the noninfarcted regions directly correlates to the left ventricular systolic pressure (Figure 7.6A, r=0.82, P<0.001), and inversely correlates to the left ventricular diastolic pressure (Figure 7.6B, r=-0.82, P<0.01) and left atrial pressure (Figure 7.6C, r=-0.79, P<0.01). No relation existed between the RMBF and the heart rate (Figure 7.6D, r=0.25).

A

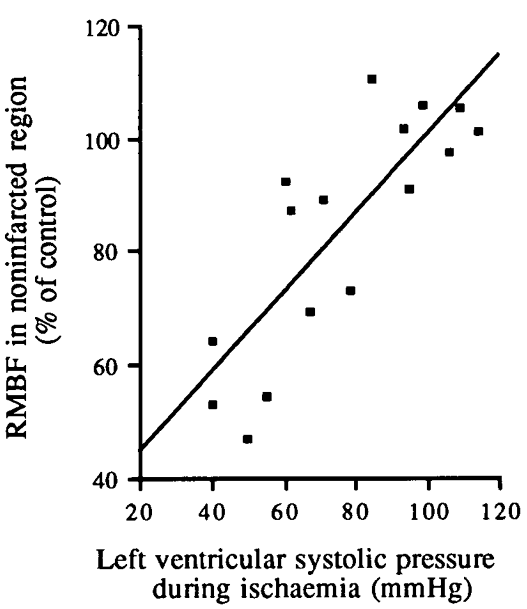

Figure 7.6A Relationship between the RMBF and the left ventricular systolic pressure during infarction by OM (n=6), LCX (n=5) and LAD (n=5) ligations (r=0.82, P=0.0001).

B

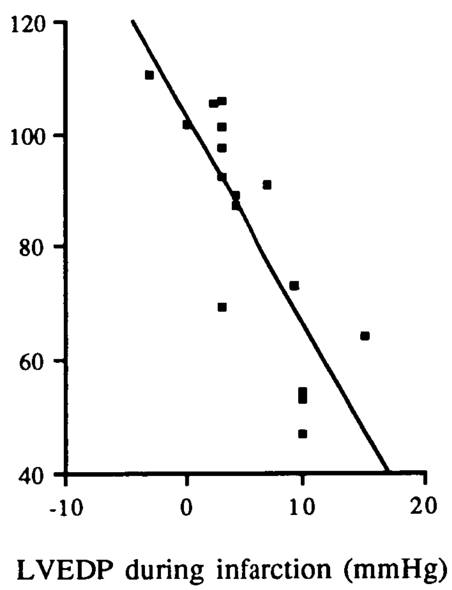

Figure 7.6B Relationship between RMBF and the left ventricular end diastolic pressure during infarction by OM (n=6), LCX (n=5) and LAD (n=5) ligations (r=-0.82, P<0.01).

C

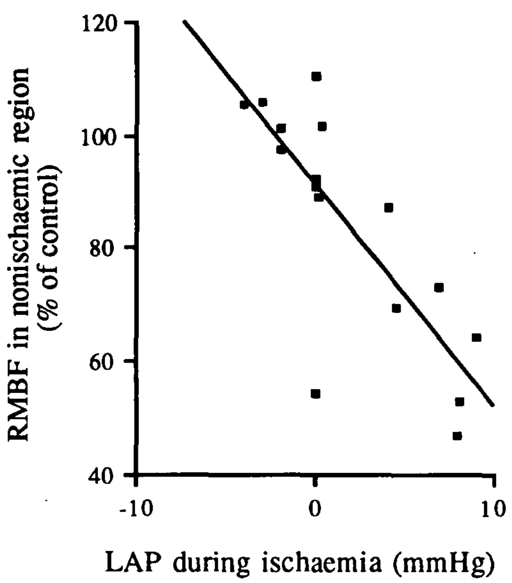

Figure 7.6C Relationship between the RMBF and the average left atrial pressure (LAP) during infarction by OM (n=6), LCX (n=5) and LAD (n=5) ligations (r=-0.79, P<0.01).

D

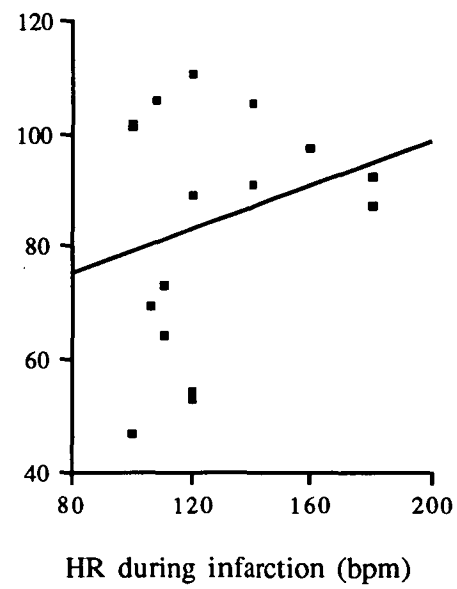

Figure 7.6D Relationship between the RMBF and the heart rate during infarction by OM (n=6), LCX (n=5) and LAD (n=5) ligations (r=0.25).

7.3.3 Epicardial Potential Distributions in Small Size Infarction

Representative maps of epicardial ST potential distributions from three typical experiments are displayed in Figure 7.7. Before OM ligation (control), the epicardial ST potentials showed a slight variation in magnitude. Over all the epicardial sites, the ST magnitude ranged from +2 mV to -4 mV. Total occlusion of the OM produced a graduated but even peak of ST elevation in the ischaemic centre, with the magnitude decreasing toward the border. The ST segment was depressed slightly in the surrounding regions (Figure 7.7). Figure 7.8 demonstrates the epicardial potential distributions at different time intervals of OM ligation in one experiment. ST elevation started from the ischaemic centre and as ischaemia progressed, it spread to the surrounding regions, with the maximum change in the centre. Minor ST depression occurred around the perimeter of the ST elevation. ST elevation reached its maximum of +36 mV at 10 minutes of OM ligation, and started to decrease 20 minutes later. Figure 7.9 shows the average epicardial potential changes at different times from the 8 animals.

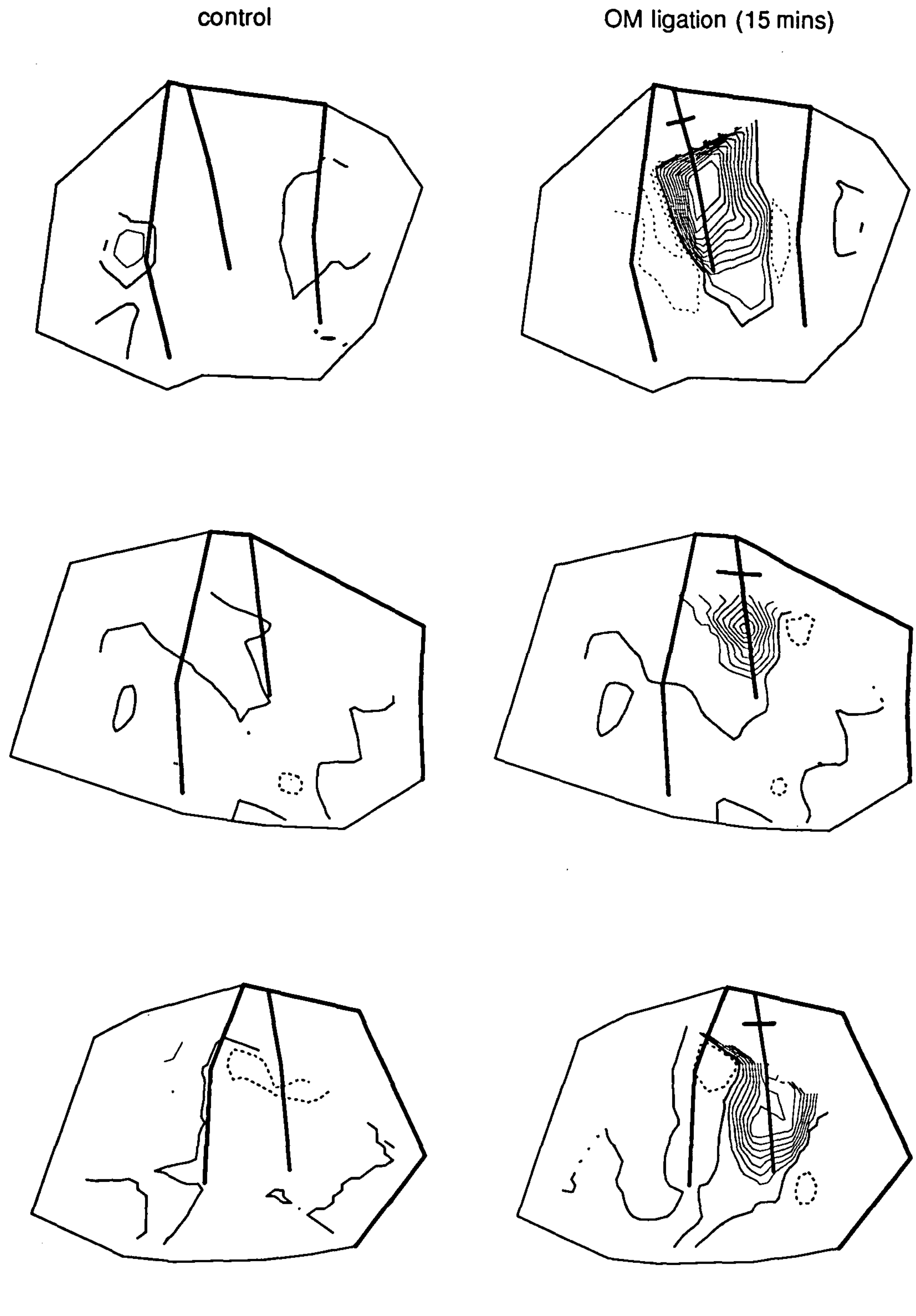

Figure 7.7 Epicardial ST potential distributions before and during OM ligation. Maps were constructed from the data of 3 animals (each two parallel maps are from one animal). The thin solid lines indicate ST elevation and dotted lines ST depression. The thicker solid contour lines represent zero potential. For the top four maps, the contour interval=2 mV; for the bottom two maps, the contour interval=4 mV.

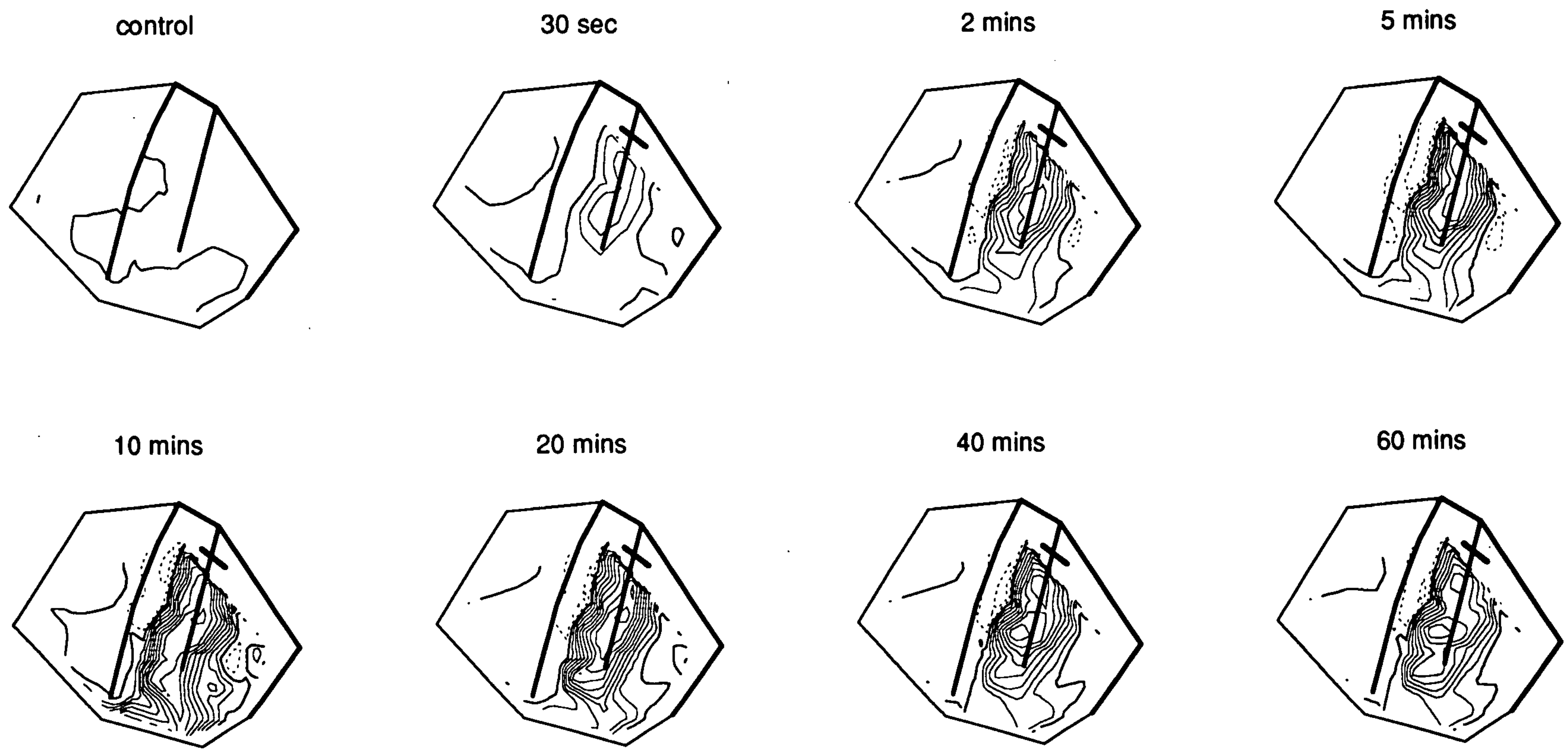

Figure 7.8 Epicardial potential distributions at different time intervals in OM ligation. Thin soild contour lines represent ST elevation, dotted lines ST depression, and thicker solid contour lines zero potential. Contour interval=4mV. Data are from one experiment.

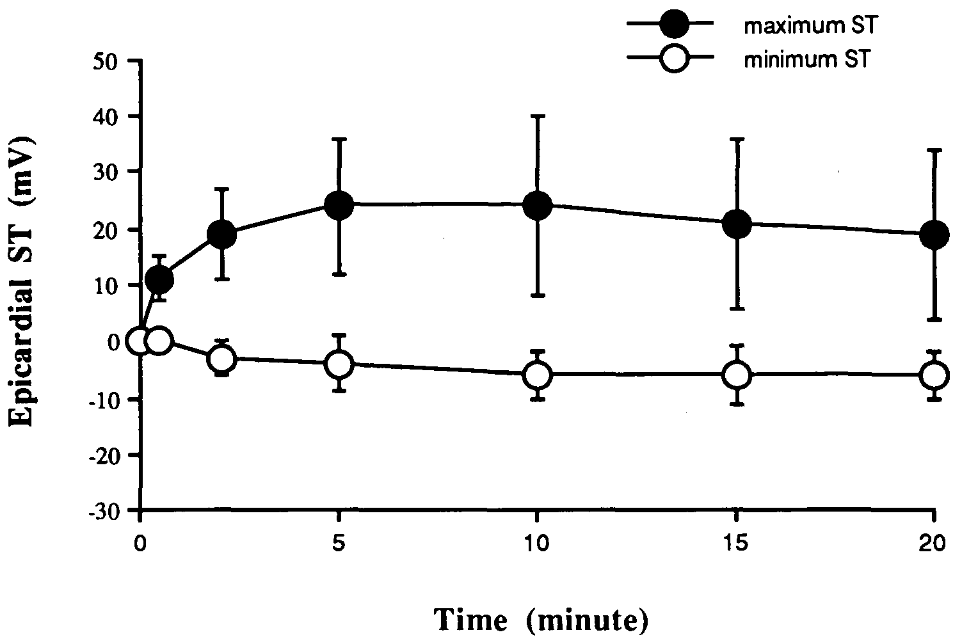

Figure 7.9 Peak epicardial ST potentials during OM ligation (n=8). Both maximum and minimum potentials occurred at 10 minutes of OM ligation. The maximum potentials started to decrease from then onwards, while the minimum potentials remained unchanged.

7.3.4 Epicardial Potential Distributions in Large Size Infarction

-Compared with small size infarction

Representative maps of epicardial ST potential distributions from six typical experiments are displayed in Figure 7.10. Total occlusion of either the LCX or the LAD produced a powerful dipole between ST elevation over the infarcted regions and ST depression over the noninfarcted regions. The regions of ST elevation are markedly asymmetric, with the highest amplitude at the boundary, a pattern of ST elevation quite different from that of the total occlusion of the OM (Figure 7.11). Figure 7.11 demonstrates the typical epicardial distributions in varied infarctions with significantly different ST alterations.

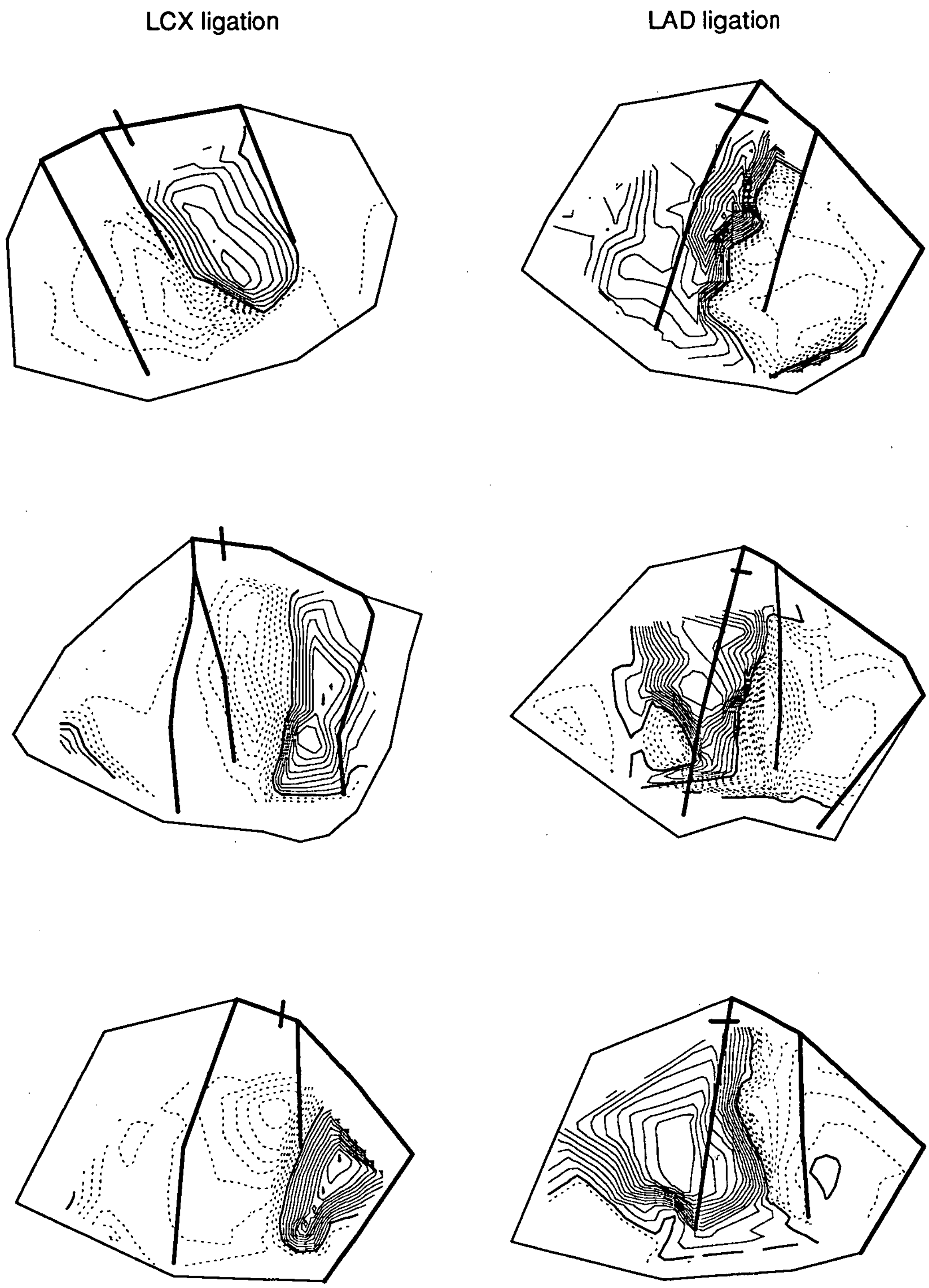

Figure 7.10 Isopotential difference maps represent epicardial ST potential distributions in LCX (left) and LAD (right) ligations. The thin solid lines indicate ST elevation, and dotted lines ST depression. The thicker solid contour lines represent zero potential. Potentials were recorded at 15 minutes of coronary artery ligations in 6 animals. Each map represents the recording from one animal. For the top four maps, the contour interval=2 mV; for the bottom two maps, the contour interval=4 mV.

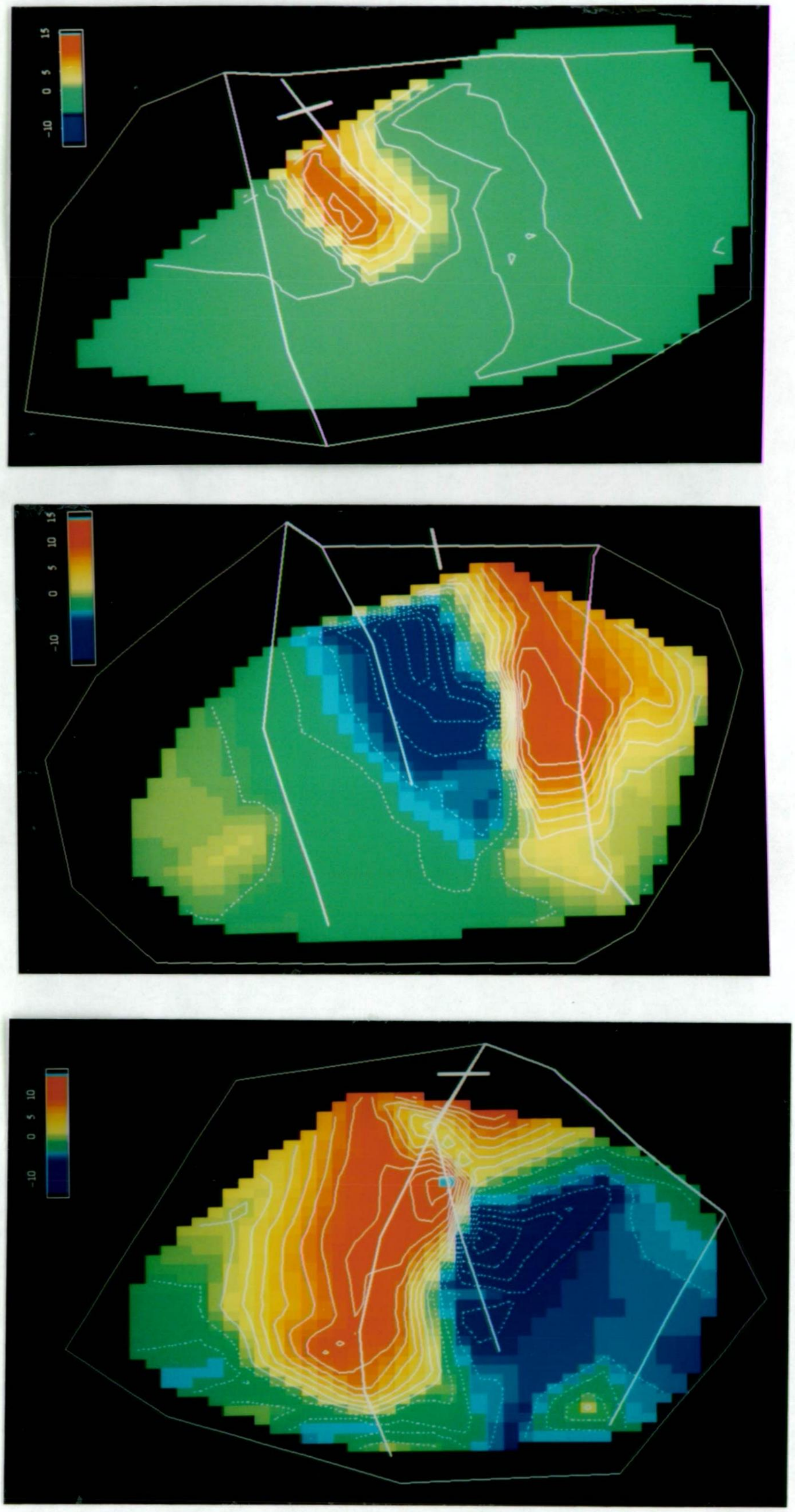

Figure 7.11 Epicardial potential distributions for OM ligation (top), LCX ligation (middle) and LAD ligation (bottom) in 3 animals. The red colour represents positive potential and the blue colour negative potential. The green colour indicates zero potential.

-Compared with endocardial potential distributions

From the endocardium, both ST elevation and ST depression were recorded during infarction, a pattern of change which was unexpected. The results are shown in Figures 7.12 and 7.13, which display the simultaneous epicardial and endocardial ST potential recordings during LCX/LAD ligations. The distribution patterns of ST changes in the endocardium are similar to those in the epicardium in both LCX and LAD ligations, but with lower potentials in the endocardium. The changes in the amplitude of the ST potentials with the timecourse were also similar in the epicardium and the endocardium. Figures 7.14 & 7.15 show the average epicardial potential changes at different times from the 8 animals in LCX and LAD ligations. Epicardial and endocardial ST potential changes occurred within 30 seconds after the occlusion of either the LCX or the LAD, reaching their maximum within 5 to 10 minutes, and then decreased from 15 minutes onwards.

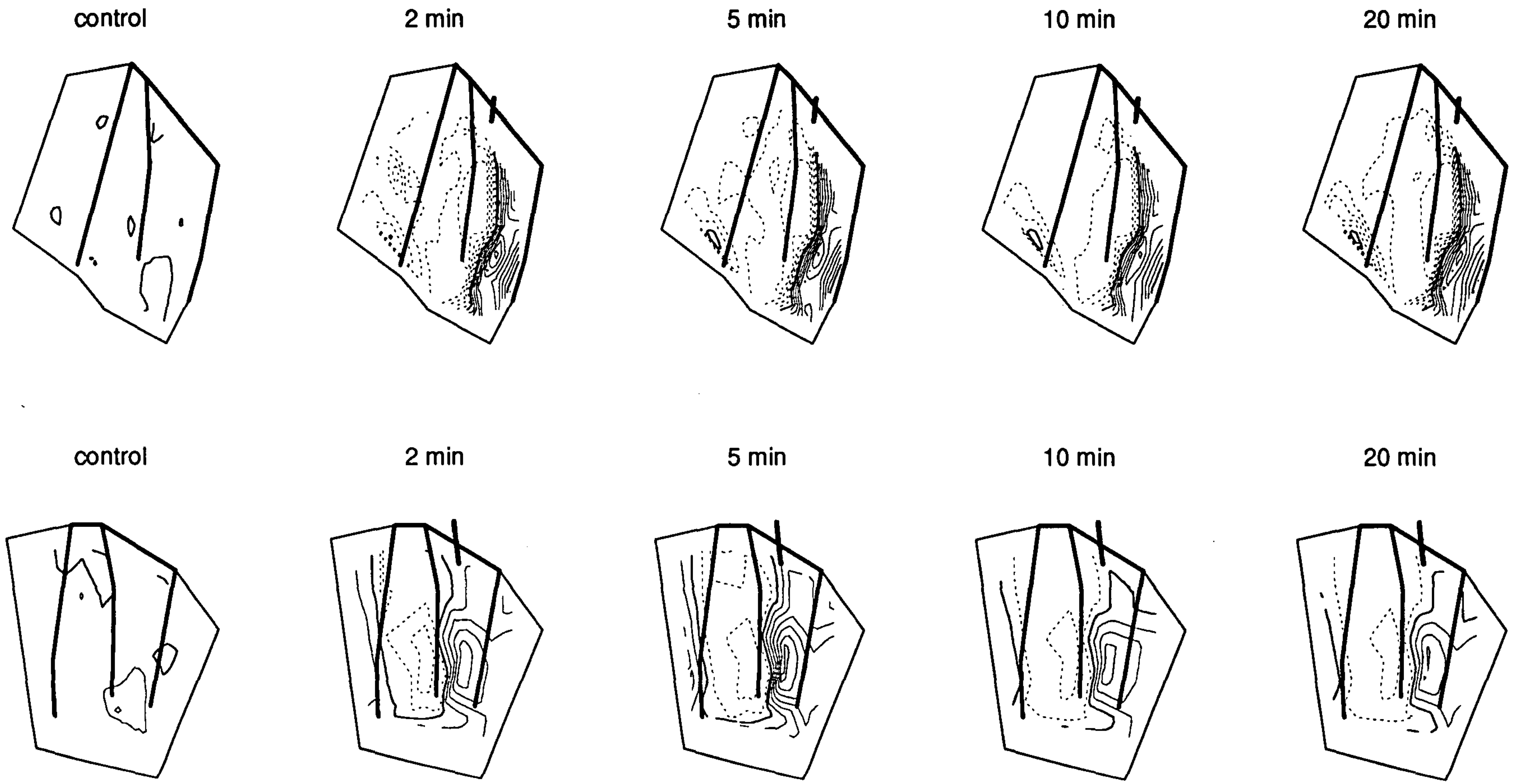

Figure 7.12 Simultaneous epicardial (top) and endocardial (bottom) potential distributions in LCX ligation. Thin solid and dotted contour lines indicate ST elevation and depression respectively. Thicker solid contour lines respresent zero potential. For epicardial maps, contour interval=4mV; for endocardial maps, contour interval=2 mV.

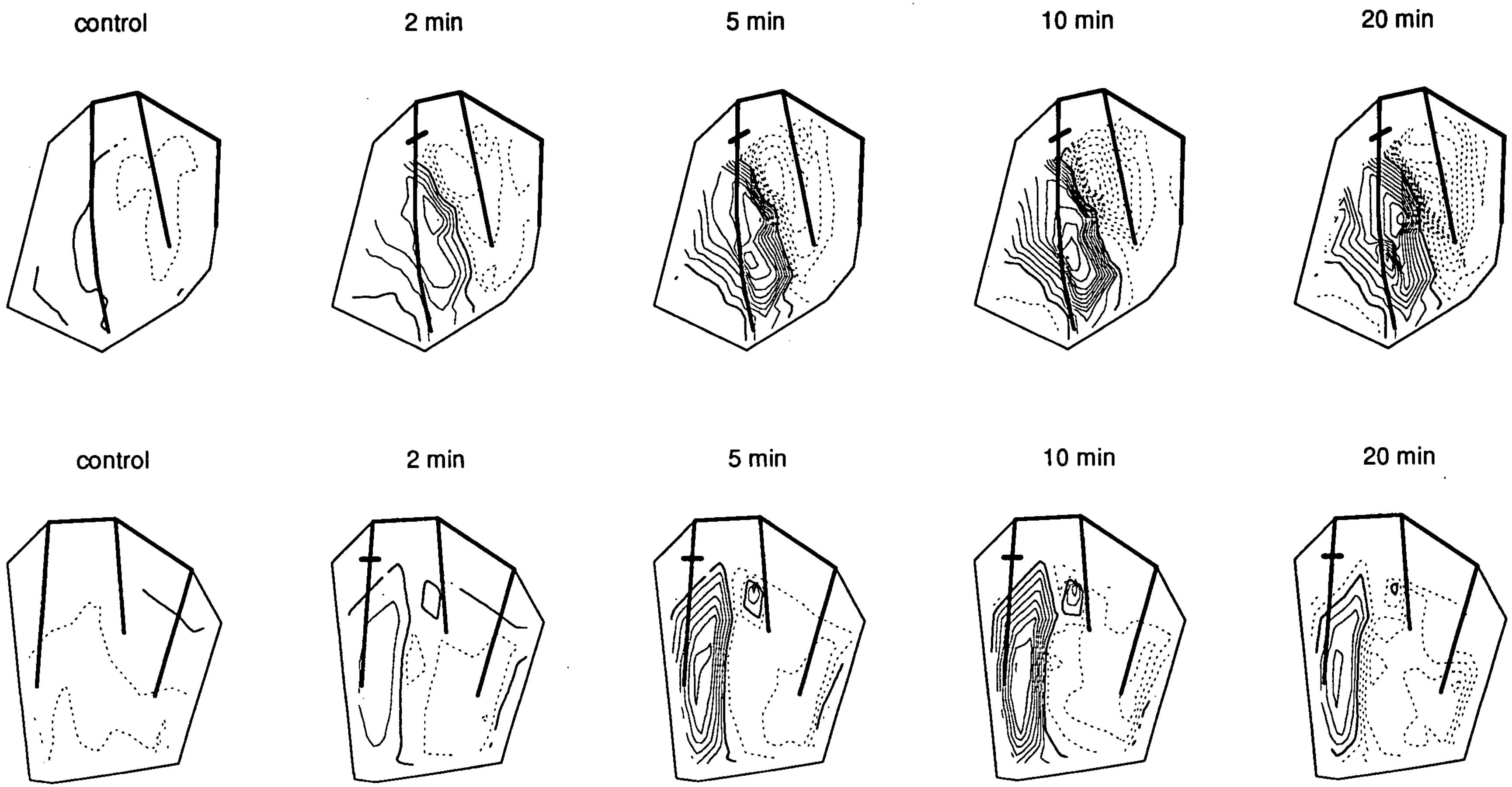

Figure 7.13 Simultaneous epicardial (top) and endocardial (bottom) potential distributions during LAD ligation. Thin solid and dotted contour lines indicate ST elevation and depression respectively. Thicker solid contour lines represent zero potential. For epicardial maps, contour interval=4 mV; for endocardial maps, contour interval=2 mV.

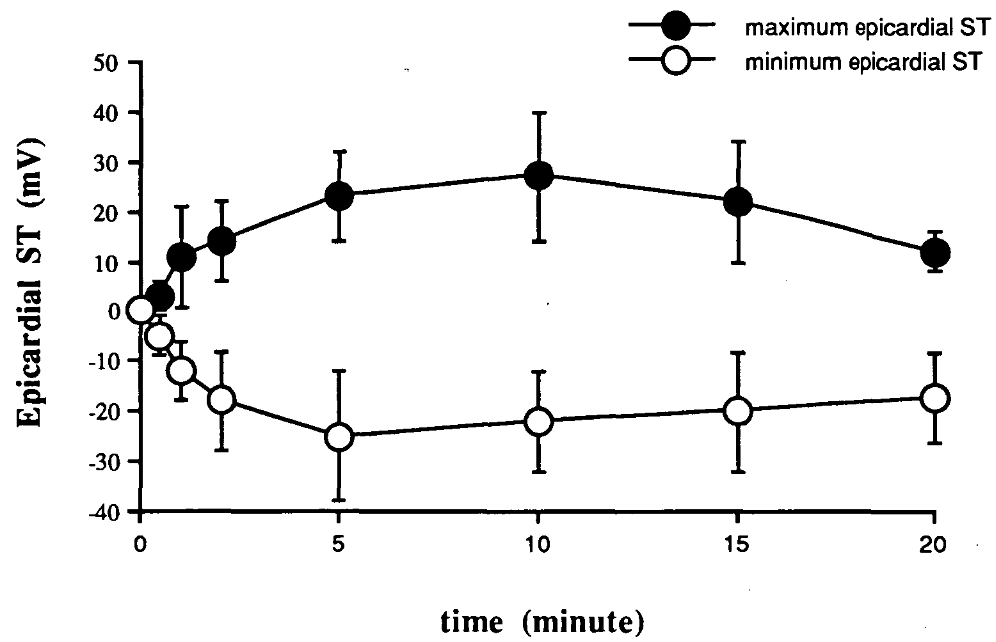

Figure 7.14A Peak epicardial ST potentials during LCX ligation (n=8). Maximum ST occurred at 10 minutes, and minimum at 5 minutes of LCX ligation. The magnitudes of both ST elevation and depression started to decrease from 10 minutes onwards.

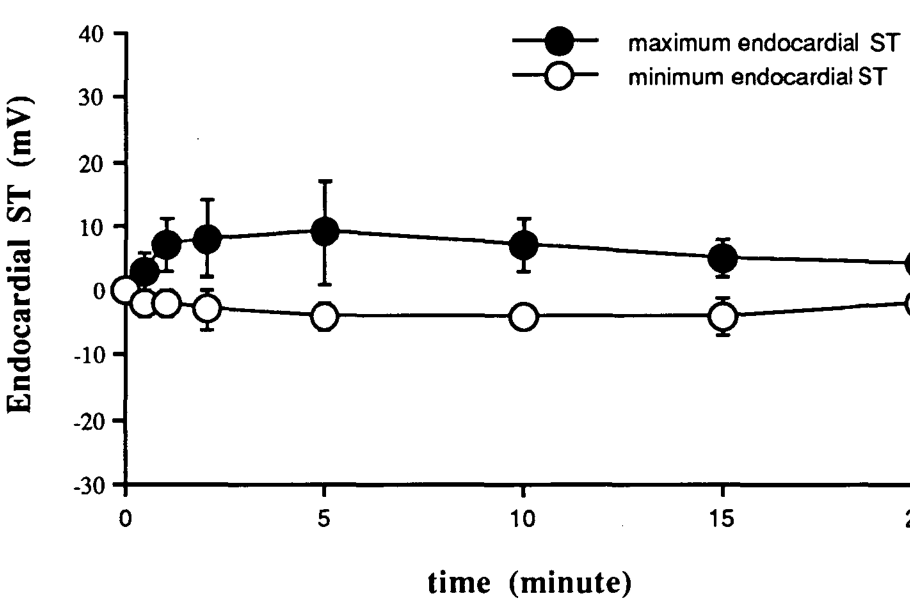

Figure 7.14B Peak endocardial ST potentials during LCX ligation (n=5). The maximum magnitudes of both ST elevation and depression occurred at 5 minutes of LCX ligation, and started to decrease from then onwards.

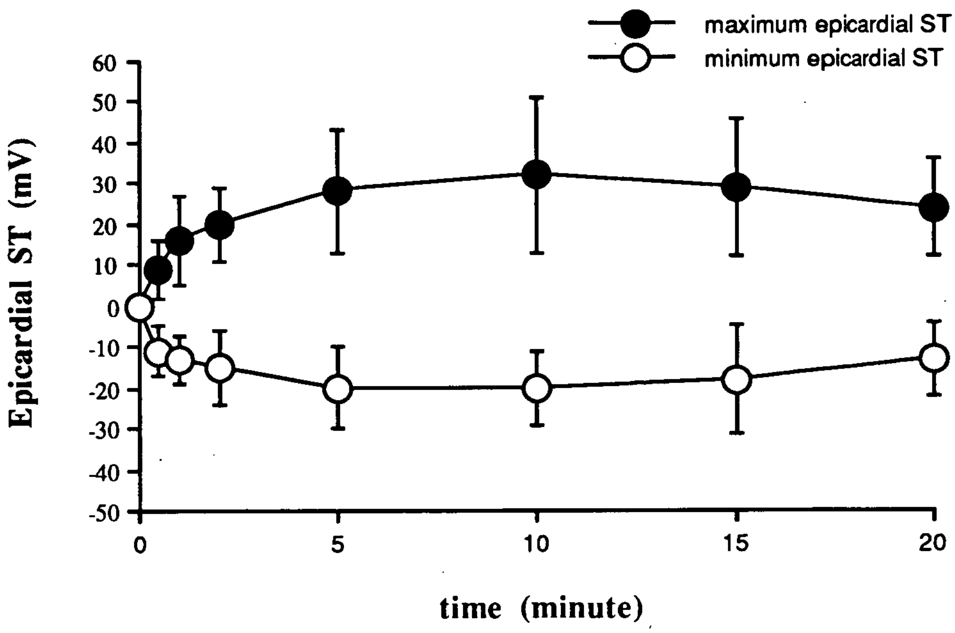

Figure 7.15A Peak epicardial potentials during LAD ligation (n=8). The maximum magnitudes for both of the ST depression and elevation occurred at 10 minutes of LAD ligation, and started to decrease from then onwards.

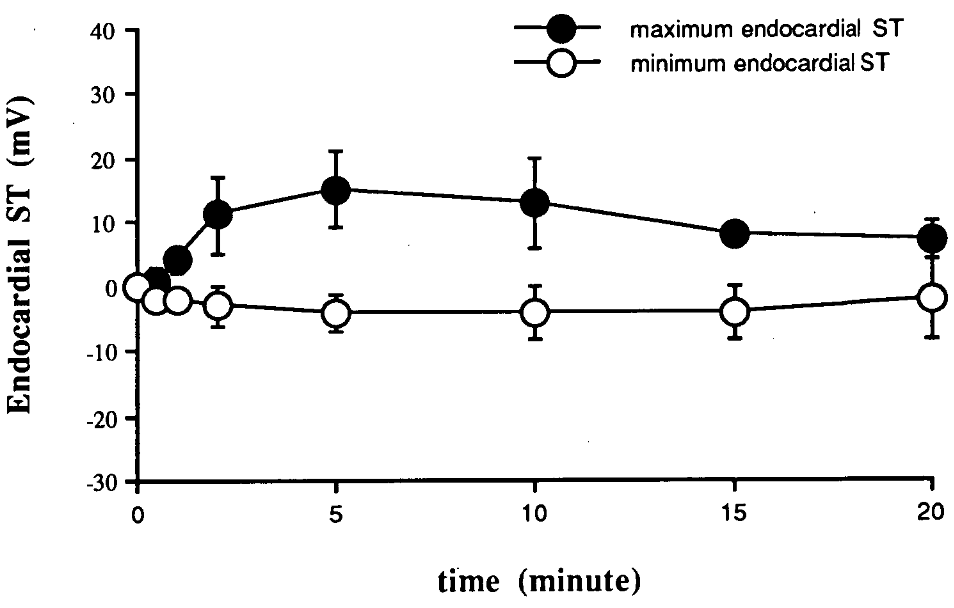

Figure 7.15B Peak endocardial ST potentials during LAD ligation (n=5). The maximum magnitudes for both of the ST elevation and depression occurred at 5 minutes of LAD ligation, and started to decrease from then onwards.

-Correlation between ST depression and ST elevation

The relationship between the epicardial ST elevation in the infarcted regions and the epicardial ST depression in the noninfarcted regions was examined by using linear correlation. As shown in Figure 7.16, there was a highly significant inverse correlation between these two variables (r=-0.61, P<0.0001).

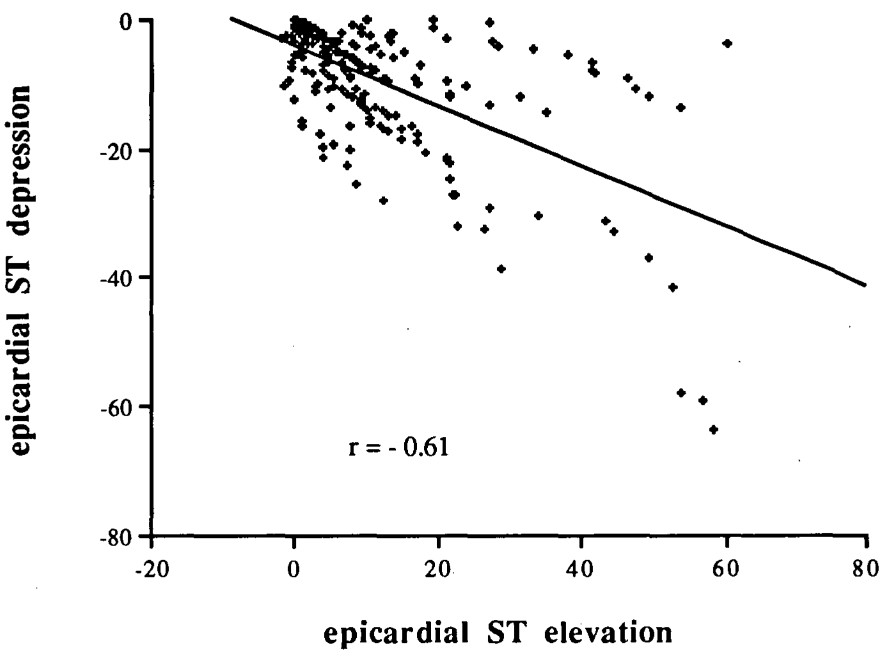

Figure 7.16 Relationship between the epicardial ST depression in the noninfarcted regions and the epicardial ST elevation in the infarcted regions (n=224 data points, P<0.0001).

-In relation to regional myocardial blood flow

Linear correlation was used to determine whether a statistically significant relation existed between the simultaneous measurements of the epicardial flow change and the epicardial ST elevation in the infarcted regions. Both measurements were obtained simultaneously 20 minutes after coronary occlusion. The RMBF is expressed as the percent of control flow measured before infarction. In general, ST elevation greater than 4 mV did not occur unless RMBF was reduced to less than 50% of the control level. The greatest degree of ST elevations occurred in the lowest flow regions. However, there was a wide range of ST elevation for a given flow value. Linear correlation analysis demonstrated a correlation coefficient of -0.45 (Figure 7.17, P< 0.01).

A similar analysis was performed between the endocardial flow change and the epicardial ST depression. As shown in Figure 7.18, although there is a wide scatter of ST depression data points in the noninfarcted regions in which the RMBF was changed to 20% to 120% of the control flow, there was a weak but highly significant positive correlation between these two (r=0.35, P<0.01).

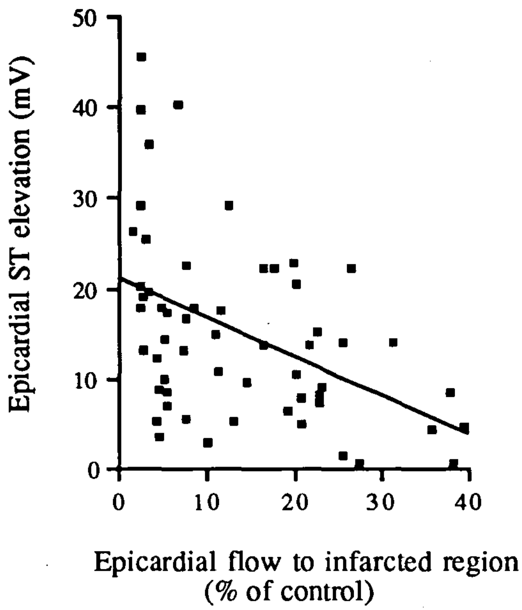

Figure 7.17 Relationship between epicardial ST elevation in the infarcted regions 20 minutes after LCX or LAD occlusion and the epicardial RMBF in the corresponding regions (57 data points from 8 animals, P<0.01).

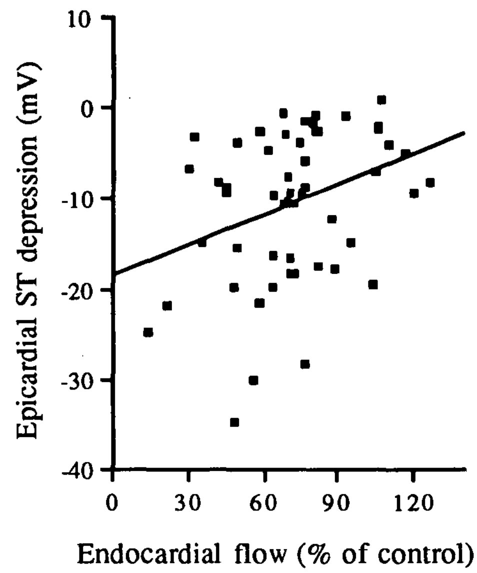

Figure 7.18 Relationship between epicardial ST depression in the noninfarcted regions 20 minutes after LCX or LAD occlusion and the RMBF to the inner third in corresponding regions (r=0.35, P=0.008, 56 data points from 8 animals).

7.4 DISCUSSION

7.4.1 Establishment of Myocardial Ischaemia

Myocardial ischaemia occurs when coronary artery blood is insufficient to meet myocardial metabolic requirements. The death of myocardial cells ensues if ischaemia lasts for a critical length of time. This usually occurs after 20 minutes of cessation of flow and continues for some hours. Ischaemia causes a series of metabolic, functional, electrical and ultrastructual changes which can be detected by different techniques. As reviewed in chapter 2 and discussed in chapter 5, the measurement of the RMBF is an early and important indicator of ischaemia. It detects both the extent and location of ischaemia. It also reflects the degree of ischaemia. According to the degree of flow reduction, ischaemia can be classified as severe, moderate and mild. Ischaemia is severe when flow is reduced to 10 to 15% or less of the nonischaemic flow; moderate when flow is reduced to 15 to 30%; mild when flow is reduced to 30 to 50% (Jennings et al. 1975).

As shown in Tables 7.3, 7.4 & 7.6, and Figure 7.4, OM occlusion reduced the flow to the infarcted region by 61%, LCX and LAD occlusion reduced the flow to the infarcted region by 81% and 84%, respectively, indicating a mild to moderate ischaemia in OM occlusion; a moderate to severe ischaemia in LAD and LCX occlusion. Electrophysiologically, ischaemia was reflected by ST elevation at infarcted regions (Figures 7.7 and 7.10). In either the LCX or the LAD ligation, there was also a 28 to 29% flow reduction to the noninfarcted regions, concomitant with ST depression over these regions, and this might reflect mild ischaemia in noninfarcted myocardium (vide infra).

7.4.2 Regional Myocardial Blood Flow and Haemodynamic Response

Ligation of either the LAD or the LCX resulted in a significant decrease in the left ventricular systolic pressure, a significant increase in the left ventricular end diastolic pressure, and a significant decrease in the blood flow to the noninfarcted regions (Table 7.8, Figure 7.4). However, no significant haemodynamic changes were observed in the OM ligation even though the RMBF decreased significantly in the infarcted regions. The haemodynamic responses in the LAD and the LCX occlusions probably resulted from the larger mass of infarction of the myocardium. As discussed in chapter 5, and shown in Table 7.1, the LAD supplies more than half and the LCX supplies almost half of the left ventricle; whereas the OM supplies only up to 20% of the left ventricle. Studies also revealed that the ovine left ventricle is exclusively supplied by the left main coronary artery and its branches; the LAD supplies the anterior wall and the apex, and the anterior two thirds of the septum; the LCX supplies the remainder of the left ventricle (Markovitz et al. 1989). In contrast to other mammalian species, the ovine heart lacks an intrinsic coronary collateral circulation (Euler et al. 1983), and thus the ischaemic size and the transmural extent are mainly determined by the size of the occluded vascular bed. Therefore, either the LAD or the LCX ligation would produce extensive ischaemia involving approximately half of the left ventricle myocardium, which has been confirmed by the measurements of the RMBF (Figure 7.5). Total occlusion of either the LAD or the LCX caused approximately an 80% flow reduction to their supplied regions (similar to those reported by others (Rivas et al. 1976; Becker 1973)). The abrupt reduction of coronary flow would rapidly lower the contractility in the ischaemic region (Sayen 1961). Since ischaemia involved almost half of the left ventricle mass, the regional impairment of myocardial contractile activity would depress global left ventricular function, causing reduction of stroke volume and cardiac output while elevating left ventricular end-diastolic volume and pressure. This explains the rapid deterioration in the haemodynamics following either the LAD or the LCX ligation.

7.4.3 Epicardial and Endocardial Potential Changes

Following ligation of a coronary artery, epicardial recordings showed ST elevation within 30-60 seconds, and tended to reach a maximum in 5 to 10 minutes (Figures 7.9, 7.14.& 7.15) (Rakita et al. 1954; Ekmekci et al. 1961). ST distribution over the epicardium showed that occluding a small vessel produces little ST depression over the noninfarcted region, and a graduated but even peak of ST elevation in the ischaemic centre, with the magnitude decreasing toward the border (Figure 7.7) (Rakita et al. 1954; Ekmekci et al. 1961). In contrast, either the LAD or the LCX occlusions resulted in a powerful electrical dipole with ST elevation over the infarcted region and ST depression over the noninfarcted region (Figure 7.11). These typical epicardial potential distributions of ST changes for the three different coronary arteries correspond well to the derived epicardial maps of humans with acute infarction reported by Kilpatrick et al. (1989). Small artery occlusion produces localised ST elevation corresponding to a good prognosis; large artery occlusion produces a dipole corresponding to a poor prognosis. Early experimental work (Rakita et al. 1954) reported "reciprocal" ST depressions in leads taken from the posterior wall of the heart following the ligation of the LAD. However, ST depression was noted just outside the cyanotic area (Ekmekci et al. 1961) when only a branch of the LAD was ligated. Posterior wall ST depression was also observed following LAD occlusion in an isolated, perfused rabbit heart (Brody et al. 1973) and in an in-situ baboon model (Crawford et al. 1984). More recent work (Kleber et al. 1978) showed uniform ST elevation over the infarcted region and little change over the border region following the LAD ligation in the isolated pig heart. The different results may be due to the lack of the epicardial electrodes in the noninfarcted region in this study (Kleber et al. 1978).

According to the modern ischaemic models of the heart (Holland & Brooks 1975; Kleber et al. 1978; Smith et al. 1979), within the first 20 minutes of ischaemia the highest epicardial ST elevation is expected to occur near the ischaemic boundary, with a small progressive decrease approaching the ischaemic centre but no ST depression in the other regions. These models do not fully explain the epicardial potential patterns in either the small or the large infarcts from this study. The reasons are uncertain. But there are two common aspects in these studies (Holland & Brooks 1975; Kleber et al. 1978; Smith et al. 1979), which are different from the present one. One is that relatively smaller infarcts were produced by ligating a small coronary artery (Holland & Brooks 1975; Smith et al. 1979); the other is that the mapping electrodes were distributed only in the ischaemic and the surrounding regions, the transition in electrophysiological measurements with respect to the distance from an ischaemic or infarcted border were not examined and therefore the spatial features of the electrophysiological changes in the infarcted and noninfarcted areas were not estimated. In the present study, the occluders were placed on the proximal LAD and the LCX rather than a distal end or a side branch. The ischaemic areas would be expected to be larger than in those carried out by other investigators. Furthermore, the epicardial electrodes covered the whole surfaces of both the left and the right ventricles, and the endocardial electrodes covered the entire endocardium of the left ventricle, which made it possible to record detailed signals from both the infarcted and the noninfarcted areas. Such differences may have contributed to the different results from this study.

Previous ST mapping studies have been focused on the epicardial potential (Holland & Brooks 1975; Kleber et al. 1978; Smith et al. 1979). Little information about endocardial ST potential mapping is available. From the present study, the distribution patterns of endocardial ST potentials are similar to those of the epicardium (Figures 7.12 & 7.13); but quite different from those of the endocardial ST potentials in the subendocardial ischaemia (chapter 6, Figures 6.8, 6.9 & 6.10). Typical subendocardial ischaemia yields endocardial ST elevation (chapter 6, Figures 6.8, 6.9 & 6.10), and therefore the endocardial ST depression in the noninfarcted regions in this study suggests either no subendocardial ischaemia occurred in these regions, or relative elevation of ST levels on the endocardium might have been missed due to changes in the reference signal (vide infra).

7.4.4 Possible Mechanisms of ST Segment Depression

Changes in ST segment in acute myocardial infarction are attributed to injury currents flowing between the ischaemic regions and the normal myocardium (Kleber et al. 1978; Samson & Scher 1960); electrodes directly overlying the injured zones usually recorded ST segment elevation (Kleber et al. 1978; Samson & Scher 1960), whereas those positioned in opposite areas of the heart detect "reciprocal" ST depression (Wolferth et al. 1945). In clinical studies, two findings are generally discussed, ie. the anterior ST depression associated with inferior myocardial infarction, and inferior ST depression associated with anterior myocardial infarction. The significance of these findings are still debated. They may reflect remote myocardial ischaemia secondary to multivessel coronary artery disease ("ischaemia at a distance") (Haraphongse et al. 1984; Salcedo et al. 1981; Jennings et al. 1983; Krone et al. 1993), extensive infarction (Wong et al. 1993a; Wong & Freedman 1994; Edmunds et al. 1994) and/or a benign electrical phenomenon (reciprocal or mirror changes) (Putini et al. 1993; Fletcher et al. 1993; Stevenson et al. 1993 & 1994; Birnbaum et al. 1994).

In this study, ST depression occurred exclusively in large infarcts whereas little ST depression accompanied small infarcts (Figure 7.11). This finding suggests that ST depression in myocardial infarction indicates larger infarcts. These results corroborate both clinical findings (Wong et al. 1993a; Wong & Freedman 1994; Edmunds et al. 1994; Berland et al. 1986; Gibson et al. 1982; Lew et al. 1985) and animal experiments. (Rakita et al. 1954; Ekmekci et al. 1961).

In clinical studies, it has been found that the amount of ischaemia and infarction was greater in the patients with ST segment depression in both inferior and anterior myocardial infarction (Wong & Freedman 1994; Edmunds et al. 1994; Willems et al. 1990) and that artery size and distribution were smaller in patients without ST depression (Bates 1988; Sato et al. 1989; Brymer et al. 1985). Patients with ST depression also had worse ventricular function than those without (Bates et al. 1990; Billadello et al. 1983; Mukharji et al. 1984; Shah et al. 1980; Haraphongse et al. 1984). Others (Kilpatrick 1989) found that a dipole on the epicardium is a powerful predictor of mortality in inferior infarction. That analysis (Kilpatrick 1989) shows clearly that the dipoles were present in patients with single vessel disease as well as in those with triple vessel disease and that the dipole predicted the death of those with single vessel disease (Kilpatrick 1989). In the present study, 14 of the 25 animals with large infarcts died from ventricular tachycardia and ventricular fibrillation; another 3 animals died from bradycardia due to atrio-ventricular block. Yet all the 8 animals with small infarcts survived, and arrhythmias were seldom observed in this group.

Furthermore, the author observed that with large infarcts there was approximately a 30% flow reduction in the noninfarcted regions (Figure 7.4B), whereas with small infarcts there was a normal or slightly increased perfusion in these regions (Figure 7.4B). In addition, the flow reduction in the noninfarcted regions directly correlates to the perfusion pressure drop ($r=0.82$, $P<0.001$) (Figure 7.6A), and a weak but highly significant correlation exists between the epicardial ST depression and the endocardial flow reduction ($r=0.35$, $P<0.01$) (Figure 7.18). These findings suggest that ST depression during myocardial infarction might reflect remote ischaemia secondary to a reduced perfusion pressure, rather than a passive electrical phenomenon.

Results of both clinical (Schuster & Bulkley 1980; Salcedo et al. 1981; Jennings et al. 1983) and experimental (Naccarella et al. 1984; Gascho et al. 1987) studies have demonstrated that "ischaemia at a distance" occurred when acute occlusion of one vessel produces ischaemia in the myocardium perfused by a second stenotic coronary artery. In this experiment, the reduction of myocardial blood flow in the noninfarcted regions was associated with reduced perfusion pressure and increased left ventricular end diastolic pressure, suggesting multiple mechanisms interact to produce such remote ischaemia (Naccarella et al. 1984; Gascho et al. 1987; Mirvis 1988; Edmunds et al. 1994; Schuster & Bulkley 1980 & 1981). Firstly, reduced perfusion due to the drop of the perfusion pressure directly produces ischaemia in the noninfarcted regions. Secondly, the increased oxygen demand after arterial ligation, resulting from factors including increased heart rate and increased chamber size, may provoke relative ischaemia in the noninfarcted region. Thirdly, increased back pressure on the distal coronary bed produced by increased left ventricular end-diastolic pressure may reduce the transcoronary pressure gradient to reduce flow. Finally, the stress to sustain cardiac output by overcompensation by the noninfarcted myocardium may also contribute to the "relative" ischaemia in the noninfarcted regions (Scott & Kerber 1992; Trevi GP & Sheiban 1991). Detailed studies of the energy state of the noninfarcting muscle and other indications of ischaemia such as lactate accumulation, left ventricular wall motion abnormalities and increases in tissue pCO_2 would be required to confirm these postulates.

However, conflicting results were obtained from this study. Firstly, if there was typical ischaemia, one would predict that the endocardial electrogram should record ST elevation in the noninfarcted regions. Nevertheless, the endocardial ST potential distribution patterns were similar to that of the epicardial, ie, a dipole formed by ST depression over the noninfarcted region and ST elevation over the infarcted region (Figures 7.12 and 7.13). It is possible that relative elevation of ST levels on the endocardium might be missed due to changes in the reference signal. Secondly, there was a good correlation between the magnitude of epicardial ST depression in the noninfarcted regions and the magnitude of epicardial ST elevation in the infarcted regions ($r=-0.61$, $P<0.0001$, Figure 7.16), suggesting a relationship between ST elevation and ST depression. Finally, in two animals with large infarcts in which the blood pressure and the remote flow were not changed during ischaemia, epicardial ST depression was still recorded in the noninfarcted regions. These data suggest that the epicardial ST depression was not purely secondary to subendocardial ischaemia of the noninfarcting myocardium. This distinction is important because management strategies may differ depending on the underlying pathophysiologic mechanisms of the ST depression.

Early work showed that intracavity leads immediately beneath the infarcted myocardium registered ST elevation of a slight degree (Rakita et al. 1954). In regions where ST depression developed after the LAD occlusion, ST elevation was not recorded from the subendocardial leads at the same location (Ekmekci et al. 1961), which suggested that the depression could not be explained on the basis of a local reciprocal effect of subendocardial injury. The authors associated ST segment depression with moderate ischaemia (Ekmekci et al. 1961) and this point of view was supported by Case et al. (1966). However, no measurements of RMBF were made to support this contention. Mirvis (1988) explained, based on the dipole theory, that such ST depression is a biophysical phenomenon, which should always be expected with primary ST elevation. Little ST depression was observed in small infarcts (Figures 7.7 & 7.11) however and this does not fit the electrical "reciprocal change" theory (Mirvis 1988).

These results show that the ST changes with acute infarction are more complex than previously thought. In particular ST depression closely associated with the ST elevation has not been explained. It is possible that it reflects ischaemia but it does not behave identically to subendocardial ischaemia in that the expected endocardial ST elevation was absent. As shown in Tables 7.4 & 7.6, and Figures 7.2, 7.3 & 7.5, there was a similar reduction in the RMBF to each third of the myocardium in both the infarcted and the noninfarcted regions. This uniform reduction in transmural flow caused a nonsignificant change in the endo/epi flow ratio. In the study described in chapter 6, endocardial ST elevation occurred during subendocardial ischaemia when the endo/epi flow ratio was reduced by 35%. Other studies (Euler 1983; Markovitz 1989) also found that in sheep, in contrast to dogs, the subepicardial zone is as severely ischaemic as the subendocardial region because of the lack of native collateral blood flow to the ischaemic regions. Another possible reason for the absence of the expected endocardial ST elevation in the noninfarcted regions may be due to the relative ST elevation of the reference lead caused by the strong positive ST shift in the infarcted regions.

7.4.5 Clinical implication and limitations

In spite of the complex nature of ST changes in myocardial infarction, findings from this study suggest that ST depression in myocardial infarction reflected large infarctions, was associated with reduced perfusion of the noninfarcted myocardium and might be a marker of patients who should receive increased treatment to maintain better perfusion pressure. Intervention studies are required to further elucidate the pathogenesis, electrophysiological mechanism and clinical significance of such ST depression.

Chapter 8

CONCLUSION

8.1 GENERAL DISCUSSION AND CONCLUSION

The primary objective of this thesis was to explore the origin of ST depression in subendocardial ischaemia, and a number of experiments were performed to estimate the ischaemic source.

Firstly, RMBF was used to measure the location, the extent and the degree of ischaemia. Although there are other ways to detect the occurrence of ischaemia, such as the measurements of metabolic parameters (myocardial lactate, tissue pCO_2 and enzyme changes) and histological changes, RMBF measurement was the only method which suited the purpose of this study. To measure the RMBF, a modified fluorescent microsphere technique was developed. It was found that RMBF could be precisely and effectively measured without filtering myocardial tissues, which reduced both work and measurement error due to transferring containers. It was also found that injection of fluorescent microspheres directly into the coronary artery was comparable with the classic left atrial injection, but the former method consumed only 5% of the number of microspheres.

Secondly, a model of subendocardial ischaemia was developed by partially ligating either the LCX or the LAD coupled with atrial pacing in the anaesthetised sheep. The position and the extent of the ensuing ischaemia were validated by the measurement of the RMBF using fluorescent microspheres. Subendocardial ischaemia occurred when the coronary blood flow was decreased by 40-50% and the heart paced at 180 bpm. Mapping of the spatial flow distributions demonstrated that during subendocardial ischaemia there was a gradual transition in flow reduction from the endocardium to the epicardium while there was a sharp change at the lateral boundary. The susceptibility to ischaemia was similar for the LAD and the LCX territories, although the amount of myocardium supplied by the LAD was slightly larger.

Based on this model, five series of experiments were conducted.

(1) Epicardial ST potentials were mapped at various regions of ischaemia in different animals. The results showed that the epicardial ST potential distribution was independent of the ischaemic region. The epicardial potential mapping was then tested in the same animal, when different regions of ischaemia were produced alternately. The results showed even more similar epicardial ST potential distributions in various regions of ischaemia ($r=0.77\pm0.14$). This finding shows that epicardial ST segment depression can not localise an ischaemic region which explains the clinical difficulty in identifying stenosed arteries from body surface ST depression.

(2) Simultaneous measurements of epicardial and endocardial potentials were performed, and RMBF measured. General ST depression was recorded from the epicardium while localised ST elevation was recorded over the ischaemic region from the endocardium. The endocardial ST elevation was closely associated with the reduction of the RMBF, but not the epicardial ST depression. These data suggest that the source of epicardial ST depression was related to the ischaemia of subendocardium but not the ischaemia of epicardium.

(3) The heart was insulated from the surrounding tissue to evaluate the source currents. It was found that insulation increased the magnitude of epicardial and endocardial ST and QRS potentials without altering their distribution patterns, but decreased the potentials from limb leads. If ST depression was due to the endocardial current flow back on to the cardiac surface, insulation should have eliminated or changed the epicardial ST depression. The important ischaemic current path might be in the myocardium in terms of the similar increase in the magnitudes of the epicardial ST potential and QRS potential by insulation.

(4) The contribution of intracavity blood to the epicardial ST depression was assessed by intracavity injection of high resistance glucose. This manoeuvre did not cause significant changes in either the magnitude or the distribution of ST potentials. Comparison of the resistance of the cavity blood before and during the fluid injection showed little change in resistance, and thus the contribution of the cavity blood to the epicardial ST depression is inconclusive.

(5) To test the contention that the important current path is in the myocardium, the subendocardial ischaemia was transformed to full-thickness ischaemia by increasing the percent stenosis of a coronary artery while the epicardial potential changes were recorded either intermediately or continuously. Epicardial potential recordings demonstrated that as ischaemia progressed ST depression increased at the lateral boundary, ST elevation developed firstly from the ischaemic centre when ischaemia

become transmural and then gradually toward the ischaemic boundary. These results suggest that the major source of subendocardial ischaemia might be at the lateral boundary, and this postulate was supported by the RMBF distributions which showed a sharp lateral flow change but a gradual transmural flow transition. To verify this contention, transmural recordings were performed by using four quadripolar needle electrodes implanted at the ischaemic boundary and the ischaemic and nonischaemic regions. Unfortunately, such recordings were not satisfactory due to strong, irreversible injury currents produced by the intramural electrodes.

These studies have provided systematic information on the distribution of epicardial and endocardial ST potentials during subendocardial ischaemia in the in-situ heart. However, the origin of ST depression was not fully defined because of the order of injury currents from the ST elevation.

The secondary objective of this study was to investigate the electrophysiologic and pathophysiologic mechanisms of ST depression occurring with ST elevation during acute myocardial infarction. To pursue this purpose, different sizes of myocardial infarction were produced, and epicardial and endocardial potentials were mapped. RMBF was measured and related to the regions of ischaemia and the changes of potentials. Epicardial ST distributions showed that occluding a small vessel produced the expected ST elevation over the infarcting region and little ST depression over the noninfarcting region, whereas left anterior descending coronary artery and left circumflex coronary artery occlusions resulted in a powerful electrical dipole with ST elevation over the infarcted region and ST depression over the noninfarcted region. Examination of fluorescent microsphere delivery into the tissues showed that with smaller infarcts the flow remained unchanged in the noninfarcted region. With large infarcts there was approximately a 30% flow reduction in the noninfarcted region which directly correlated to the perfusion pressure drop. These data suggest that ST depression is associated with reduced perfusion in the noninfarcted region secondary to an extensive infarction. However, from the endocardium, ST elevation was not recorded over noninfarcted myocardium; epicardial ST depression in animals with normal perfusion to the noninfarcted myocardium did not disappear as expected; and epicardial ST elevation was correlated to the epicardial ST depression. These results demonstrate that ischaemia is not the only reason for the epicardial ST depression in the noninfarcted region.

In conclusion, epicardial ST depression in subendocardial ischaemia does not reflect the position of ischaemia. The ischaemic source does relate spatially to the endocardial ST change but not to the epicardial ST change. The main current path during subendocardial ischaemia is in the myocardium and ST depression might originate from the injury current which flows at the lateral boundary of the ischaemia. These effects are not explained by conventional theory. ST depression does not localise cardiac ischaemia even on the epicardium. Epicardial ST depression in acute myocardial infarction reflects extensive infarction; it is associated with reduced perfusion of the noninfarcted myocardium, and may be an indicator of patients who should have increased treatment to maintain better perfusion pressures.

8.2 FUTURE WORK

To further understand the origin of ST depression, the three dimensional current and potential fields could be measured by recording intramyocardial potentials simultaneously with epicardial and endocardial potentials using multiple electrode needles. The intramural electrodes should be placed to the ischaemic region, ischaemic boundary and nonischaemic regions. Using these data, three dimensional current and potential fields could be plotted by computer, and a clear image of the current path in subendocardial ischaemia could be obtained.

To confirm that ST depression occurring with ST elevation in acute myocardial infarction relates to underperfusion of normal myocardium, the following experiments could be performed. (1) Record the epicardial and endocardial potentials continuously with small size infarction while transforming it to large size infarction by a series of ligations at different sites from the distal to the proximal of an artery. The changes of ST potential fields during this process should reveal the significance of ST depression. (2) Measure myocardial lactate accumulation, myocardial tissue pCO_2 increase and left ventricular wall motion abnormalities to clarify whether the flow reduction in noninfarcted region is sufficient to cause myocardial ischaemia. (3) Correct the low perfusion to the normal myocardium by the following manoeuvres: a. balloon pumping to increase coronary perfusion pressure; b. Dopamine to raise blood pressure; c. colloid solution to increase preload. Coronary sinus pO_2 and RMBF should be measured and O_2 consumption calculated. Epicardial potential fields before and after the correction of the low perfusion should be measured and compared. These studies should solve whether ST depression in the noninfarcted region indicates reversible ischaemia, and whether clinical treatment should be altered by the observation of epicardial ST depression from inverse transformation.

REFERENCES

Abel FL, Cooper RH, Beck RR. Use of fluorescent latex to measure coronary blood flow distribution. Circulatory Shock 41:156-161, 1993.

Abouantoun S, Ahnve S, Savvides M, Witztum K, Jensen D, Froelicher V. Can areas of myocardial ischemia be localized by the exercise electrocardiogram? A correlative study with thallium-201 scintigraphy. Am Heart J 108:933-941, 1984.

Adams JE III, Abendschein DR, Jaffe AS. Biochemical markers of myocardial injury: Is MB creatine kinase the choice for the 1990s? Circulation 88:750-763, 1993.

Altman DG. Practical statistics for medical research. Chapman and Hall London, pp277-299, 1991.

Archie JP, Fixler DE, Ullyot DJ, Buckberg GD, Hoffman JIE. Regional myocardial blood flow in lambs with concentric right ventricular hypertrophy. Circ Res 34: 143-154, 1974.

Austin RE Jr, Hauck WW, Aldea GS, Flynn AE, Coggins DL, Hoffman JIE. Quantitating error in blood flow measurements with radioactive microspheres. Am J Physiol 257:H280-288, 1989.

Bache RJ, Cobb FR. Effect of maximal coronary vasodilation on transmural myocardial perfusion during tachycardia in the awake dog. Circ Res 41:648-653, 1977.

Bache RJ, McHale PA, Greenfield JC. Transmural myocardial perfusion during restricted coronary inflow in the awake dog. Am J Physiol 232:H645-651, 1977.

Bache RJ, Schwartz JS. Effect of perfusion pressure distal to a coronary stenosis on transmural myocardial blood flow. Circulation 65: 928-935, 1982.

Bache RJ, Vrobel TR, Ring WS, Emery RW, Andersen RW. Regional myocardial blood flow during exercise in dogs with chronic left ventricular hypertrophy. Circ Res 48:76-87, 1981.

Barber MR, Fischmann EJ. Heart dipole regions and the measurement of dipole moment. Nature 192:141-142, 1961.

Bassingthwaighte JB, Malone MA, Moffett TC, King RB, Chan IS, Link JM, Krohn KA. Molecular and particulate depositions for regional myocardial flows in sheep. Circ Res 66:1328-1344, 1990.

Bates ER, Clemmensen PM, Califf RM, Gorman LE, Aronson LG, George BS, Kereiakes D, Topol E. Precordial ST segment predicts a worse prognosis in inferior infarction despite reperfusion therapy. J Am Coll Cardiol 16:1538-1544, 1990.

Bates ER. Reperfusion therapy in inferior myocardial infarction. J Am Coll Cardiol 12:44A-51A, 1988.

Bayley RH. An interpretation of the injury and ischemic effects of myocardial infarction in accordance with the laws which determine the flow of electric currents in homogeneous volume conductors and in accordance with relevant pathologic changes. Am Heart J 24:514-528, 1942.

Bayley RH. The electrocardiographic effects of injury at the endocardial surface of the left ventricle. Am Heart J 31:677-684, 1946.

Becker LC, Ferreira R, Thomas M. Mapping of left ventricular blood flow with radioactive microspheres in experimental coronary artery occlusion. Cardiovasc Res 7:391-400, 1973.

Becker LC, Fortuin NJ, Pitt B. Effect of ischemia and antianginal drugs on the distribution of radioactive microspheres in the canine left ventricle. Circ Res 28:263-269, 1971.

Becker LC, Schuster EH, Jugdutt BI, Hutchins GM, Bulkley BH. Relationship between myocardial infarct size and occluded bed size in the dog: difference between left anterior descending and circumflex coronary artery occlusions. Circulation 67:549-557, 1983.

Becker RC, Alpert JS. Electrocardiographic ST segment depression in coronary heart disease. Am Heart J 115:862-868, 1988.

Bell AJ, Briggs CM, Nichols P, Kilpatrick D. Relationship of ST-segment elevation to eventual QRS loss in acute anterior wall myocardial infarction. J Elctrocardiol 26:177-185, 1993.

Berland J, Cribier A, Behar P, Letac B. Anterior ST depression in inferior myocardial infarction: correlation with results of intracoronary thrombolysis. Am Heart J 111:481-488, 1986.

Billadello JJ, Smith JL, Ludbrooke PA, Tiefenbrunn AJ, Jaffe AS, Sobel BE, Geltman EM. Implications of "reciprocal" ST segment depression associated with acute myocardial infarction identified by positron tomography. J Am Coll Cardiol 2:616-624, 1983.

Birnbaum Y, Solodky A, Herz I, Kusniec J, Rechavia E, Sulkes J, Sclarovsky S. Implications of inferior ST-segment depression in anterior acute myocardial infarction: electrocardiographic and angiographic correlation. Am Heart J 127:1467-1473, 1994.

Blackburn H, Katigbak R. What electrocardiographic lead to take after exercise? Am Heart J 67:184-185, 1963.

Bland JM, Altman DG. Measurement. Statistical methods for assessing agreement between two methods of clinical measurement. The Lancet (i):307-310, 1986.

Boatwright RB, Downey HF, Bashour FA, Crystal GJ. Transmural variation in autoregulation of coronary blood flow in hyperfused canine myocardium. Circ Res 47:599-609, 1980.

Braash W, Gudbjarnason S, Puri PS, Ravens KG, Bing RJ. Early changes in energy metabolism in the myocardium following acute coronary artery occlusion in anesthetized dogs. Circ Res 23:429-438, 1968.

Brazier J, Cooper N, Buckberg G. The adequacy of subendocardial oxygen delivery: the interaction of determinants of flow, arterial oxygen content and myocardial oxygen need. Circulation 49: 968-977, 1974.

Brody DA, Terry FH, Ideker RE. Eccentric dipole in a spherical medium: generalized expression for surface potentials. IEEE Trans Biomed Eng 20:141-143, 1973.

Brody DA. A theoretical analysis of intracavity blood mass influence on the heart-lead relationship. Circ Res 4:731-738, 1956.

Bruyneel KJJ. Use of moving epicardial electrodes in defining ST segment changes after acute coronary occlusion in the baboon. Relation to primary ventricular fibrillation. Am Heart J 89:731-741, 1975.

Brymer JF, Khaja F, Marzilli M, Goldstein S. "Ischemia at a distance during intermittent coronary artery occlusion: a coronary anatomic explanation. J Am Coll Cardiol 6:41-45, 1985.

Buckberg GD, Luck JC, Payne DB. Some sources of error in measuring regional blood flow with radioactive microspheres. J Appl Physiol 31:598-604, 1971.

Camara EJN, Chandra N, Ouyang P, Gottlieb SH, Shapiro EP. Reciprocal ST change in acute myocardial infarction: assessment by electrocardiography and echocardiography. J Am Coll Cardiol 2:251-257, 1983.

Campbell MJ, Machin D. Medical Statistics. John Wiley & Sons England, pp80-96, 1990.

Case RB, Felix A, Castellana FS. Rate of rise of myocardial pCO_2 during early myocardial ischemia in the dog. Circ Res 45:324-330, 1979.

Case RB, Roselle HA, Crampton RS. Relation of S-T depression to metabolic and haemodynamic events. Cardiologia 48:32-41, 1966.

Cinca J, Janse MJ, Morena H, Candell J, Valle V, Durrer D. Mechanism and time course of the early electrical changes during acute coronary artery occlusion. Chest 77:499-505, 1980.

Cohen D, Savard P, Rifkin RD, Lepeschkin E, Strauss WE. Magnetic measurement of S-T and T-Q segment shifts in humans. Part II. Exercise induced S-T segment depression. Circ Res 53:274-279, 1983.

Cohen D, Savard P, Rifkin RD, Lepeschkin E, StraussWE. Magnetic measurement of S-T and T-Q segment shifts in humans. part II Exercise induced S-T segment depression. Circ Res 53:274-279, 1983.

Colli-Franzone P, Guerri L, Viganotti C, Macchi E, Baruffi S, Spaggiari S, Taccardi B. Potential fields generated by oblique dipole layer modeling excitation wavefronts in the anisotropic myocardium. Comparison with potential fields elicited by paced dog hearts in a volume conductor. Circ Res 51:330-346, 1982.

Connelly C, Vogel WM, Hernandez YM, Apstein CS. Movement of necrotic wave front after coronary artery occlusion in rabbit. Am J Physiol 243:H682-H690, 1982.

Conrad LL, Cuddy TE. The influence of boundary conditions on the amplitude of R and other accession potentials in leads from the ventricular wall. Circ Res 8:82-87, 1960.

Cook RW, Edwards JE, Pruitt RD. Electrocardiographic changes in acute subendocardial infarction. I. Large subendocardial and large nontransmural infarcts. Circulation 18:603-612, 1958.

Coronel R, Fiolet JWT, Wilms-Schopman FJG, Schaapherder AFM, Johnson TA, Gettes LS, Janse M. Distribution of extracellular potassium and its relation to electrophysiologic changes during acute myocardial ischemia in the isolated perfused porcine heart. Circulation 77:1125-1138, 1988.

Corr PB, Gross R, Sobel BE. Amphipathic metabolites and membrane dysfunction in ischemic myocardium. Circ Res 55:135-154, 1984.

Crawford MH, O'Rourke RA, Grover FL. Mechanism of inferior electrocardiographic ST-segment depression during acute anterior myocardial infarction in a baboon model. Am J Cardiol 54:1114-1117, 1984.

Crozatier B, Ross J Jr, Franklin D, Bloor CM, White FC, Tomoike H, McKown DP. Myocardial infarction in the baboon: Regional function and the collateral circulation. Am J Physiol 235: H413-H421, 1978.

DeWood MA, Heit J, Spores J, Eugster GS, Coulston D, Reisig AH, Hinnen ML, Shields JP. Significance of precordial ST segment depression in acute inferior transmural myocardial infarction: assessment by coronary arteriography and ventriculography during the early hours (abstr). Circulation 66(suppl II):II-182, 1982.

Dole WP, Jackson DL, Rosenblatt JI, Thompson WL. Relative error and variability in blood flow measurements with radiolabeled microspheres. Am J Physiol 243:H371-H378, 1982.

Domenech RJ, Hoffman JIE, Noble MIM, Saunders KB, Henson JR, Subijanto S. Total and regional coronary blood flow measurement by radioactive microspheres in conscious and anaesthetised dogs. Circ Res 25:581-596, 1969.

Dunn RB, Griggs DM Jr. Transmural gradients in ventricular tissue metabolites produced by stopping coronary blood flow in the dog. Circ Res 37:438-445, 1975.

Dunn RB, Griggs DM Jr. Ventricular filling pressure as a determinant of coronary blood flow during ischemia. Am J Phsiol 244:H429-H436, 1983.

Dunn RF, Freedman B, Bailey IK, Uren RF, Kelly DT. Localization of coronary artery disease with exercise electrocardiography. Correlation with thallium-201 myocardial perfusion scanning. Am J Cardiol 48:837-843, 1981.

Edmunds JJ, Gibbons RJ, Bresnahan JF, Clements IP. Significance of anterior ST depression in inferior wall acute myocardial infarction. Am J Cardiol 73 (2):143-148, 1994.

Einthoven W, Fahr G, DeWaart A. On the direction and manifest size of the variations of potential in the human heart and on the influence of the position of the heart on the form of the electrocardiogram. Pflugers Arch 150:275-315, 1913. (Translated by Hoff PE and Sekelj P: Am Heart J 40:163-211, 1950.)

Ekmekci A, Toyoshima H, Kwoczynski JK, Nagaya T, Prinzmetal M. Angina Pectoris. IV. Clinical and experimental difference between ischemia with S-T elevation and ischemia with S-T depression. Am J Cardiol 7:412-426, 1961.

Ellis AK. Serum protein measurements and the diagnosis of acute myocardial infarction. Circulation 83:1107-1109, 1991.

Euler DE, Spear JE, Moore EN. Effect of coronary occlusion on arrhythmias and conduction in the ovine heart. Am J Physiol 245:H82-89, 1983.

Factor SM, Okun EM, Kirk ES. The histological lateral border of acute canine myocardial infarction: A function of microcirculation. Circ Res 48:640-649,1981.

Fedor JM, McIntosh DM, Rembert JC, Greenfield JC Jr. Coronary and transmural myocardial blood flow responses in awake pigs. Am J Physiol. Heart Circ Physiol 235: H435-H444, 1978.

Ferro G, Duilio C, Spinelli L, Liucci GA, Mazza F. Relation between diastolic perfusion time and coronary artery stenosis during stress-induced myocardial ischemia. Circulation 92:342-347, 1995.

Fisch C. Electrocardiography and vectorcardiography. In Heart Disease, Braunwald E, ed., W. B. Saunders Company, pp136-149, 1992.

Fisher DJ, Heymann MA, Rudolph AM. Effects of hemorrhage on myocardial consumption of oxygen and carbohydrate in fetal sheep in utero. J Dev Physiol 2:151-159, 1980.

Fisher DJ. Increased regional myocardial blood flows and oxygen deliveries during hypoxemia in lambs. Pediatr Res 18: 602-606, 1984.

Fletcher WO, Gibbons RJ and Clements IP. The relationship of inferior ST depression, lateral ST elevation, and left precordial ST elevation to myocardium at risk in acute anterior myocardial infarction. Am Heart J 126:526-535, 1993.

Flynn AE, Coggins DL, Goto M, Aldea GS, Austin RE, Doucette JW, Husseini W, Hoffman JIE. Does systolic subepicardial perfusion come from retrograde subendocardial flow? Am J Physiol 262:H1759-H1769, 1992.

Fox KM, Selwyn A, Oakley D, Shillingford JP. Relation between the precordial projection of S-T segment changes after exercise and coronary angiographic findings. Am J Cardiol 44:1068-1075, 1979.

Fozzard HA, Arnsdorf MF. Cardiac electrophysiology. In: The Heart and Cardiovascular System, Fozzard HA et al., ed. New York, Raven Press, pp63-94, 1992.

Fozzard HA, Friedlander IR. Cellular electrophysiology. In: Comprehensive Electrocardiology, Macfarlane PW & Lawrie TD, ed. Pergamon Press, pp79-99, 1989.

Freifeld AG, Schuster EH, Bulkley BH. Nontransmural versus transmural myocardial infarction. A morphologic study. Am J Med 75:423-432, 1983.

Fuchs RM, Achuff SC, Grunwald L, Yin FCP, Griffith LSC. Electrocardiographic localization of coronary artery narrowings. Studies during myocardial ischemia and infarction in patients with one-vessel disease. Circulation 66:1168-1176, 1982.

Ganz P, Braunwald E. Coronary blood flow and myocardial ischemia. In: Heart Disease. Braunwald E ed., W B Saunders Company, pp1161-1183, 1997.

Gascho JA, Beller GA. Adverse effects of circumflex coronary artery occlusion on blood flow to remote myocardium supplied by a stenosed left anterior descending coronary artery in anesthetized open-chest dogs. Am Heart J 113:679-683, 1987.

Geselowitz DB. Dipole theory in electrocardiography. Am J Cardiol 14: 301-306, 1964.

Gettes LS, Cascio WE. Effects of acute ischemia on cardiac electrophysiology. In: The heart and cardiovascular system. Fozzard HA ed., Raven Press, Ltd., pp2021-2054, 1992.

Gevers W. Generation of protons by metabolic processes in heart cells. J Mol Cell Cardiol 9:867-874, 1979.

Gheorghiade M, Shivkumar K, Schultz L, Jafri S, Tilley B, Goldstein S. Prognostic significance of electrocardiographic persistent ST depression in patients with their first myocardial infarction in the placebo arm of the Beta-Blocker Heart Attack Trial. Am Heart J 126:271-278, 1993.

Gibson RS, Crampton RS, Watson DD, Taylor GJ, Carabello BA, Holt ND, Beller GA. Precordial ST-segment depression during acute inferior myocardial infarction: clinical, scintigraphic and angiographic correlations. Circulation 66:732-741, 1982.

Glenny RW, Bernard S, Brinkley M. Validation of fluorescent-labelled microspheres for measurement of regional organ perfusion. J Appl Physiol 74:2585-2597, 1993.

Gould KL, Lipscomb K, Hamilton GW. Physiologic basis for assessing critical coronary stenosis: instantaneous flow response and regional distribution during coronary hyperemia as measures of coronary flow reserve. Am J Cardiol 33:87-94, 1974.

Green LS, Taccardi B, Ershler PR, Lux RL. Epicardial potential mapping: effects of conducting media on isopotential and isochrone distributions. Circulation 84:2513-2521, 1991.

Guilbault GG. Practical Fluorescence. In: Modern Monographs in Analytical Chemistry, Guilbault GG ed., 1990.

Guyton RA, McClenathan JH, Newman GE, Michaelis LL. Significance of Subendocardial S-T segment elevation caused by coronary stenosis in the dog. Am J Cardiol 40:373-380, 1977.

Hale SL, Alker KJ, Kloner RA. Evaluation of nonradioactive, coloured microspheres for measurement of regional myocardial blood flow in dogs. Circulation 78:428-434, 1988.

Hales JRS, Cliff WJ. Direct observations of the behaviour of microspheres in microvasculature. Bibliotheca Anatonica 15:87-91, 1977.

Haraphongse M, Tanomaup S, Jugdutt BI. Inferior ST segment depression during acute anterior myocardial infarction: clinical and angiographic correlations. J Am Coll Cardiol 4:467-476, 1984.

Harken AH, Simson MB, Haselgrove J, Wetstein L, Harden WR, Barlow CH. Early ischemia after complete coronary ligation in the rabbit, dog, pig, and monkey. Am J Physiol 241:H202-H210, 1981.

Harris AS, Bisteni A, Russell RA, Brigham CB, Firestone JE. Excitatory factors in ventricular tachycardia resulting from myocardial ischemia. Potassium a major excitant. Science 119:200-203, 1954.

Heller GV, Aroesty JM, McKay RG, Parker JA, Silverman KJ, Corne PC, Grossman W. The pacing stress test: a reexamination of the relation between coronary artery disease and pacing-induced electrocardiographic changes. Am J Cardiol 54:50-55, 1984.

Heng MK, Singh BN, Norris RM, John MB, Elliott R. Relationship between epicardial ST-segment elevation and myocardial ischemic damage after experimental coronary artery occlusion in dogs. J Clin Invest 58:1317-1326, 1976.

Heymann MA, Payne BD, Hoffman JIE, Rudolph AM. Blood flow measurements with radionuclide-labeled particles. Prog Cardiovasc Dis 20:55-79, 1977.

Hill JL, Gettes LS. Effect of acute coronary artery occlusion on local myocardial extracellular K+ activity in swine. Circulation 61:768-778, 1980.

Hodgkin BC, Millard RW, Nelson CV. Effect of hematocrit on electrocardiographic potentials and dipole moment of the pig. Am J Physiol 232:H406-H410, 1977.

Hoffman JIE. Transmural myocardial perfusion. Prog Cardiovasc Dis 29: 429-464, 1987.

Holland R.P, Arnsdorf MF. Solid angle theory and the electrocardiogram: Physiologic and Quantitation Interpretations. Prog Cardiovasc Dis 19:431-457, 1977.

Holland RP, Brook H. TQ-ST segment mapping: Critical review and analysis of current concepts. Am J Cardiol 40:110-129, 1977a.

Holland RP, Brooks H. Precordial and epicardial surface potentials during myocardial ischemia in the pig. A theoretical and experimental analysis of the TQ and ST segments. Circ Res 37:471-480, 1975.

Holland RP, Brooks H. Spatial and nonspatial influences on the TQ-ST segment deflection of ischemia. Theoretical and experimental analysis in the pig. J Clin Invest 60:197-214, 1977b.

Holmberg S, Serzyskol W, Varnauskas E. Coronary circulation during heavy exercise in control subjects and patients with coronary heart disease. Acta Med Scand 190:465-480, 1971.

Holmberg S, Varnauskas E. Coronary circulation during pacing-induced tachycardia. Acta Med Scand 190:481-490, 1971.

Holt JH Jr, Barnard ACL, Lynn MS, Svendsen P. A study of the human heart as a multipole electrical source. I. Normal adult male subjects. Circulation 40:687-696, 1969.

Horan LG, Flowers NC. Electrocardiography and vectorcardiography. In Heart Disease, Braunwald E, ed. W. B. Saunders Company, pp198-250, 1980.

Horan LG, Flowers NC. Limitations of the dipole concept in electrocardiography. New York, Grune & Stratton, pp9-18, 1972.

Irvin RG, Cobb FR. Relationship between epicardial ST-segment elevation, regional myocardial blood flow, and extent of myocardial infarction in awake dogs. Circulation 55:825-832, 1977.

Janse MJ, Cinca J, Morean H, Fiolet JWT, Kleber AG, de Vries GP, Becker AE, Durrer D. The 'border zone' in myocardial ischaemia. An electrophysiological, metabolic, and histochemical correlation in the pig heart. Circ Res 44:576-588, 1979.

Janse MJ, Frans JL, van Capelle, Morsink H, Kleber AG, Wilms-Schopman F, Cardinal R, d'Alnoncourt CN, Durrer D. Flow of "injury" current and patterns of excitation during early ventricular arrhythmias in acute regional myocardial ischemia in isolated porcine and canine hearts. Circ Res 47:151-165, 1980.

Jennings K, Reld DS, Julian DG. "Reciprocal" depression of the ST-segment in acute myocardial infarction. Br Med J 287:634-637, 1983.

Jennings RB, Ganote CE, Reimer KA. Ischemic tissue injury. Am J Pathol 81:179-198, 1975.

Jennings RB, Reimer KA, Hill ML, Mayer SE. Total ischemia in dog hearts, in vitro. 1. Comparison of high-energy phosphate production, utilization, and depletion, and of adenine nucleotide metabolism in total ischemia in vitro vs severe ischemia in vivo. Circ Res 49:892-900, 1981.

Jennings RB, Reimer KA. Factors involved in salvaging ischaemic myocardial: Effects of reperfusion of arterial blood. Circulation 68 (Suppl. I):I-25, 1983.

Jennings RB, Schaper J, Hill ML, Steenbergen C, Reimer KA. Effect of reperfusion late in the phase of reversible ischemic injury. Changes in cell volume, electrolytes, metabolites and ultrastructure. Circ Res 56:262-278, 1985.

Jugdutt BI, Hutchins GM, Bulkey BH, Becker LC. Myocardial infarction in the conscious dog: Three-dimensional mapping of infarct, collateral flow and region at risk. Circulation 60:1141-1150, 1979a.

Jugdutt BI, Hutchins GM, Bulkley BH, Pitt B, Becker LC. Effect of indomethacin on collateral blood flow and infarct size in the conscious dog. Circulation 59:734-743, 1979b.

Katz R, Conroy RM, Robinson K, Mulcahy R. The etiology and prognostic implications of reciprocal electrocardiographic changes in acute myocardial infarction. Br Heart J 55:423-427, 1986.

Khuri SF, Flaherty JT, O'Riordan JB, Pitt B, Brawley RK, Donahoo JS, Gotl VL. Changes in intramyocardial ST segment voltage and gas tensions with regional myocardial ischaemia in the dog. Circ Res 37:455-463, 1975.

Kilpatrick D, Bell AJ, Walker SJ. Derived epicardial potentials differentiate ischaemic ST depression from ST depression secondary to ST elevation in acute inferior myocardial infarction in man. J Am Coll Cardiol 14:695-702, 1989.

Kilpatrick D, Walker SJ, Bell AJ. Importance of the Great Vessels in the Genesis of the Electrocardiogram. Circ Res 66:1081-1087, 1990.

Kilpatrick D, Walker SJ. A validation of derived epicardial potential distributions by prediction of the coronary artery involved in acute myocardial infarction in humans. Circulation 76:1282-1289, 1987.

Kjekshus JK, Maroko PR, Sobel BE. Distribution of myocardial injury and its relation to epicardial ST-segment changes after coronary artery occlusion in the dog. Cardiovasc Res 6:490-499, 1972.

Kjekshus JK. Mechanism for flow distribution in normal and ischemic myocardium during increased ventricular preload in the dog. Circ Res 33: 489-499, 1973.

Kleber AG, Janse MJ, van Capelle FC. Mechanism and time course of S-T and T-Q segment changes during acute regional myocardial ischemia in the pig heart determined by extracellular and intracellular recordings. Circ Res 42:603-613, 1978.

Kleber AG. Extracellular potassium accumulation in acute myocardial ischemia. J Mol Cell Cardiol 16:389-394, 1984.

Kleber AG. Resting membrane potential, extracellular potassium activity and intracellular sodium activity during acute global ischemia in isolated perfused guinea pig hearts. Cir Res 52:442-450, 1983.

Klocke FJ, Braunwald E, Ross J Jr. Oxygen cost of electrical activation of the heart. Circ Res 18:357-365, 1966.

Kloner RA, Rude RE, Carlson N, Maroko PR, DeBoer LWV, Braunwald E. Ultrastructural evidence of microvascular damage and myocardial cell injury after coronary artery occlusion: Which comes first? Circulation 62:945- 952, 1980.

Kornreich F, Montague TJ, Rautaharju PM. Body surface potential mapping of ST segment changes in acute myocardial infarction. Implications for ECG enrolment criteria for thrombolytic therapy. Circulation 87:773-782, 1993.

Kowallik P, Schulz R, Guth BD, Schade A, Paffhausen W, Gross R, Heusch G. Measurement of regional myocardial blood flow with multiple coloured microspheres. Circulation 83:974-982, 1991.

Krone RJ, Greenberg H, Dwyer EM, Kleiger RE Jr, Boden WE. Long-term prognostic significance of ST segment depression during acute myocardial infarction. The Multicenter Diltiazem Postinfarction Trial Research Group. J Am Coll Cardiol 22(2):361-367, 1993.

Kubota I, Hanashima K, Ikeda K, Tsuiki K, Yasui S. Detection of diseased coronary artery by exercise ST-T maps in patients with effort angina pectoris, single-vessel disease, and normal ST-T wave on electrocardiogram at rest. Circulation 80:120-127, 1989.

Kubota I, Ikeda K, Ohyama T, Yamaki M, Kawashima S, Igarashi A, Tsuiki K, Yasui S. Body surface distributions of ST segment changes after exercise in effort angina pectoris without myocardial infarction. Am Heart J 110:949-955, 1985.

Kubota I, Yamaki M, Shibata T, Ikeno E, Hosoya Y, Tomoike H. Role of ATP-sensitive K^+ channel on ECG ST segment elevation during a bout of myocardial ischemia. A study on epicardial mapping in dogs. Circulation 88:1845-1851, 1993.

Lavalee M, Vatner SF. Regional myocardial blood flow and necrosis in primates following coronary occlusion. Am J Physiol 246:H635-H639, 1984.

Lembo NJ, Starling MR, Dell'Italia LJ, Crawford MH, Chaudhuri TK, O'Rourke RA. Clinical and prognostic importance of persistent precordial (V_1-V_4) electrocardiographic ST segment depression in patients with inferior transmural infarction. Circulation 74:56-63, 1986.

Levick JR. Excitation and contraction of a cardiac myocyte. In: An Introduction to Cardiovascular Physiology. Levick JR eds. Butterworth-Heinemann Ltd, pp25-43, 1995.

Lew AS, Hanoch H, Cercek B, Shah PK, Ganz W. Inferior ST segment changes during acute anterior myocardial infarction: a marker of the presence or absence of concomitant inferior wall ischemia. J Am Coll Cardiol 10:519-526, 1987.

Lew AS, Weiss AT, Shah PK, Maddahi J, Peter T, Ganz W, Swan HJC, Berman DS. Precordial ST segment depression during acute inferior myocardial infarction: early thallium-201 scintigraphic evidence of adjacent posterolateral or inferoseptal involvement. J Am Coll Cardiol 5:203-209, 1985.

Lindner E, Katz L. The relative conductivity of the tissue in contact with the heart. Am J Physiol 125:625-630, 1939.

Lowe JE, Cummings RG, Adams DH, Hull-Ryde EA. Evidence that ischemic cell death begins in the subendocardium independent of variations in collateral flow or wall tension. Circulation 68:190-202, 1983.

Lubbe WF, Peisach M, Pretorius R, Bruyneel KJJ, Opie LH. Distribution of myocardial blood flow before and after coronary artery ligation in the baboon: relation to early ventricular fibrillation. Cardiovasc Res 8:478-487, 1974.

Macdonald RG, Hill JA, Feldman RL. ST segment response to acute coronary occlusion: coronary hemodynamic and angiographic determinants of direction of ST segment shift. Circulation 74:973-979, 1986.

Macfarlane PW, Tweddel A, Macfarlane D, Watts MP, Lawrie TDV. Body surface ECG mapping on exercise. Eur Heart J 5(supp. 1):279, 1984.

Makowski EL, Meschia G, Droegemuller W, Battaglia FC. Measurement of umbilical arterial blood flow to the sheep placenta and fetus in utero. Circ Res 23: 623-631, 1968.

Mallory GK, White PD, Salcedo-Salgar J. The speed of healing of myocardial infarction. A study of the pathologic anatomy in 72 cases. Am Heart J 18:647-671, 1939.

Mark DB, Hlatky MA, Lee KL, Harrell FE, Califf RM, Pryor DB. Localizing Coronary Artery Obstructions with the Exercise Treadmill Test. Ann Intern Med 106:53-55, 1987.

Markovitz LJ, Savage EB, Ratcliffe MB, Bavaria JE, Kreiner G, Iozzo RV, Hargrove WC, Bogen DK, Edmunds LH Jr. Large animal model of left ventricular aneurysm. Annals Thoracic Surgery 48:838-845, 1989.

Maroko PR, Kjekshus JK, Sobel BE, Watanabe T, Covell JW, Ross J Jr, Braunwald E. Factors influencing infarct size following experimental coronary artery occlusions. Circulation 43:67-82, 1971.

McKeever WP, Gregg DE, Canney PC. Oxygen uptake of the nonworking left ventricle. Circ Res 6:612-623, 1958.

McLachlan EM. Fundamentals of Electrocardiography. Oxford University Press, pp 135-154, 1981.

Miller WT, Geselowitz DB. Simulation studies of the electrocardiogram I. The normal heart. Circ Res 43: 301-314, 1978a.

Miller WT, Geselowitz DB. Simulation studies of the electrocardiogram II. Ischemia and infarction. Circ Res 43:315-323, 1978b.

Mills RM Jr, Young E, Gorlin R, Lesch M. Natural history of ST-segment elevation after acute myocardial infarction. Am J Cardiol 35:609-614, 1975.

Mirvis D, Ramanathan K, Wilson J. Regional blood flow correlates of ST segment depression in tachycardia-induced myocardial ischaemia. Circulation 73:365-373, 1986.

Mirvis D, Ramanathan K. Alterations in transmural blood flow and body surface ST segment abnormalities produced by ischaemia in the circumflex and left anterior descending coronary arterial beds of the dog. Circulation 76:697-704, 1987.

Mirvis DM, Gordey RL. Electrocardiographic effects of myocardial ischemia induced by atrial pacing in dogs with coronary stenosis I. Repolarization changes with progressive left circumflex coronary artery narrowing. J Am Coll Cardiol 1:1090-1098, 1983.

Mirvis DM, Keller FW, Ideker RE, Zettergren DG, Dowdie RF. Equivalent generator properties of acute ischemic lesions in the isolated rabbit heart. Circ Res 42:676-685, 1978.

Mirvis DM. Physiologic bases for anterior ST segment depression in patients with acute inferior wall myocardial infarction. Am Heart J 116:1308-1322, 1988.

Momomura S, Ferguson JJ, Miller MJ, Parker JA, Grossman W. Regional myocardial blood flow and left ventricular diastolic properties in pacing-induced ischemia. J Am Coll Cardiol 17:781-789, 1991.

Morena H, Janse MJ, Fiolet JWT, Krieger WJG, Crijns H, Durrer D: Comparison of the effects of regional ischemia, hypoxia, hyperkalemia and acidosis on intracellular potentials and metabolism in the isolated porcine heart. Circ Res 46:634-646, 1980.

Mukharji J, Murray S, Lewis SE, Croft CH, Corbett JR, Willerson JT, Rude RE. Is anterior ST depression with acute transmural inferior infarction due to posterior infarction? J Am Coll Cardiol 4:28-34, 1984.

Murdock RH Jr, Harlan DM, Morris JJ III, Pryor WW Jr, Cobb FR. Transitional blood flow zones between ischemic and nonischemic myocardium in the awake dog. Analysis based on distribution of the intramural vasculature. Circ Res 52:451-459, 1983.

Nabel EG, Selwyn AP, Ganz P. Paradoxical narrowing of atherosclertic coronary arteries induced by increases in heart rate. Circulation 81:850-859, 1990.

Naccarella FF, Weintraub WS, Agarwal JB, Helfant RH. Evaluation of "ischemia at a distance": effects of coronary occlusion on remote area of the left ventricle. Am J Cardiol 54:869-874, 1984.

Nakayama K, Fan Z, Marumo F, Hiraoka M. Interrelation between pinacidil and intracellular ATP concentrations on activation of the ATP-sensitive K+ current in guinea pig ventricular myocytes. Circ Res 67:1124-1133, 1990.

Nelson CV, Lange RL, Hecht HH, Carlisle RP, Ruby AS. Effect of intracardiac blood and of fluids of different conductivities on magnitude of surface vectors. Circulation 14:977, 1956.

Nelson CV, Rand PW, Angelakos ET, Hugenholtz PG. Effect of intracardiac blood on the spatial vectorcardiogram. Part I. Results in the dog. Circ Res 31:95-104, 1972.

Nelson CV. Relative influence of intracardiac blood hematocrit and volume on the electrocardiogram. J Electrocardiol 13:387-392, 1980.

Nesarajah MS, Matalon S, Krasney JA, Farhi LH. Cardiac output and regional oxygen transport in the actually hypoxic conscious sheep. Respiration Physiology 53:161-172, 1983.

Odle SG, Wechsler L, Silveerberg JH. The electrocardiographic diagnosis of coronary insufficiency by leads demonstrating the left ventricular cavity. Am Heart J 39:532-543, 1950.

Okada RH, Langner PH, Briller SA. Synthesis of precordial potentials from the SVEC III vectorcardiogrphic system. Circ Res 7:185-191, 1959.

Okada RH. A critical review of vector electrocardiography. IEEE Trans Biomed Eng 10:95-98, 1963.

Okin PM, Kligfield P. Population selection and performance of the exercise ECG for the identification of coronary artery disease. Am Heart J 127:296-304, 1994a.

Okin PM, Kligfield P. Solid-angle theory and heart rate adjustment of ST-segment depression for the identification and quantification of coronary artery disease. Am Heart J 127:659-667, 1994b.

Otto HL. The ventricular electrocardiogram. An experimental study. Arch Int Med 43:335-350, 1929.

Page E. The electrical potential difference across the cell membrane of heart muscle. Biophysical considerations. Circulation 26:582-595, 1962.

Pardee HBE. An electrocardiographic Sign of coronary artery obstruction. Arch Intern Med 26:244-257, 1920.

Pichler M, Shah PK, Peter T, Singh B, Berman D. Wall motion abnormalities and electrocardiographic changes in acute transmural myocardial infarction: implications of reciprocal ST segment depression. Am Heart J 105:1003-1009, 1983.

Plonsey R. Limitations on the equivalent cardiac generator. Biophysical J 6:163-173, 1966.

Prinzmetal M, Ekmekci A, Toyoshima H, Kwoczynski JK. Demonstration of a chemical origin of ST deviation in classic angina pectoris, its variant form, early myocardial infarction, and some noncardiac conditions. Am J Cardiol 3:276-293, 1959a.

Prinzmetal M, Goldman A, Shubin H, Bor N, Wada T. Angina pectoris: II. Observations on the classic form of angina pectoris. Am Heart J 57:530-543, 1959b.

Prinzmetal M, Ishikawa K, Nakashima M, Oishi H, Ozkan E, Wakayama J, Baines JM. Correlation between intracellular and surface electrocardiograms in acute myocardial ischemia. J Electrocardiology 1:161-166, 1968.

Prinzmetal M, Toyoshima H, Ekemckei A, Mizuno Y, Nagaya T. Myocardial Ischemia. Nature of ischemic electrocardiographic patterns in the mammalian ventricles as determined by intracellular electrographic and metabolic changes. Am J Cardiol 8:493-503, 1961.

Prinzmetal M, Toyoshima H, Ekmekci A, Nagaya T. Angina pectoris. 6. The nature of ST Segment elevation and other ECG changes in acute severe myocardial ischemia. Clin Sci 23:489-514, 1962.

Pruitt RD, Valencia F. The immediate electrocardiographic effects of circumscribed myocardial injuries: an experimental study. Am heart J 35:161-197, 1948.

Putini RL, Natale E, Ricci R, Minardi G, Tubaro M, Lioy E, Boccardi L, Pucci E, Disegni M, Giovannini E. Dipyridamole echocardiography evaluation of acute inferior myocardial infarction with concomitant anterior ST segment depression. Eur Heart J 14(10):1328-1333, 1993.

Quyyumi AA, Rubens MB, Rickards AF, Crake T, Levy RD, Fox KM. Importance of "reciprocal" electrocardiographic changes during occlusion of left anterior descending coronary artery. Lancet 1:347-350, 1986.

Rakita L, Borduas JL, Rothman S, Prinzmetal M. Studies on the mechanism of ventricular activity. XII. Early changes in the RS-T segment and QRS complex following acute coronary artery occlusion. Experimental study and clinical applications. Am Heart J 48:351, 1954.

Reimer KA, Jennings RB, Hill MA. Total ischemia in dog hearts, in vitro. 2. High-energy phosphate depletion and associated defects in energy metabolism, cell volume regulation, and sarcolemmal integrity. Circ Res 49:901-911, 1981.

Reimer KA, Jennings RB. Myocardial ischemia, hypoxia, and infarction. In: The Heart and Cardiovascular System. Fozzard HA, Haber E, Jennings RB, Katz AM and Morgan HE ed., Raven Press Ltd, pp1875-1953, 1992.

Reimer KA, Jennings RB. The 'wavefront phenomenon' of ischemic cell death. II. Transmural progression of necrosis within the framework of ischemic bed size (myocardium at risk) and collateral flow. Lab Invest 40:633-644, 1979.

Reimer KA, Lowe JE, Rasmussen MM, Jennings RB. The wavefront phenomenon of ischemic cell death. I. Myocardial infarct size vs duration of coronary occlusion in dogs. Circulation 56:786-794, 1977.

Rivas F, Cobb FR, Bache RJ, Greenfield JC Jr. Relationship between blood flow to ischemic regions and extent of myocardial infarction. Serial measurement of blood flow to ischemic regions in dogs. Circ Res 38:439-447, 1976.

Ross J Jr. Mechanisms of regional ischaemia and antianginal drug action during exercise. Prog Cardiovasc Dis 31:455-466, 1989.

Ross J, Covell JW, Feld GK, Schmid-Schoenbein G. The coronary circulation. In: Physiological Basis in Medical Practice. West JB eds., Williams & Wilkins, Baltimore, PP: 261-273, 1990.

Rouleau J, Boerboom LE, Surjadhana A, Surjadhana A, Hoffman JIE. The role of autoregulation and tissue diastolic pressures in the transmural distribution of left ventricular blood flow in anesthetized dogs. Circ Res 45:804-815, 1979.

Rudolph AM, Heymann MA. The circulation of the fetus in utero: Methods for studying distribution of blood flow, cardiac output and organ blood flow. Circ Res 21:163-184, 1967.

Rush S, Abildskov JA, McFee R. Resistivity of body tissues at low frequencies. Circ Res 12:40-50, 1963.

Sabbah HN, Stein PD. Effect of acute regional ischemia on pressure in the subepicardium and subendocardium. Am J Physiol 242:H240-H244, 1982.

Salcedo JR, Baird MG, Chambers RJ, Beanlands DS. Significance of reciprocal ST-segment depression in anterior precordial leads in acute inferior myocardial infarction: concomitant left anterior descending coronary artery diseased? Am J Cardiol 48:1003-1008, 1981.

Samson WE, Scher AM. Mechanism of ST segment alteration during acute myocardial injury. Circ Res 8:780-787, 1960.

Sato H, Kodama K, Masuyama T, Nanto S, Hori M, Kitabatake A, Inoue M, Kamada T. Right coronary artery occlusion: its role in the mechanism of precordial ST segment depression. J Am Coll Cardiol 14:297-302, 1989.

Savard P, Cohen D, Lepeschkin E, Cuffin BN, Madias JE. Magnetic measurement of S-T and T-Q segment shifts in humans. Part I. Early repolarisation and left bundle branch block. Circ Res 53:264-273, 1983.

Sayen JJ, Peirce G, Katcher AH, Sheldon WF. Correlation of intramyocardial electrocardiogram with polarographic oxygen and contractility in the nonischemic and regionally ischemic left ventricle. Circ Res 9:1268-1279, 1961.

Schaper W. Pathophysiology of coronary circulation. Prog Cardiovasc Dis 14:275-296, 1971.

Scher AM, Young AC, Meredith WM. Factor analysis of the electrocardiogram. Test of electrocardiographic theory: Normal Hearts. Circ Res 8:619-626, 1960.

Schlesinger MJ, Reiner L. Focal myocytolysis of the heart. Am J Pathol 31:443-459, 1955.

Schmitt OH, Levine RB, Simonson E. Electrocardiographic mirror from pattern studies, experimental validity test of dipole test and of central terminal theory. Am Heart J 45:416-428, 1953.

Schosser R, Arfors KE, Messmer K. MIC-II--a program for the determination of cardiac output, arterio-venous shunt and regional blood flow using the radioactive microsphere method. Comp Prog Biomed Res 9:19-38, 1979.

Schulz R, Miyazaki S, Miller M, Thaulow E, Heusch G, Ross JJr, Guth BD. Consequences of regional inotropic stimulation of ischaemic myocardium on regional myocardial blood flow and function in anaesthetised swine. Circ Res 64:1116-1126, 1989.

Schuster EH, Bulkley BH. Early post-infarction angina: ischemia at a distance and ischemia in the infarct zone. N Engl J Med 305:1101-1105, 1981.

Schuster EH, Bulkley BH. Ischemia at a distance after acute myocardial infarction: a cause of early postinfarction angina. Circulation 62:509-515, 1980.

Schwartz JS, Carlyle PF, Cohn JN. Decline in blood flow in stenotic coronary arteries during increased myocardial energetic demand in response to pacing-induced tachycardia. Am Heart J 101:435-440, 1981.

Scott BD, Kerber RE. Clinical and experimental aspects of myocardial stunning. Prog Cardiovasc Dis 35:61-76, 1992.

Selwyn AP, Ogunro EA, Shillingford JP. Natural history and evolution of ST-segment changes and MB CK release in acute myocardial infarction. Br Heart J 39:988-994, 1977.

Shah A, Green CL, Trollinger KM, Wilderman NM, Pope JE, Califf RM, Wagner GS, Krucoff MW. Reassessing the clinical significance of ST-segment depression that occurs concomitantly with the ST-segment elevation during acute myocardial infarction with the use of continuous ST-segment analysis. J Electrocardiol 27(Suppl):256-259, 1994.

Shah PK, Pichler M, Berman DS, Singh BN, Swan HJC. Left ventricular ejection fraction determined by radionuclide ventriculography in early stages of first transmural myocardial infarction: relation to short-term prognosis. Am J Cardiol 45:542-546, 1980.

Sheffield LT. Exercise stress testing. In: Heart Disease. Braunwald E. ed., Harcourt Brace Jovanovich Inc., pp223-241, 1988.

Shenasa M, Hamel D, Nasmith J, Nadeau R, Dutoy J, Derome D, Savard P. Body surface potential mapping of ST-segment shift in patients undergoing percutaneous transluminal coronary angioplasty. Correlations with the ECG and Vectorcardiogram. J Electrocardiology 26:43-51, 1993.

Smith FM. The ligation of coronary arteries with electrocardiographic study. Arch Intern Med 22:8, 1918.

Smith GT, Geary G, Blanchard W, Roelofs TH, Ruf W, McNamara JJ. An electrocardiographic model of myocardial ischemic injury. J Electrocardiology 16:223-234, 1983.

Smith GT, Geary G, Ruf W, Roelofs TH, Ruf W, McNamara JJ. Epicardial mapping and electrocardiographic models of myocardial ischemic injury. Circulation 60:930-938, 1979.

Smith HJ, Singh BN, Norris RM, John MB, Hurley PJ. Changes in myocardial blood flow and S-T segment elevation following coronary artery occlusion in dogs. Circ Res 36:697-705, 1975.

Snedecor GW, Cochran WG. Statistical methods. Iowa State University Press, Ames, pp175-191, 1980.

Sodi-Pallares D, Calder RM. Intracavitary potentials in subendocardial ischaemia. In: New bases of electrocardiography. CV Mosby, St Louis, pp593-594, 1956.

Sodi-Pallares D, Calder RM. The monophasic wave in angina pectoris, In: New bases of electrocardiography. C V Mosby, St Louis, pp211-213, 1956.

Spach MS, Barr RC, Serwer GA, Kootsey JM, Johnson EA. Extracellular potentials related to intracellular action potentials in the dog Purkinje system. Circ Res 30: 505-519, 1972.

Spach MS, Miller WT III, Miller-Jones E, Warren RB, Barr RC. Extracellular potentials related to intracellular action potentials during impulse conduction in anisotropic canine cardiac muscle. Circ Res 45:188-204, 1979.

Spach MS. Microscopic basis of anisotropic propagation in the heart. In: Cardiac Electrophysiology-from cell to bedside, Zipes DP and Jalife J ed., New York, W.B. Saunders Company, pp204-216, 1995.

Stanley PC, Pilkington TC, Morrow MN. The effects of thoracic inhomogeneities on the relationship between epicardial and torso potentials. IEEE Trans Biomed Eng 33:273-284, 1986.

Stephan K, Meesmann W, Sadony V. Oxygen demand and collateral vessels of the heart: Factors influencing the severity of myocardial ischemic injury after experimental coronary artery occlusion. Cardiovasc Res 9:640-648, 1975.

Stevenson RN, Ranjadayalan K, Umachandran V, Timmis AD. Significance of reciprocal ST depression in acute myocardial infarction: a study of 258 patients treated by thrombolysis. Br Heart J 69(3):211-214, 1993.

Stevenson RN, Umachandran V, Ranjadayalan K, Roberts RH, Timmis AD. Early exercise testing after treatment with thrombolytic drugs for acute myocardial infarction: importance of reciprocal ST segment depression. British Medical Journal 308(6938):1189-1192, 1994.

Taccardi B. Changes in cardiac electrogenesis following coronary occlusion. In: Coronary Circulation and Energetics of the Myocardium. Marchetti G, Taccardi B, eds., Karger: Basel. 259-267, 1967.

Taccardi B. La distribution spatiale des potentiels cardiaques. Acta Cardiol 13:173-189, 1958.

Tada M, Yamagishi M, Kodama K, Kuzuya T, Nanto S, Inoue M, Abe H. Transient collateral augmentation during coronary arterial spasm associated with ST-segment depression. Circulation 67:693-698, 1983.

Theroux P, Franklin D, Ross J, Kemper WS. Regional myocardial function during acute coronary artery occlusion and its modification by pharmacologic agents in dog. Circ Res 35:896-908, 1974.

Theroux P, Ross J, Frankin D, Kemper WS, Sasayam S. Regional myocardial function in the conscious dog during acute coronary occlusion and responses to morphine, propranolol, nitroglycerin and lidocaine. Circulation 53: 302-313, 1976.

Tomoike H, Franklin D, Ross J. Detection of myocardial ischemia by regional dysfunction during and after rapid pacing in conscious dogs. Circulation 58:48-56, 1978.

Toyoshima H, Ekmekci A, Flamm E, Mizuno Y, Nagaya T, Nakayama R, Yamada K, Prinzmetal M. Angina Pectoris. VII. The nature of S-T depression in acute myocardial ischemia. Am J Cardiol 13:498-509, 1964.

Trevi GP, Sheiban I. Chronic ischemia ("hibernating") and postischaemic ("stunned") dysfunction but viable myocardium. Eur Heart J 12(Suppl G):20-26, 1991.

Tung T. A bidomain model for describing ischaemic myocardial DC potentials. PhD thesis, M.I.T, 1978.

Uren N, Melin JA, De Bruyne B, Wijins W, Baudhuin T, Camici P. Relation between myocardial blood flow and the severity of coronary artery stenosis. N Engl J Med. 330:1782-1788, 1994.

Utley J, Carlson EL, Hoffman JIE, Martinez HM, Gerald D. Total and regional myocardial blood flow measurements with 25μ, 15μ, 9μ, and filtered 1-10μ diameter microspheres and antipyrine in dogs and sheep. Circ Res 34:391-404, 1974.

Vatner SF. Correlation between acute reduction in myocardial blood flow and function in conscious dogs. Circ Res. 47:201-207, 1980.

Vincent GM, Abildskov JA, Burgess MJ. Mechanisms of ischemic ST-segment displacement, evaluation by direct current recordings. Circulation 56:559-566, 1977.

Vokonas PS, Malsky PM, Paul SJ, Robbins SL, Hood WB. Radioautographic studies in experimental myocardial infarction: Profiles of ischemic blood flow and quantification of infarct size in relation to magnitude of ischemic zone. Am J Cardiol 42:67-75, 1978.

Walker SJ, Bell AJ, Loughhead MG, Lavercombe PS, Kilpatrick D. Spatial distribution and prognostic significance of ST segment potential determined by body surface mapping in patients with acute inferior myocardial infarction. Circulation 76:289-297, 1987.

Walker SJ, Kilpatrick D. Forward and inverse electrocardiographic calculations using resistor network models of the human torso. Circ Res 61:504-513, 1987.

Walker SJ, Lavercombe PS, Loughhead MG, Kilpatrick D. A body surface mapping system with immediate interactive data processing. IEEE Computers In Cardiology pp305-308, 1983.

Warltier DC, Zyvoloski MG, Gross GJ, Brooks HL. Subendocardial versus transmural myocardial infarction: Relationship to the collateral circulation in canine and porcine hearts. Can J Physiol Pharmacol 60:1700-1706, 1982.

Watabe S, Taccardi B, Lux R, Ershler PR. Effect of nontransmural necrosis on epicardial potential fields. Correlation with fiber direction. Circulation 82:2115-2127, 1990.

Wegria R, Segers M, Keating RP, Ward HP. Relationship between the reduction in coronary flow and the appearance of electrocardiographic changes. Am Heart J 38:90-96, 1949.

Wilde AAM, Kleber AG. The combined effects of hypoxia, high K^+, and acidosis on the intracellular sodium activity and resting potential in guinea pig papillary muscle. Circ Res 58:249-256, 1986.

Willems JL, Willems RJ, Willems GM, Arnold AER, Van de Werf F, Verstraete M, for the European Cooperative Study Group for Recombinant Tissue-type Plasminogen Activator. Significance of initial ST segment elevation and depression for the management of thrombolytic therapy in acute myocardial infarction. Circulation 82:1147-1158, 1990.

Wilson FN, Hill IGW, Johnston FD. The interpretation of the galvanometric curves obtained when one electrode is distant from the heart and the other near or in contact with the ventricular surface. I. Observations on the cold-blooded heart. Am Heart J 10:163-175, 1934.

Wilson FN, MacLeod AG, Barker PS. The distribution of the action currents produced by heart muscle and other excitable tissue immersed in extensive conducting media. J Gen Physiol 16:423-456, 1933a.

Wilson FN, Macleod AG, Barker PS. The distribution of the currents of action and injury displayed by heart muscle and other excitable tissues. Univ Mich Studies Sci Ser 10:1-57, 1933b.

Wilson FN, Macleod AG, Barker PS. The distribution of the currents of action and injury displayed by heart muscle and other excitable tissues. Univ Mich Studies Sci Ser 18:58-115, 1933c.

Wolferth CC, Bellet S, Livezey MM, Murphy FD. Negative displacement of the RS-T segment in the electrocardiogram and its relationships to positive displacement; an experimental study. Am Heart J 29:220-245, 1945.

Wong CK, Freedman SB, Bautovich G, Bailey BP, Bernstein L, Kelly DT. Mechanism and significance of precordial ST depression during inferior wall acute myocardial infarction associated with severe narrowing of the dominant right coronary artery. Am J Cardiol 71:1025-1030, 1993a.

Wong CK, Freedman SB. Implications of ST changes in reperfusion management of acute inferior myocardial infarction. Eur Heart J 15 (10):1385-1390, 1994.

Wong CK, Freedman SB. Usefulness of continuous ST monitoring in inferior wall acute myocardial infarction for describing the relation between precordial ST depression and inferior ST elevation. Am J Cardiol 72:532-537, 1993b.

Woodbury JW, Brady AJ. Intracellular recording from moving tissues with a flexibly mounted ultramicroelectrode. Science 123:100-101, 1956.

Wyatt HL, Forrester JS, Tyberg JV, Goldner S, Logan SE, Parmley WW, Swan HJC. Effect of gradual reductions in regional coronary perfusion on regional and total cardiac function. Am J Cardiol 36:185-192, 1975.

Yamagishi M, Kuzuya T, Kodama K, Nanto S, Tada M. Functional significance of transient collaterals during coronary artery spasm. Am J Cardiol 56:407-412, 1985.

Yasue H, Omote S, Takizawa A, Masao N, Hyon H, Nishida S, Horie M. Comparison of coronary arteriographic findings during angina pectoris associated with S-T elevation or depression. Am J Cariol 47:539-546, 1981.

Yu PNG, Stewart JM. Subendocardial myocardial infarction with special reference to the electrocardiogrphic changes. Am Heart J 39:862-880, 1950.

Zwissler B, Schosser R, Weiss C, Iber V, Weiss M, Schwicker C, Spengler P, Messmer K. Methodologic error and spatial variability of organ blood flow measurements using radiolabeled microspheres. Res Exp Med 191: 47-63, 1991.

Appendix A STATISTICAL DEFINITIONS

SIMPLE LINEAR REGRESSION

The simple linear regression reflects the linear dependence of one variable on a second variable (Campbell & Machin 1990). The linear relationship between variables X and Y can be expressed by the equation:

$$Y = a + bX$$

Where Y is termed the dependent variable and X independent variable. b is termed the regression coefficient or the slope of the best fit regression line, and a intercept. b is given by:

$$b = \frac{\sum(x-\bar{x})(y-\bar{y})}{\sum(x-\bar{x})^2}$$

The intercept is estimated by $a = \bar{y} - b\bar{x}$

The standard error of estimate is calculated by:

$$SEE(b) = \frac{\sqrt{\sum(y-\bar{y})^2 - b^2\sum(x-\bar{x})^2}}{(n-2)\sum(x-\bar{x})^2}$$

In this study, the simple linear regression was used to estimate the linear relationship between the intensity of the fluorescent signal and the number of fluorescent microspheres (chapter 4, appendix C).

CORRELATION COEFFICIENT

The correlation coefficient (r) is a measure of the closeness of a linear relationship between two sets of variables x and y (Altman 1991). The correlation coefficient is calculated by the formula:

$$r = \frac{\sum(x-\bar{x})(y-\bar{y})}{\sqrt{\sum(x-\bar{x})^2\sum(y-\bar{y})^2}}$$

The correlation coefficient is always between -1 and 1; a correlation coefficient approaches 1 if the data sets are identically shaped; a zero correlation coefficient if there is no association between the two data sets. A positive correlation implies that for an increase in one of the variables, the other variable also increases; a negative correlation indicates that an increase in one of the variables is accompanied by a decrease in the other variable. When the correlation coefficient is used, it is often associated with a P value (Snedecor & Cochran 1980). The P value indicates a relationship greater than would be expected by chance. A P value less than 0.05 indicates the probability of a correlation arising by chance is less than 5 in 100. In this study, the correlation coefficient was used to analyse the similarity between two measurements (chapters 4 and 6), and the relationship between the ST potential change and the regional myocardial blood flow (chapters 6 and 7).

Appendix B CALIBRATION FOR MAGNETIC FLOW TRANSDUCER

The following graphs demonstrate the relationship between the magnetic flowmeter readings and the actual flow rate at the specific calibration factor of the transducer. At the flow rate range of 20-100 mL/min, the flow readings correlated exceptionally well with the actual flow. The diameters of the flow transducers were 3 mm (A) and 2.5 mm (B) respectively.

A

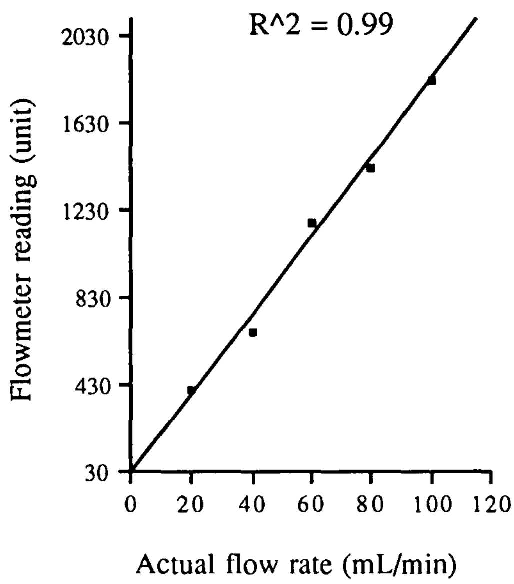

B

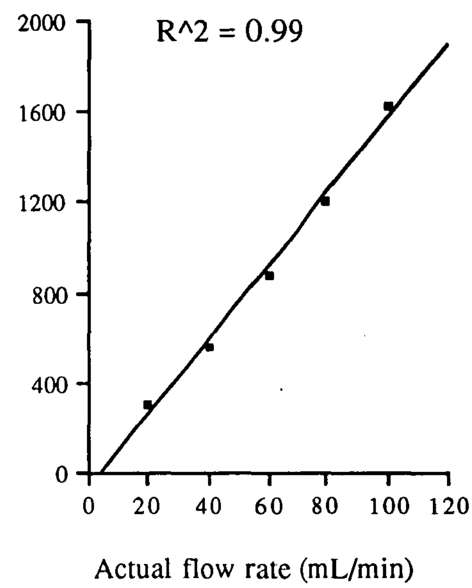

Appendix C REGRESSION AND CORRELATION ANALYSIS FOR CHAPTER 4

Tables 1 and 2 show the fluorescent intensity as a function of the microsphere numbers. Table 3 shows the correlation between fluorescent intensity measured by using pure fluorescence and fluorescent intensity measured by using the mixture of fluorescence and myocardium.

Table 1 Fluorescent intensity vs microsphere number
-measurements of pure fluorescence samples

fluorescent dye	R^2	slope	intercept	SEE
blue-green	0.999	0.40	20.10	28.61
green	0.999	0.30	6.56	23.60
yellow-green	0.999	0.22	17.80	14.14
orange	0.999	0.16	15.66	9.23
red	0.998	0.29	5.13	27.71
crimson	0.997	6.20	3.03	7.41

Table 2 Fluorescent intensity vs microsphere number
-measurements of fluorescence-myocardium samples

fluorescent dye	R^2	slope	intercept	SEE
blue-green	0.997	0.35	6.38	47.80
green	0.999	0.31	24.03	21.19
yellow-green	0.999	0.24	3.79	16.15
orange	0.999	0.13	1.25	12.94
red	0.998	0.34	19.91	32.39
crimson	0.999	7.27	12.31	6.04

Table 3 Relationship between the fluorescent intensity of pure fluorescence and the fluorescent intensity of fluorescence-myocardium

fluorescent dye	r
blue-green	0.998
green	0.998
yellow-green	0.999
orange	0.999
red	0.998
crimson	0.998

Appendix D HAEMODYNAMIC RECORDINGS

The following graphs are haemodynamic recordings from one experiment. Graph A shows the measurements before ischaemia; graph B shows the measurements during partial coronary artery ligation. Data were recorded by a Macintosh II computer via an analogue-to-digital converter (NB-DMA-8, NI-488 for Mac-SN 3643 and LabView software) at a sampling rate of 100 Hz.

CQ: coronary artery flow
LVP: left ventricular pressure
LAP: left atrial pressure

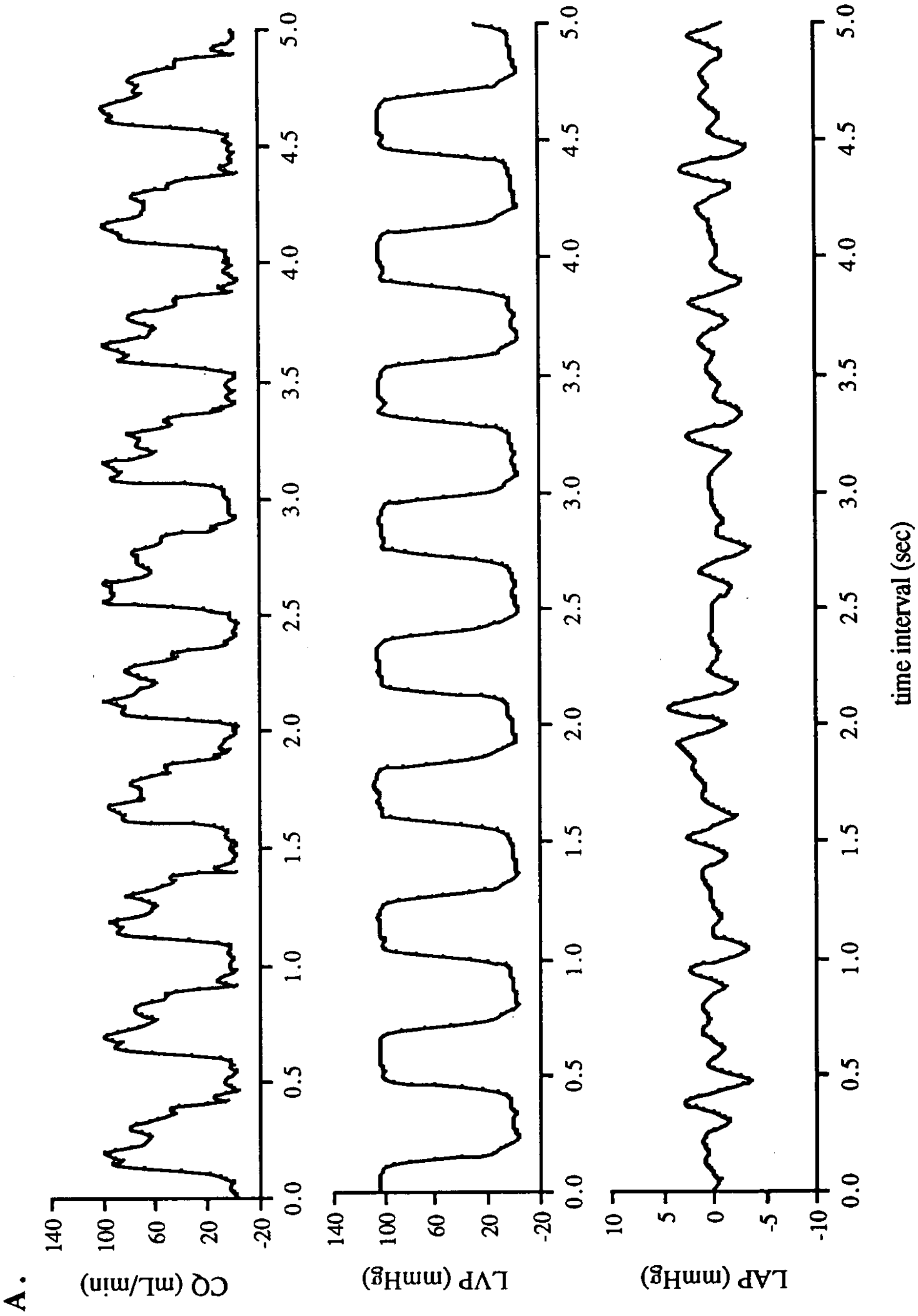

A.
CO (mL/min)
LVP (mmHg)
LAP (mmHg)
time interval (sec)

B .

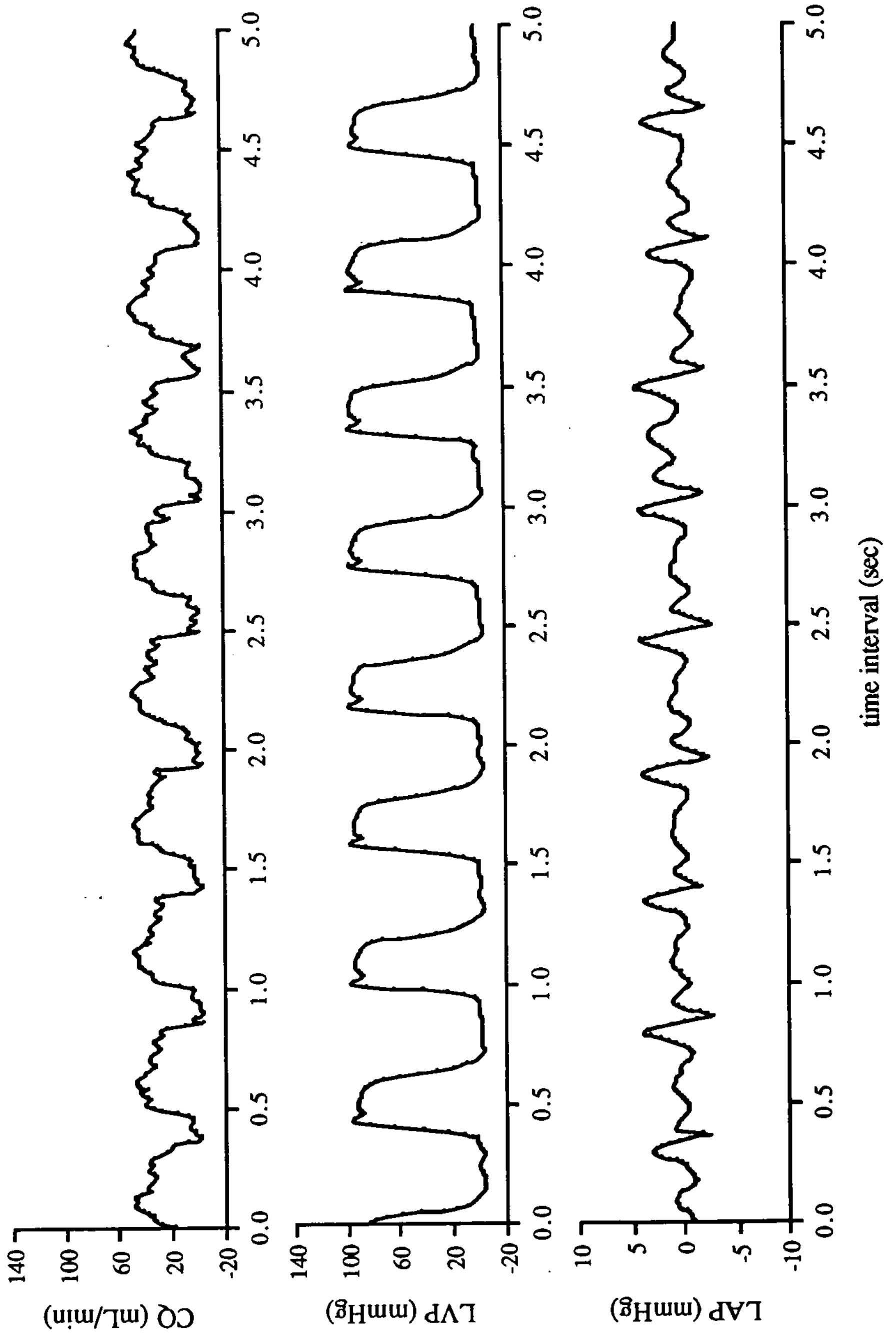
CQ (mL/min)
LVP (mmHg)
LAP (mmHg)
time interval (sec)
0.0 0.5 1.0 1.5 2.0 2.5 3.0 3.5 4.0 4.5 5.0
140 100 60 20 -20
10 5 0 -5 -10